INSTITUTE OF SOUND AND VIBRATION RESEARCH
FACULTY OF ENGINEERING AND APPLIED SCIENCE

UNIVERSITY OF SOUTHAMPTON

The Vibration and Acoustic Properties of Pipes with Squeeze Film and Some Friction Damping Systems

by

MENG LI

A thesis submitted for the degree of Doctor of Philosophy

August 1991

UNIVERSITY OF SOUTHAMPTON

ABSTRACT

FACULTY OF ENGINEERING AND APPLIED SCIENCE
INSTITUTE OF SOUND AND VIBRATION RESEARCH

Doctor of Philosophy

The Vibration and Acoustic Properties of Pipes with Squeeze Film and Some Friction Damping Systems.

By MENG LI

This study was motivated by the need to decrease the noise radiation and vibration of pipework in power plants, particularly at elevated temperature.

A thin circular cylindrical shell has been studied theoretically. The exact solutions for natural frequencies of the symmetrical and anti-symmetrical modes for cylindrical shell vibration have been derived in matrix form. Using this theory, numerical results for natural frequencies and mode shapes with free-free, clamped-free and clamped-clamped boundary conditions have been evaluated.

Based upon studies of the thin cylindrical shell theory and the physical phenomenon of air film damping of two parallel plates, the theory for predicting the loss factor of an annular double pipe damping system with a very small air gap has been developed. Flügge's thin shell equations of motion and the Navier-Stokes equation for viscous fluid were employed in the analysis. The fluid motion was expressed in terms of shell displacement by using a travelling wave type solution. The solutions gave the fluid velocity profiles and stresses in the clearance between two cylindrical, concentric shells. According to the definition of energy dissipated in the fluid, an equation was derived for predicting the loss factor of the whole damping system. Based on the principle of similarity, an optimum design for a system generating squeeze film damping in pipes has been made. The theory was then extended to study the damping caused by various kinds of viscous fluid in the gap between the two annular structures. Experiments have been carried out to investigate the loss factor of the double pipe system with in-phase and out-of-phase modes of vibration.

Friction damping has been studied experimentally on a thin-walled pipe with a coiled steel spring or wire rope attached or with a mineral wool wrapping. Flexural vibration was examined in the experiments.

This study included an experimental investigation of reduction of internally generated high level noise through a pipe wall, and the sound transmission losses of pipes with a coiled spring friction damper or wire rope and conventional lagging were measured. The transmission losses of a double pipe system with air or oil in the gap were also measured.

ACKNOWLEDGEMENTS

I wish to thank Professor R. G. White for allowing me the opportunity to do this research and for his excellent supervision, patience and encouragement throughout the project. I also gratefully acknowledge the financial support by the Central Electricity Generating Board under which the research was carried out.

Thanks are also extended to Professor Frank Fahy and Dr. R. J. Pinnington for their suggestions and help in the experimental work, and to Mr. Terry A. Vass for his kind help in administrative matters.

Many thanks are due to ISVR technicians for their technical assistance.

CONTENTS

NOMENCLATURE

chapter 2.

B	constant
C	constant
[D]	matrix differential operator
E	Young's modulus
h	thickness of pipe wall
j	$\sqrt{-1}$
L	length of shell
m	number of axial waves
M_x	axial moment
n	number of circumferential waves
N_x	axial force
$N_{x\theta}$	shear force
R	radius of cylindrical shell
S_x	Kirchhoff force
u	displacement in longitudinal direction
U_0	the amplitude of u
v	displacement in tangential direction
V_0	the amplitude of v
w	displacement in radial direction
W_0	the amplitude of w
x	axial co-ordinate
α	frequency function coefficient
β	thickness/radius ratio
Δ	differential operator
θ	angular co-ordinate
ν	Poisson's ratio
ω	circular frequency, rads/sec.
Ω	nondimensional frequency, rads/sec
ρ	density of material

chapter 3 & 4

C_0	velocity of sound
$\bar{c}$	average speed of the molecules of gas

f	frequency, Hz
Δf	frequency bandwidth
h	thickness of pipe wall
$I_n(kr)$, $K_n(kr)$	modified first and second order Bessel functions
k	wave number
L	characteristic length
M	Mach number
p	pressure of fluid
P_{ij}	surface loading component per unit area
R	mean radius
r, θ, z	radial, tangential and longitudinal direction
S	constant
T_{60}	the reverberation time
T	temperature
V	mean velocity of flow
$V_{r,\theta}$	fluid velocity
$v_{r,\theta,z}$	particle velocity of pipe
δ	boundary layer thickness of flow
ε_{xy}	strain in fluid
η	loss factor
Λ	the mean free path of the molecules of gas
μ	dynamic viscosity
ν	kinematic viscosity
π	3.14159··· : ratio of circumference to diameter of circle
ρ	density of fluid
τ_{xy}	stress in fluid
ψ	stream function

chapter 5

a	acceleration
D_s	diameter of spring coil
d_s	diameter of spring wire
D_w	diameter of wire rope
d_w	diameter of a wire
F	force
f_s	the lowest natural frequency of spring
G	modulus of rigidity of spring material

G_{aa}	acceleration spectral density
G_{af}	cross spectral density of acceleration and force
g	constant of gravitation
H_i	transfer function
K_s	stiffness of spring
l_s	spacing between two spring coils
N	normal force to surface of pipe wall
N_s	number of strands of wire rope
N_w	number of wires in a strand
n	number of active coils
R	radius of pipe
y	displacement of spring mass
δ	deflection of spring
μ	coefficient of dry friction
γ	weight density of spring material

chapter 6

B	the bending stiffness per unit width of the pipe wall
c	speed of sound in fluid
c_0	speed of sound in the air
c_L	the longitudinal wave speed in a pipe wall
D	diameter of pipe
f_c	critical frequency of pipe
f_r	ring frequency of pipe
h	thickness of pipe wall
I	sound intensity
I_0	reference sound intensity
L_I	sound intensity level
L_p	sound pressure level
$<L_p>$	the space-average sound pressure level in a pipe
n	circumferential mode of pipe
m	axial mode of pipe, mass per unit surface area of pipe wall
p	sound pressure
$<p^2>$	the space-average mean square pressure
p_{ref}	sound reference pressure
S	the sound radiation surface area
TL	sound transmission loss

u	particle velocity of sound wave in air
W_t	the sound power transmitted through a measured surface
ϕ	phase of sound pressure
η_{air}	acoustic air gap loss factor
ρ_0	density of air
τ	sound transmission coefficient

CHAPTER 1. GENERAL INTRODUCTION.

1.1 DEFINITION OF THE PROBLEM.

In electrical power stations, large machinery installations such as turbo alternator sets are composed of an assembly of machine elements, including, for example pumps, etc. The pipework forms a set of transmission paths by which vibration is carried from sources to areas where unacceptable vibration levels are produced or noise is radiated. In addition to high pipe wall vibration levels and subsequent acoustic radiation, these vibrations often excite attached structures. In some instances this can result in component failure which is both costly and hazardous. As this type of pipework generally carries a mixture of high temperature water and steam, there are limitations when applying damping treatments or noise absorbing materials, which should be capable of working at high temperature. Suitable damping treatment and noise reduction systems for pipework are needed for reasons of safety and legislation.

1.2 VIBRATION OF A THIN CYLINDRICAL SHELL AND ITS DAMPING TREATMENT.

When unwanted energy is transmitted along a pipe in the form of random structural vibration resulting from random exitation, the vibrational response of the piping system is dominated by the responses of the structural modes. To control the vibration and noise level radiated from a pipe system, it is essential to study the dynamic response of thin circular cylindrical shells which represent the types of pipes used in power stations. Calculation of the free vibration characteristics of circular cylindrical shells of finite length has been of interest to engineers and scientists for a long time. An excellent survey and discussion of the literature on the free vibration of cylindrical shells has been given by Leissa in reference [1], which contains approximately 1000 references on this topic. The theory of vibration of thin cylindrical shells included the study of free vibration of finite shells with various boundaries [2, 3, 4] , and the study of forced vibration of finite shells with structural damping [5]. Experimental studies on the vibration of a circular cylindrical shell have been published which concerned measurements of mode shape and resonance frequency [6].

Damping treatments are a conventional means for reducing mechanical vibration levels by the removal of energy from a system. The role of damping controlling structural response has been examined [7] and quantitive studies of the damping of beams have

been made by a number of investigators [8,9]. In study of vibration damping, the loss factor is a important parameter which is a ratio of energy dissipated to total energy of the structure. Two experimental methods have been applied to determine loss factors of pipe, they are an energy method and the decay method [10, 11]. Using the decay method, loss factors of pipe can be measured within a frequency band at high frequencies or at a single frequency associated with response in a dominant mode.

Surface damping treatments are often used to solve a variety of resonant noise and vibration problems, especially those associated with vibration of structures made of thin sheet metal. Such treatments can easily be applied to existing structures and provide high damping capability over wide temperature and frequency ranges. The surface damping treatments are usually classified in one of two categories, according to whether the damping material is subjected to extensional or shear deformation [12]. One of the most commonly used surface damping treatments is extensional damping. Sometimes this method is referred to as the unconstrained or free layer damping treatment. The treatment is coated on one or both sides of a structure, the damping material will be subjected to tension-compression deformation [13]. The dependence of the free-layer damping treatment performance on temperature is very significant. However, the shear type of damping treatment or constrained damping [14] [15] is more efficient than the unconstrained-layer damping treatment. This efficiency is balanced by great complication in analysis and application. The constrained damping treatment is similar to the unconstrained layer, except that the viscoelastic material is constrained by a metal layer. Therefore, whenever the structure is subjected to cyclic bending, the metal layer will constrain the viscoelastic material and force it to deform in shear. Shear deformation is the mechanism by which the energy is dissipated. Both unconstrained and constrained damping are a function of temperature. Low damping is usually found at high temperature.

1.3 VIBRATION CONTROL IN DOUBLE-PLATE OR DOUBLE PIPE SYSTEMS.

One possible method for increasing the damping of a pipe is to make a system which consists of two concentric circular cylindrical shells with a very narrow annulus. A damping study is needed for this kind of double pipe system for assessing both vibration and noise radiation characteristics.

The transmission of vibration and structural damping are topics which have been studied over the years at the ISVR (Institute of Sound and Vibration Research). The

damping of machine structures has been studied with the ultimate objective of reducing radiated noise; double plate arrangements have been examined [21] and have been shown to be relatively economical and robust sources of damping. The damping arises due to air pumping in the gap between the plates. The important advantage of this approach is its possible application at high temperature working conditions. Therefore, to increase damping of pipework, the principle of "air pumping" will be adopted, for which a double pipe system is designed. The double pipe system consists of two coaxial thin-walled pipes with air or oil in the gap between them.

The initial discovery of 'air pumping' loss came from the investigation of damping in joints which started in 1962 as a continuing effort to refine methods for prediction and control of structural vibration [16] [17]. Maidanik [18] attempted to find a gas pumping mechanism which would lead to damping values that agree in order of magnitude with those observed in experiments. In Maidanik's research, an expression for the loss factor associated with the dissipation in the gas was derived. It has shown that the loss factor was a function of the vibration frequency and ambient pressure. Following this initial work, the phenomena of gas or liquid pumping were studied in the vibration of double plate systems and coaxial cylindrical shells.

1) Damping of double plates.

Möser [19] carried out research on the influence of the viscosity of a gas or fluid-like layer between two plates on structure borne sound. The analysis involved the determination of the wave number of the system. From this analysis the frequency variation of the damping was found and the dependence of the losses on the thickness of the layer and on the mass loading of the plates became evident. More recently, Trochidis [20] has developed a theoretical model for predicting loss factors of double plate systems and it was assumed that the fluid in between was incompressible. Comparisons of predicted values with experimental results were only given at frequencies well below the excited plate critical frequency. Chow [21] carried out experiments to measure loss factors of plates separated by a fluid layer. Attached plates were used in Chow's work, one was a perforated plate with equally spaced circular holes and the other was a flexible plate. The damping due to squeeze film motion of gas between two plates was predicted. An impedance approach was used to calculate the loss factor of the vibration system. Theoretical and experimental results showed a very low damping level. It was claimed that the ratio of the dynamic viscosity of the fluid to its density was the controlling parameter. This ratio was favourable with gas but not for liquid. However, high loss factors can still be achieved if the viscosity can be increased significantly. Although the impedance method can be used to predict

energy loss in a vibrating system either for squeeze film damping or material damping, the contribution of gas pumping in the modes of coupled plate systems is unknown. In other words, concerning fluid dynamics the motion of fluid caused by the vibration of a double plate system was not evaluated in the theory. The velocity distribution of squeezed flow has to be assumed for impedance calculation.

From previous studies, it is understood that the mechanism of so called "squeeze film damping" has not been adequately theoretically modelled. For example, how do the mode shapes and vibration coupling of two plates affect the air pumping and system damping? The object of this study was trying to develop the mathematical modelling to describe the phenomena of air or oil squeeze film damping in a double pipe system and to predict the damping level or loss factor of this system. Some relevant experiments are carried out to prove the theory. Furthermore, the squeeze flow in double pipe system vibration is deduced from the equation of motion of pipe vibration and theory of fluid dynamics. The energy dissipated in the squeezed fluid is also calculated.

2) Dynamics of a cylindrical shell system coupled by a viscous fluid.

Chen [22,23,24] in his research, attempted to find the expression for the natural frequencies of two coaxial cylindrical shells containing fluid, in which a rod vibrating in a static or flowing fluid annulus was considered. The beam-like vibration of a fluid-structural system including a cylindrical shell was used in the theory. It was found that, because of the increase in the added mass due to the boundary constraint, the natural frequencies and critical flow velocity (maximum fluid velocity within annulus) for a rod vibrating in a flowing fluid annulus were smaller than those of an isolated rod surrounded by an axial flow. The increase of added mass depends on the ratio of the wavelength to the rod radius and the ratio of the pipe wall thickness to the rod radius. In the study of structural modes, acoustic modes and coupled structural-acoustic modes, it was found that the fluid inertia effect was always very large in out-of-phase modes. In the study of hydrodynamic effects on two body motions with fluid coupling, Frits [25] presented an expression for hydrodynamic mass in a long cylindrical annulus of a finite length as well as for various shapes of vibrating body.

The first study of the breathing vibrations of two thin-walled cylinders in a fluid initially at rest was made by Levin [26]. It was found that the lowest resonance frequencies of combined structures were always associated with the out-of-phase modes. Au-Yang [27,28] also studied the virtual mass in free vibration of fluid coupled coaxial cylindrical shells of

different lengths, where the uncoupled modes were used, in which a cylinder vibrates with the other being rigid.

Yeh and Chen [29,30], in order to design the thermal shield inside a reactor and other system components to avoid detrimental flow induced vibrations, analyzed the dynamics of a cylindrical shell system coupled by a viscous fluid. In the theory, Flügge's shell equation and the Navier-Stokes equation for a viscous fluid were employed by using a travelling wave type and beam mode solution. Natural frequencies for coupled and uncoupled systems with a rigid inner or outer shell, or both vibrating, were discussed. The effects of a water fluid gap on damping ratio were examined in their experiments.
Based on the fluid forces, lumped added mass and linear dashpot, modelling of an annular gap support was employed by Mulcahy [31] to predict the fundamental natural frequency and modal damping, of a type of structure typically found in nuclear reactors. Fox [32] suggested in a theoretical and experimental investigation that thin layer of gas trapped between surfaces of a structure might contribute to damping of structural vibrations. Brown [33] showed that the three-dimensional computation of fluid effects was difficult for finite length cylinders with complex boundary conditions, but the finite element method was easier to apply than classical methods in modelling the physical boundary conditions. Modal damping was also studied by Dowell [34] and Chung [35], where a cylindrical shell vibrating in fluid was analysed. Garner [36] found that for short lengths or higher modes, the effect of the fluid on the cylinder motion diminishes compared to that for the infinite cylinder case.

Heckl [37] studied the special case of a double-pipe system, where two pipes were made together with a very narrow air gap. This air gap was controlled by high air pressure (about 4 atm) in the inner pipe. Natural frequencies and mode shapes were studied theoretically. An interesting phenomenon observed was that when the air gap was very small and the inner pressure was varied, the system loss factor appeared to remain unchanged.

3) Friction damping and its role in vibration control.

Friction between contacting interfaces which undergo relative vibrating motion is known to dissipate the energy of vibration, resulting in damped oscillations. The phenomenon of friction between contacting surfaces is probably the most elusive physical mechanism that defies clear comprehension.
There are many friction phenomena existing in vibrating machinery structures and other engineering systems. In some instances, artificial devices are designed and introduced into

the structural system with the sole purpose of developing friction forces leading to vibration damping.
Many efforts have been made to understand the dry friction damping mechanism in the area of surface science and characterization of friction forces at mating surfaces and to develop damping technology.

In principle, the friction force is determined by the normal load and the coefficient of friction and so is the energy dissipation. Friction occurs because surfaces of real components used in engineering practice are never ideally smooth, so that when they come into contact with each other, the contact cannot be continuous and only certain parts of the surface will carry the applied load. Thus, the true contact area is the sum of those parts of the surfaces where the interaction between the bodies is strong. This true contact area could be determined on the basis of measurement of electrical conductivity [38] which changes in direct proportion to the normal load N. A theoretical study was carried out by Zhuravlev [39] to calculate the true surface area in elastic contact of two rough bodies. The relationships of modulus of elasticity and Poisson's ratio with this true surface were also concerned [40].

The characteristics of friction forces have been discussed in many references previously. A great variety of phenomena occur in rubbing contact between surfaces of structural components. The apparent simplicity of the relationship is that the friction force induced at a point on an interface is proportional to the normal load. In addition to the problem of obtaining a reliable estimate of the constant of proportionality, i.e. the coefficient of friction μ, the representation $F=\mu N$ led to computational complications even when applied to the study of a single degree freedom system by Den Hartog [41]. However, this simplicity of approach has been the primary reason for its use in most studies of dry friction, and continuing attempts have been made to use modifications of this basic model, such as a single degree of freedom spring-mass system with viscous damping and Coulomb friction [42, 43], application of Fourier series to represent the friction force [44] and mathematical modelling of an unknown force dependent on the prescribed displacement [45, 46] as well as the exact solutions for a two degree freedom system with friction damping.

There have been very few studies to calculate the coefficient of dry friction since it has usually been considered as a constant dependent only on the natures of the material and contacting surfaces, as discussed in chapter 5. There are also only very few published experimental data which may be used to estimate coefficients of friction, such as Srinivasan's research on turbojet engine blade damping [47]. Most theories discussed above were mainly concerned with forced response of a vibrating structure. To determine

coefficients of friction as a function of loading and through the frequency range of vibrating structures is a most difficult problem.

Dry friction damping technology has been divided into two aspects. One is investigation or prediction of friction damping which occurs in a substructure of a vibrating body. For example, the friction damping and energy dissipation have been predicted for joints in the cases of riveted and bolted plates [48], or rotational slip [49]. Another aspect is the "added friction damper" to minimize the vibration of a structure. This was based on creating an extra friction damping source on the vibrating structure. One such design was applied to limit a particular resonant amplitude of a compressor blade [50]. A useful application of friction damping was the silencing treatments to reduce rock drilling noise carried out at the ISVR, University of Southampton a few years ago [51]. In this study, a compression spring like a steel coil was wound around a drill bit to give friction damping when driven by a pneumatic or hydraulic drill. It was found that damped drill rod noise was reduced to below 100 dBA compared with that from an undamped drill of 115 dBA. No theoretical work was carried out for this design and there has been little previous research on friction damping created by use of springs, although the internal damping of helical springs has been studied using hysteretic and viscous models [52]. A wire rope damper has also been used in vibration isolation [53].

1.4 THE EFFECTS OF CLADDING/DAMPING MATERIAL ON SOUND TRANSMISSION THROUGH PIPE WALLS.

Pipe systems in power stations are often covered with cladding which consists of absorbent or thermal protecting material for the purpose of both noise control and thermal protection.

Damping is normally created when cladding is clamped on a pipe system. For air-borne sound inside the pipe, the portion of the propagating sound energy, which is transmitted through the pipe wall, depends on the nature of the internal sound field, the acoustical properties of the internal and external fluids, the geometry of the pipe, and the acoustical and damping properties of the pipe material [54].

When added damping of the pipe system is large compared with radiation losses, structural damping will affect the acoustical transmission loss. Sound transmission loss can be expected to exhibit 3 dB decrease per doubling of structural loss factor according to Manning and the experimental data of others [55] [56]. Some other research also showed that the acoustical transmission loss below the ring frequency was unaffected by the change in loss factor [54].

A layer of porous material as wrapping is typically applied to noisy pipes and to the interior of aircraft fuselages to attenuate noise [57]. A porous material, when used as a sound-attenuating layer, attenuates a sound wave partly by acting as a reflecting surface (as does a solid wall), and partly by conversion of the acoustical energy that penetrates the material to heat by viscous losses in the interstices [58]. Most applications of wrappings or cladding consist of a porous layer and added metal plate to enhance the noise reduction [59].

Sound transmission into a thin cylindrical shell has been studied by many researchers. Much of the work involved study of sound transmission through cylindrical shells in the mass-law controlled region, the regions above the ring frequency and the critical frequency [60]. However, only very few studies have been carried out on noise reduction through double walled pipes or cylinders. Balena's studies [61] gave a double-wall fuselage design which provides a highly efficient treatment for reducing the transmission of propeller noise to the interior of propfan aircraft. A prediction method was given for noise reduction of single-walled and double-walled cylinders.

Acoustical transmission loss (TL) measurement is an important approach used to study the above problem. Fahy [62] in a recently published book "Sound Intensity" introduced a new technique for sound intensity measurement, fully describing the physical processes involved.

1.5 THE IMPORTANCE OF PREDICTING THE NATURAL FREQUENCIES OF A CIRCULAR CYLINDRICAL SHELL.

The type of pipe studied in this project belongs to a type of structure classified as a thin cylindrical shell, which is the kind of pipe used in most power stations. Free-free boundary conditions were used for convenience in the experimental work and it is therefore essential to be able to evaluate natural frequencies and mode shapes of a thin walled shell in these conditions. The Rayleigh-Ritz method or other approximate methods have been used in most previous studies. Few examples of calculations for the free-free pipe were found. Thus, there were few suitable data available for use in this study. The exact theory was found in reference [2], where an approximate solution was also deduced to compute natural frequencies for clamped end conditions and the Rayleigh-Ritz method was used for free-free end conditions of a thin-walled cylindrical shell.

1.6 THE OBJECTIVES OF THE INVESTIGATION.

1). Studies of a thin walled cylindrical shell, squeeze film damping-theory and associated experiments.

In the present research, a thin-walled isotropic, circular cylindrical shell is of interest. The primary objective is to produce the equations from the exact theory to predict the natural frequencies and mode shapes of a thin-walled pipe. The theory would then be a basis for further study of vibration of a double pipe system.

The vibration characteristics of thin-walled cylindrical shells are studied in chapter 2. Based on Flügge's differential operator, the exact solutions for natural frequencies and mode shapes of a thin-walled pipe with free-free, free-clamped and clamped-clamped boundary conditions have been derived in matrix form. The difference between the approach used here and previous work is that all the computed results are derived from exact theory and no approximate procedures have been applied. Computer programmes were developed to perform the numerical calculations. In a study of the natural frequency and mode shape data of thin-walled pipes with free-free boundary conditions, the Rayleigh and Love inextensional modes are discussed.

To increase damping of pipework, the principle of "air pumping" is adopted, for which a double pipe system is required. The double pipe system consists of two coaxial thin-walled pipes with air or oil in the gap between them.

From previous studies, it is understood that the mechanism of so called "squeeze film damping" is not so clear. For example, how do the mode shapes and vibration coupling of two plates affect the air pumping and system damping? The object of the present study was to develop theoretical models required to describe the phenomena of air or oil squeeze film damping in the double pipe system and to predict the damping level or loss factor in this system. Experimental work is obviously also required to substantiate the theory.

Based on the study of the thin cylindrical shell theory and investigation of the physical phenomenon of squeeze film damping between two parallel plates, the theory for predicting the loss factor of a double pipe system, which consists of two thin-walled cylindrical shells with an air filled annulus, has been developed in chapter 3. In this theory, the fluid-solid interaction is concerned. The velocity profile and stresses in the gas between the two pipes are derived. Then, the energy dissipated in the damping

system can be calculated. The principle of an optimum design for maximum damping is deduced from the theory.

Both "air pumping" and "oil pumping" have also been examined experimentally in a coaxial double pipe system in chapter 4. In the theory and experimental work, the effects of the squeezed fluid motion in in-phase and out-of-phase modes on the damping are discussed.

2). Friction damping.

Friction damping has been examined experimentally in chapter 5 though there was not the time to develop suitable theory within the scope of this project. Two kinds of additive damping devices were developed. Two damping approaches are

a. a pipe wrapped with coiled spring,

b. a pipe wrapped with wire rope.

Experiments have also been carried out to measure the loss factor of a pipe with constrained and unconstrained mineral wool laggings.

3). Sound transmission loss through a pipe wall.

Vibration damping has been studied by means of squeeze film damping and friction damping. Concerning the acoustical properties, can these added damping devices affect or control the acoustical radiation from pipes? An investigation has been carried out for a pipe with internal acoustical excitation. This is so called "air borne sound". Acoustical transmission loss may be obtained from the measured sound pressure inside a pipe and sound intensity outside the pipe. Investigations of acoustical transmission loss versus frequency were made for pipes in the following arrangements:

a. a plain pipe,
b. a double pipe system with an air or oil-filled annulus,
c. a pipe wrapped with coiled springs or wire ropes,
d. a industrial pipe with cladding which consists of mineral wool lagging and a steel sheet cover, as it would be useful to compare acoustical properties achieved by a double pipe system or a pipe with an added friction device to those of a practical pipe with cladding.

CHAPTER 2.
THE STUDY OF NATURAL FREQUENCIES AND MODE SHAPES OF THIN-WALLED ISOTROPIC, CIRCULAR CYLINDRICAL SHELLS.

2.1 INTRODUCTION.

To study natural frequencies and mode shapes of the thin-walled pipes, which are used in the experiments on added damping and acoustic radiation, equations for natural frequency and mode shape are derived in this chapter. The natural frequency and mode shape are important factors in the analysis of damping treatments and prediction of acoustic radiation from a pipe. The deduced equations of motion form the basis of the theory required to analyse a double pipe system, in which the mechanism of 'squeeze film' damping is employed.

Shell theories are usually classified into thick-walled and thin-walled circular cylindrical shell theories according to the ratio of radius to thickness of the shell. In thin shell theory, the radius to thickness ratio is greater than 20 while in thick shell theory the radius to thickness ratio is less than 20 and three dimensional elasticity theory is used. The following assumptions are made in the thin shell theory: the material is assumed to be linearly elastic, isotropic and homogeneous; displacements are assumed to be small, shear deformation and rotary inertia effects are neglected, and the thickness is taken to be constant. The deformation of a thin shell will be completely determined by the displacements of its middle surface.

In the present research, the difference from previous studies is that natural frequencies and mode shapes of a thin-walled pipe with various boundary conditions are computed directly from deduced exact theory and there is no approximate procedure applied during the computation.

2.1.1 Thin-Walled Circular Cylindrical Shell Theory.

Many studies in earlier work have summarised the basic theory. The standard or classical theories of thin shells are governed by eighth order systems of differential equations. The Donell-Mushtari theory [63] has been commonly used to model the vibrational behaviour of circular cylindrical shells. A "modifying" differential operator which alters the Donnell-Mushtari operator yields another shell theory. There are various modifying theories described by the differential operators. Many researchers have used the Flügge operator

[64]. Rayleigh and Love [65, 66] assumed that the bending rigidity of a shell is negligible at every point, thus the differential equation of motion can be reduced to fourth order. The natural frequency equation and mode shapes of a finite length of shell can be deduced by an exact theory which is based upon the assumption of functions in the solution which satisfy the boundary conditions. Another method is the Rayleigh-Ritz method or energy method which uses beam functions and equates the maximum strain energy stored in the undamped shell during vibration to the maximum kinetic energy.

The importance of studying the free-free pipe in damping studies has been stated earlier. Very few previous researches have concerned the free-free pipe though many references yield results for pipes with various end conditions. There was no direct equation or data available to meet the above requirements. To obtain solutions for natural frequencies, the Rayleigh-Ritz method or other approximate methods were applied in previous work. In this chapter, the equations of motion from exact theory are used to obtain solutions for natural frequencies and mode shapes, by use of Warburton's [2] method. The basic equation is then used later for describing structural vibration of pipes in the study of a double pipe system. Equations for natural frequencies and mode shapes are written in matrix form. No approximate procedure is applied in the theory. A "half interval search" method is employed for obtaining the roots of the natural frequency equation via computing with high resolution.

2.1.2 Mode Shapes and Rayleigh and Love's Inextensional Theory.

For studying the vibration characteristics of free-free shells, several parameters can be varied which are

(1) Number of axial waves, m.
(2) Number of circumferential waves, n.
(3) Thickness / radius ratio, β.
(4) Length / radius ratio.
(5) Material.

In an early study [65], Rayleigh studied the relationship between bending and stretching energy to describe the deformation and vibration of thin shells of revolution. The kinematics of deformation in this theory require that the middle surface of the shell deforms without stretching. Rayleigh claimed that, if the shell were sufficiently thin and vibrating in one of its lower modes, the middle surface behaves as if it is inextensible. Rayleigh applied the theory to the circular cylindrical shell; this theory consists of two sets of vibration modes for the shells. According to Rayleigh, the first set is characterized by displacements,

$$u = 0$$

$$v = C \sin n\theta \cos \omega t \tag{2.1}$$

$$w = C \cos n\theta \cos \omega t$$

where u,v,w are displacements in the longitudinal, tangential and radial directions (see figure 2.1), C is a constant, θ the angular co-ordinate and ω the natural circular frequency. These functions were assumed to be applicable to a long shell. Setting the maximum strain energy stored in a shell during vibration equal to the maximum kinetic energy, Rayleigh obtained

$$\Omega^2 = \beta \frac{n^2(n^2-1)^2}{n^2+1} \tag{2.2}$$

where Ω^2 is nondimensional frequency and β the ratio of thickness to radius. The expressions of Ω and β are

$\Omega = \rho R^2(1-\nu^2)\omega^2/E$,
$\beta = h / R$,
n = circumferential wave number,
E = Young's modulus,
ν = Poisson's ratio.

The second set, more applicable to shells of arbitrary length, assumed displacements of the following form:

$$u = \frac{R}{n} C \cos n\theta \cos \omega t$$

$$v = xC \sin n\theta \cos \omega t \tag{2.3}$$

$$w = nxC \cos n\theta \cos \omega t$$

where R is radius and x the length coordinate measured from the centre section of the shell. Using this set of mode shapes, Love [66] obtained the following natural frequency formula:

$$\Omega^2 = \beta \frac{n^2(n^2-1)^2}{n^2+1} \frac{1+24(1-\nu)R^2/n^2L^2}{1+12n^2L^2/n^2(n^2+1)L^2} \qquad (2.4)$$

where ν is Poisson's ratio, L the length of shell. When $L/R \rightarrow \infty$, equation (2.4) is equal to (2.2), so equation (2.4) is a modified form of (2.2). Rayleigh and Love mode shapes are shown in figure 2.2, which indicates the constant radial movement of the Rayleigh mode as in equation (2.1) and linear movement of the Love mode as in equation (2.3) at a circumferential mode. The first three circumferential modes are shown in figure 2.3.

2.2 EQUATIONS OF MOTION OF A THIN CIRCULAR CYLINDRICAL SHELL.

In the present study, a uniform thin cylindrical shell of length L, mean radius R and thickness h has been considered. The shell coordinates to be used are x and θ shown in figure 2.1. A point in the middle surface of the shell is defined by the axial co-ordinate x and angular co-ordinate θ. The components of displacement u,v, and w at any point (x,θ), are each function of x, θ and time t. The mode is defined by the number of circumferential waves (n) and the number of axial waves (m) or nodes, as shown in figure 2.3.

The equations of motion for thin circular cylindrical shells can be written in matrix form as

$$[D]\{u_i\} = \{0\} \qquad (2.5)$$

where $\{u_i\}$ is the displacement vector,

$$\{u_i\} = \begin{Bmatrix} u \\ v \\ w \end{Bmatrix} \qquad (2.6)$$

u,v, and w are the components of displacement in the axial, tangential and radial directions, respectively.

Solutions are assumed to be of the form

$$u = U_0 \cos n\theta \exp(\alpha x/R) \cos \omega t$$

$$v = V_0 \sin n\theta \exp(\alpha x/R) \cos \omega t \qquad (2.7)$$

$$w = W_0 \cos n\theta \exp(\alpha x/R) \cos \omega t$$

where ω is the circular frequency, U_0, V_0, W_0 the amplitudes of u,v, and w and α is the frequency function coefficient. [**D**] is a matrix differential operator which can be treated as the sum of two operators;

$$[\,\mathbf{D}\,] = [\,\mathbf{D}_{d\text{-}m}\,] + \beta[\,\mathbf{D}_{mod}] \qquad (2.8)$$

where $[\,\mathbf{D}_{d\text{-}m}\,]$ is the differential operator according to the Donnell-Mushtari theory [2], $[\mathbf{D}_{mod}]$ a "modifying" operator which alters the D-M operator to yield another shell theory, and β the nondimensional thickness parameter defined by

$$\beta = h^2 / 12\,R^2 \qquad (2.9)$$

β is normally very small for a thin shell. For the various shell theories the modifying operators are simple in some cases and complicated in others. Here the Flügge-Byrne-Lurye operator is used according to Warburton's shell theory. The differential operators $[\mathbf{D}_{d\text{-}m}]$ and $[\mathbf{D}_{mod}]$ are

$$[\,\mathbf{D}_{d\text{-}m}\,] = \begin{bmatrix} \left[R^2\frac{\partial^2}{\partial x^2}+\frac{(1-\nu)}{2}\frac{\partial^2}{\partial\theta^2}-\Omega^2\frac{\partial^2}{\partial t^2}\right] & R\frac{(1+n)}{2}\frac{\partial^2}{\partial x\partial\theta} & R\nu\frac{\partial}{\partial x} \\ R\frac{(1+\nu)}{2}\frac{\partial^2}{\partial x\partial\theta} & \left[\frac{(1-\nu)}{2}R^2\frac{\partial^2}{\partial x^2}+\frac{\partial^2}{\partial\theta^2}-\Omega^2\frac{\partial^2}{\partial\theta^2}\right] & \frac{\partial}{\partial\theta} \\ R\nu\frac{\partial}{\partial x} & \frac{\partial}{\partial\theta} & \left[1+\beta\nabla^4+\Omega^2\frac{\partial^2}{\partial t^2}\right] \end{bmatrix}$$

(2.10)

where $\nabla^4 = \nabla^2\nabla^2$, $\nabla^2 = R^2\frac{\partial^2}{\partial x^2} + \frac{\partial^2}{\partial\theta^2}$, $\Omega^2 = \rho R^2(1-\nu^2)\omega^2/E$, E is Young's modulus, ν the Poisson's ratio, ρ the density of material,

$$[\mathbf{D}_{mod}] = \begin{bmatrix} \left[\frac{(1-\nu)}{2}\frac{\partial^2}{\partial\theta^2}\right] & 0 & -R^3\frac{\partial^3}{\partial x^3}+\frac{(1-\nu)}{2}R\frac{\partial^3}{\partial x\partial\theta^2} \\ 0 & \frac{3}{2}R^2(1-\nu)\frac{\partial^2}{\partial x^2} & -\frac{(3-\nu)}{2}R^2\frac{\partial^3}{\partial x^2\partial\theta}+\frac{\partial^2}{\partial\theta^2} \\ -R^3\frac{\partial^3}{\partial x^3}+\frac{(1-\nu)}{2}R\frac{\partial^2}{\partial\theta^2} & -\frac{(3-\nu)}{2}R^2\frac{\partial^3}{\partial x^2\partial\theta} & 1+2\frac{\partial^2}{\partial\theta^2} \end{bmatrix} \tag{2.11}$$

equation (2.5) becomes

$$[\mathbf{D}_{d\text{-}m}]\{u_i\} + \beta[\mathbf{D}_{mod}]\{u_i\} = 0. \tag{2.12}$$

The three equations of motion become

$$\begin{bmatrix} \alpha^2-0.5(1+\nu)(1+\beta)n^2+\Omega^2 & 0.5(1+\nu)n\alpha & -\beta\alpha^3+[\nu-0.5(1-\nu)n^2\beta]\alpha \\ -0.5(1+\nu)n\alpha & 0.5(1-\nu)(1+3\beta)\alpha^2-n^2+\Omega^2 & 0.5(3-\nu)\beta n\alpha^2-n \\ -\beta\alpha^3+[\nu-0.5(1-\nu)\beta n^2]\alpha & -0.5(3-\nu)\beta n\alpha^2+\nu & \beta\alpha^4-2\beta n^2\alpha^2+1+\beta(1-2n^2)-\Omega^2+\beta n^4 \end{bmatrix} \begin{Bmatrix} U_0 \\ V_0 \\ W_0 \end{Bmatrix} = 0 \tag{2.13}$$

or

$$\begin{bmatrix} a_{11} & a_{12} & a_{13} \\ a_{21} & a_{22} & a_{23} \\ a_{31} & a_{32} & a_{33} \end{bmatrix} \begin{Bmatrix} U_0 \\ V_0 \\ W_0 \end{Bmatrix} = 0 \tag{2.14}$$

For free vibration and free-free boundary conditions

$$\begin{Bmatrix} U_0 \\ V_0 \\ W_0 \end{Bmatrix} \neq \begin{Bmatrix} 0 \\ 0 \\ 0 \end{Bmatrix}$$

so that

$$\begin{vmatrix} a_{11} & a_{12} & a_{13} \\ a_{21} & a_{22} & a_{23} \\ a_{31} & a_{32} & a_{33} \end{vmatrix} = 0 \qquad (2.15)$$

where $a_{i,j}$ is shown in appendix 2.

This is the characteristic determinant or characteristic equation. Eigenvalues are the roots of the corresponding equation (2.15). By developing equation (2.15), a polynomial of eighth degree in α, the characteristic polynomial, is obtained. That is

$$A_1\alpha^8 + A_2\alpha^6 + A_3\alpha^4 + A_4\alpha^2 + A_5 = 0 \qquad (2.16)$$

where

$$A_1 = 0.5\beta(1-\nu)(1+3\beta)(1-\beta)$$

$$A_2 = \beta(\Omega^2-n^2)(1-\beta)+0.25\beta(1-\nu)(1+3\beta)[4(\nu-n^2)-(1-\nu)(1+3\beta)n^2+2\Omega^2] +[0.5\beta n(3-\nu)]^2-0.25\beta^2\nu^2(1-\nu)(3-\nu)+0.25\beta n^2(1+\nu)^2$$

$$A_3 = 2\beta(\Omega^2-n^2)[\nu-0.5\beta n^2(1-\nu)-n^2]+0.5(1-\nu)(1+3\beta)\{[1+\beta(n^2-1)-\Omega^2]-[\nu-0.5\beta n^2 (1-\nu)]^2\}+0.5\beta n^2(1+\nu)[2+(3-\nu)(\nu-0.5\beta n^2)]-0.5\beta^2 n^4(1+\nu)^2-\beta n^2(3-\nu)-[0.5 n^2(1-\nu)(1+\beta)-\Omega^2][(\Omega^2-n^2)\beta-(1-\nu)(1+3\beta)\beta n^2+0.25(\beta n)^2(3-\nu)^2]$$

$$A_4 =[0.5n^2(1-\nu)(1+\beta)-\Omega^2]\{2\beta n^2(\Omega^2-n^2)-0.5(1-\nu)(1+3\beta)[1+\beta(n^2-1)^2-\Omega^2] +(3-\nu)\beta n^2\}-0.5n^2(1+\nu)\{\nu-0.5\beta n^2(1-\nu)-0.5(1+\nu)[1+\beta(n^2-1)^2-\Omega^2]\} -[\nu-0.5n^2(1-\nu)]\{0.5n^2(1+\nu)+(\Omega^2-n^2)[\nu-0.5\beta n^2(1-\nu)]\}+(\Omega^2-n^2) [1+\beta(n^2-1)^2-\Omega^2]+n^2$$

$$A_5 = -[0.5n^2(1-\nu)(1+\beta)+\Omega^2]\{(\Omega^2-n^2)[1+\beta(n^2-1)^2-\Omega^2]+n^2\}$$

For the real values of A_i (i=1,2...5) equation (2.16) has two real roots, one positive and one negative, two imaginary roots and four complex roots, according to reference [2]. That is

$$\alpha_r = \pm\alpha_1, \pm j\alpha_2, \pm\alpha_3 \pm j\alpha_4$$

where $j^2 = -1$.

Thus the complete solution for the radial component of displacement is

$$w = W(x)\ (\cos n\theta \cos \omega t)$$

with

$$W(x) = \sum_{r=1}^{8} B_r \exp(\alpha_r x/R) \tag{2.17}$$

where B_r (r=1, 2 ... 8) is a constant.

Equation (2.14) is then rewritten in the following form

$$\begin{bmatrix} a_{11} & a_{12} \\ a_{21} & a_{22} \end{bmatrix} \begin{Bmatrix} U_0/W_0 \\ V_0/W_0 \end{Bmatrix} = - \begin{bmatrix} a_{13} \\ a_{23} \end{bmatrix} \tag{2.18}$$

where

$$U_0/W_0 = - \begin{vmatrix} a_{13} & a_{12} \\ a_{23} & a_{22} \end{vmatrix} / \begin{vmatrix} a_{11} & a_{12} \\ a_{21} & a_{22} \end{vmatrix}$$

$$= \frac{a_{12}a_{23} - a_{13}a_{22}}{a_{11}a_{22} - a_{12}a_{21}}$$

and

$$V_0/W_0 = - \begin{vmatrix} a_{11} & a_{13} \\ a_{21} & a_{23} \end{vmatrix} / \begin{vmatrix} a_{11} & a_{12} \\ a_{21} & a_{22} \end{vmatrix}$$

$$= \frac{a_{13}a_{21} - a_{11}a_{23}}{a_{11}a_{22} - a_{12}a_{21}}$$

equation (2.7) becomes

$$\begin{Bmatrix} u \\ v \\ w \end{Bmatrix} = \sum_{r=1}^{8} B_r \begin{Bmatrix} U_0/W_0 \\ V_0/W_0 \\ 1 \end{Bmatrix} \exp(\alpha_r x/R) \begin{Bmatrix} \cos n\theta \\ \sin n\theta \\ \cos n\theta \end{Bmatrix} \cos \omega t \tag{2.19}$$

If the definitions are made as

$K_1 = U_0/W_0$ and	$K_2 = V_0/W_0$	when	$\alpha_r = \alpha_1$
$-K_1 = U_0/W_0$	$K_2 = V_0/W_0$		$\alpha_r = -\alpha_1$
$K_3 = U_0/W_0$	$K_4 = V_0/W_0$		$\alpha_r = j\alpha_2$
$-K_3 = U_0/W_0$	$K_4 = V_0/W_0$		$\alpha_r = -j\alpha_2$
$K_5 + K_6 = U_0/W_0$	$K_7 + jK_8 = V_0/W_0$		$\alpha_r = \alpha_3 + j\alpha_4$
$K_5 - K_6 = U_0/W_0$	$K_7 - jK_8 = V_0/W_0$		$\alpha_r = \alpha_3 - j\alpha_4$
$-K_5 - K_6 = U_0/W_0$	$K_7 + jK_8 = V_0/W_0$		$\alpha_r = -\alpha_3 - j\alpha_4$
$-K_5 + K_6 = U_0/W_0$	$K_7 - jK_8 = V_0/W_0$		$\alpha_r = -\alpha_3 + j\alpha_4$

(2.20)

Using (2.19) and (2.16), equation (2.17) can be rewritten in another form, after some manipulation, as

$$U(x) = C_2K_1\cosh \alpha_1x/R + C_1K_1\sinh \alpha_1x/R + C_4K_3\cos \alpha_2x/R - C_3K_3\sin \alpha_2x/R + \cos \alpha_4x/R[(C_6K_5+C_7K_6)\cosh \alpha_3x/R + (C_5K_5+C_8K_6)\sinh \alpha_3x/R)] + \sin \alpha_4x/R[(C_8K_5-C_5K_6)\cosh \alpha_3x/R + (C_7K_5-C_6K_6)\sinh \alpha_3x/R)] \quad (2.21a)$$

$$V(x) = C_1K_2\cosh \alpha_1x/R + C_2K_2\sinh \alpha_1x/R + C_3K_4\cos \alpha_2x/R - C_4K_4\sin \alpha_2x/R + \cos \alpha_4x/R[(C_5K_7+C_8K_8)\cosh \alpha_3x/R + (C_6K_7+C_7K_8)\sinh \alpha_3x/R)] + \sin \alpha_4x/R[(C_7K_7-C_6K_8)\cosh \alpha_3x/R + (C_8K_7-C_5K_8)\sinh \alpha_3x/R)] \quad (2.21b)$$

$$W(x) = C_1\cosh \alpha_1x/R + C_2\sinh \alpha_1x/R + C_3\cos \alpha_2x/R + C_4K_3\sin \alpha_2x/R + \cos \alpha_4x/R(C_5\cosh \alpha_3x/R + C_6\sinh \alpha_3x/R) + \sin \alpha_4x/R(C_7\cosh \alpha_3x/R + C_8\sinh \alpha_3x/R) \quad (2.21c)$$

C_i $(i=1,2 \cdots 8)$ = constant

or written in a matrix form

$$\begin{Bmatrix} U(x) \\ V(x) \\ W(x) \end{Bmatrix} = \begin{bmatrix} A_{11} & A_{12} & \cdots & A_{18} \\ A_{21} & A_{22} & \cdots & A_{28} \\ A_{31} & A_{32} & \cdots & A_{38} \end{bmatrix} \begin{Bmatrix} C_1 \\ C_2 \\ \cdot \\ \cdot \\ \cdot \\ C_8 \end{Bmatrix} \quad (2.22)$$

where $A_{i,j}$ is written in appendix 2. All deductions of equation (2.21) are also shown in appendix 2.

Equation (2.22) is the solution of the equation of motion for a thin circular cylindrical shell, the constant C_i is determined by the boundary conditions of the shell.

2.3 NATURAL FREQUENCIES OF A THIN CYLINDRICAL SHELL WITH VARIOUS BOUNDARY CONDITIONS.

2.3.1 Boundary Conditions.

According to Flügge's theory [1], free boundary conditions in terms of displacement are

axial force $N_x = 0$;
axial moment $M_x = 0$;
shear force $N_{x\theta} = 0$;
Kirchhoff force $S_x = 0$.

So they are,

$$\partial u/\partial x + v/R\,(\partial v/\partial\theta - w) + \beta R\partial^2 w/\partial x^2 = 0 \qquad (2.23\ a)$$

$$\partial^2 w/\partial x^2 + v/R\,(\partial v/\partial\theta + \partial^2 w/\partial\theta^2) + 1/R\ \partial u/\partial x = 0 \qquad (2.23\ b)$$

$$1/R\ \partial u/\partial\theta + \partial v/\partial x + b(\partial v/\partial x + \partial^2 w/\partial x\partial\theta) = 0 \qquad (2.23\ c)$$

$$\partial^3 w/\partial x^3 + 1/R\ \partial^2 u/\partial x^2 + (3 - v)/2R^2\ \partial^2 v/\partial x\partial\theta + (2 - v)/R^2$$
$$\partial^3 w/\partial x\partial\theta^2 - (1 - v)/2R^3\ \partial^2 u/\partial\theta^2 = 0 \qquad (2.23\ d)$$

The clamped conditions are

$$u = 0 \qquad (2.24\ a)$$

$$v = 0 \qquad (2.24\ b)$$

$$w = 0 \qquad (2.24\ c)$$

$$\partial w/\partial x = 0 \qquad (2.24\ d)$$

2.3.2 Equations for Natural Frequencies with Free-free Boundary Conditions.

There are four mathematical expressions to indicate the boundary condition at each of the two ends of a cylindrical shell, x = - L/2 and x = L/2. Substituting free-free boundary conditions into equation (2.22) leads to an eighth order matrix;

$$[B_{ij}]\{C_j\} = \{0\} \tag{2.25}$$

$$i = 1, 2 \ldots 8 \quad , \quad j = 1, 2 \ldots 8$$

because matrix $\{C_j\} \neq \{0\}$, then

$$|B_{ij}| = 0 \tag{2.26}$$

For a cylindrical shell of length L, the only unknown is the frequency ω or non-dimensional frequency Ω; equation (2.26) is the frequency equation, where operator $B_{i,j}$ is given in appendix 2.

By taking the origin of x in the middle section of the cylinder, symmetrical and antisymmetrical characteristics are used in the determinant. The boundaries are at x=-L/2 and x=L/2. Substituting x=-L/2, L/2 for x=0, L in the determinant of equation (2.26) by using

$$\begin{aligned} \cos x &= \cos(-x) \quad , \quad \cosh x = \cosh(-x) \\ \sin x &= -\sin(-x) \quad , \quad \sinh x = -\sinh(-x) \end{aligned} \tag{2.27}$$

A following relation is found as;

$B_{11}=B_{21}$, $B_{12}=-B_{22}$, $B_{13}=B_{23}$, $B_{14}=-B_{24}$ ... and etc.

Equation (2.26) is rewritten at x=-L/2 and x=L/2 as

$$\begin{vmatrix} B_{11} & B_{12} & B_{13} & B_{14} & B_{15} & B_{16} & B_{17} & B_{18} \\ B_{11} & -B_{12} & B_{13} & -B_{14} & B_{15} & -B_{16} & -B_{17} & B_{18} \\ B_{31} & B_{32} & . & . & . & . & . & . \\ B_{31} & -B_{32} & . & . & . & . & . & . \\ \cdots & & & & & & & \end{vmatrix} = 0$$

and via this rearrangement, we obtain the determinant for the symmetrical or even modes and antisymmetrical or odd modes as

$$\left|\begin{array}{cc|c} B_{11} & B_{13} & B_{15} & B_{18} \\ B_{31} & B_{33} & B_{35} & B_{38} \\ B_{51} & B_{53} & B_{55} & B_{58} \\ B_{71} & B_{73} & B_{75} & B_{78} \\ \hline & 0 & & \end{array}\right| \quad \left|\begin{array}{c} 0 \\ \hline B_{12} \; B_{14} \; B_{16} \; B_{17} \\ B_{32} \; B_{34} \; B_{36} \; B_{37} \\ B_{52} \; B_{54} \; B_{56} \; B_{57} \\ B_{72} \; B_{74} \; B_{76} \; B_{77} \end{array}\right| = 0 \qquad (2.28)$$

That is

$$\left|\begin{array}{c|c} \text{Symmetrical mode} & \\ \hline & \text{Anti-symmetrical mode} \end{array}\right| = 0$$

2.3.3 Equations for Natural Frequencies with Clamped-clamped Boundary Conditions.

Substituting clamped-clamped boundary conditions for equation (2.22), equation (2.26) becomes

$$\begin{vmatrix} B_{11} & B_{13} & B_{15} & B_{18} & & & & \\ B_{21} & B_{23} & B_{25} & B_{28} & & 0 & & \\ B_{31} & B_{33} & B_{35} & B_{38} & & & & \\ B_{41} & B_{43} & B_{45} & B_{48} & & & & \\ & & & & B_{12} & B_{14} & B_{16} & B_{17} \\ & 0 & & & B_{22} & B_{24} & B_{26} & B_{27} \\ & & & & B_{32} & B_{34} & B_{36} & B_{37} \\ & & & & B_{42} & B_{44} & B_{46} & B_{47} \end{vmatrix} = 0 \qquad (2.29)$$

where $B_{i,j}$ clamped-clamped condition is in appendix 2.

2.3.4 Equation for Natural Frequencies with Clamped-Free Boundary Conditions.

Substituting clamped-free boundary conditions into equation (2.22) with x = - L/2 and x = L/2, The natural frequency equation is

$$| D_{ij} | = 0 \qquad (2.30)$$

where

$D_{ij} = B_{ij}$ of (2.29) when i = 1, 2, 3, 4 , j = 1, 2, 3, ...8

when i > 4, expression of $D_{i,j}$ is stated in appendix 2.

2.4 MODE SHAPES OF THE CYLINDRICAL SHELLS.

2.4.1 Free-Free Ends.

The shapes of the symmetrical and antisymmetrical modes are studied separately. For the symmetrical modes of equation (2.28), there is a matrix similar to equation (2.25), as follows

$$\begin{bmatrix} B_{11} & B_{13} & B_{15} & B_{18} \\ B_{31} & B_{33} & B_{35} & B_{38} \\ B_{51} & B_{53} & B_{55} & B_{58} \\ B_{71} & B_{73} & B_{75} & B_{78} \end{bmatrix} \begin{Bmatrix} C_1 \\ C_3 \\ C_5 \\ C_8 \end{Bmatrix} = 0 \tag{2.31}$$

Let $C_8 = 1$, then equation (2.31) can be written as

$$\begin{bmatrix} B_{11} & B_{13} & B_{15} \\ B_{31} & B_{33} & B_{35} \\ B_{51} & B_{53} & B_{55} \end{bmatrix} \begin{Bmatrix} C_1 \\ C_3 \\ C_5 \end{Bmatrix} = - \begin{bmatrix} B_{18} \\ B_{38} \\ B_{58} \end{bmatrix} \tag{2.32}$$

Solving for C_1, C_3, C_5, gives

$$C_1 = \frac{\begin{vmatrix} -B_{18} & B_{13} & B_{15} \\ -B_{38} & B_{33} & B_{35} \\ -B_{58} & B_{53} & B_{55} \end{vmatrix}}{\begin{vmatrix} B_{11} & B_{13} & B_{15} \\ B_{31} & B_{33} & B_{35} \\ B_{51} & B_{53} & B_{55} \end{vmatrix}} \quad , \quad \text{and so on.}$$

Then use the same method to obtain C_3, C_5 and the antisymmetric modes. Therefore, the equations of motion can be written as the following forms

SYMMETRIC MODES

$$\begin{Bmatrix} U(x) \\ V(x) \\ W(x) \end{Bmatrix} = \begin{bmatrix} A_{11} & A_{13} & A_{15} & A_{18} \\ A_{21} & A_{23} & A_{25} & A_{28} \\ A_{31} & A_{33} & A_{35} & A_{38} \end{bmatrix} \begin{Bmatrix} C_1 \\ C_3 \\ C_5 \\ 1 \end{Bmatrix} \tag{2.33}$$

ANTISYMMETRIC MODES

$$\begin{Bmatrix} U(x) \\ V(x) \\ W(x) \end{Bmatrix} = \begin{bmatrix} A_{12} & A_{14} & A_{16} & A_{17} \\ A_{22} & A_{24} & A_{26} & A_{27} \\ A_{32} & A_{34} & A_{36} & A_{37} \end{bmatrix} \begin{Bmatrix} C_2 \\ C_4 \\ C_6 \\ 1 \end{Bmatrix} \tag{2.34}$$

Using equations ($2.23_{a\text{-}d}$), (2.25) and (2.28), equations in N_x, M_x, $N_{x\theta}$ and S_x can be written directly,

SYMMETRIC MODES

$$\begin{Bmatrix} N_x \\ M_x \\ N_{x\theta} \\ S_x \end{Bmatrix} = \begin{bmatrix} B_{11} & B_{13} & B_{15} & B_{18} \\ B_{31} & B_{33} & B_{35} & B_{38} \\ B_{51} & B_{53} & B_{55} & B_{58} \\ B_{71} & B_{73} & B_{75} & B_{78} \end{bmatrix} \begin{Bmatrix} C_1 \\ C_3 \\ C_5 \\ C_8 \end{Bmatrix} \tag{2.35}$$

ANTISYMMETRIC MODES

$$\begin{Bmatrix} N_x \\ M_x \\ N_{x\theta} \\ S_x \end{Bmatrix} = \begin{bmatrix} B_{12} & B_{14} & B_{16} & B_{17} \\ B_{32} & B_{34} & B_{36} & B_{37} \\ B_{52} & B_{54} & B_{56} & B_{57} \\ B_{72} & B_{74} & B_{76} & B_{77} \end{bmatrix} \begin{Bmatrix} C_2 \\ C_4 \\ C_6 \\ C_7 \end{Bmatrix} \tag{2.36}$$

2.4.2 Clamped-Clamped Ends.

The same procedure described in 2.4.1 is used for calculating the mode shapes with clamped-clamped boundary conditions. Again, for symmetrical form, using the equation (2.29), there is an equation which satisfies clamped-clamped boundaries as

$$\begin{bmatrix} B_{11} & B_{13} & B_{15} & B_{18} \\ B_{21} & B_{23} & B_{25} & B_{28} \\ B_{31} & B_{33} & B_{35} & B_{38} \\ B_{41} & B_{43} & B_{45} & B_{48} \end{bmatrix} \begin{bmatrix} C_1 \\ C_2 \\ C_3 \\ C_4 \end{bmatrix} = 0 \tag{2.37}$$

Let $C_8 = 1$, then equation (2.35) can be written as

$$\begin{bmatrix} B_{11} & B_{13} & B_{15} \\ B_{21} & B_{23} & B_{25} \\ B_{31} & B_{33} & B_{35} \end{bmatrix} \begin{bmatrix} C_1 \\ C_2 \\ C_3 \end{bmatrix} = - \begin{bmatrix} B_{18} \\ B_{28} \\ B_{38} \end{bmatrix} \tag{2.38}$$

Solving for C_1, C_2, C_3 gives

$$C_1 = \frac{\begin{vmatrix} -B_{18} & B_{13} & B_{15} \\ -B_{28} & B_{23} & B_{25} \\ -B_{38} & B_{33} & B_{35} \end{vmatrix}}{\begin{vmatrix} B_{11} & B_{13} & B_{15} \\ B_{21} & B_{23} & B_{25} \\ B_{31} & B_{33} & B_{35} \end{vmatrix}} \quad , \quad \text{and so on.}$$

Then using equations (2.33) and (2.34), equations of the antisymmetrical mode shapes can be obtained.

2.4.3 Clamped-Free Ends.

The equation of motion for a shell with clamped-free ends is

$$[D_{ij}] \{C_i\} = 0 \tag{2.39}$$

$i = 1, 2, ...8 \quad , \quad j = 1, 2, ...8$

Let $C_8 = 1$, then equation (2.37) can be written as

$$[D_{i-1,j-1}] \{C_{i-1}\} = - [D_{i-1,8}] \tag{2.40}$$

Solving for C_{i-1},

$$C_{i-1} = \frac{|D_k|}{|D|} \tag{2.41}$$

where $|D_k|$ is the determinant obtained from $|D|$ by replacing the k^{th} column with the column having elements of $- D_{i-1,8}$.

Then the mode shapes are

$$\begin{Bmatrix} U(x) \\ V(x) \\ W(x) \end{Bmatrix} = [A_{ij}] \{C_j\} \tag{2.42}$$

2.5 NUMERICAL RESULTS

To examine the theory derived above, the natural frequencies and the mode shapes of an aluminium alloy cylindrical shell, under free-free, free-clamped and clamped-clamped boundary conditions, were calculated. To compare with published experimental and numerical results, the data and dimensions used were as follows:

Young's modulus $E = 68.9 \times 10^9$ N/m^2
Density of material $\rho = 2720$ kg/m^3
Poisson's ratio $\nu = 0.3$

		Clamped-Clamped	Clamped-Free	Free-Free
Length	L (mm)	610.7	625.3	637.4
Radius	R (mm)	242.4	242.4	242.4
Thickness	h (mm)	0.648	0.648	0.648

2.5.1. Natural Frequencies and Mode Shapes.

To evaluate the theory, the data given above were used for computing natural frequencies and mode shapes of a thin-walled pipe. Then comparisons were made between theory and published experimental results. Further evaluations and comparisons are made in the following chapters.

Table 2.1 shows the natural frequencies of the first four axial wave numbers for various circumferential wave numbers n with free-free boundary conditions.

Figure 2.4 shows the comparison of theoretical results for natural frequencies of free-free modes to experimental data from reference [67], where the data were results from experiments and numerical results from approximate theory. Comparing the theoretical natural frequencies of the first three axial modes (m =1, 2 and 3) with data from reference [67] in figure 2.4, it is found that curves for theoretical results from this work and reference data agree quite well. The interesting phenomenon is that the axial mode numbers are different in the theoretical results and reference data although their curves of frequencies versus circumferential wave number are similar. It is found that theoretically predicted natural frequencies in the axial wave mode m =1 coincide with the frequencies of Rayleigh and Love modes which were believed to be lower than that of the mode with m =1, according to some previous work. In figure 2.4, theoretical frequencies in mode m = 2

coincide with that of published data with m = 1, theoretical frequencies in wave mode m = 3 coincide with that of published data with m = 2, and so on. To verify the mode shapes in the present theory, mode shapes at relevant frequencies have been computed.

The mode shapes for the first three axial waves are given in figures 2.5, 2.6 and 2.7. By studying the mode shapes of figure 2.5 - 2.7, it can be seen that radial displacement in a vibrating shell is the largest compared with tangential and axial motions, so that radial displacement predominantly governs shell vibration. The radial displacement mode is similar to that of a beam in bending.

The natural frequencies and mode shapes with free-clamped and clamped-clamped boundary conditions are also given in figures 2.8 and 2.9. The first three axial mode shapes at relevant frequencies are shown in figures 2.10 to 2.15.

2.5.2. Further Study of Rayleigh and Love's Inextensional Theory.

Frequencies of Rayleigh and Love modes have been calculated by use of equations (2.2) and (2.4), and compared with theoretical results, which are shown in table 2.2. Similar results are found as stated above that theoretically predicted natural frequencies in the first axial wave mode m =1 coincide with the frequencies of Rayleigh and Love modes. Further comparisons are given in figure 2.16, where theoretical natural frequencies and frequencies of Rayleigh and Love modes are computed versus ratio of length to mean radius of pipe. Comparisons are made between natural frequencies of the first axial mode (m = 1) with two circumferential modes (n = 2, 3) and the frequencies of Rayleigh or Love modes. It is found from these figures that coincidences of frequencies of the first axial mode with those of Rayleigh and Love modes could occur only if the ratio of length to mean radius of pipe is very large.

It may be concluded that Rayleigh and Love modes may be simply and quickly estimated for a free-free shell but they may not be independent modes compared with the first axial mode (m=1).

An assumption may be made that when the length of a shell is large enough, the first axial wave mode becomes the Rayleigh mode approximately, in which the dynamic displacement is essentially parallel movement. When the length is short enough, the differential equation of motion may not be satisfied and the Love mode may be a modified mode in which the behaviour is similar to that of a ring in rigid movement. So that the Rayleigh or Love mode might be treated as a special case of the first axial wave mode but not an independent mode.

2.6 CONCLUSIONS.

(1) The exact theory of circular, cylindrical, thin-walled shells gives the natural frequencies and mode shapes of symmetrical and antisymmetical modes in matrix form. The results agree quite well with published data. Results for natural frequencies and mode shapes with free-free, clamped-clamped and clamped-free boundaries have been presented.

(2) Examination of the numerical results suggest that Rayleigh and Love modes might not be independent modes. They could be considered as a special case of the first axial wave mode of shell vibration when the shell is either very long or very short.

Table 2.1 Numerical result of natural frequencies of a free-free cylindrical shell. Material is aluminum; length = 637.4 mm, mean radius = 242.4 mm, thickness = 0.648 mm.

Frequency (Hz)	m=1	m=2	m=3	m=4
n=2		1176.40	2052.40	2645.60
3		730.71	1143.30	2057.30
4	37.08	490.76	1048.20	1599.20
5	62.58	352.08	787.88	1259.70
6	92.66	273.12	613.63	1011.60
7	127.50	235.98	498.16	830.28
8	167.68	231.44	426.82	702.67
9	213.19	251.38	391.56	615.76
10	263.23	288.28	386.59	564.36
11	320.27	336.87	406.07	543.94
12	381.84	394.16	444.24	550.11
13	448.76	458.59	496.40	578.22
14	521.04	529.35	559.29	623.81
15	598.66	606.02	630.83	683.19
16	681.63	679.78	709.76	753.62

Table 2.2 Comparison of frequencies of Rayleigh and Love modes and natural frequencies of a cylindrical shell with first axial wave mode (m=1). All frequencies are computed with various circumferential wave modes.

Material is aluminum; length = 637.4 mm, mean radius = 242.4 mm, thickness = 0.648 mm.

n = circumferential wave mode, $f_{Rayleigh}$ = frequency of Rayleigh mode, f_{Love} = frequency of Love mode, $f_{m=1}$ = frequency of first axial mode.

n	$f_{Rayleigh}$(Hz)	f_{Love}(Hz)	$f_{m=1}$(Hz)	Difference % ($\lvert f_{Ray.}-f_{m=1}\rvert/f_{Ray.}$)
1				
2	2.42	3.58		
3	20.51	25.31		
4	39.32	45.00	37.08	6.00
5	63.58	69.57	62.58	1.60
6	93.28	99.45	92.66	0.66
7	128.38	134.65	127.50	0.69
8	168.90	175.24	167.68	0.72
9	214.80	221.19	213.19	0.75
10	266.15	272.57	263.23	1.10
11	322.89	329.34	320.27	0.81
12	385.02	391.48	381.84	0.83
13	452.57	459.05	448.76	0.84
14	525.50	531.99	521.04	0.85
15	603.87	610.37	598.66	0.86
16	687.62	694.13	681.63	0.87

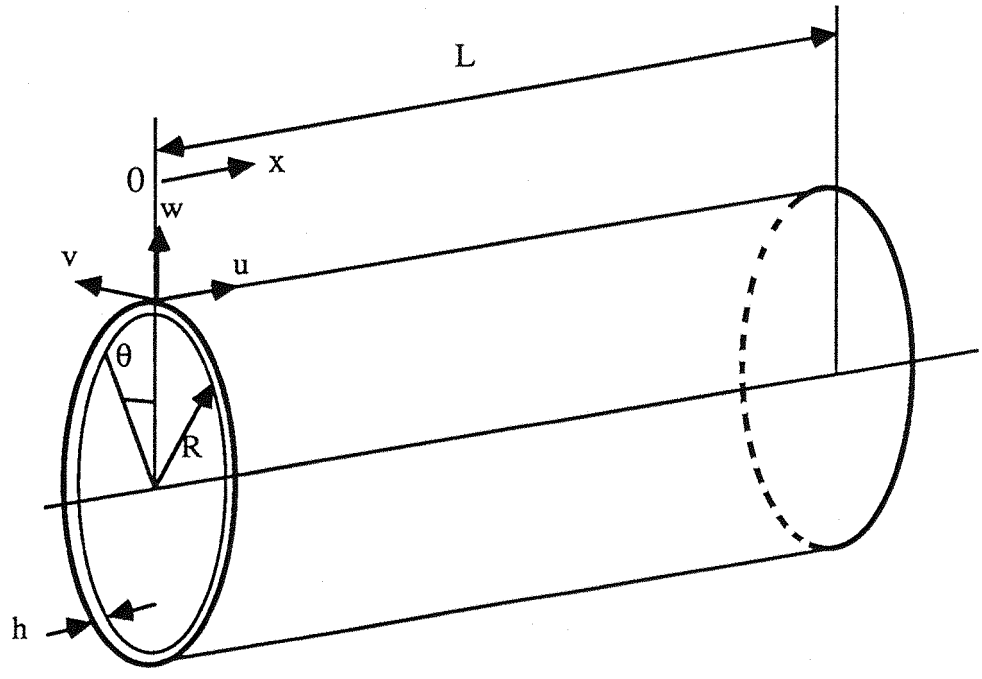

Figure 2.1 Circular cylindrical shell and coordinate system.

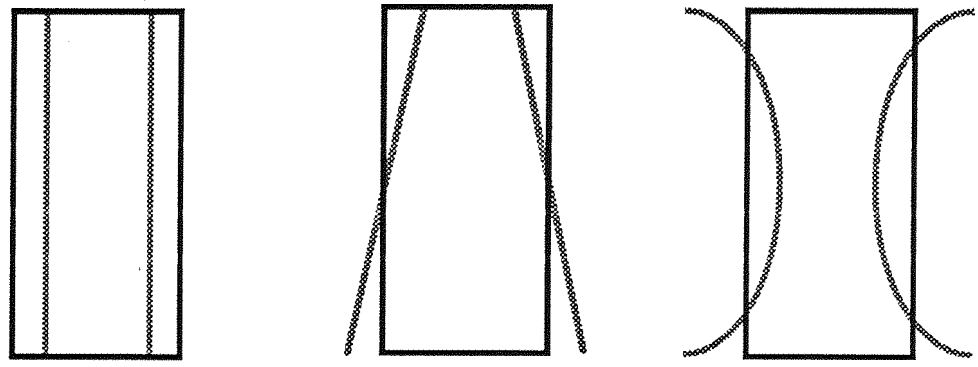

Figure 2.2 Rayleigh, Love mode shapes and the first axial mode shape of a free-free circular cylindrical shell.

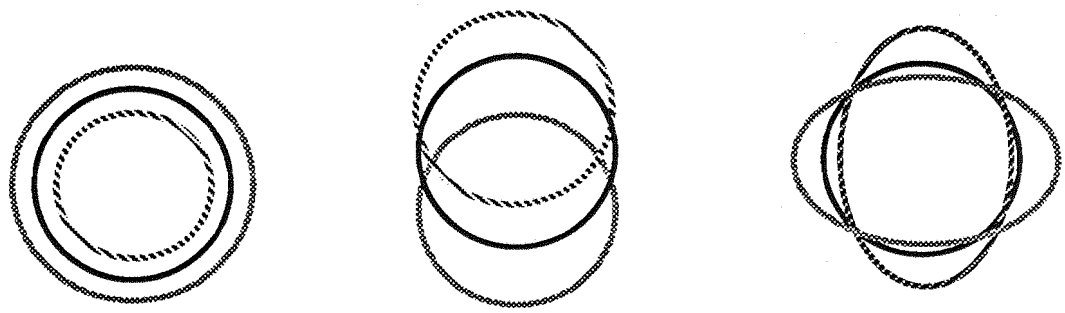

n = 0 n = 1 n = 2

CIRCUMFERENTIAL MODE SHAPES

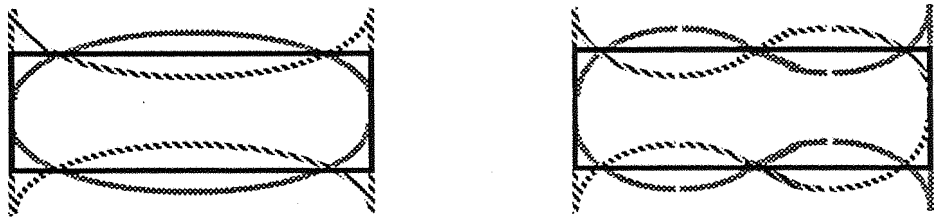

m = 1 m = 2

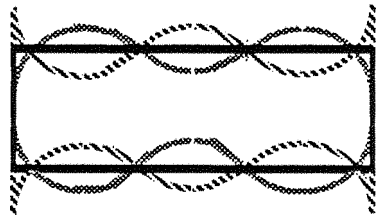

m = 3

AXIAL MODE SHAPES

Figure 2.3 Some mode shapes and nodal patterns of a circular cylindrical shell with free-free boundary conditions.

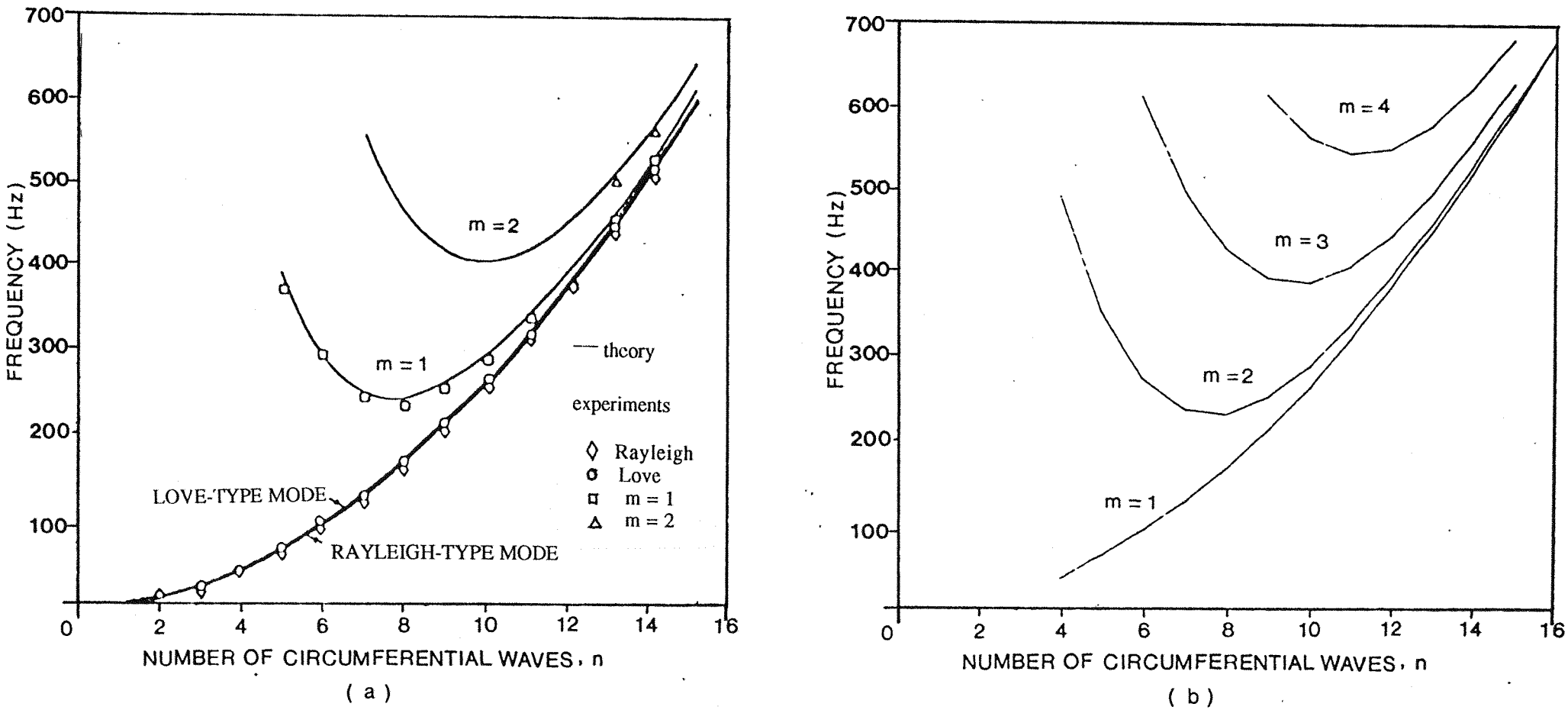

Figure 2.4 Comparison of theoretical results with published experimental data.

(a) data from reference [67],
(b) theoretical results.

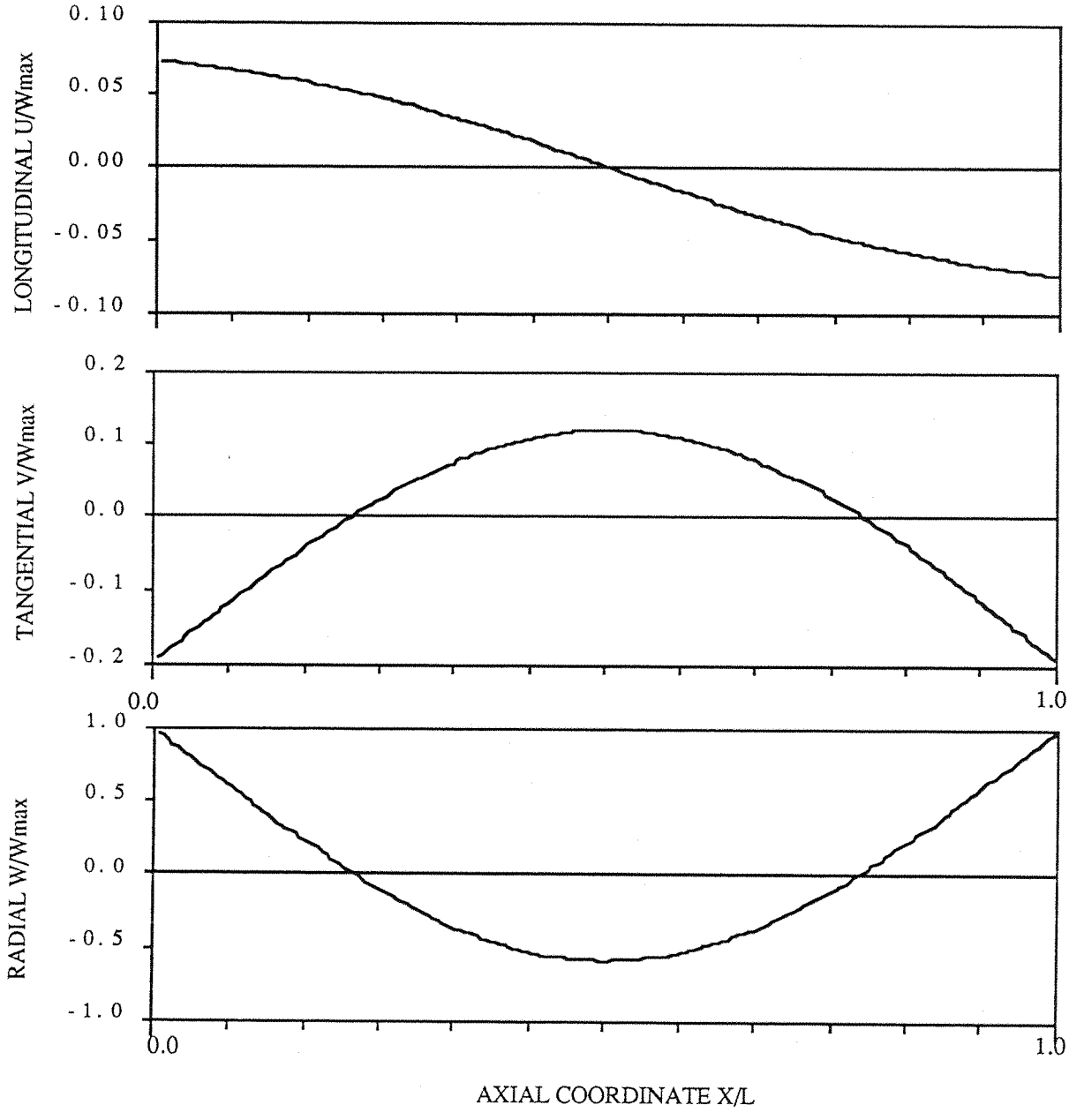

Figure 2.5 Mode shape of a free-free shell, m=1, n=4.

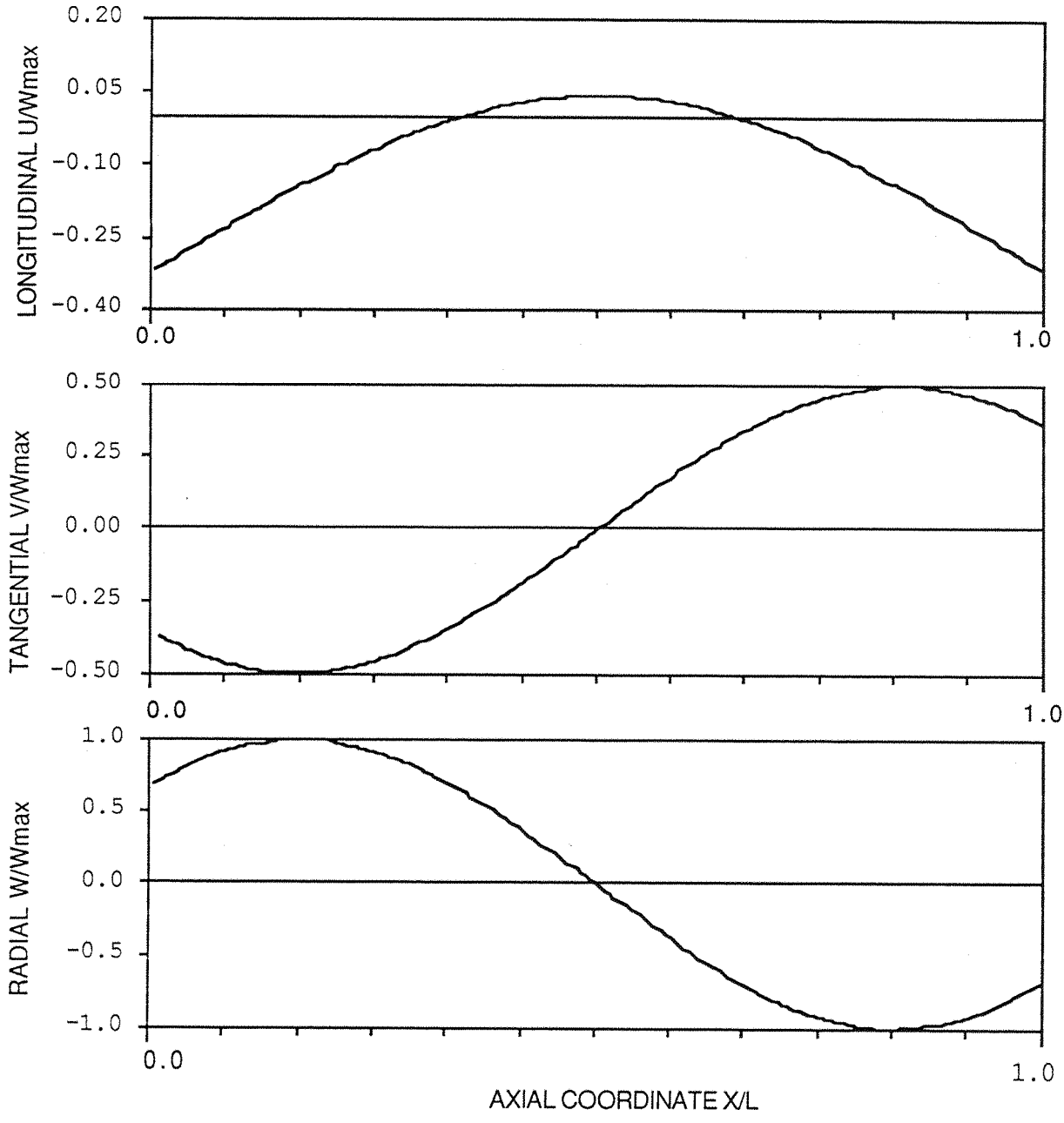

Figure 2.6 Mode shape of a free-free shell, m=2, n=2.

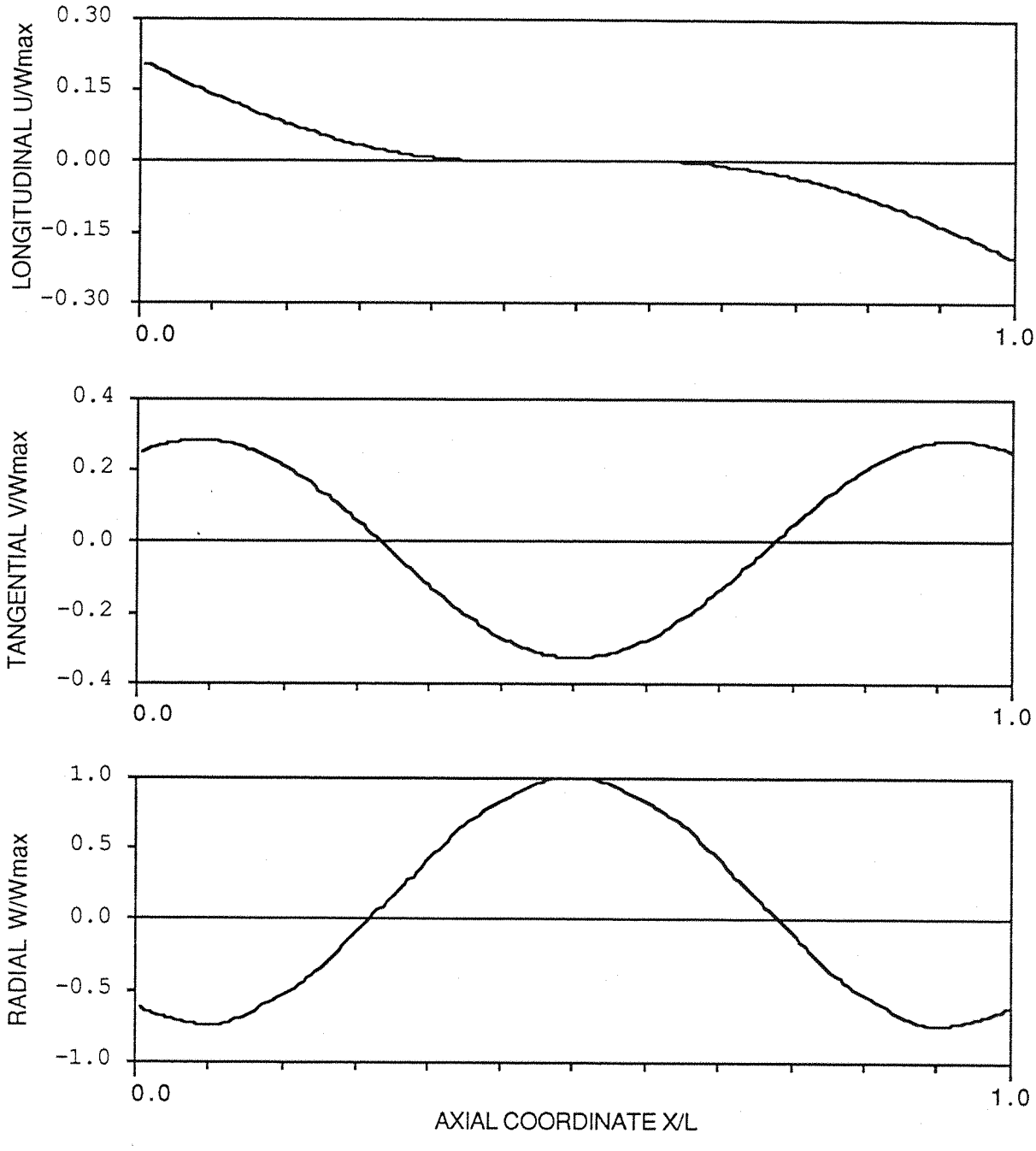

Figure 2.7 Mode shape of a free-free shell, m=3, n=4.

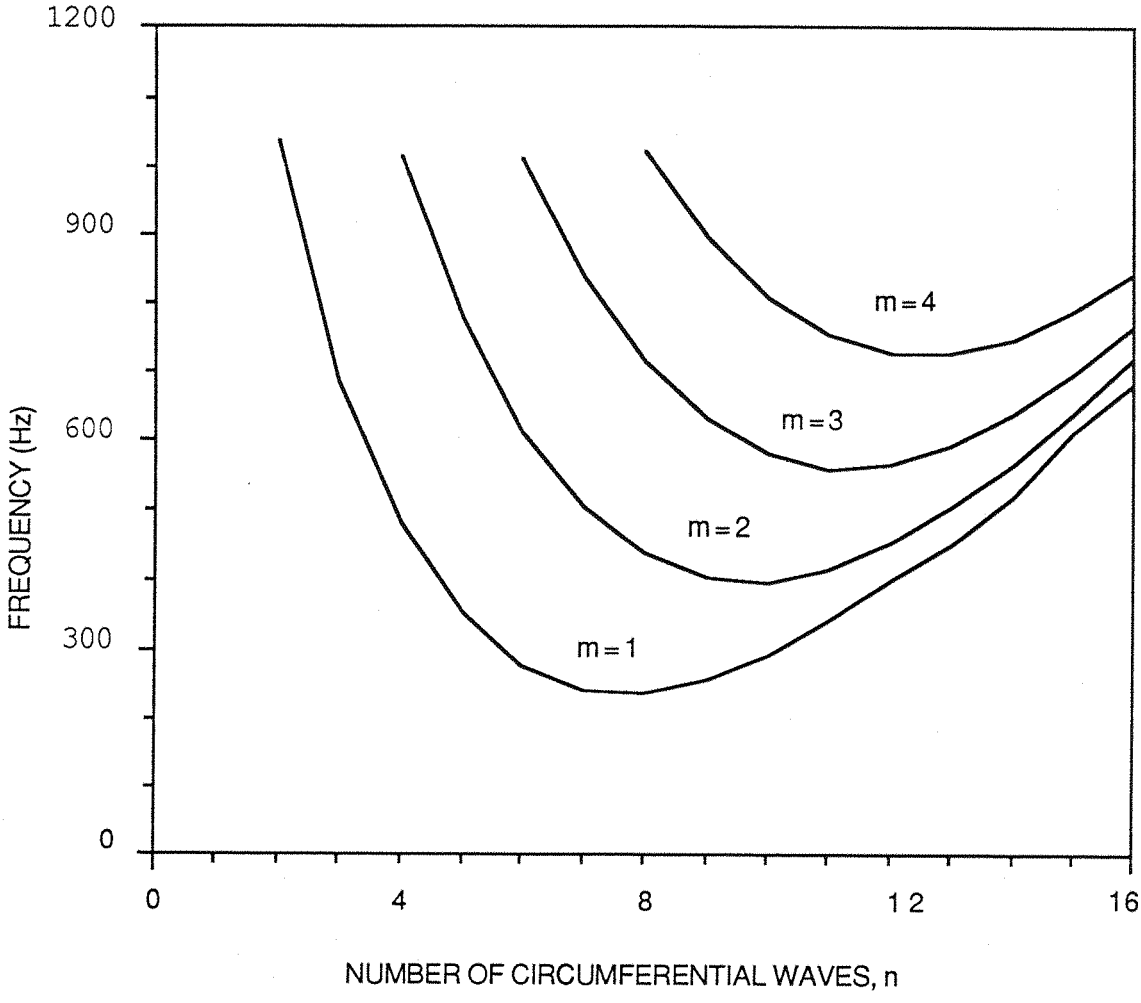

Figure 2.8 Theoretical results for natural frequencies of clamped-clamped cylindrical shell.

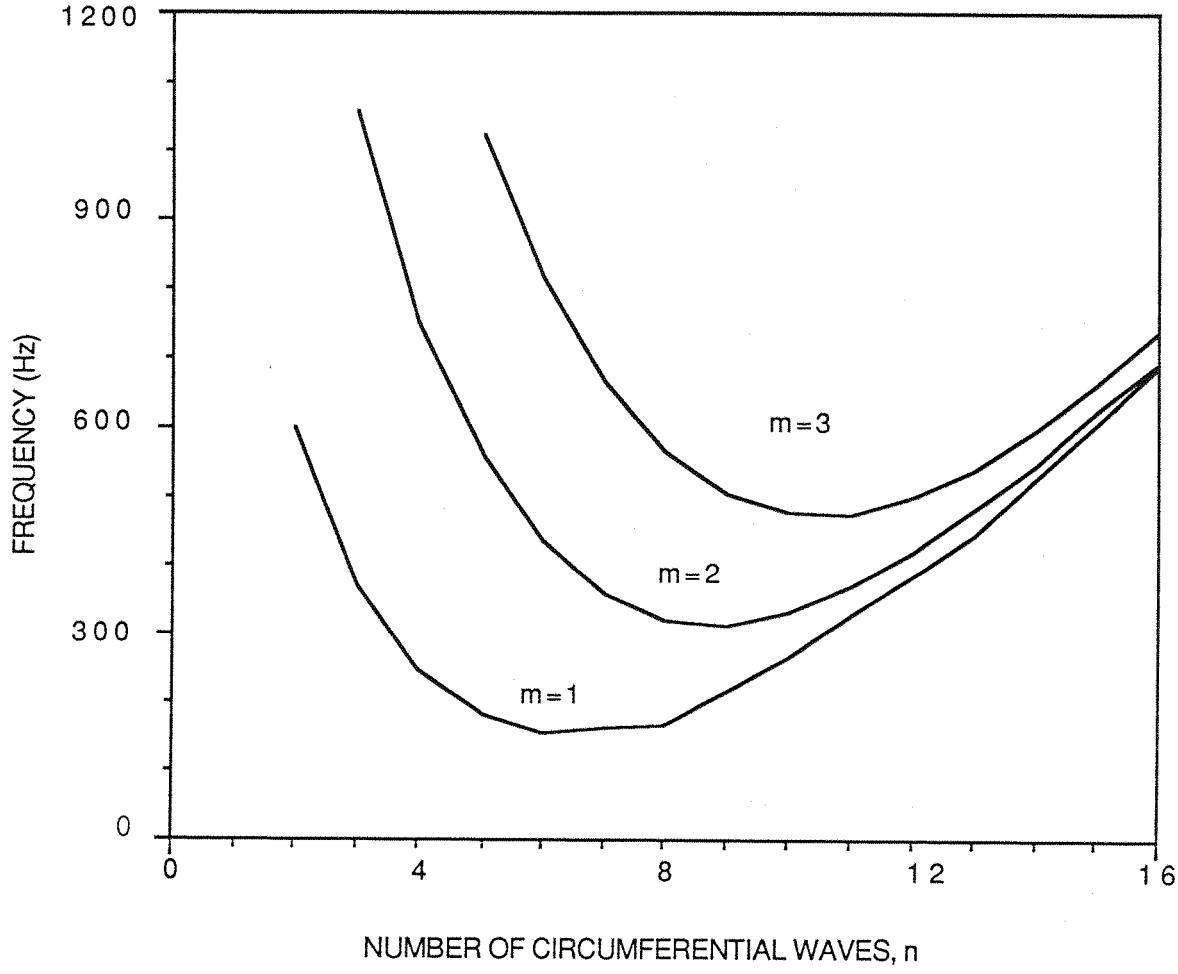

Figure 2.9 Theoretical results for natural frequencies of clamped-free cylindrical shell.

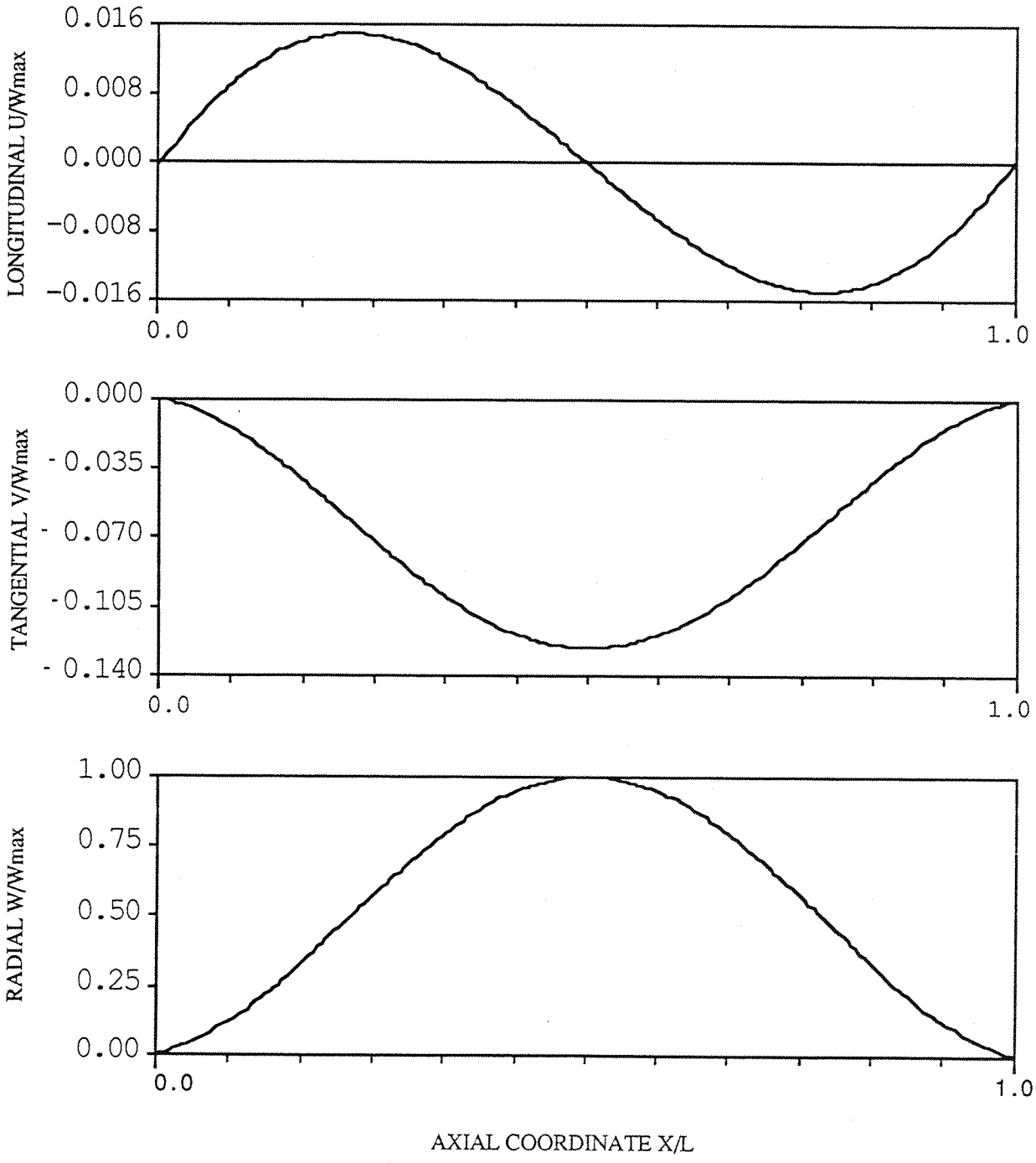

Figure 2.10 Mode shape of a clamped-clamped cylindrical shell.
m=1, n=8, natural frequency=237.1 Hz.

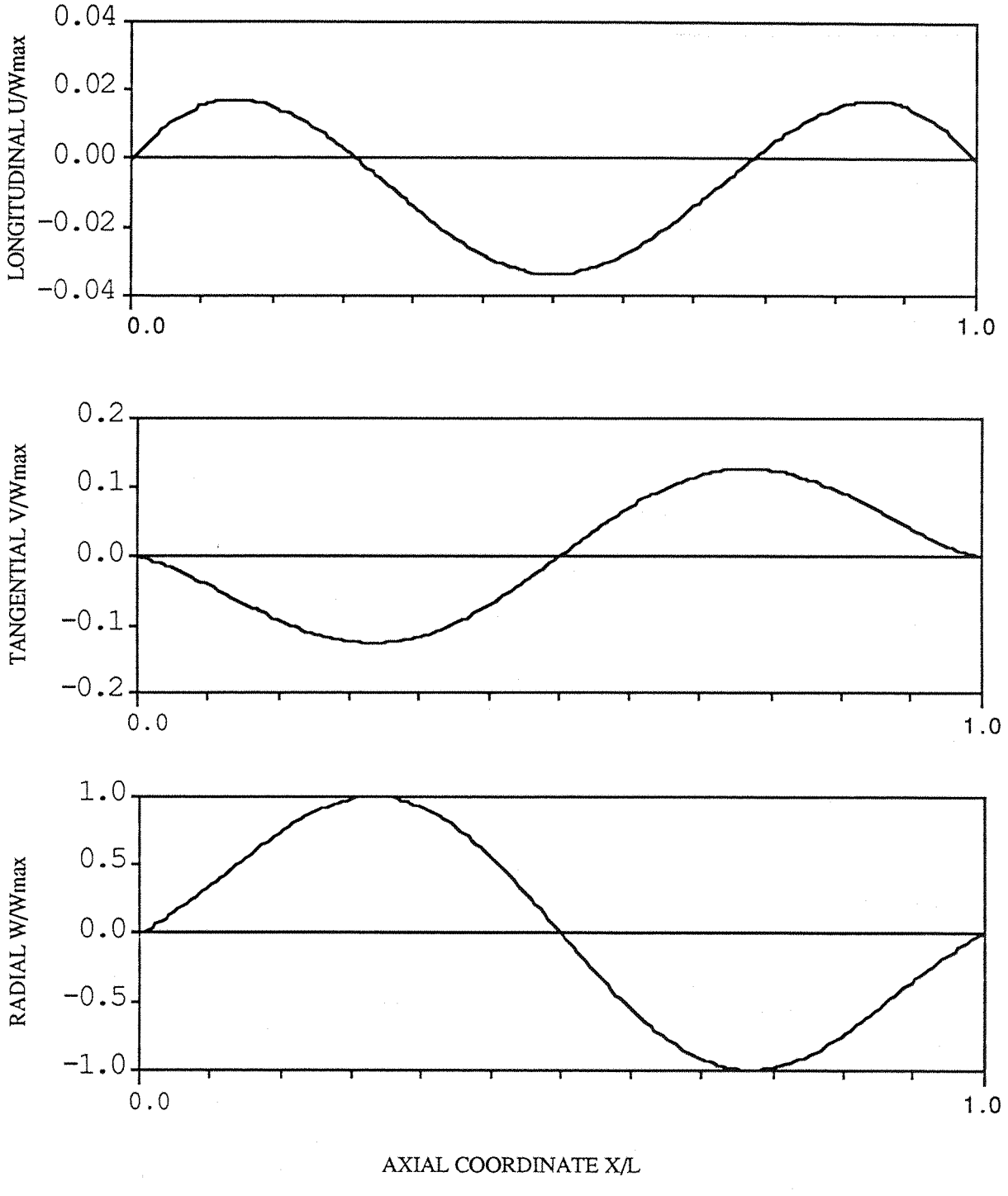

Figure 2.11 Mode shape of a clamped-clamped cylindrical shell.
m=2, n=8, natural frequency=437.0 Hz.

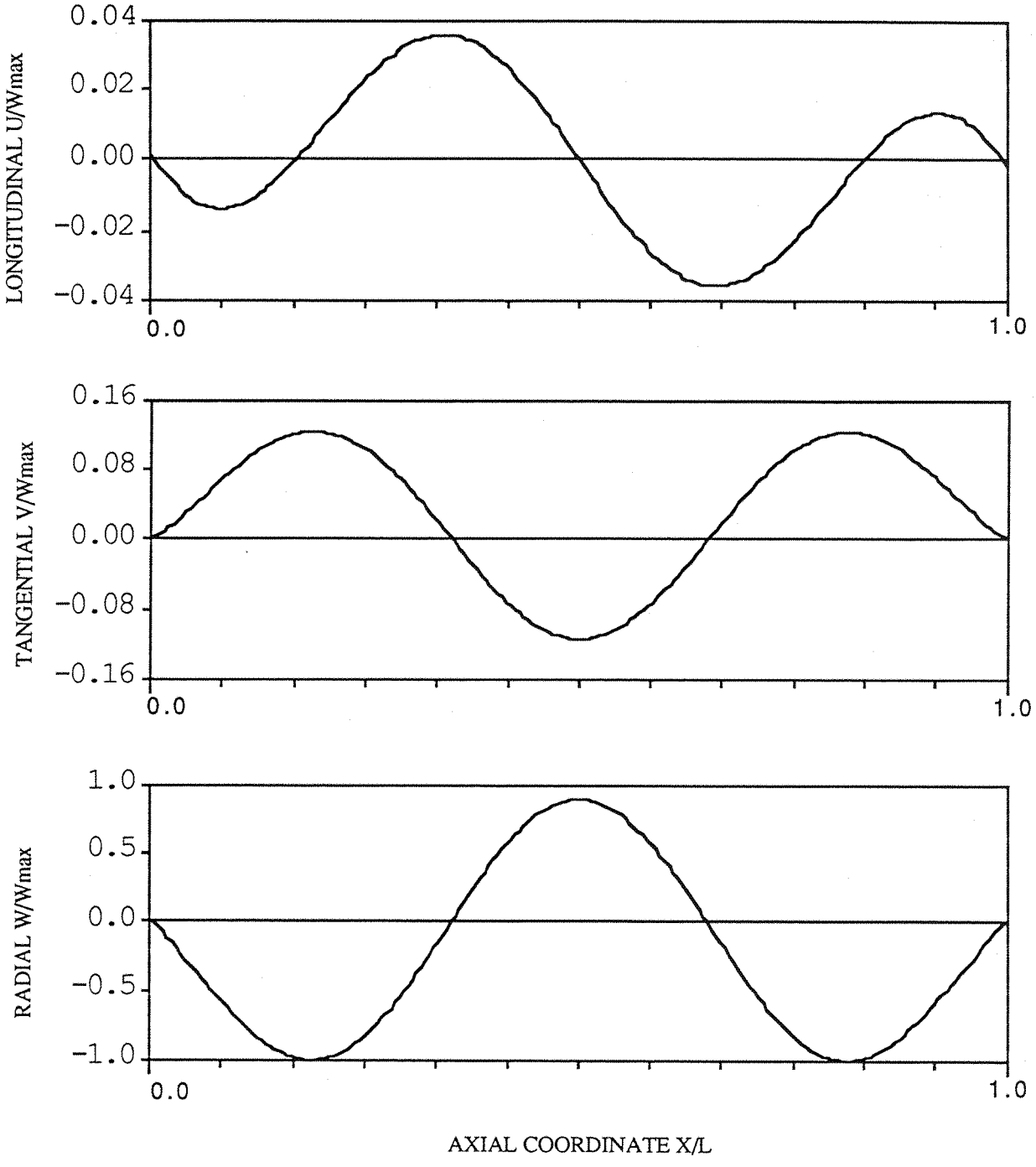

Figure 2.12 Mode shape of a clamped-clamped cylindrical shell.
m=3, n=8, natural frequency= 714.0 Hz.

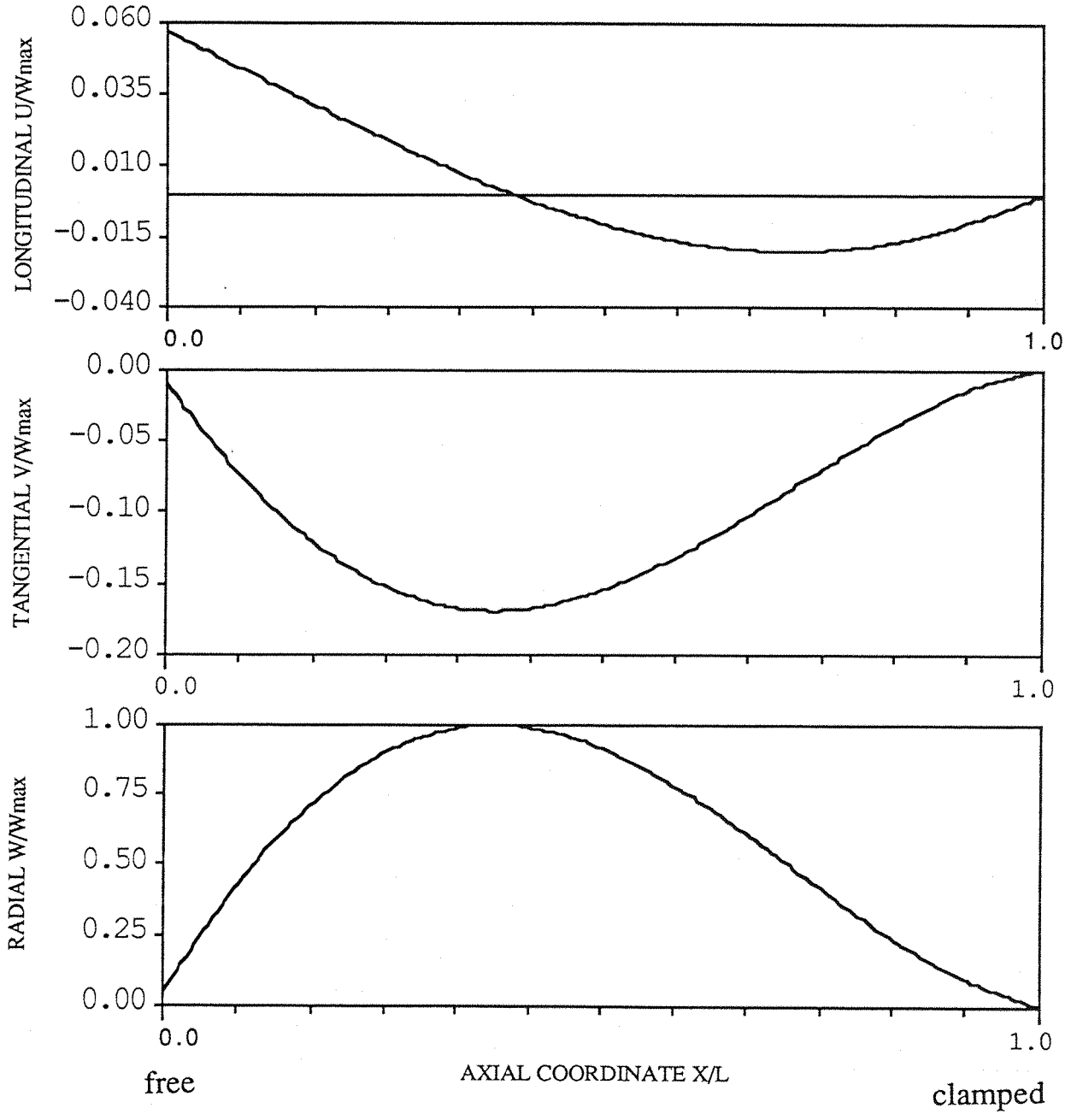

Figure 2.13 Mode shape of a free-clamped cylindrical shell.
m=1, n=6, natural frequency= 154.6 Hz.

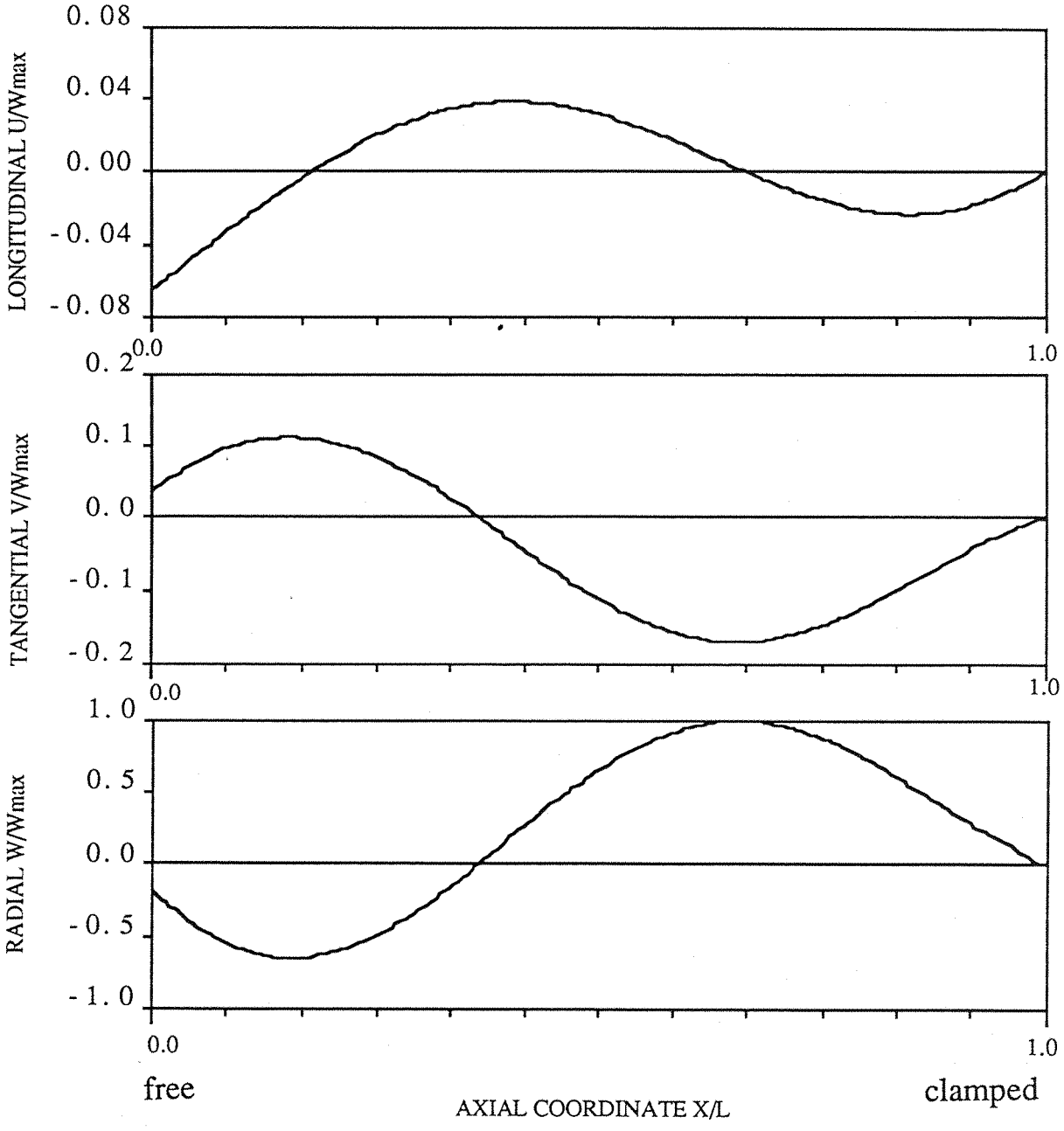

Figure 2.14 Mode shape of a free-clamped cylindrical shell.
m=2, n=6, natural frequency= 433.0 Hz.

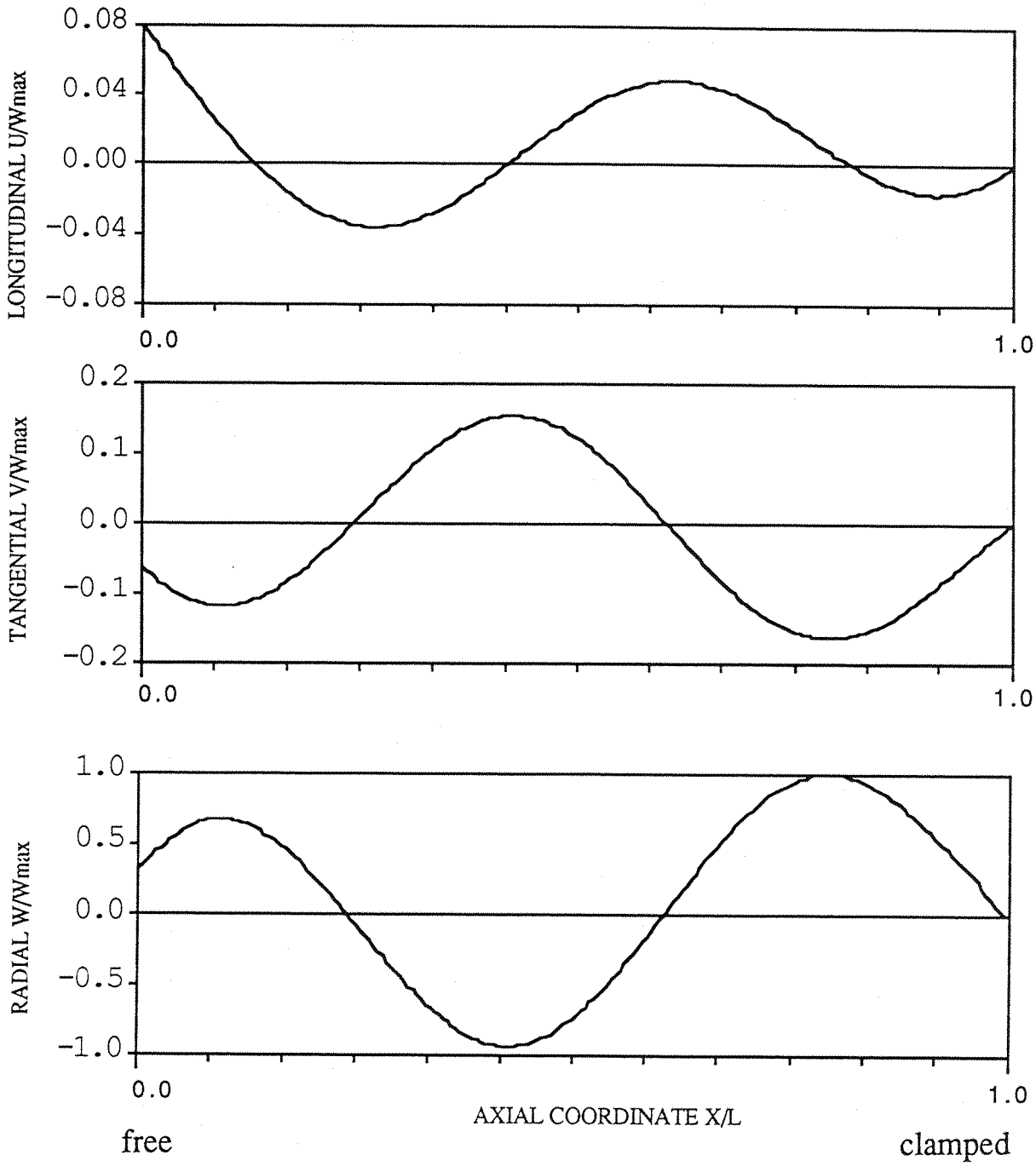

Figure 2.15 Mode shape of a free-clamped cylindrical shell.
m=3, n=6, natural frequency= 811.0 Hz.

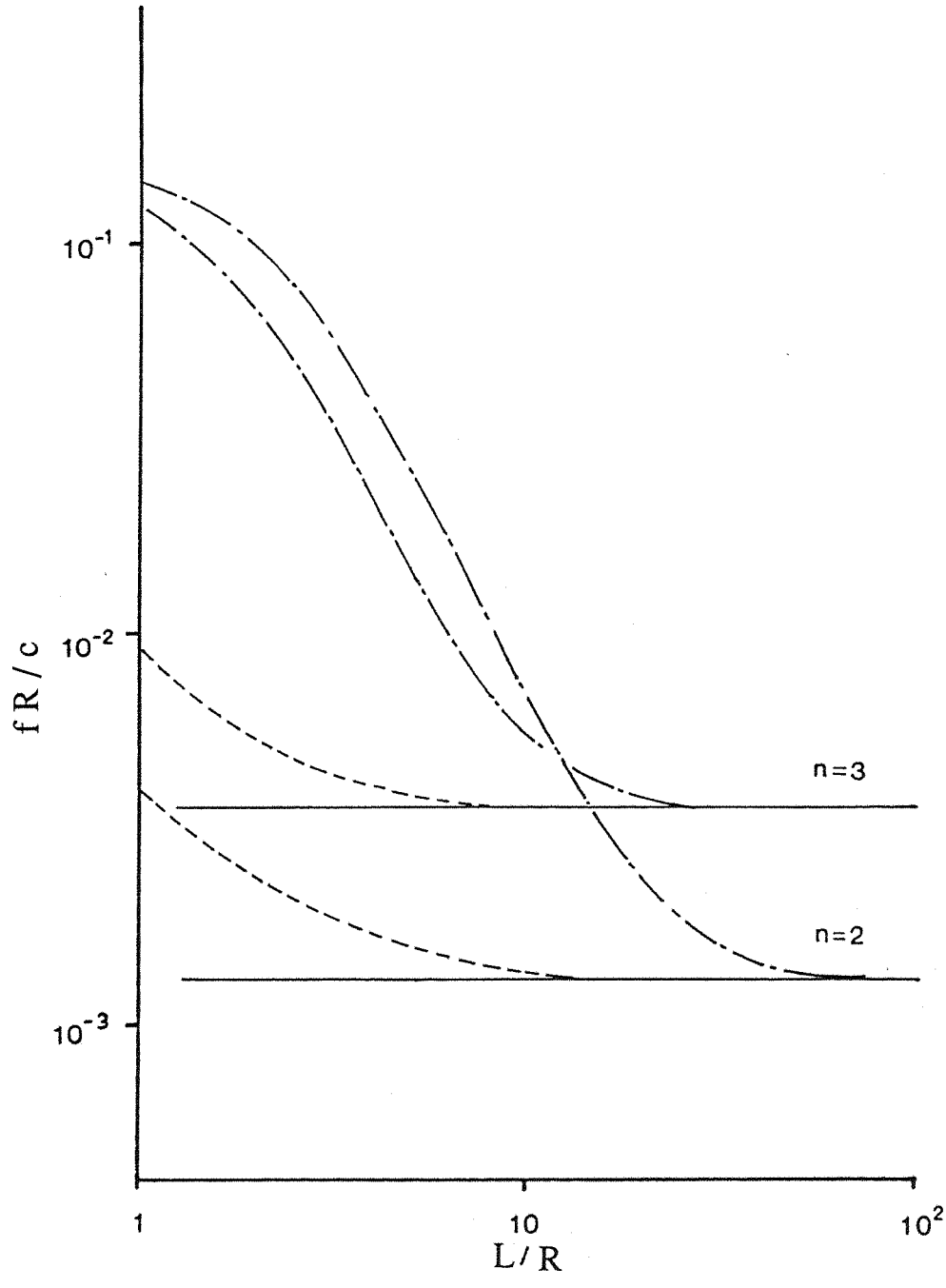

Figure 2.16 Comparison between frequencies of Rayleigh, Love modes and the first axial wave mode .
R/h = 100, f = frequency, h = thickness of the pipe,
R = radius of the pipe, L = length of the pipe,
c = speed of sound.
—— Rayleigh mode, --- Love mode,
—— - —— first axial wave mode.

CHAPTER 3. PREDICTION OF PIPE DAMPING DUE TO SQUEEZE FILM DAMPING.

3.1 INTRODUCTION.

It was stated in the introduction of this thesis that an objective of the work was to increase the damping of pipes using robust methods which would create high loss factors through a wide temperature and frequency range. One possible method is to have concentric thin-walled pipes with an air or fluid-filled annular gap between. The inner pipe must, of course, be of sufficient dimensions to carry the contained fluid at the required flow rate and pressure. The outer pipe could be of different material and wall thickness. It is probable that if such a system is to generate high damping, then the gap between the two pipes will be small. This chapter is therefore concerned with theoretical analysis of a concentric double pipe system and complementary experimental work is described in Chapter 4.

Gas or fluid pumping in the annulus is studied. From knowledge of the pumping mechanism and the mode shapes established in Chapter 2, it is possible to calculate the loss factor of the system - neglecting initial dissipation in the structural materials of the pipes which will generally be small. Work has already been carried out on damping due to gas pumping and this is examined first before proceeding to the concentric pipe problem.

In the present study, the theory for predicting the loss factor of a double pipe system, which consists of two thin cylindrical shells with an air filled annulus, is developed. In this theory, the fluid-solid interaction is considered; the velocity profile and stresses in the gas between the two pipes are derived; then the energy dissipated in the system can be calculated. Finally, an optimum design for maximum damping is deduced from the theory. The theory can be extended to study the damping with various kinds of viscous fluid in the gap between the two annular structures.

3.2 PRINCIPLE OF SQUEEZE-FILM DAMPING.

3.2.1 Characteristics of Gas.

A. Newtonian fluid.

Viscosity controls the ability of a fluid to flow freely. A real fluid, gas or liquid, has its viscous resistance. The coefficient of viscosity indicates its ability to flow or the property of resistance. Mathematically, the coefficient of viscosity is the ratio of applied stress to the resulting strain in the fluid. A simple and widely used example of a fluid sheared between

two plates is shown in figure 3.1, where an ideal linear velocity profile is displayed for viscous fluid flow when one plate is moving and the other is fixed. The assumption is made for the above viscous flow model that there is no slip or movement between fluid and solid boundaries. For simple fluids such as water, oil or gases, there is a linear relationship between stress τ_{xy} and strain ε_{xy} as

$$\tau_{xy} = 2\,\mu\varepsilon_{xy} = \mu\,\frac{dV}{dy} \qquad (3.1)$$

where μ is dynamic viscosity and V is fluid velocity; this is called Newtonian flow. Nonnewtonian fluids have a nonlinear relationship between τ_{xy} and ε_{xy}.

B. Viscosity as a function of temperature and pressure.

The coefficient of viscosity of a Newtonian fluid is directly related to molecular interactions and thus it may be considered as a thermodynamic property in the macrosopic sense, varying with temperature and pressure. From previous studies the following statements can be made:

1. The viscosity of liquids decreases rapidly with increasing temperature.
2. The viscosity of low pressure gases increases with increasing temperature.
3. The viscosity of liquids and gases always increases with increasing pressure.

Since the pressure dependence of gas viscosity needs only to be considered at pressure above 2 atm, it is common in aerodynamics to ignore the pressure dependence of gas viscosity and consider only the temperature variations. The properties of gas viscosity discussed above may have the advantage of generating viscous damping in a squeeze film and giving high damping at high temperatures.

3.2.2 Mechanism of Damping by Air Pumping.

A. Energy dissipation in a boundary layer.

In a Newtonian fluid, the viscous stress depends linearly on velocity gradient. For a flow of air or other gases the effect of viscosity is normally neglected as the coefficient of viscosity is very small; gases are usually treated as the perfect or ideal gas and it is often assumed that no energy is dissipated in the flowing fluid.

To describe flow conditions, the Reynolds number is used, which is the ratio of inertia force to viscous force, that is

$$Re = \frac{\rho V^2}{\mu V/L} = \frac{\rho VL}{\mu} = \frac{VL}{\nu} \qquad (3.2)$$

where ρ = density of fluid,

$\nu = \mu/\rho$ = kinematical viscosity,

L = characteristic length.

Large Reynolds number means that the viscous force is relatively small. The boundary conditions for an ideal fluid require only that the normal component of velocity should vanish; but for a viscous fluid, however, the velocity at a solid wall must vanish entirely. When the Reynolds number is relatively large, e.g. Re >> 1, the decrease of velocity to zero occurs almost exclusively in a thin layer adjoining the wall. In this situation there are two flow regions to be considered:

1. A very thin layer exists in the immediate neighbourhood of the body within which the velocity gradient normal to the wall, $\partial V/\partial y$, is very large. It is called the boundary layer. In this region, the very small viscosity μ of the fluid exerts an essential influence as the shearing stress $\tau = \mu(\partial V/\partial y)$ may assume large values.
2. In the remaining region no such large velocity gradients occur and the influence of viscosity is relatively unimportant.

The flow in the boundary layer may be either laminar or turbulent. The rapid decrease of velocity at the boundary is due to the viscosity. It cannot be neglected even if Re is large. In fact velocity gradients in boundary layers are usually large, and therefore the viscous force is large even if ν is small. Then most energy dissipation occurs in the boundary layer.

B. Air pumping in the double plate and double pipe system

Figure 3.2 shows air pumping by double plate and double pipe systems. In principle, the air between the structures is squeezed by structural vibration. As energy is dissipated by air viscosity, the structural vibrations are damped. It is immediately apparent that:

1. Mode shapes are important in the air pumping process.
2. The gap size is important: a small gap will produce a large pumping effect.
3. In a double plate system, the structure can be modelled by using beam mode shape functions. However in a double pipe system, vibration is more complex than that occurring with a pair of plates.

3.3. THEORETICAL PREDICTION OF THE LOSS FACTOR OF A DOUBLE PIPE DAMPING SYSTEM.

3.3.1 Mathematical modelling

A double pipe damping system is shown in Figure 3.3, which is considered as two concentric circular cylindrical shells separated by an annulus filled with a viscous fluid.

The motion of the shell is described by the following Flügge's shell equation:

$$[D_{d\text{-}m}]\{u_{ij}\} + \beta_j [D_{mod}]\{u_{ij}\} = \{P_{ij}\} \qquad (3.1)$$

$i = 1,2,3 \quad j = 1,2$

$u_{ij} = (u,v,w)_j$,

the components of displacements are in the z, θ and r (longitudinal, tangential and radial) directions, respectively; j = 1 indicates the inner pipe and j = 2 indicates the outer pipe,

$\beta_j = h_j^2/12R_j^2$,

h_j = thickness of the pipe,

$h = r_2 - r_1$,

R_j = mean radius,

P_{ij} = surface loading components per unit area (P_{zj}, $P_{\theta j}$,P_{rj}) in the longitudinal, tangential and radial directions.

$[D_{d\text{-}m}]$ and $[D_{mod}]$ = differential operators shown in appendix 3.1, are the same as that in chapter 2.

For a non-steady, small amplitude oscillatory motion, the equation for a contained viscous gas can be expressed as:

(i) Continuity equation

$$\frac{D\rho_a}{Dt} + \rho_a \nabla.\bar{V} = 0$$

or $$\frac{\partial \rho_a}{\partial t} + \nabla.(\rho_a \bar{V}) = 0 \qquad (3.2)$$

where ρ_a is the density of gas

$$\rho_a = \rho_o + \rho$$

ρ_o = density of gas at atmosphere or ambient pressure

ρ = change of density which relates to the change in volume of the compressed fluid

So,

$$\frac{\partial \rho}{\partial t} + \rho_o \nabla.\bar{V} = 0 \tag{3.3}$$

where

$\bar{V} = (V_z, V_\theta, V_r)$

$V_{z,\theta,r}$ = flow velocity in the z, θ, r directions

(ii) Equation of motion of a viscous fluid

$$\frac{D\bar{V}}{Dt} = -\frac{1}{\rho_o} \nabla p + \nu_o \nabla^2 \bar{V} + (\nu_b + \tfrac{1}{3}\nu_o) \nabla\nabla.\bar{V}$$

or

$$\frac{\partial \bar{V}}{\partial t} + (\bar{V}.\nabla)\bar{V} = -\frac{1}{\rho_o} \nabla p + \nu_o \nabla^2 \bar{V} + (\nu_b + \tfrac{1}{3}\nu_o) \nabla\nabla.\bar{V} \tag{3.4}$$

where

$\nu_o = \mu/\rho_o$ is dynamic viscosity coefficient

ν_b = bulk viscosity

p = change of pressure due to flow.

(iii) Equation of state

$$\frac{\partial p}{\partial \rho} = C_o^2$$

C_o = velocity of sound

The bulk viscosity or second viscosity is usually of the same order of magnitude as ν_o. As is known, the bulk viscosity appears in processes which are accompanied by a change in volume (or density) of the fluid. In compression or expansion, the processes increase entropy and therefore involve energy dissipation.

In order to consider whether it is necessary to take into account the compressibility of a gas in problems of fluid flow, it is required to consider if the changes in pressure brought about by motion of the fluid cause large changes in volume or density. The density changes according to

$$\frac{\Delta\rho}{\rho_o} \approx \frac{1}{2}\left(\frac{V}{C_o}\right)^2 = \frac{1}{2}M^2 \qquad (3.5)$$

where Mach number $M = V/C_o$

V = mean velocity of flow

C_o = velocity of sound

According to the theory of fluid dynamics, when

$\frac{\Delta\rho}{\rho_o} = \frac{1}{2}M^2 << 1$, compressibility can be neglected.

The following assumptions are made for solving the above equation:

(1) For many applications, the length of the pipe is much larger than the radius R_i. A fluid field in the gap can then be considered to be two dimensional, that is, the axial motion of the fluid is neglected.

(2) The fluid is incompressible at the low Mach number involved, and no bulk viscosity effect is included in the equations.

(3) In the structural vibration of cylindrical shells, longitudinal vibration is neglected as it contributes little to the fluid flow, and the effect due to longitudinal vibration is relatively small compared with those due to radial and tangential vibration.

(4) In theory, for the circumferential modes of the two pipes, only modes with the same mode number n can couple, shown in figure 3.4, while the contributions from different circumferential modes of the two pipes are neglected. Only identical axial modes of the two pipes are concerned in the theory.

From the above assumptions, ρ = constant. For a non-steady and small amplitude oscillation the equations of motion (Navier-Stokes equation) and continuity of fluid are

$$\nabla.\bar{V} = 0 \tag{3.6}$$

$$\frac{\partial \bar{V}}{\partial t} + (\bar{V}.\nabla)\bar{V} = -\frac{1}{\rho_o}\nabla p + \nu_o \nabla^2 \bar{V} \tag{3.7}$$

Due to the condition of incompressibility, the stream function $\psi(r,\theta)$ can be introduced, which satisfies the continuity equation according to

$$V_r = \frac{1}{r}\frac{\partial \psi}{\partial \theta} \tag{3.8}$$

$$V_\theta = -\frac{\partial \psi}{\partial r} \tag{3.9}$$

Now introduce the vector of vorticity, curl Ω,

$$\Omega = -\nabla^2\psi \tag{3.10}$$

Equation (3.7) can be rewritten as the vorticity transfer equation,

$$\frac{D\Omega}{Dt} = \nu_o \nabla^2\Omega \tag{3.11}$$

Because of $(\bar{V}.\nabla) << \partial\bar{V}/\partial t$ (seeing Appendix 3.2),

$$\frac{\partial \Omega}{\partial t} = \nu_o \nabla^2\Omega$$

$$\text{or} \quad \nabla^4\psi - \frac{1}{\nu_o}\frac{\partial}{\partial t}\nabla^2\psi = 0 \tag{3.12}$$

using the travelling wave type solution in two cylindrical shells as

$$v_i = \bar{v}_i \sin(n\theta) \exp[j(\omega t - k_z Z)] \tag{3.13a}$$

$$w_i = \bar{w}_i \cos(n\theta) \exp[j(\omega t - k_z Z)] \tag{3.13b}$$

where

v_i = tangential displacement of pipe wall,

w_i = radial displacement of pipe wall,

$\bar{v}_i$, $\bar{w}_i$ = amplitudes of displacements of v_i and w_i respectively,

$i = 1, 2$ denote inner and outer pipes,

n = circumferential mode number for both inner and outer pipes,

k_z = axial wave number

$$= \frac{m\,\pi}{L},$$

m = axial mode number,

L = length of pipe (both pipes have same length),

$j^2 = -1$

Let

$$\psi = \psi(r) \sin(n\theta) \exp[j(\omega t - k_z Z)] \tag{3.14}$$

and using cylindrical coordinates,

$$\nabla^2 = \frac{\partial^2}{\partial r^2} + \frac{1}{r^2}\frac{\partial^2}{\partial \theta^2} + \frac{1}{r}\frac{\partial}{\partial r} + \frac{\partial^2}{\partial z^2}$$

equation (3.11) becomes

$$\nabla^2\left(\nabla^2\psi - \frac{1}{\nu_o}\frac{\partial}{\partial t}\psi\right) = 0 \tag{3.15}$$

The solution is (Appendix 3.2),

$$\psi(r) = Ar^n + Br^{-n} + CI_n(kr) + DK_n(kr) \tag{3.16}$$

where A, B, C, D are constants, n = circumferential mode number,

$I_n(kr)$, $K_n(kr)$ = modified first and second order Bessel functions,

$k^2 = k_z^2 + j\,\omega/\nu_o$,

k_z = axial wave number,

ω = circular frequency.

At the interfaces between the shells and fluid, the following conditions must be satisfied:

$$V_r \Big|_{r=r_i} = \frac{\partial w_i}{\partial t} \tag{3.17}$$

$$V_\theta \Big|_{r=r_i} = \frac{\partial v_i}{\partial t} \tag{3.18}$$

that is

$$V_r = \dot{w}_i, \quad V_\theta = \dot{v}_i, \qquad \text{at } r = r_i,$$

where $\dot{w}_i$ = radial velocity of pipe wall, $\dot{v}_i$ = tangential velocity of pipe wall.

By using equations (3.8), (3.9) and (3.16), fluid velocities are

$$V_r = V_r(r) \cos(n\theta) \exp[j(\omega t - k_z Z)]$$

$$V_\theta = V_\theta(r) \sin(n\theta) \exp[j(\omega t - k_z Z)]$$

or

$$V_r = \frac{n}{r}[Ar^n + Br^{-n} + C\, I_n(kr) + D\, K_n(kr)] \tag{3.19a}$$

$$V_\theta = -\, nr^{n-1} A + nr^{-(n+1)} B - k\, I'_n(kr)\, C - k\, K'_n(kr)\, D \tag{3.19b}$$

where the terms $\cos(n\theta) \exp[j(\omega t - k_z Z)]$ and $\sin(n\theta) \exp[j(\omega t - k_z Z)]$ are omitted in writing, only the amplitude terms being given.

Substituting equations (3.13) and (3.19) into (3.17) and (3.18), the relation of structural vibration and fluid flow becomes

$$\begin{bmatrix} a_{11} & a_{12} & a_{13} & a_{14} \\ a_{21} & \cdots & \cdots & a_{24} \\ \cdots & \cdots & \cdots & \cdots \\ a_{41} & \cdots & \cdots & a_{44} \end{bmatrix} \begin{bmatrix} A \\ B \\ C \\ D \end{bmatrix} = j\omega \begin{bmatrix} \bar{v}_1 \\ \bar{w}_1 \\ \bar{v}_2 \\ \bar{w}_2 \end{bmatrix} \tag{3.20}$$

where,

$$a_{11} = -nr_1^{n-1}$$
$$a_{12} = -nr_1^{-(n+1)}$$
$$a_{13} = -\frac{n}{r_1} I_n(kr_1) - k\, I_{n+1}(kr_1)$$
$$a_{14} = -\frac{n}{r_1} K_n(kr_1) + k\, K_{n+1}(kr_1)$$

$$a_{21} = nr_1^{n-1}$$
$$a_{22} = nr_1^{-(n+1)}$$
$$a_{23} = \frac{n}{r_1} I_n(kr_1)$$
$$a_{24} = \frac{n}{r_1} K_n(kr_1)$$

$$a_{31} = -nr_2^{n-1}$$
$$a_{32} = nr_2^{-(n+1)}$$
$$a_{33} = -\frac{n}{r_2} I_n(kr_2) - k\, I_{n+1}(kr_2)$$
$$a_{34} = -\frac{n}{r_2} K_n(kr_2) + k\, K_{n+1}(kr_2)$$

$$a_{41} = nr_2^{n-1}$$
$$a_{42} = nr_2^{-(n+1)}$$
$$a_{43} = \frac{n}{r_2} I_n(kr_2)$$
$$a_{44} = \frac{n}{r_2} K_n(kr_2)$$

The derivitation of the Bessel function is

$$\frac{\partial I_n(z)}{\partial z} = \frac{n}{z} I_n(z) + I_{n+1}(z)$$

$$\frac{\partial K_n(z)}{\partial z} = \frac{n}{z} K_n(z) - K_{n+1}(z)$$

The matrix of constants can be written as

$$\begin{bmatrix} A \\ B \\ C \\ D \end{bmatrix} = j\omega \left[a_{ij} \right]^{-1} \begin{bmatrix} \bar{v}_1 \\ \bar{w}_1 \\ \bar{v}_2 \\ \bar{w}_2 \end{bmatrix} \tag{3.21}$$

where the inverse of matrix $[a_{ij}]$ is a function of r_1/r_2, $I_n(kr)$, $K_n(kr)$ and n.
Let velocities $\dot{v}_i$ and $\dot{w}_i$ have the form of

$$v_i = j\omega \, \bar{v}_2 \sin(n\theta) \exp[j(\omega t - k_z z)] \tag{3.22a}$$

$$w_i = j\omega \, \bar{w}_2 \cos(n\theta) \exp[j(\omega t - k_z z)] \tag{3.22b}$$

by using

$$P_{\theta i} = \tau_{r\theta} \Big|_{r=r_i}, \tag{3.23a}$$

$$P_{ri} = \tau_{rr} \Big|_{r=r_i}, \tag{3.23b}$$

where the fluid stresses are

$$\tau_{rr} = - p + 2\mu \frac{\partial V_r}{\partial r} \tag{3.24a}$$

$$\tau_{r\theta} = \mu \left(\frac{\partial V_\theta}{\partial r} - \frac{V_\theta}{r} + \frac{1}{r} \frac{\partial V_r}{\partial \theta} \right) \tag{3.24b}$$

equation (3.1) can be rewritten in the following form by using equations (3.19), (3.21), (3.23) and (3.24):

$$\begin{bmatrix} A_{11} & A_{12} & 0 & 0 \\ A_{21} & A_{22} & 0 & 0 \\ 0 & 0 & A_{33} & A_{34} \\ 0 & 0 & A_{43} & A_{44} \end{bmatrix} \begin{bmatrix} \bar{v}_1 \\ \bar{w}_1 \\ \bar{v}_2 \\ \bar{w}_2 \end{bmatrix} = \frac{(1-\nu_i^2) R_i^2}{E_i h_i} \begin{bmatrix} -P_{\theta 1} \\ P_{r1} \\ -P_{\theta 2} \\ -P_{r2} \end{bmatrix} \tag{3.25}$$

or

$$[\,A_{ij}\,]\begin{bmatrix} \bar{v}_1 \\ \bar{w}_1 \\ \bar{v}_2 \\ \bar{w}_2 \end{bmatrix} = [\,B_{ij}\,]\,[\,C_{ij}\,]\begin{bmatrix} A \\ B \\ C \\ D \end{bmatrix}$$

$$= [\,B_{ij}\,]\,[\,C_{ij}\,]\,[\,a_{ij}\,]^{-1}\begin{bmatrix} \bar{v}_1 \\ \bar{w}_1 \\ \bar{v}_2 \\ \bar{w}_2 \end{bmatrix} \qquad (3.26)$$

where

$$[\,B_{ij}\,] = \begin{bmatrix} -\gamma_1 & & & \\ & \gamma_1 & & 0 \\ 0 & & +\gamma_2 & \\ & & & -\gamma_2 \end{bmatrix}$$

and

$$\gamma_i = \frac{\mu(1-\nu_i^2)\,R_i^2}{E_i h_i}(j\omega),$$

E_i = Young's modulus of the *i* th pipe,
ν_i = Poisson's ratio of the *i* th pipe
= ν if both pipes are of the same material,

$A_{11} = -n^2 - 0.5k_z^2R_1^2(1-\nu)(1+3\beta_1) + \Omega_1^2$
$A_{12} = -n\,[1 + 0.5k_z^2R_1^2(3-\nu)\beta_1]$
$A_{21} = n + 0.5nk_z^2R_1^2(3-\nu)\beta_1$
$A_{22} = 1+ \beta_1(1+k_z^4R_1^2+n^4-2n^2k_z^2R_1^2) - \Omega_1^2$

where
$\Omega_i^2 = \rho_iR_i^2(1-\nu^2)\omega^2/E_i$,
$\beta_i = h_i^2/12R_i^2$,
h_i = thickness of the shell wall,
$k_z = m\pi/L$.

The expressions for A_{33}, A_{34}, A_{43}, A_{44} are similar to those for A_{11}, A_{12}, A_{21}, A_{22} and can be obtained by replacing Ω_1, β_1, ρ_1, R_1 and E1 with Ω_2, β_2, ρ_2, R_2 ans E_2.

And

$$C_{11} = -2n(n-1)r_1^{n-2},$$
$$C_{12} = -2n(n+1)r_1^{-(1+2)},$$
$$C_{13} = [nr_1^{-2}(1-2n)+nr_1^{-1}]\, I_n(k\, r_1) + k[1-(2n+1)\, r_1^{-1}]\, I_{n+1}(k\, r_1) - k^2\, I_{n+2}(k\, r_1),$$
$$C_{14} = [nr_1^{-2}(1-2n)+nr_1^{-1}]\, K_n(k\, r_1) + k[(2n+1)\, r_1^{-1} -1]\, K_{n+1}(k\, r_1) - k^2\, K_{n+2}(k\, r_1),$$

$$C_{21} = 2n^2 r_1^{n-2} + j\omega\rho_0 r_1^n,$$
$$C_{22} = -2n^2 r_1^{-(n+2)} + j\omega\rho_0 r_1^n,$$
$$C_{23} = 2n^2 r_1^{-2}\, I_n(k\, r_1) + 2nr_1^{-1}\, k\, I_{n+1}(k\, r_1) + j\omega\rho_0\, I_n(k\, r_1),$$
$$C_{24} = 2n^2 r_1^{-2}\, K_n(k\, r_1) - 2nr_1^{-1}\, k\, K_{n+1}(k\, r_1) + j\omega\rho_0\, K_n(k\, r_1).$$

The expression of C_{ij} for i=3 & 4 can be obtained by replacing r_1 with r_2.
Rewriting equation (3.26) gives

$$\{[\mathbf{A}_{ij}] - [\mathbf{B}_{ij}][\mathbf{C}_{ij}][\mathbf{a}_{ij}]^{-1}\}[\ \bar{v}_l,\ \bar{w}_l]^T = 0$$

or $$[\mathbf{G}_{ij}]\ [\ \bar{v}_l,\ \bar{w}_l]^T = 0 \qquad (3.27)$$

where l is equal to 1 or 2 and the matrix G_{ij} is a function of frequency, r_i, R_i and μ.

3.3.2 Vibration Mode Shapes of a Double Pipe System.

Let $\bar{w}_1$=1, and from equation (3.27), vibration mode shapes are $\bar{v}_1/\ \bar{w}_1$, $\bar{v}_2/\ \bar{w}_1$, $\bar{w}_2/\ \bar{w}_1$, or ratios of velocities $\dot{v}_1/\dot{w}_1$, $\dot{v}_2/\dot{w}_1$ and $\dot{w}_2/\dot{w}_1$ can be derived, where

$\dot{v}_i$ = tangential velocity of pipe wall,
$\dot{w}_i$ = radial velocity of pipe wall,
i = 1, 2 denote inner and outer pipes,

$$\dot{v}_1/\dot{w}_1 = \mathbf{H}_1/\mathbf{H},$$

$$\dot{v}_2/\dot{w}_1 = \mathbf{H}_2/\mathbf{H}, \qquad (3.28)$$

$$\dot{w}_2/\dot{w}_1 = \mathbf{H}_3/\mathbf{H},$$

and

$$\mathbf{H} = \begin{vmatrix} G_{11} & G_{13} & G_{14} \\ G_{21} & G_{23} & G_{24} \\ G_{31} & G_{33} & G_{34} \end{vmatrix}$$

$$\mathbf{H}_1 = \begin{vmatrix} -G_{12} & G_{13} & G_{14} \\ -G_{22} & G_{23} & G_{24} \\ -G_{32} & G_{33} & G_{34} \end{vmatrix}$$

$$\mathbf{H}_2 = \begin{vmatrix} G_{11} & -G_{12} & G_{14} \\ G_{21} & -G_{22} & G_{24} \\ G_{31} & -G_{32} & G_{34} \end{vmatrix}$$

$$\mathbf{H}_3 = \begin{vmatrix} G_{11} & G_{13} & -G_{12} \\ G_{21} & G_{23} & -G_{22} \\ G_{31} & G_{33} & -G_{32} \end{vmatrix}$$

By the same method, V_r, V_θ, τ_{rr} and $\tau_{r\theta}$ can be calculated by use of equations (3.19), (3.21) and (3.24). The expressions of V_r, V_θ, the velocities of squeeze flow in radial and tangential directions, are

$$\begin{bmatrix} V_r \\ V_\theta \end{bmatrix} = \begin{bmatrix} nr^{n-1} & nr^{-n-1} & \frac{n}{r} I_n(kr) & \frac{n}{r} K_n(kr) \\ -nr^{n-1} & nr^{-(n+1)} & -k\, I'_n(kr) & -k\, K'_n(kr) \end{bmatrix} [\, a_{ij} \,]^{-1} \begin{bmatrix} \dot{v}_1 \\ \dot{w}_1 \\ \dot{v}_2 \\ \dot{w}_2 \end{bmatrix} \qquad (3.29)$$

where

$\dot{v}_i = j\omega\bar{v}_i \sin(n\theta) \exp[j(\omega t - k_z Z)]$

$\dot{w}_i = j\omega\bar{w}_i \cos(n\theta) \exp[j(\omega t - k_z Z)]$

3.3.3 Expression of the Loss Factor in the Double Pipe System.

Neglecting energy dissipation in the pipes, the definition of loss factor in the double pipe system in steady state harmonic vibration is

$$\eta = \frac{\text{Energy dissipated in the viscous gas in a cycle } *}{2\pi(\text{Maximum total energy stored in the pipes + energy stored in the gas})}$$

$$= \frac{E_{dissipated}}{2\pi\, E_{total}}. \qquad (3.30)$$

Energy dissipated is

$$E_{dissipated} = \int_{r_1}^{r_2} \int_{0}^{\frac{2\pi}{\omega}} \int_{0}^{L} \int_{0}^{2\pi} \mu[2(\varepsilon_{rr}^2+\varepsilon_{\theta\theta}^2) + \varepsilon_{r\theta}^2]\, dtdz\, rd\theta dr \qquad (3.30\ a)$$

where $\varepsilon_{rr} = \frac{\partial V_r}{\partial r}$

$$\varepsilon_{\theta\theta} = \frac{1}{r}\frac{\partial V_\theta}{\partial \theta} + \frac{V_r}{r}$$

$$\varepsilon_{r\theta} = \frac{1}{r}\frac{\partial V_r}{\partial \theta} + \frac{\partial V_\theta}{\partial r} - \frac{V_\theta}{r}.$$

The total energy in the system is

$$E_{total} = \frac{1}{2}\rho \int_0^L \int_0^{2\pi} \sum_{i=1}^{2} h_i R_i \left[\left(\frac{\partial v_i}{\partial t}\right)^2 + \left(\frac{\partial w_i}{\partial t}\right)^2\right] dzd\theta$$

$$+ \frac{1}{2}\rho_o \int_{r_1}^{r_2} \int_0^L \int_0^{2\pi} (V_\theta^2 + V_r^2)\, rd\theta\, drdz \qquad (3.30\ b)$$

* Loss factor is defined as the equivalent loss factor which is not a hysteretic mechanism.

where the energy dissipated in the pipes is neglected and energy is dissipated in the squeezed gas only by conversion into thermal energy. The details of this analysis are in Appendix 3.

The energy dissipated depends upon the velocity gradient created by air pumping. It is a function of the frequency (ω), the thickness of the layer of squeezed liquid or gas (h), the viscosity (μ), the circumferential mode number (n) , temperature (T) and ratio of radii of pipes (r_2/r_1). That is

$$E_{dissipated} = f(\omega, h, n, \mu, T, r_2/r_1 ...)$$

It is also a function of Reynolds number Re, where

$$Re = \frac{V_\theta h}{\nu_0} \tag{3.31}$$

Simple estimation Reynolds number of laminar flow for air pumping can be made by the following equation:

$$V_\theta = f\, w \frac{\pi\, r}{2\ h} \tag{3.32}$$

where f = frequency of oscillation of inner pipe,

w = radial displacement of inner pipe,

$\frac{\pi\ r}{2}$ = a quarter of circumference for beam mode n = 1.

In this estimation tangential velocity V_θ, the squeezed flow is created by a radial displacement of the inner pipe while the outer pipe is considered to be fixed; the largest velocity occurs within a distance of 1/4 of the first circumference. If an air filled annulus is chosen and f is chosen as 5000 Hz, $\frac{r}{h}$ as 100 and w as 10×10^{-6} (as an example), ν_0 as 17.9×10^{-6} m^2/sec, h = 1 mm, it can be shown that the Reynolds number will be in a range within laminar flow (V_θ = 7.8 m/sec and Re= 439) as will be the case for the frequency range of interest. It was also found that the Mach number (V_θ/C) is less than 0.03 in this estimation, thus the flow is considered to be incompressible and laminar.

Loss factors of a double pipe system with gas or liquid in the annulus can be calculated by use of equations (3.29), (3.30 a,b) and relevant equations (3.19), (3.20) and (3.28) deduced above. Its deduction can be seen in Appendix 3.

3.3.4. Velocity Profile of Pumping Flow.

From equation (3.19), it can be seen that the velocity profile of pumping flow between two pipes is described by Bessel functions. To simplify numerical calculation, Bessel functions can be expended by using Taylor's theorem at the point $r = r_1$ (see figure 3.4). Modified first and second order Bessel functions become

$$I_n(k\,r) = I_n(k\,r_1)\,H_1(y)+kI_{n+1}(k\,r_1)\,H_2(y)+k^2I_{n+2}(k\,r_1)\,H_3(y) \qquad (3.32a)$$

$$K_n(k\,r) = K_n(k\,r_1)\,H_1(y)-kK_{n+1}(k\,r_1)\,H_2(y)+k^2K_{n+2}(k\,r_1)\,H_3(y) \qquad (3.32b)$$

where

$$H_1(y) = 1+n\frac{y}{r_1}+0.5n(n-1)\left(\frac{y}{r_1}\right)^2$$

$$H_2(y) = y\left[1+0.5(2n+1)\frac{y}{r_1}\right]$$

$$H_3(y) = 0.5\,y^2$$

$y = 0$ to h, and $h/r_1 \ll 1$.

$$I_n(z) \sim \frac{e^z}{\sqrt{2\pi z}}\left\{1-\frac{\xi-1}{8z}+\frac{(\xi-1)(\xi-9)}{2!\,(8z)^2}-\frac{(\xi-1)(\xi-9)(\xi-25)}{3!\,(8z)^3}+\ldots\right\} \qquad (3.33)$$

$$K_n(z) \sim \frac{e^{-z}}{\sqrt{2\pi z}}\left\{1+\frac{\xi-1}{8z}+\frac{(\xi-1)(\xi-9)}{2!\,(8z)^2}-\frac{(\xi-1)(\xi-9)(\xi-25)}{3!\,(8z)^3}+\ldots\right\} \qquad (3.34)$$

where $\xi=4n^2$

$z=kr$.

From this expression the Bessel function becomes a function of y when other coefficients are fixed. Deduction of velocity is given in Appendix 3.3.

Based on these velocity expressions, the gradient of the velocity of squeeze flow and the relevant energy dissipated in equation (3.29) and (3.30) can be easily estimated numerically.

3.3.5 Effect of Thickness of Boundary Layer.

According to theory of fluid mechanics, the boundary layer thickness of squeezed flow between two vibrating plates [68] is expressed as

$$\delta = \sqrt{\frac{2\nu_0}{\omega}} \tag{3.35}$$

According to boundary layer theory, there is large velocity gradient in the thickness of the boundary layer, hence energy is dissipated. The ratio of the air gap to the boundary thickness associated with the oscillating air flow is an important parameter controlling the damping of the whole system. This ratio is

$$\frac{h}{\delta} = h \sqrt{\frac{\omega}{2\nu_0}} \tag{3.36}$$

The results from the previous study suggest that the smaller the volume h/δ, the larger the damping. From equation (3.35) the thickness of the boundary layer will vary with frequency, being thin at high frequency.

3.4 OPTIMUM DESIGN FOR MAXIMUM LOSS FACTOR OF A DOUBLE PIPE SYSTEM.

3.4.1. Loss Factor Associated with In-phase and Out-of-phase Modes.

From previous research, it is known that narrow clearance in the gas filled annulus yields high damping and that the mode shapes of the vibrating pipes are also important influences on damping. For the double pipe system the squeeze gas effect is most pronounced for the out-of-phase modes as shown in figure 3.5; the effect of fluid viscosity is very small and in fact it could be negligible for the in-phase mode.

Figure 3.5 has also given a example of circumferential mode (n) and axial mode (m) in a double pipe system, where either the circumferential mode or the axial mode has the same number for both inner and outer pipes in this study.

When the gap clearance becomes zero, there can only be in-phase modes of vibration and no energy is dissipated in the gas. Therefore there is must an optimum clearance for the gas, where the damping is a maximum. It could be supposed that the mode shape ratio $\dot{w}_2/\dot{w}_1$ is a function of h/δ. When $h = 0$, $\dot{w}_2/\dot{w}_1 = 1$, and the loss factor is zero.

3.4.2. Dependence of the Kinematic Viscosity on Separation Distance.

In previous research on gas pumping [18], it has been stated that when the gap h is as small as the mean free path of the molecules of the gas, the kinematical viscosity will depend upon the separation distance h.

The coefficient of kinematical viscosity can be expressed as [18]

$$\nu_0 = 0.5 \ \bar{c}\, h \,(S + h\,\Lambda^{-1})^{-1} \tag{3.37}$$

where

Λ = the mean free path of the molecules of gas,

$\bar{c}$ = average speed of the molecules of gas,

$S = 30$.

The kinematical viscosity decreases rapidly as h decreases, so that less energy is dissipated in the gas when h is small.

3.4.3. The Theory of Similarity.

To apply particular theoretical or experimental results in a general study, the law of similarity is often used, which describes numerous groups of phenomena by a number of nondimensional parameters. For instance Reynold's number can denote similar flow conditions for a set of parameters. Using the theory of similarity, it is possible to apply theory and experiment in studying the phenomenon at large dimensions; for example a

model test on pipe damping in a laboratory can be used for the purpose of studying large pipes in industrial plant.

3.5. PREDICTION OF LOSS FACTOR FOR AIR DAMPING.

3.5.1. Prediction of Velocity Profile of Pumping Flow.

In the principle of squeeze film damping, the velocity gradient of squeeze flow between the vibrating bodies plays an important role in the energy dissipated from the vibrating system. Because of this, the velocity profile of flow between the two pipes has been calculated. The squeeze damping of the whole system may then be easily derived from equations (3.28), (3.29) and (3.30). Appendix 3.4 gives the flow chart of the program procedure for predicting the loss factor of a double pipe system.

From the mathematical modelling, the squeezed flow has been assumed to be only in the tangential and radial directions. Figures 3.6 to 3.10 showed the theoretical results of tangential and radial velocity profiles of air pumping with various ratios of $\dot{w}_2/\dot{w}_1$, air gap h and circumferential mode number n when other parameters are fixed. In figure 3.6, it can be clearly seen that the tangential velocity is determined by the ratio of $\dot{w}_2/\dot{w}_1$; when $\dot{w}_2/\dot{w}_1 = 1$ for in-phase motion there is no pumping velocity and when $\dot{w}_2/\dot{w}_1 < 1$ or <0 for out-of-phase modes, the pumping velocity becomes greater. A narrow air gap always produces a high velocity gradient as shown in figure 3.7.

Results from further studies of the tangential velocity with various circumferential mode numbers are shown in figure 3.8; it is found that the first circumferential mode number gives the largest contribution to the air pumping. The larger the circumferential mode number, the less the contribution to the air pumping. The vibration modes have been discussed in previous sections, 3.3.1, 3.4.1, and figure 3.5.

The radial velocity profile of air flow with ratios of $\dot{w}_2/\dot{w}_1$ in figure 3.9 and with various air gap clearances in figure 3.10 indicate that the relative velocity of air flow in the radial direction is much smaller than that in the tangential direction. The radial velocity will be less important in the air pumping characteristics of the system.

3.5.2. Prediction of Loss Factor with Various Circumferential mode Numbers and In-phase or Out-of-phase Modes.

From the results in section 3.5.1., it is understood that damping in a double pipe system will be controlled by the mode shapes of the components of the vibrating system. So that circumferential mode number and in-phase or out-of-phase mode conditions are the most important.

Figure 3.11 gives a predicted loss factor for the first three circumferential mode numbers (n=1, 2 & 3). In the figure it is shown that the loss factor has the greatest magnitude when n=1 and the loss factor becomes negligible when n is greater then 3. The effect of in-phase and out-of-phase modes can also be seen in the figure 3.11. The minima in the loss factor curves denote the loss factors at frequencies where in-phase modes occur.

The loss factor with n=1 and theoretical in-phase and out-of-phase modes are demonstrated in figure 3.12. The two minima in the loss factor curves for a circumferential mode number n=1, corresponding to the two peaks in the lower plot, show that when in-phase modes occur the loss factor is very low.

3.5.3. Prediction of Loss Factor with Variation of Thickness and Radii of Pipes.

To understand how the dimensions of pipes will affect the loss factor of the system, the loss factors with various dimensions of the pipes were investigated by varying the relative dimensions of the pipe wall thickness, diameters and gap. The parameters used were: (1) the ratio of radius of the inner pipe to air gap thickness, (2) the ratio of inner and outer wall thicknesses of the pipes.

The numerical results presented in figures 3.13 to 3.16 denote the following characteristics:

(a) Effect of the ratio R_1/h on loss factor.

When the radius of the inner pipe is relatively large compared with the air gap (see figure 3.13), the loss factor increases because the air pumping effect increases. When $R_1 \rightarrow \infty$ (figure 3.14) the damping system becomes a double plate system and the loss factor has its maximum value for a given air gap h. This may explain why a double plate system has higher damping than a double pipe system.

(b) Effect of the ratio h_2/h_1 on loss factor.

The loss factor increases at low frequency as the ratio h_2/h_1 decreases (see figure 3.15). When the wall thickness of the outer pipe is relatively very large, e.g. the outer pipe tends to be fixed, the pumping effect decreases and, of course, a large weight penalty occurs. At high frequencies, the squeeze air effect of the pipes is quite weak, so that the loss factor at high frequencies is insensitive to changes in the ratio h_2/h_1 (see figure 3.16).

3.5.4. Prediction of Loss Factor with Various Air Gap Clearances.

There is an optimum air gap h_{opt} at which the loss factor is maximum at a given frequency. The reason for this has already been discussed in sections 3.4.1 and 3.4.2. It is supposed that the optimum air gap should occur at twice the thickness of the boundary layer δ,

$$h_{opt} = 2\delta = 2\sqrt{2\nu_0/\omega} \qquad (3.38)$$

Figure 3.17 is a three dimensional plot of predicted loss factor versus air gap h and frequency. It can be clearly seen that when the air gap h is small to a certain level, the loss factor will reach its maximum value and further reduction in h then causes the loss factor to decrease, though the equation of $h_{opt} = 2\delta$ may not be proved at this stage of theoretical study.

3.5.5. Prediction of Loss Factor due to Air Pumping as a Function of Temperature.

The dynamic viscosity and density of air are functions of temperature and pressure, as shown in figures 3.18 and 3.19. The loss factor in an air filled annulus of a double pipe system will slightly increase with increasing temperature as shown in figure 3.20. This is due to the fact that the kinematical viscosity of the air will increase at high temperature.

3.5.6. Comparison of Predicted Loss Factors with Air, Water and Oil in the Annulus of a Double Pipe System.

The magnitude of the loss factor depends not only on the viscosity coefficient but also on the characteristics of the fluid within the annulus. As an example, the loss factors of a double pipe system with air, water and oil in the annulus respectively are given in figure 3.21. There is a high loss factor with oil, but low loss factor with water as water has low kinematical viscosity, although the dynamic viscosity of water is higher than that of air. The data used in computing are

	air	water	oil
density ρ (kg/m^3)	1.2	1000	890
dynamic viscosity ν (kg/m.sec)	18.2×10^{-6}	0.001	0.041
kinematical viscosity μ (m^2/sec)	15.17×10^{-6}	1×10^{-6}	46.1×10^{-6}.

Comparing above data, it can be seen that $\eta_{oil} > \eta_{air} > \eta_{water}$ and $\mu_{oil} > \mu_{air} > \mu_{water}$. The loss factor of double pipe system depends on kinematical viscosity, high damping is created by a fluid of high viscosity.

The frequencies with in-phase modes, at low loss factors points in figure 3.21,are natural frequencies of double pipe system with various liquid or gas filled annulus. The added mass effect is not obvious in the theory, the frequencies of the first in-phase mode points are listed below,

	air	water	oil
frequency (Hz) at in-phase point	758	752	753

There is little added mass effect on natural frequencies in the present theory, more discussion of added mass effects in double pipe systems can be found in reference [24].

3.6. CONCLUSIONS.

(a) High damping may be achieved by air pumping in a double pipe system. The energy dissipated by viscous forces is related to the velocity gradients caused by air flow between the two vibrating pipes.

(b) At low frequency, the velocity gradient is low and so is the energy dissipation. At high frequency the air has little time to move, and behaves as a stiff spring, resulting in low energy dissipation. At intermediate frequencies, the velocity profile is capable of maximising the damping.

(c) The velocity profile of air pumping is of parabolic-like shape. The velocity gradient is high at low circumferential mode numbers.

(d) Only the first few circumferential modes of vibrating pipes will contribute significantly to the damping according to the theory.

(e) The loss factor is high at large ratios of pipe radius to air gap since the air pumping effect is greater in this regime.

(f) Loss factors are improved at low frequency when the ratio of thickness of inner pipe to that of the outer pipe is large.

(g) Generally, loss factors are high for out-of-phase modes and low for in-phase modes.

(h) At high temperatures, the loss factor due to air pumping increases a little as the kinematical viscosity increases.

(i) If a liquid, such as oil, with high kinematical viscosity is used in the gap, the double pipe system has high damping; but loss factor decreases with increasing temperature.

(j) The assumptions were made in the theory that the squeeze fluid was considered to be two dimensional, and fluid motion along the pipe was neglected. The squeeze film damping was contributed to only by the modes where both pipes had the same circumferential mode shapes. If the length of the pipes is very short or the two pipes are made of different materials and thicknesses of the pipe walls are much different, the damping affected by axial motion of flow and different mode shapes between the two pipes may not be neglected.

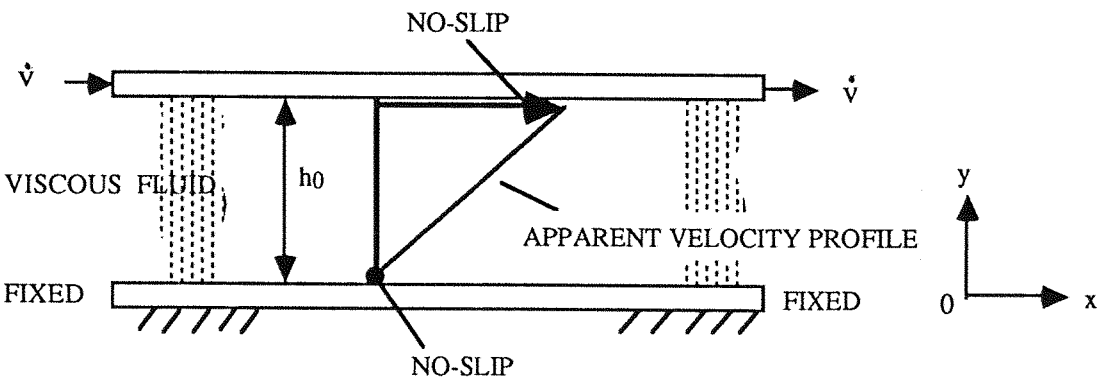

Figure 3.1 A simple representation of fluid sheared between two plates.

$\dot{v}$ = velocity of moving plate,
h_0 = thickness of fluid gap.

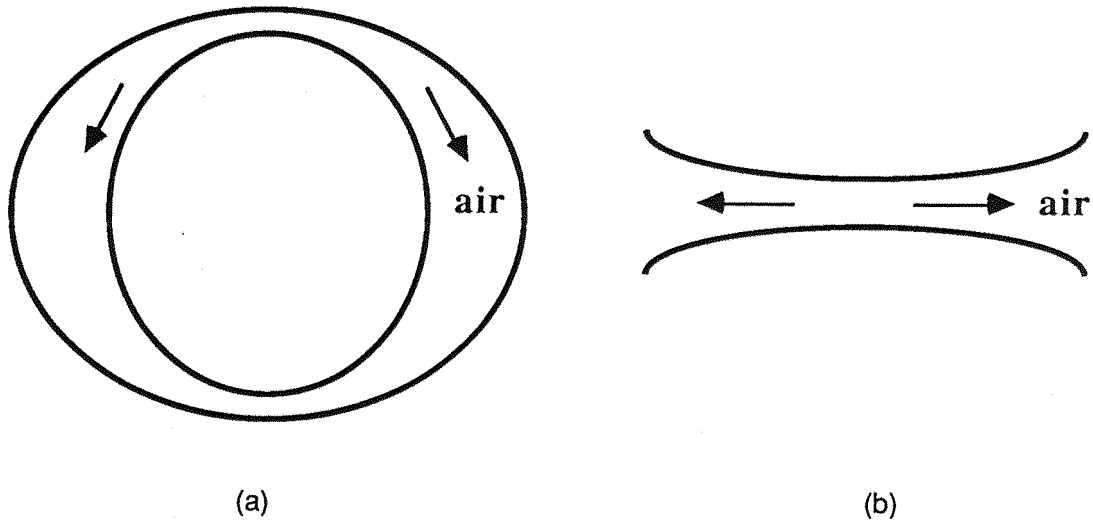

Figure 3.2 Air pumping by (a) double pipe, (b) double plate.

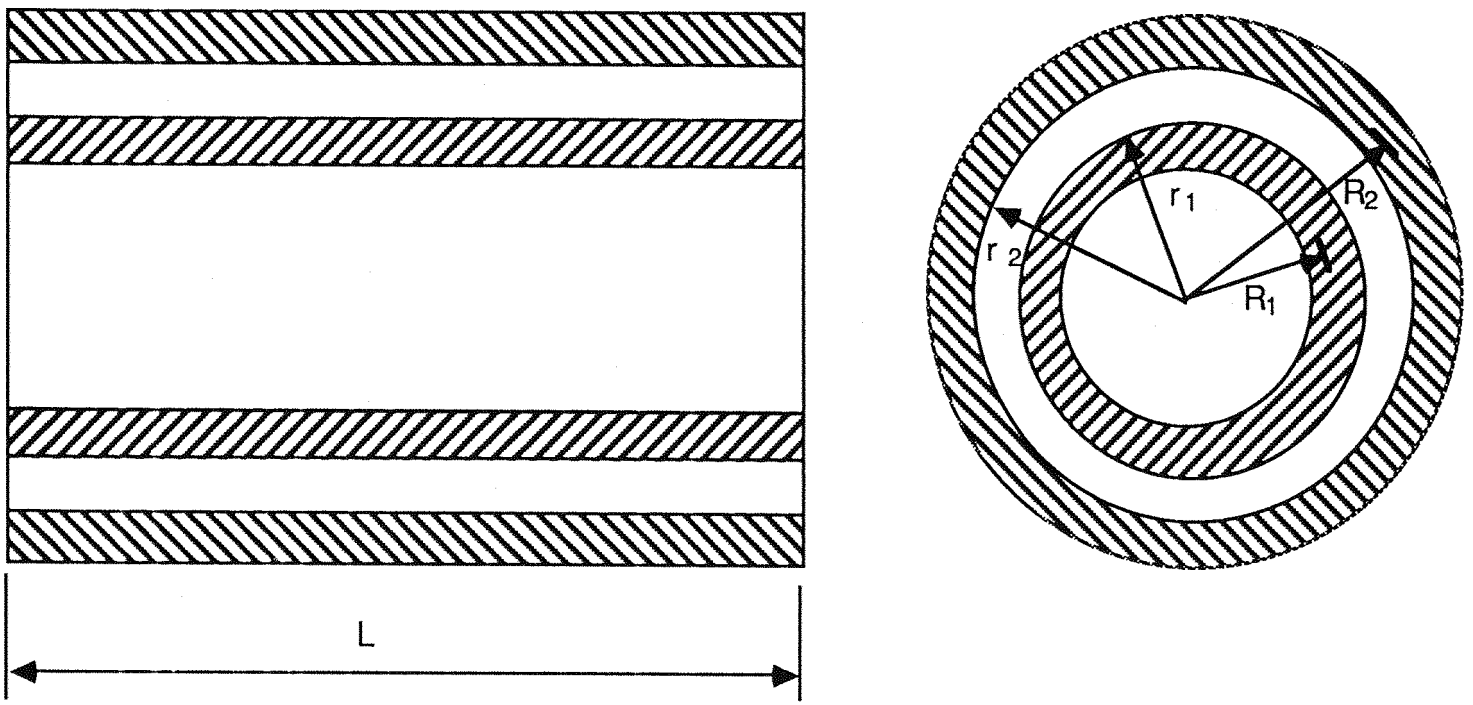

Figure 3.3 Schematic diagram of two concentric cylindrical shells containing a viscous fluid in the annulus.

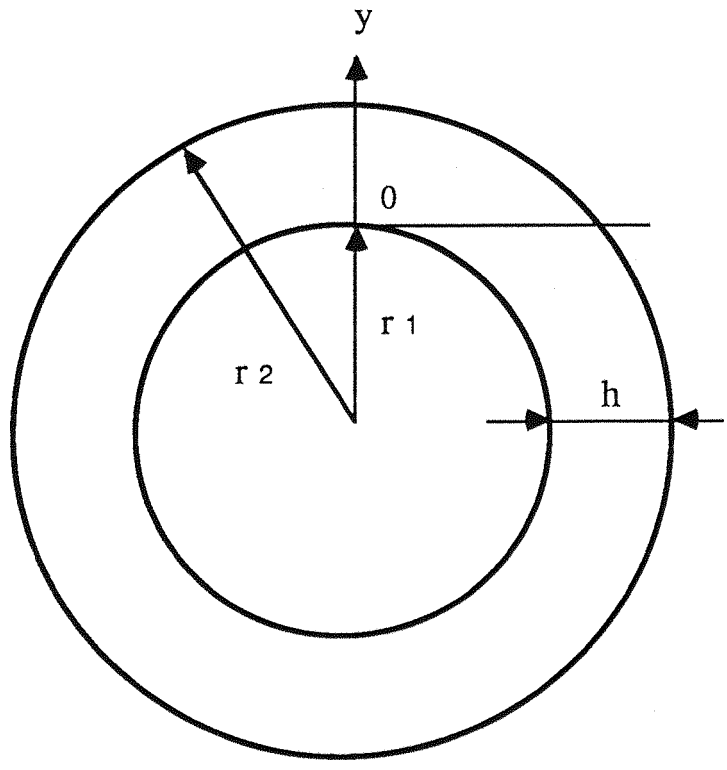

Figure 3.4 Coordinates of a double pipe system for Taylor's series.

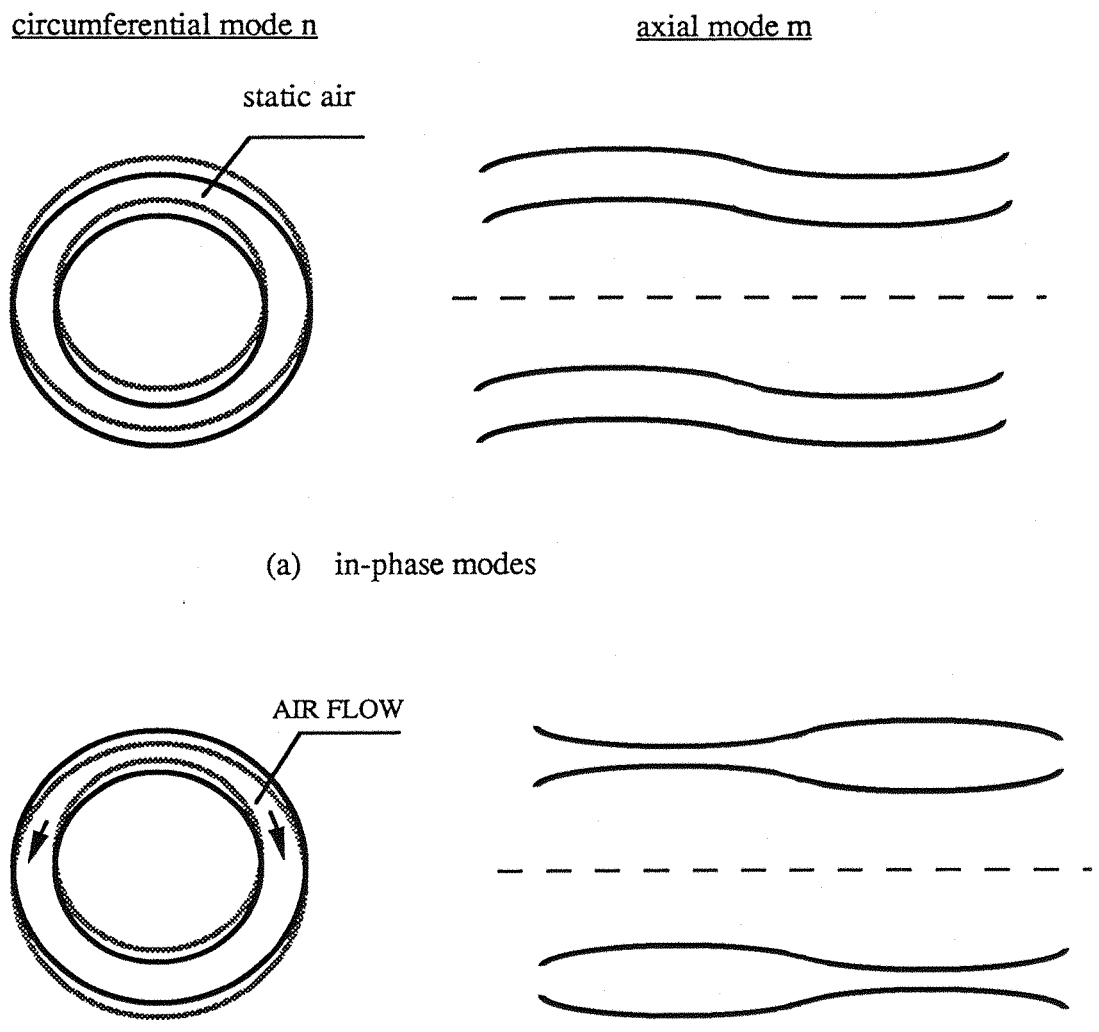

Figure 3.5 Mode shapes of double pipe vibration.
(a) In-phase modes.
(b) Out-of-phase modes.

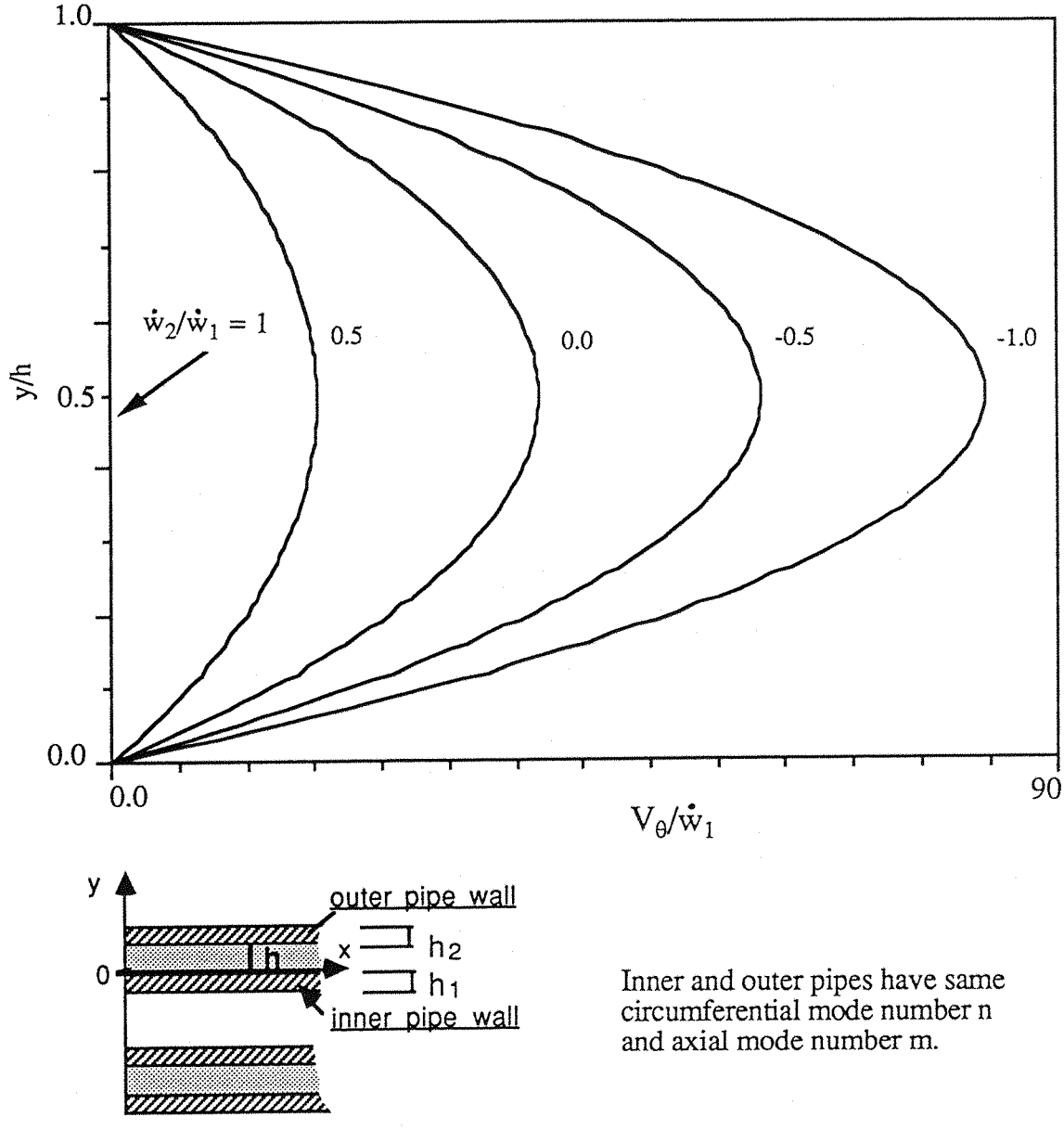

Figure 3.6 Tangential velocity profile of the air pumping with various ratios of w_2/w_1.

$\dot{w}_1$ = radial velocity of inner pipe.
$\dot{w}_2$ = radial velocity of outer pipe.
V_θ = tangential velocity of air.
n = 1, m =1. h = thickness of air gap.

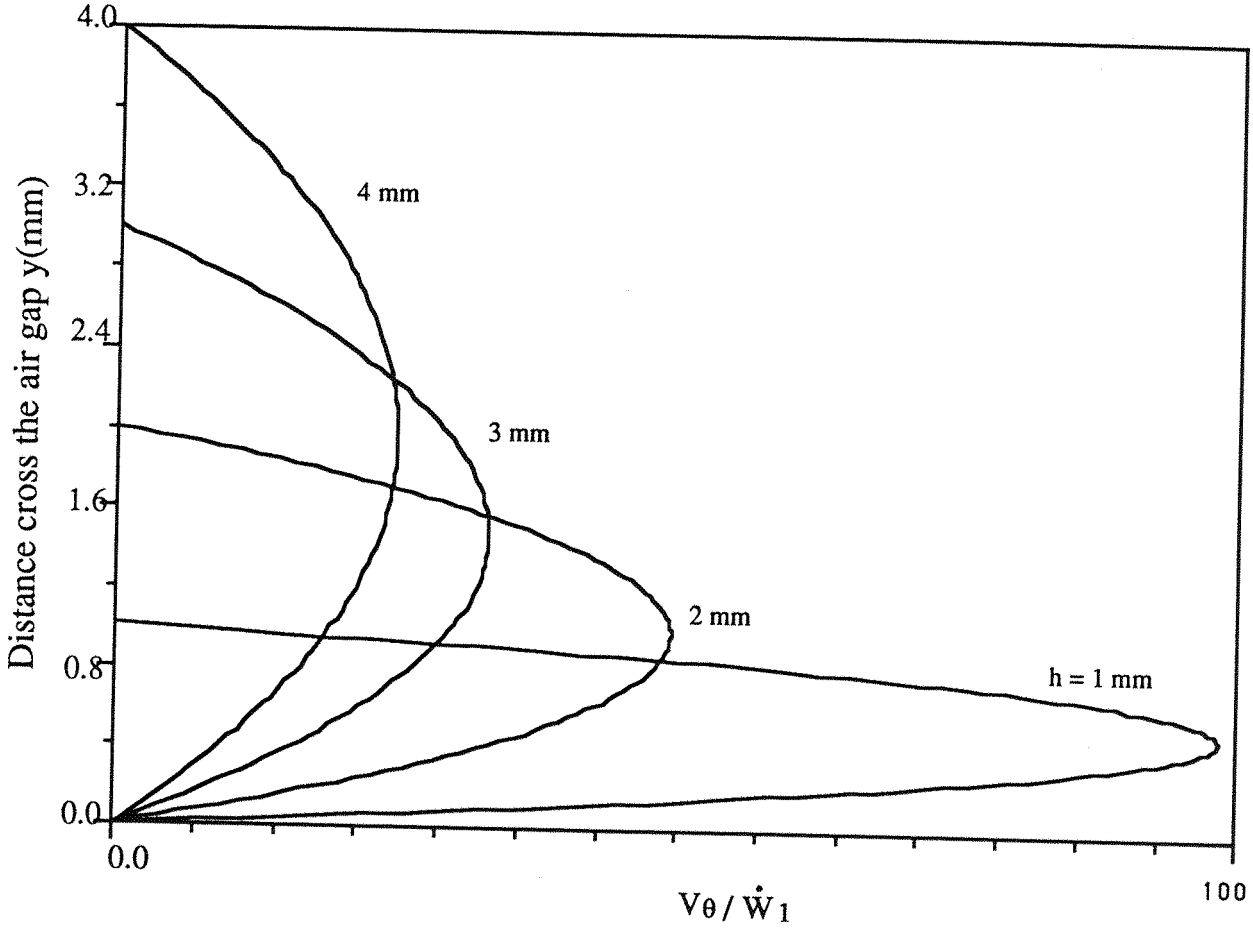

Figure 3.7 Tangential velocity profile of the air pumping with various air clearance h, n=1,m=1, w2/w1=-0.2.

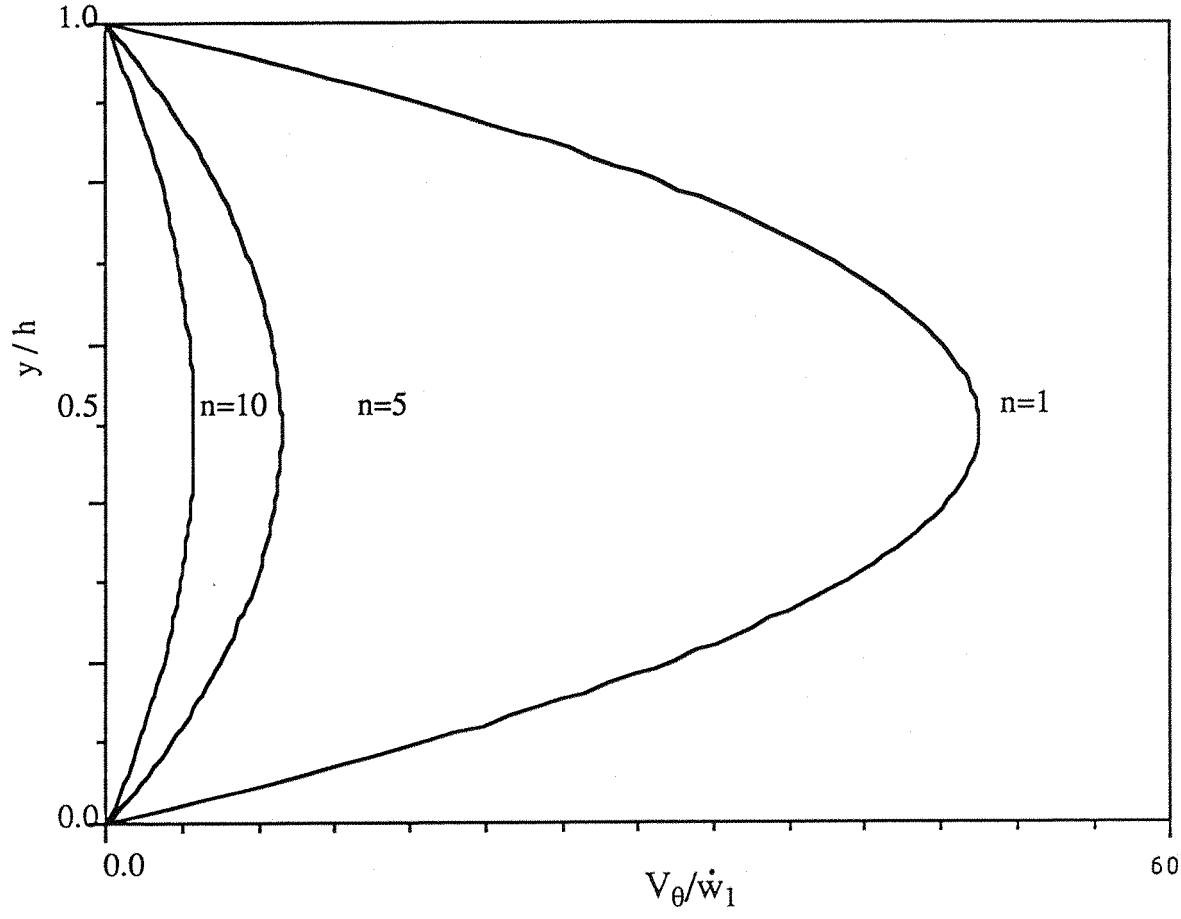

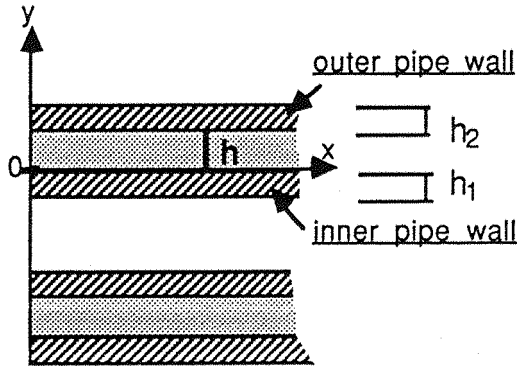

Inner and outer pipes have same circumferential mode number n and axial mode number m.

Figure 3.8 Tangential velocity profile of the air pumping with various circumferential wave numbers n.

$\dot{w}_1$ = radial velocity of inner pipe.
V_θ = tangential velocity of air.

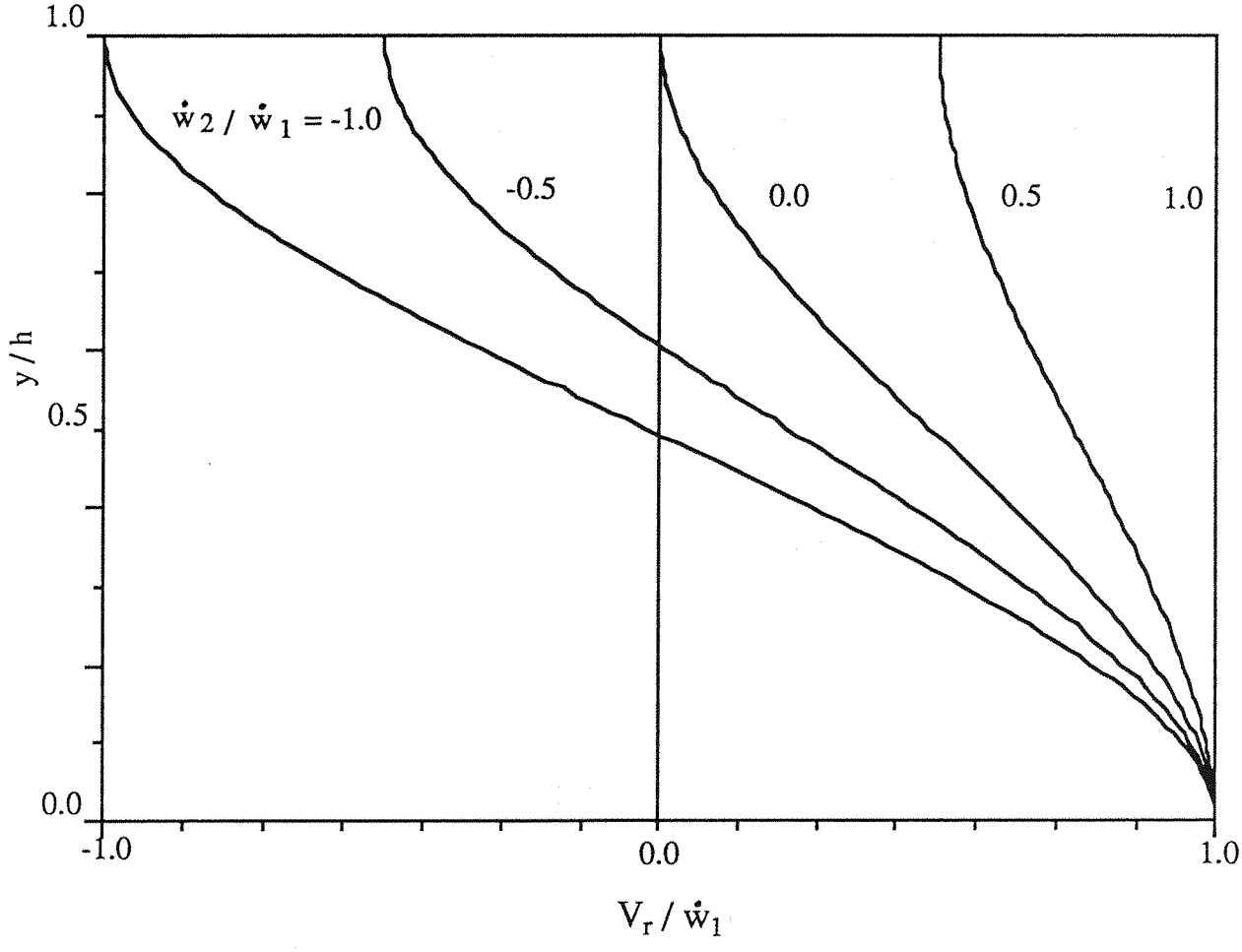

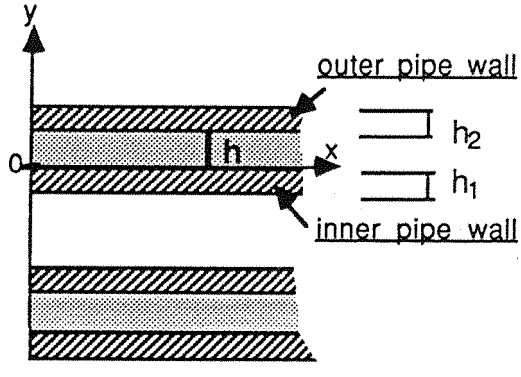

Inner and outer pipes have same circumferential mode number n and axial mode number m.

Figure 3.9 Radial velocity (V_θ) profile of the air pumping with various ratios of $\dot{w}_2/\dot{w}_1$.

$\dot{w}_1$ = radial velocity of inner pipe.
$\dot{w}_2$ = radial velocity of outer pipe.
V_r = radial velocity of air.
h = 2 mm, m = 1, n =1.

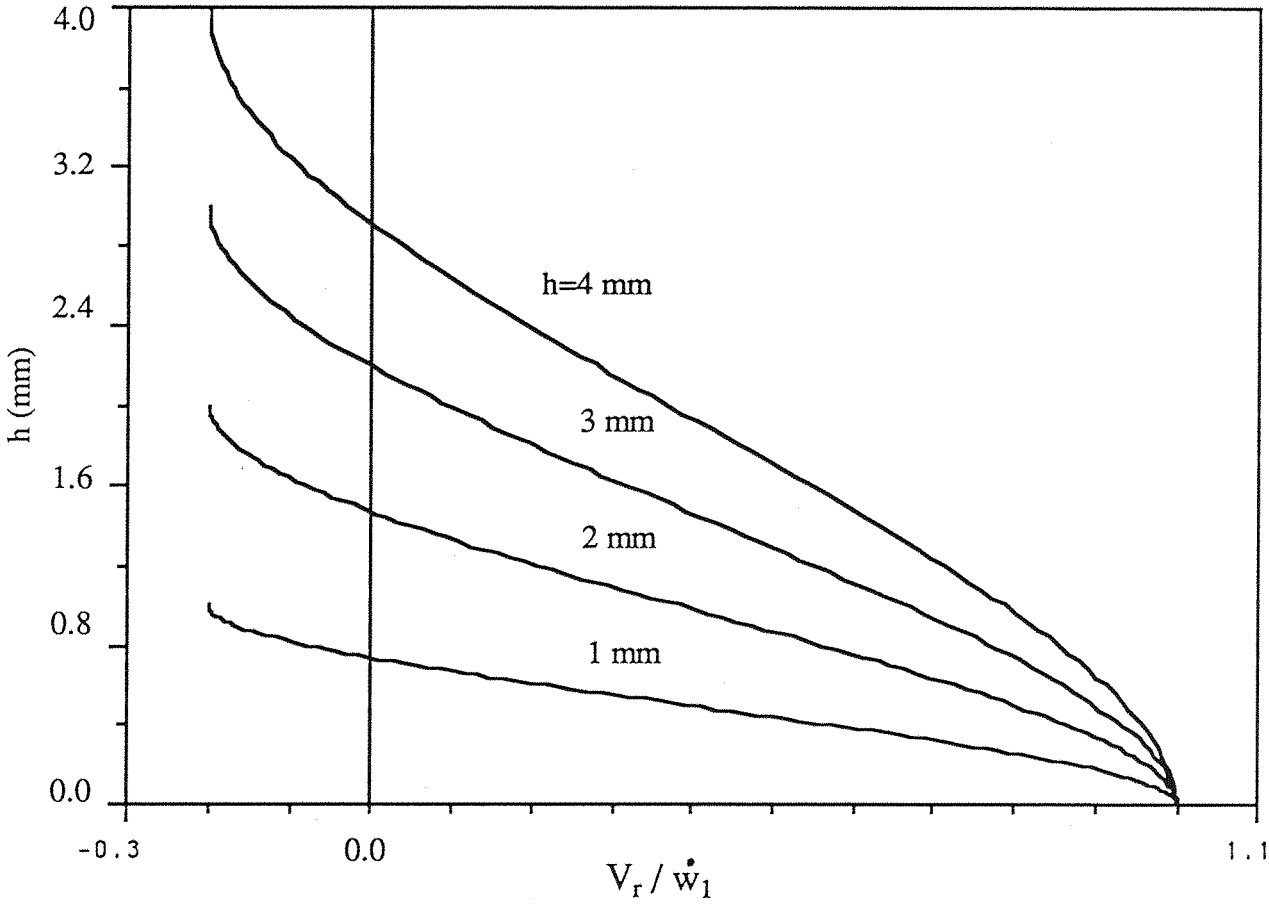

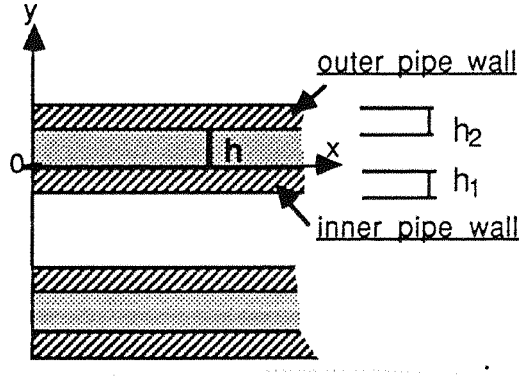

Inner and outer pipes have same circumferential mode number n and axial mode number m.

Figure 3.10 Radial velocity (V_θ) profile of the air pumping with various air gap clearances.

$\dot{w}_1$ = radial velocity of inner pipe.
V_r = radial velocity of air.
h = thickness of air gap clearance
$\dot{v}_1/\dot{w}_1 = 0.1$, $\dot{v}_2/\dot{w}_1 = 0.001$, $\dot{w}_2/\dot{w}_1 = -0.2$.
$\dot{v}_1/\dot{v}_2$ = tangential velocities of inner and outer pipes.

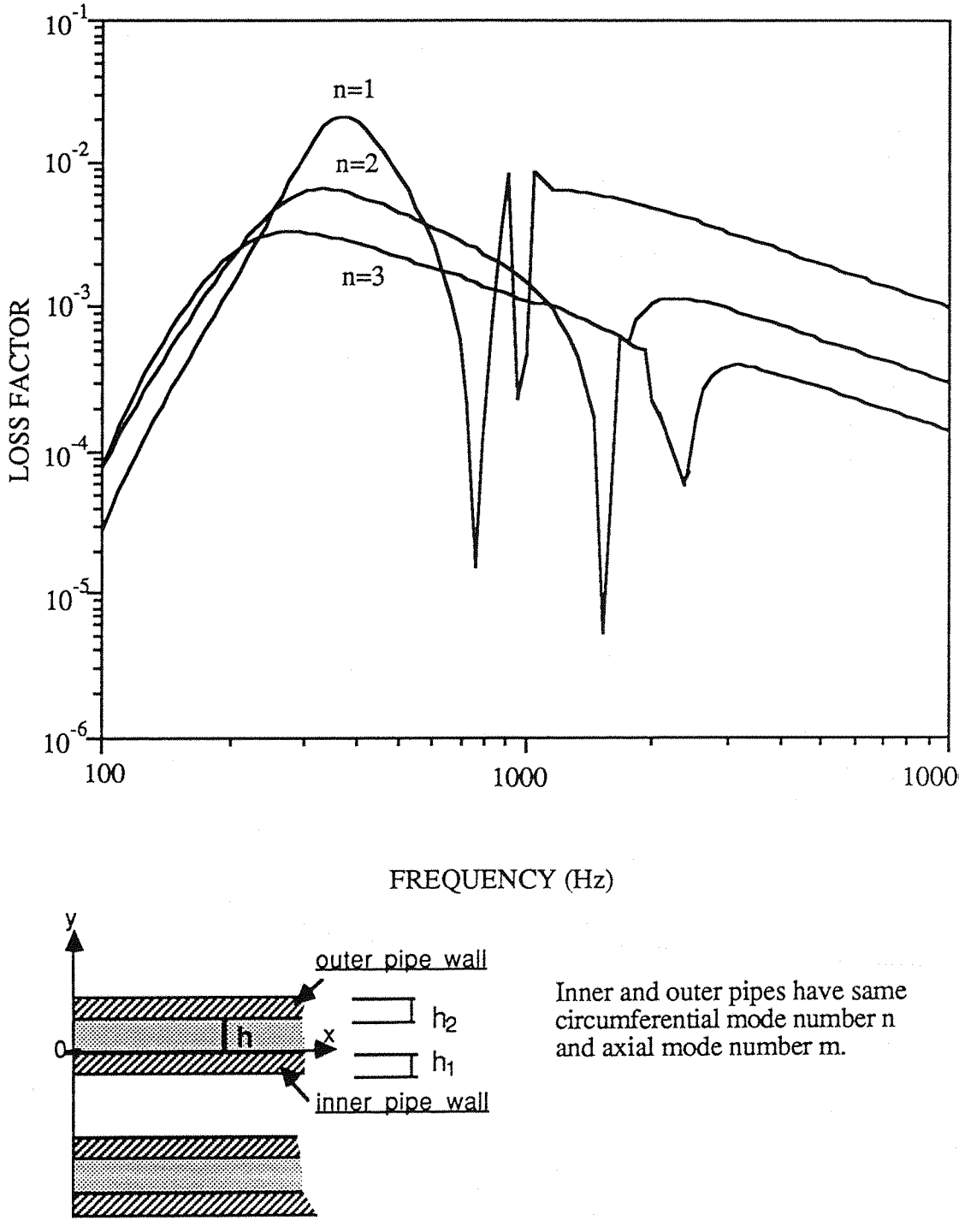

Figure 3.11 Loss factor with various circumferential mode numbers n.

r_1= 53 mm, h_1 = 2.2 mm, h_2 = 2 mm,
h = 1.0 mm, T = 20^0 C.

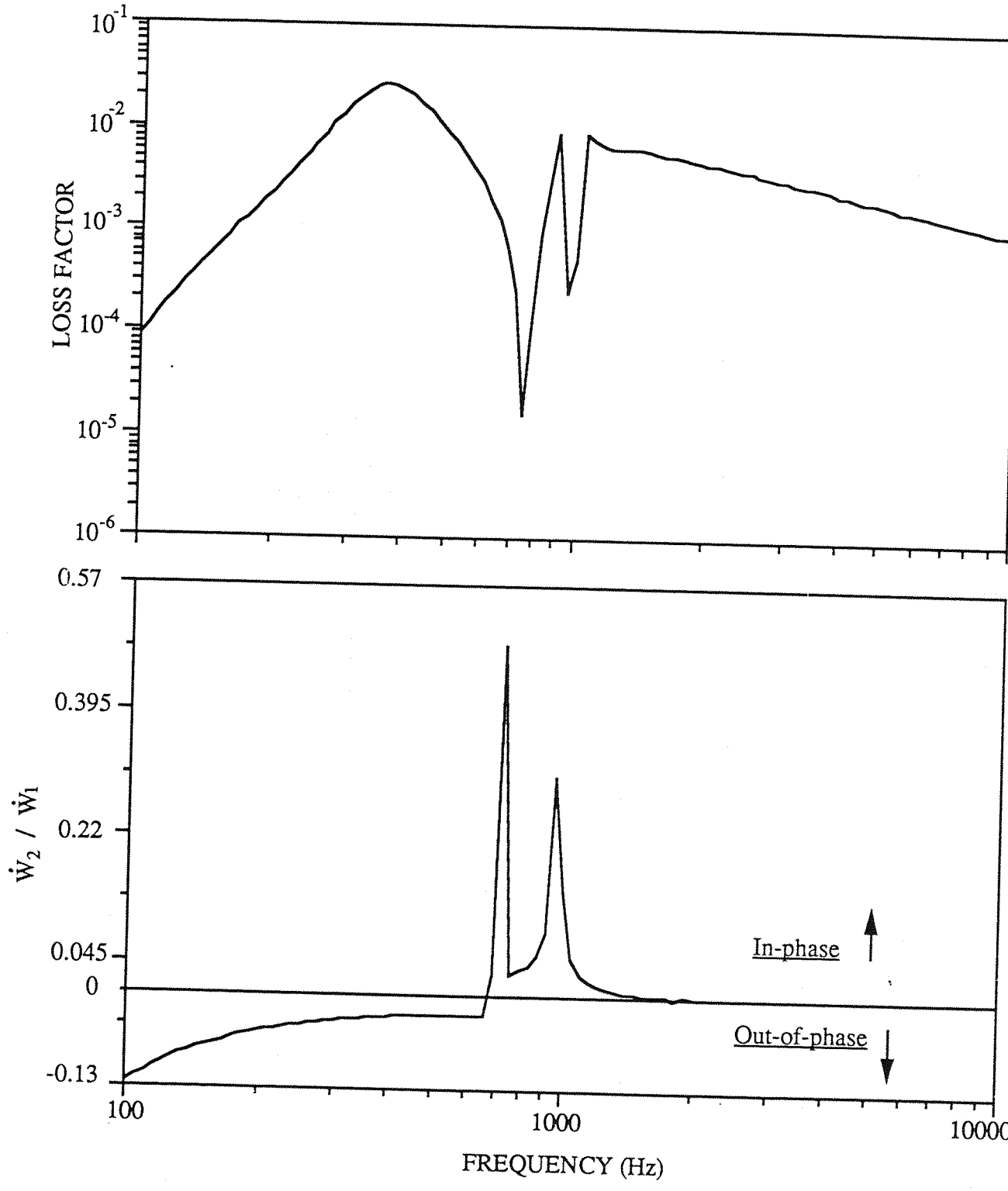

Figure 3.12 Vibration modes with in-phase and out-of-phase motion between the two pipes.

$\dot{w}_1$ = radial velocity of inner pipe.
$\dot{w}_2$ = radial velocity of outer pipe.

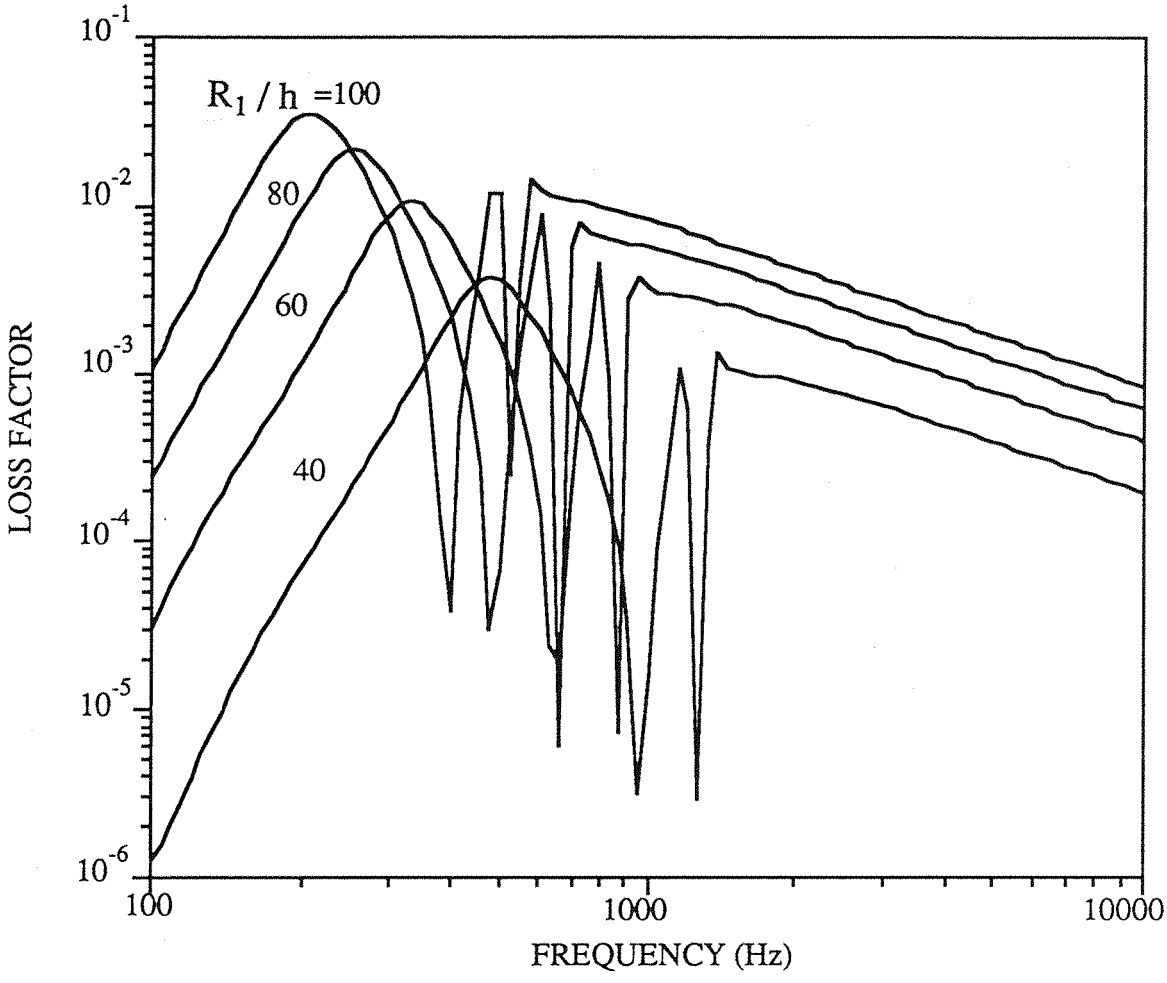

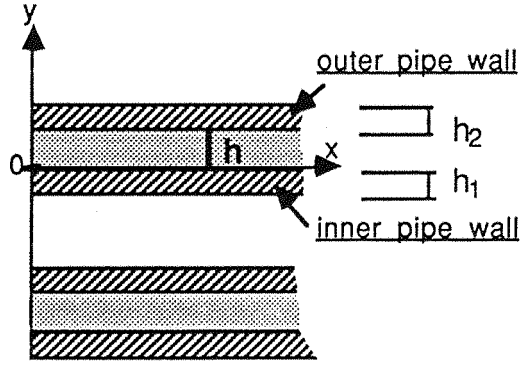

Inner and outer pipes have same circumferential mode number n and axial mode number m.

n = 1, m =1

Figure 3.13 Predicted loss factor with various ratios of radius of inner pipe to air gap.

h = 1.0 mm, h_1 = 2 mm, h_2 = 2 mm, T = 20^0 C.

R_1 = mean radius, h = thickness of air gap.

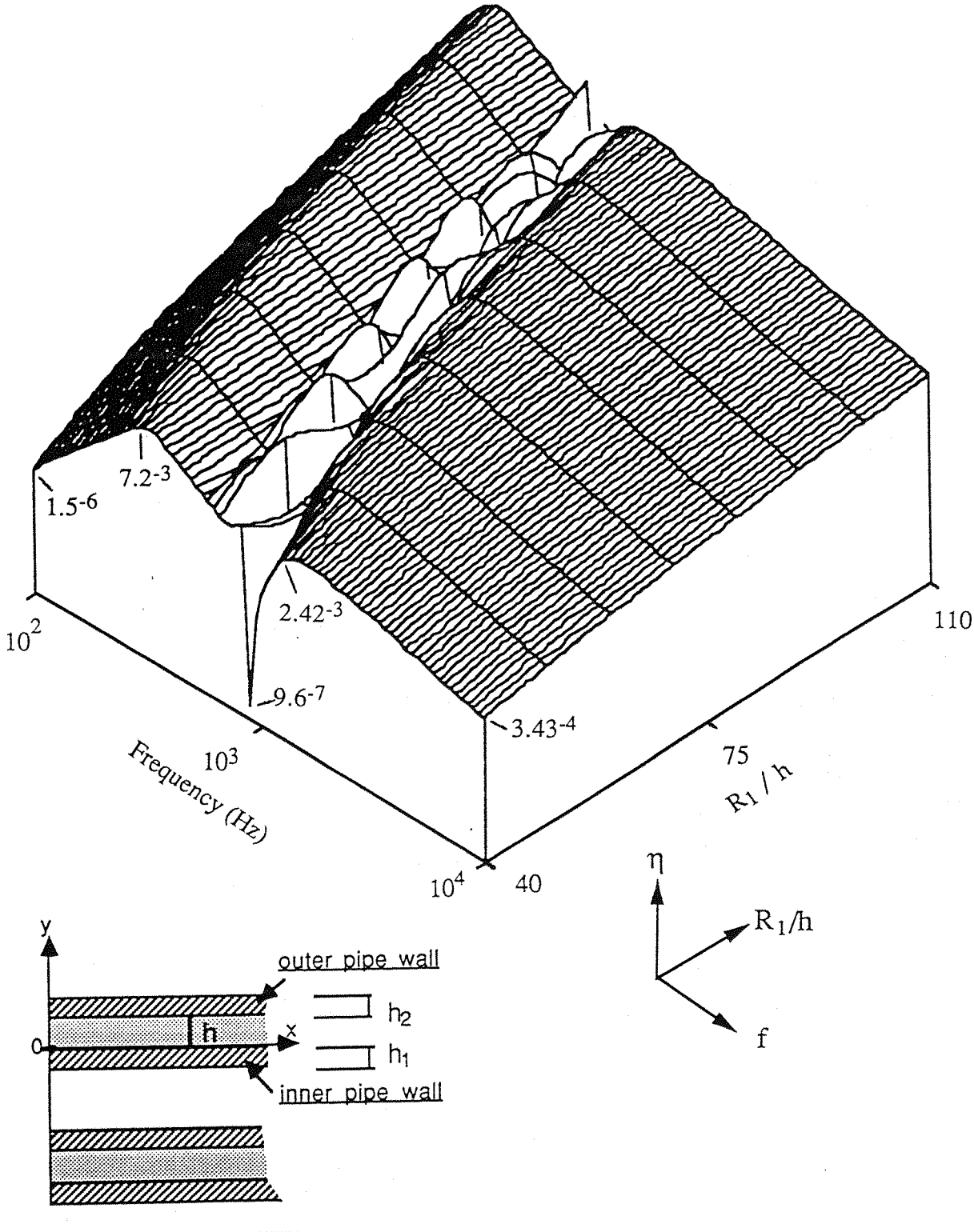

Figure 3.14 Three dimensional graph of predicted loss factor versus ratio of R_1 / h and frequency.

h = 1.0 mm, h_1 = 2.2 mm, h_2 = 2 mm, T = 20^0 C.
η = loss factor, f = frequency.
R_1 = mean radius, h = thickness of air gap clearance.

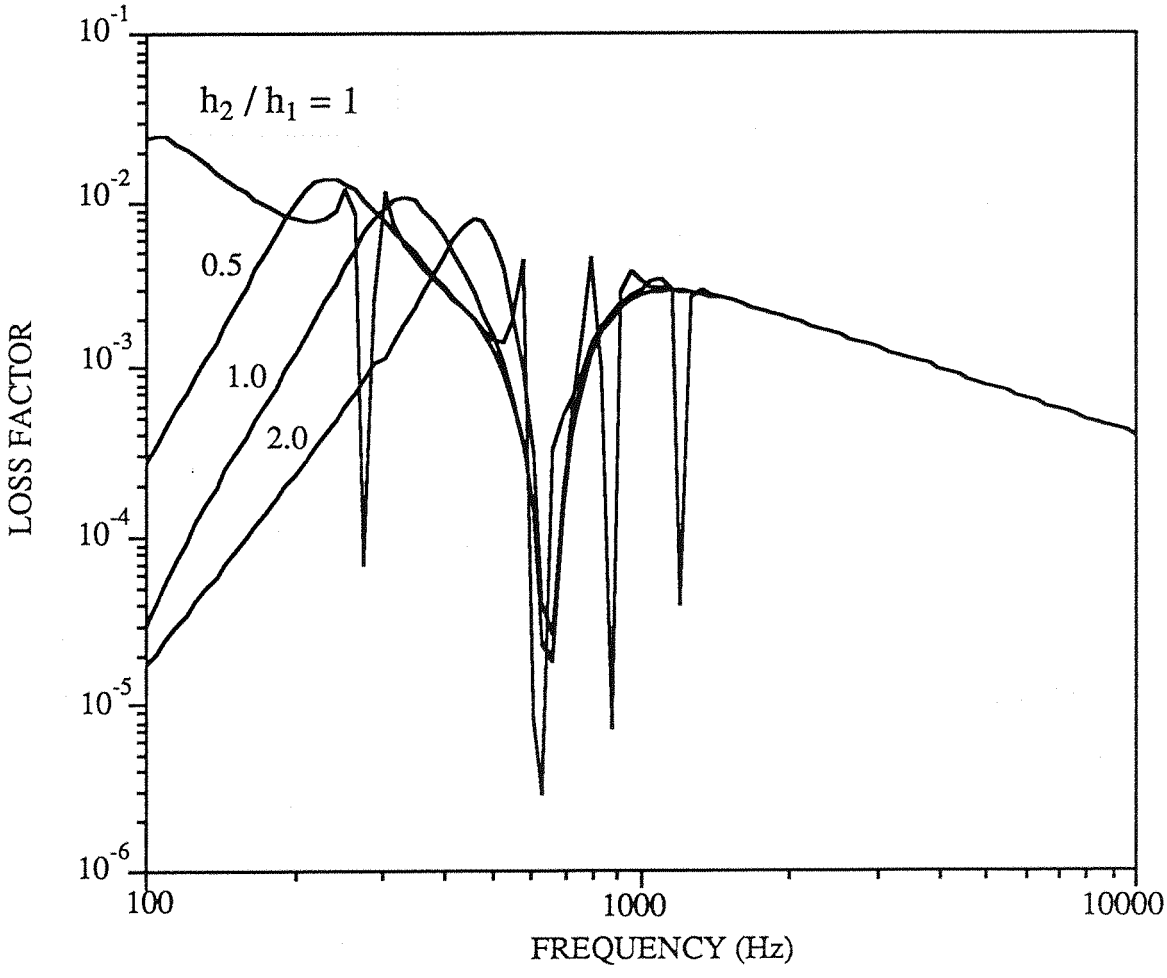

Figure 3.15 Predicted loss factor with various ratios of inner and outer thicknesses of pipe.

$h = 1.0$ mm, $h_1 = 2$ mm, $r_1 = 60$ mm, $T = 20^0$ C.

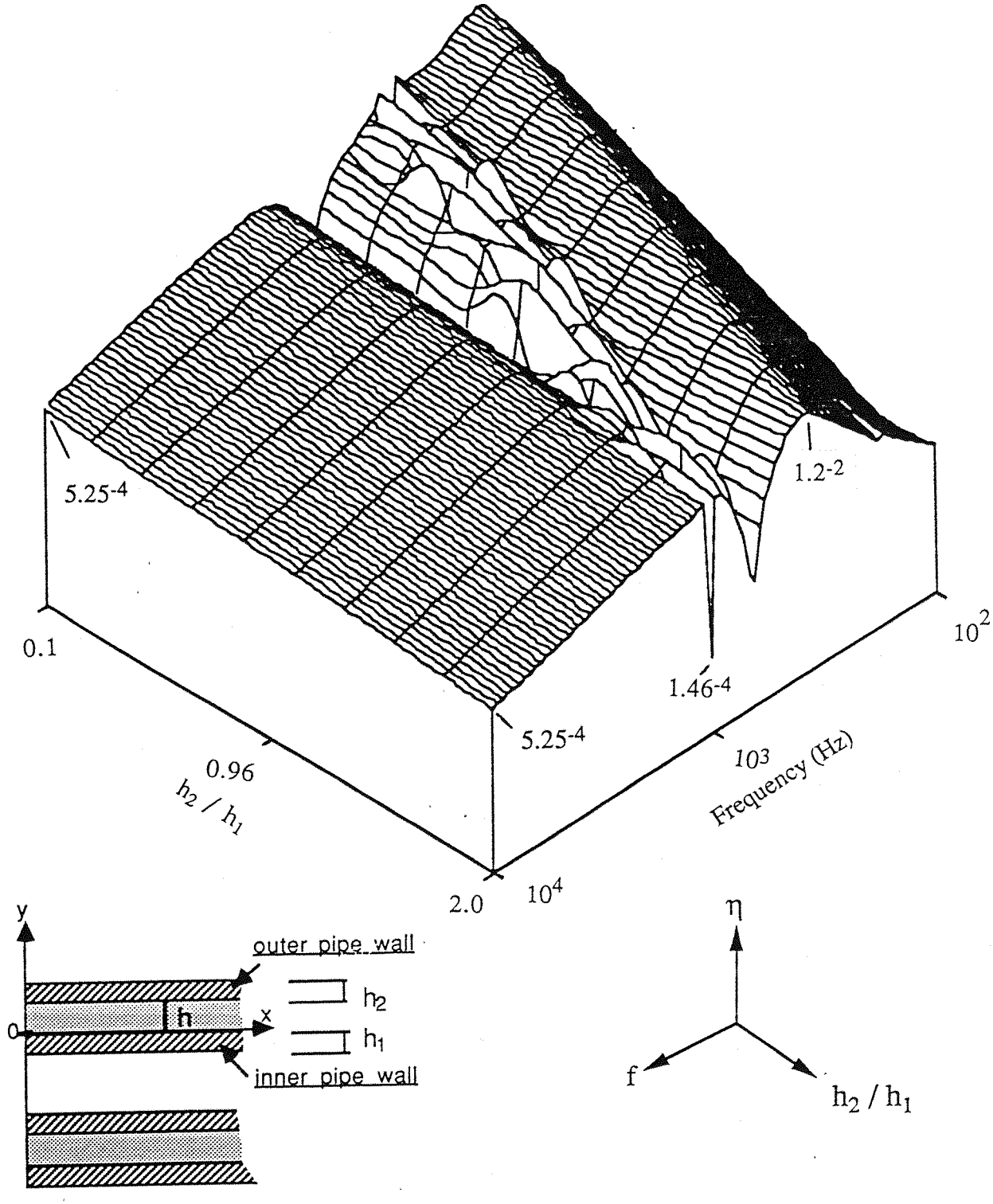

Figure 3.16 Three dimensional graph of predicted loss factor versus ratio of h_2 / h_1 and frequency.

h = 1.0 mm, h_1 = 2 mm, r_1 = 60 mm, T = 20^0 C.
η = loss factor, f = frequency.

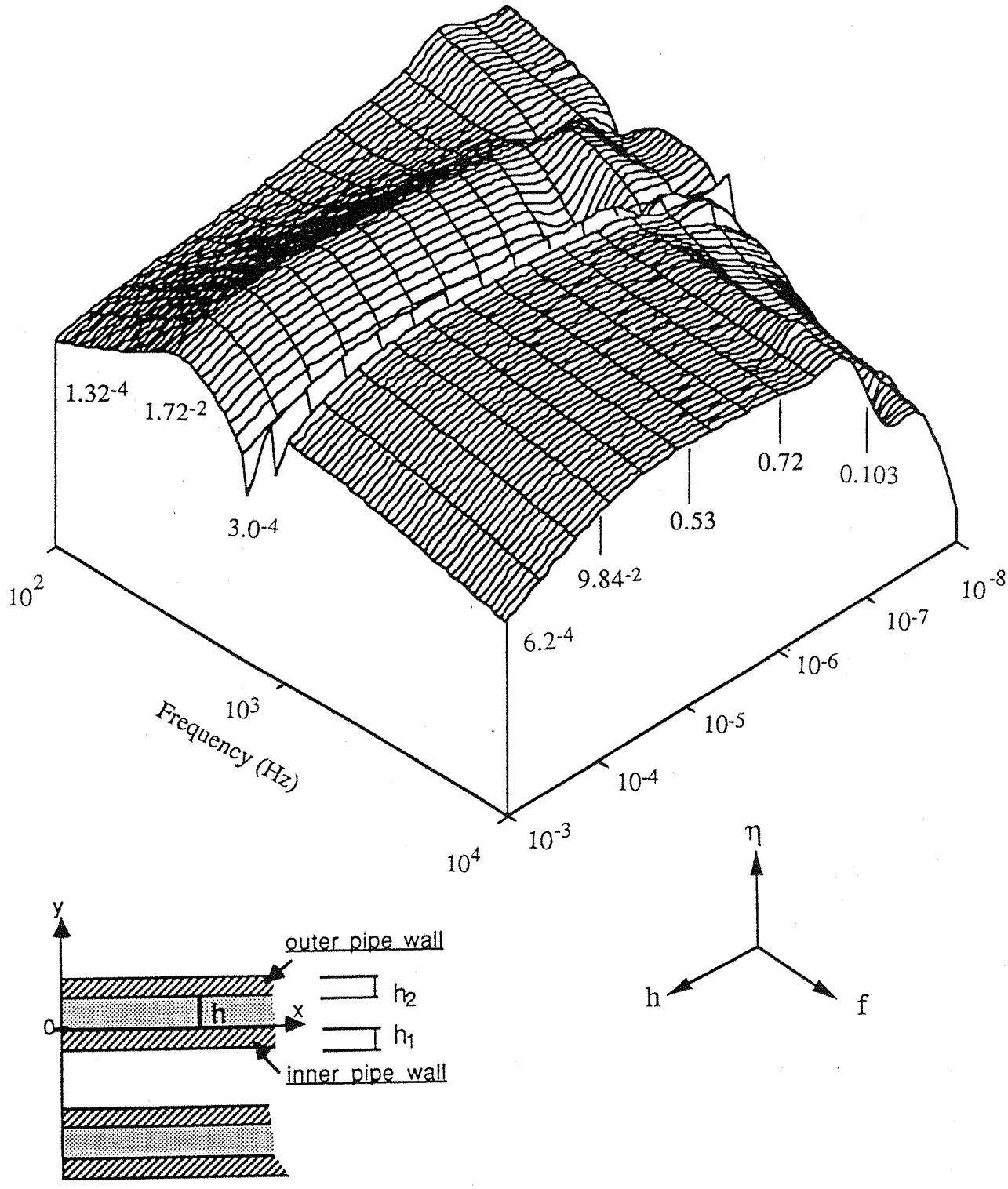

Figure 3.17 Three dimensional graph of predicted loss factor versus air gap h and frequency.

h_1 = 2 mm, h_2 = 2 mm, r_1 = 60 mm, T = 20^0 C.
η = loss factor, f = frequency.
h = thickness of air gap.

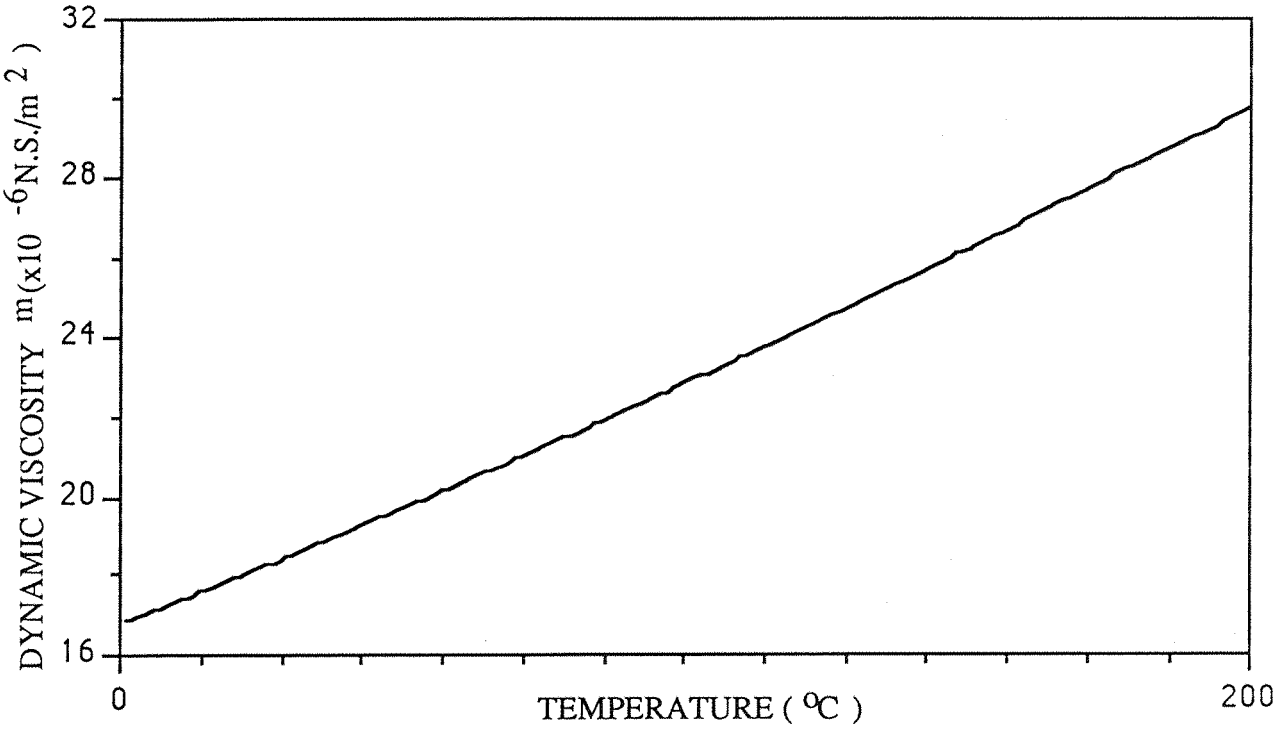

Figure 3.18 Relationship between dynamic viscosity of air and temperature at 1 atm pressure.

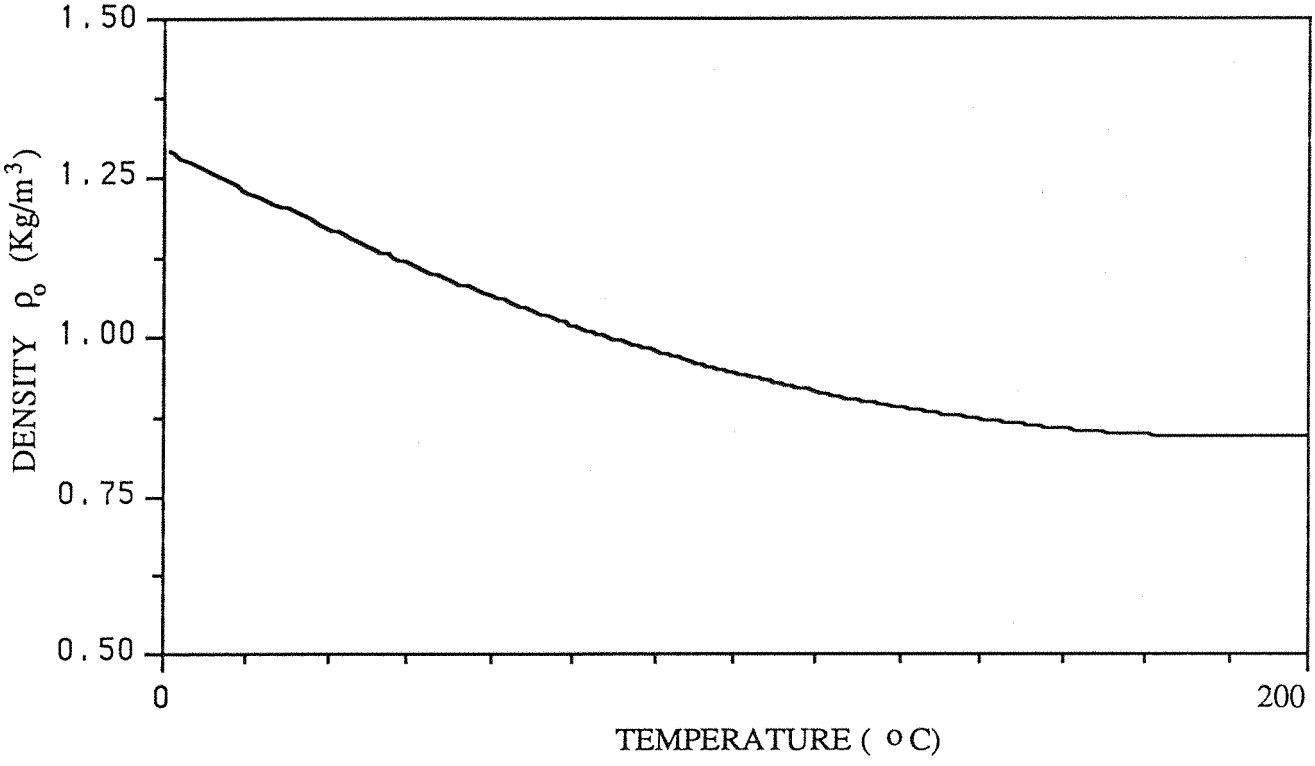

Figure 3.19 Relationship between density of air and temperature at 1 atm pressure.

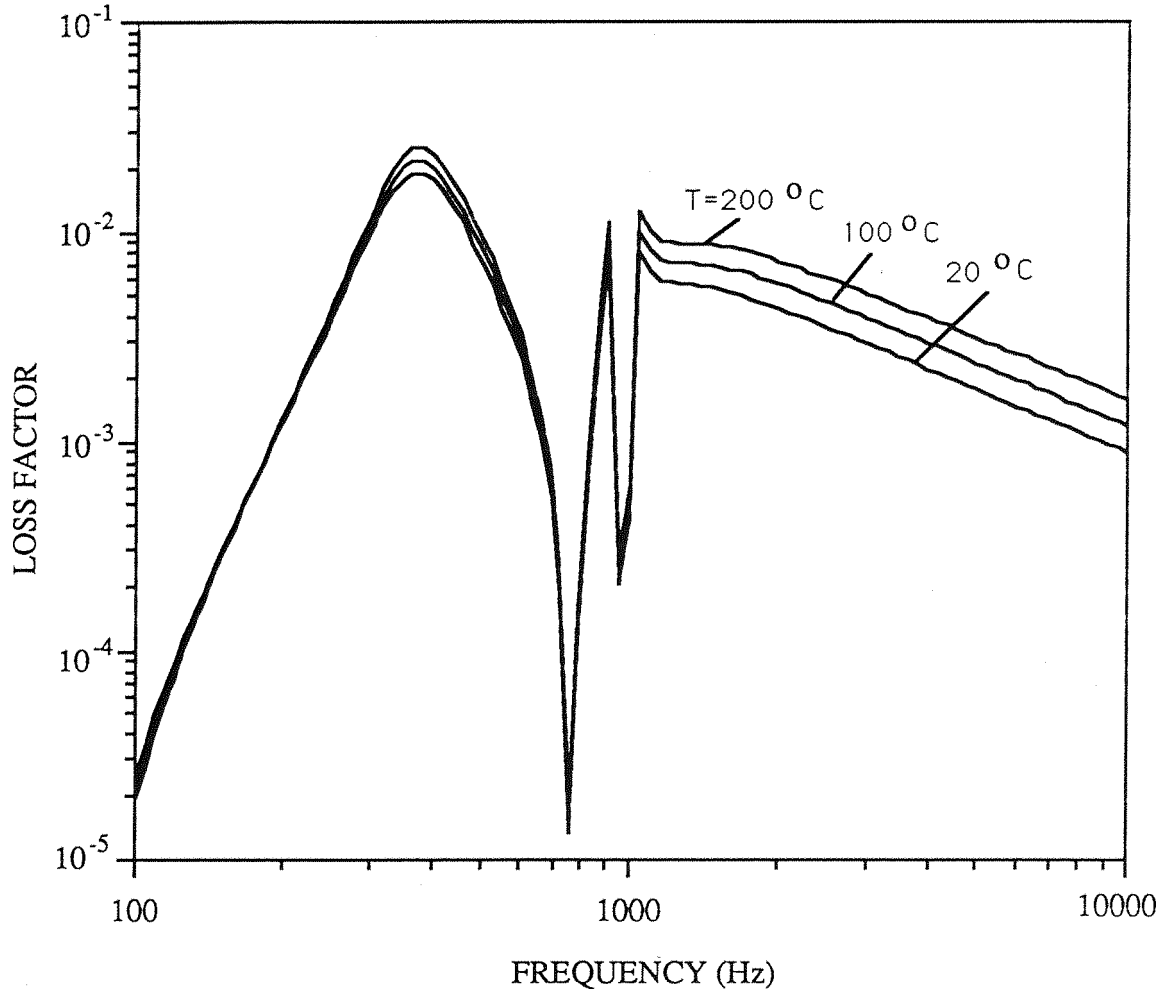

Figure 3.20 Predicted loss factors of a double pipe system at various temperatures of air

$h = 1.0$ mm, $h_1 = 2.2$ mm, $h_2 = 2$ mm,
$r_1 = 60$ mm, $T = 20^0$ C.

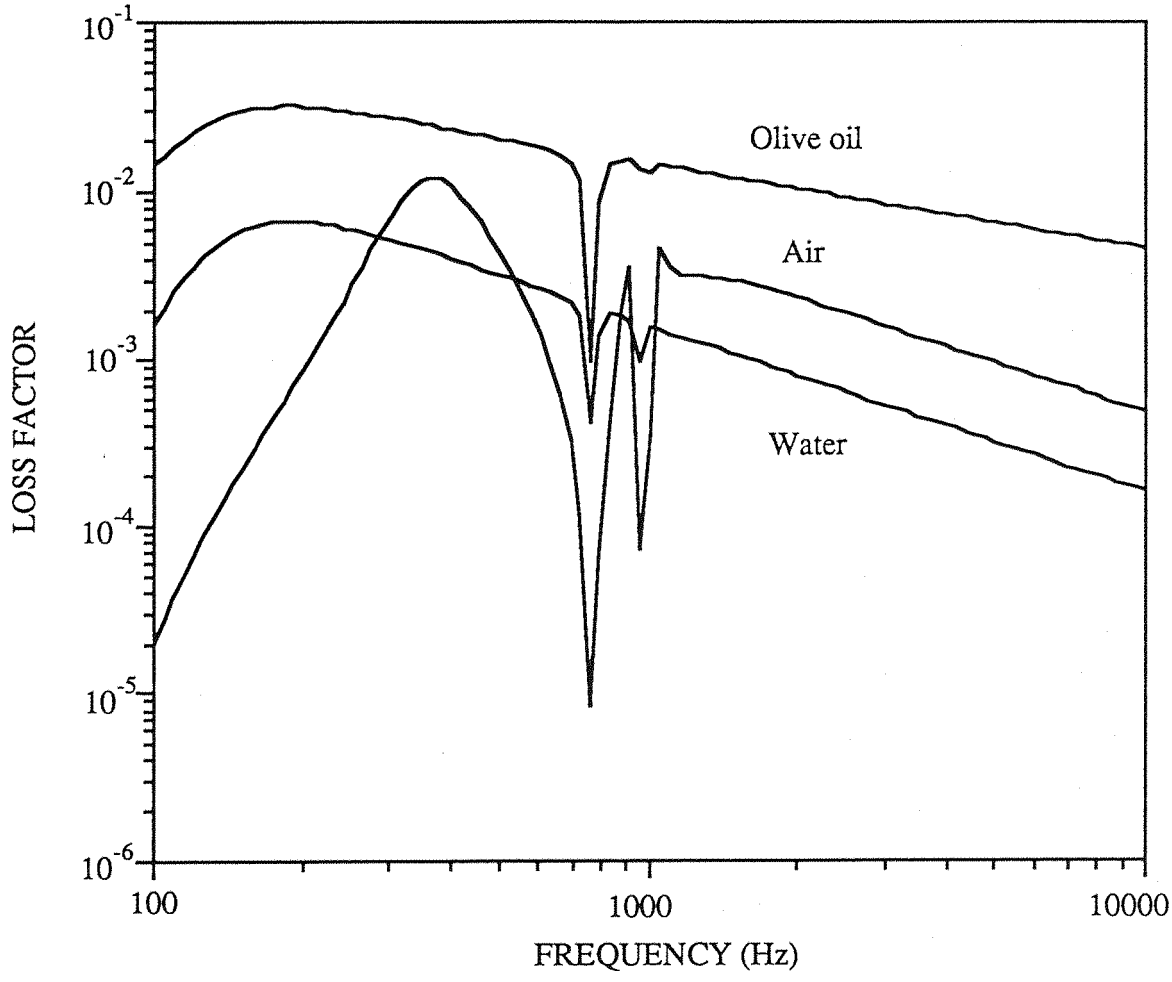

Figure 3.21 Predicted loss factors of a double pipe system with air, water and Olive oil.

$h = 1.0$ mm, $h_1 = 2.2$ mm, $h_2 = 2$ mm,
$r_1 = 60$ mm, $T = 20^0$ C.

CHAPTER 4. MEASUREMENT OF THE LOSS FACTORS OF A DOUBLE PIPE SYSTEM.

4.1 INTRODUCTION.

This chapter describes the measurements of loss factors of a double pipe system and intends to experimentally verify the theoretical predictions made in chapter 3.

As the initial energy dissipation in the structural materials of the pipes was neglected in the theory of chapter 3, the loss factor of a single pipe needs to be measured and compared with the loss factor of the double pipe system with an air or oil filled gap. To prove the squeeze film damping phenomena, loss factors were measured at reduced air pressure conditions.

Resonance frequencies and mode shapes play important roles in damping of a double pipe system. Natural frequencies of pipes are examined and in-phase and out-of-phase modes are verified experimentally.

4.2 METHOD USED FOR DAMPING MEASUREMENT.

The decay time method was chosen to measure the loss factor as it is simple to use and generally yields more accurate results than other methods. For decay measurements, the decay of the vibrations is observed after the exitation suddenly ceased. Energy decay is described by the function $e^{-\eta\omega t}$. By measuring the reverberation time T, the loss factor is determined from the relation,

$$\eta = \frac{\ln 10^6}{\omega T_{60}} \approx \frac{2.2}{f T_{60}} \qquad (4.1)$$

where

f = the measured individual resonance frequency.

T_{60} = the reverberation time which is the duration for the response to decay 60 dB.

4.3. INSTRUMENTATION.

The time decay method was used in the experiment to measure the loss factor of a single pipe and a double pipe system with an air or oil filled annular gap. The single or double

pipes studied here were all thin-walled cylindrical shells. The loss factor was determined according to equation 4.1.

The pipes to be tested were suspended to represent free-free boundary conditions as shown in figure 4.1. The inner pipe was excited in flexural vibration by a coil-magnet system driven by a random signal generator (for the purpose of transfer function measurement) or a sine wave generator (for loss factor measurement) via a power amplifer.

The vibration was detected by an accelerometer attached at the other end of the outer pipe. The acceleration signal was amplified to achieve the voltage level required by the computer, as shown in figure 4.2. The signal was acquired by an analogue to digital converter, the data could then be analysed by computer. For measuring the decay of the acceleration, the exciter was disconnected from the power amplifer and the computer was triggered to acquire data. Figure 4.2 shows the instrumentation for the loss factor measurements.

The computer was used for data processing; the acceleration waveform was converted to a logarithmic scale and then drawn into a decay curve. The decay time T_{60} was read from the decay curve and then loss factor was calculated. Accelerance (acceleration (ω)/force (ω)) could also be calculated from the acquired acceleration and force signals when a random signal was used as the excitation. Figure 4.3 shows an example of measured decay curve for a pipe.

4.4 MEASUREMENT OF LOSS FACTOR DUE TO AIR PUMPING IN A DOUBLE PIPE SYSTEM.

To measure the loss factors of a double pipe system, the three steel pipes used had the following dimensions:

	L (mm)	d (mm)	D (mm)	R (mm)	h (mm)
Pipe 1	1000	91	95	46.5	2
Pipe 2	1000	98	102.3	50.075	2.15
Pipe 3	1000	104	108	53	2

where

L = length,

d = inner diameter,

D = outer diameter,

R = mean radius,

h = thickness of pipe wall

4.4.1. Natural frequencies compared with shell theory and beam theory.

As loss factors were measured at resonance frequencies, and accelerances could also be plotted, the opportunity was taken to compare measured resonance frequencies and predicted natural frequencies. From measured transfer function of the three pipes shown in figure 4.4, natural frequencies were obtained. The results were compared with natural frequencies computed from the theory in chapter 2 and beam theory,

	Natural frequency in Hz		
	Experiment	Shell theory (n,m)	Difference($\frac{\lvert f_{exp}-f_{theory}\rvert}{f_{exp}}$) %
Pipe 1	571	551 (1,2)	3.5
	596	601 (2,1)	0.8
	640	638 (2,2)	0.3
	806	791 (2,3)	0.6
	1162	1142 (2,4)	1.7
	1440	1374 (1,3)	4.5
	Beam theory	605	
Pipe 2	527	536 (1,2)	1.7
	571	570 (2,1)	0.2
	615	601 (2,2)	2.3
	776	786 (2,3)	1.3
	1176	1170 (2,4)	0.5
	1440	1436 (1,3)	0.3
	Beam theory	651	
Pipe 3	464	495 (2,1)	6
	522	537 (2,2)	2.9
	640	609 (1,2)	4.8
	752	755 (2,3)	0.4
	1191	1177 (2,4)	1.2
	Beam theory	690	

where (n,m) = (circumferential mode, axial mode).
Experimental results and verification of mode shapes will be discussed further in chapter 5.
The equation for natural frequencies according to beam theory [69] is

$$\cos \beta L \cosh \beta L = 1$$

where

$\beta^4 = m \omega^2 / EI$

m = mass per length

$\omega = 2 \pi f$

f = frequency

E = Young's modulus

I = second moment of area of the cross-section.

Predicted natural frequencies from the theory of thin-walled cylindrical shells in chapter 2 agree quite well with experimental data.

4.4.2 Measurement of the loss factors of a double pipe system for a range of air pressure.

To establish whether or not the damping observed was due to air damping, a double pipe system was suspended in a vacuum chamber shown in figure 4.5. Loss factors of the double pipe system were measured at various air pressures. The double pipe system consisted of two pipes (Pipe 1+2), pipe 1 was the inner pipe and pipe 2 the outer pipe, with a 1.5 mm air gap. The two pipes were separated by silicon rubber at both ends, as shown in figure 4.6

Loss factors of the double pipe with 1.5 mm air gap were measured at air pressures of 1 atm (780 mmHg), 0.43 atm (335.6 mmHg) and 0.166 atm (127 mmHg) respectively. The results, shown in figure 4.7, indicate that loss factors decreased with decreasing air pressure. Thus, it is proved that damping can be created by the air gap of a double pipe system.

The measured loss factor is low at the first distinct in-phase mode shown in figure 4.7. This result is consistent with the theoretical prediction in chapter 3 that the loss factor is low at the frequencies where in-phase modes occur. The experimental results also indicated that the loss factor at the in-phase mode condition is little dependent upon air pressure, which means that there is less effect of air pumping at the in-phase condition, as would be

expected. The effect of the squeeze air film on resonance frequency can also be observed from transfer functions (accelerance) of the double pipe system at two air pressures as shown in figure 4.8, where the frequencies are slightly shifted to higher frequency with low air pressure.

4.5 COMPARISON OF MEASURED LOSS FACTORS OF THE DOUBLE PIPE SYSTEM WITH THEORETICAL VALUES.

4.5.1 Theoretical and experimental loss factors of a double pipe system with 1.5 mm and 0.85 mm air gaps.

Two double pipe systems were used in the study, Pipes 1+2 with 1.5 mm air gap and Pipes 2+3 with 0.85 mm air gap. Again, free-free boundary conditions were used. The measured loss factors of a double pipe system (pipes 1+2) are compared with those of a single pipe (pipe 2) in figure 4.9. The results show increase of loss factors from $2x10^{-3}$ to $1x10^{-2}$ achieved by squeeze air film damping. Figures 4.10 and 4.11 show measured and theoretical loss factors of Pipes 1+2 and 2+3 respectively. The comparison of results shows that the theoretical results agree with experimental values fairly well. Thus, it may be concluded from the trends observed that loss factor in a double pipe system is low at low frequencies because of low air pumping velocities created and the loss factor is high in the mid-frequency range but low again at high frequencies since the frequency becomes too high to allow air flow and less energy is dissipated by the air in the gap..

4.5.2 Detecting of in phase and out-of-phase modes.

It is necessary to know whether the pipes are moving in-phase or out-of-phase, because there is no air pumping flow at the in-phase condition according to the theory in chapter 3. For measuring relative phase, two accelerometers were fixed at the ends of the pipes as shown in figure 4.6. Two measured responses of in-phase and out-of phase modes are shown in figure 4.12 (a) and (b), from which the vibration behaviour of the double pipe system can be seen clearly. (Note the relative orientation of the accelerometers in fig 4.6)

4.5.3 Theoretical and experimental loss factors due to oil damping.

To investigate the loss factor due to liquid damping in a double pipe system, the experimental loss factor measurement was extended to oil damping. The double pipe

system with oil in the annulus was used, composed of pipes 2+3 with 0.85 mm oil annulus gap. The oil in the gap between the pipes was Shell Oil (SEA 15W/40). The oil data are,

	40° C	100° C
Kinematical viscosity (10^{-6} m^2/sec)	116.6	14.4
Density (Kg/m^3)	890	890

where kinematical viscosity was from data supplied by Shell [70], density was measured at 25^0 C temperature on presumption that the density of the oil would be constant up to 100^0C.

The oil was sealed in the annulus by thin rubber film or by silicon rubber seals as shown in figure 4.13. Measured loss factors are shown in figures 4.14 and 4.15. Figure 4.14 gives the loss factors with the gap sealed by silicon rubber and figure 4.15 is the loss factor of thin rubber film sealed double pipes. Both sets of experimental data were measured at normal room temperature (approximately 20° C). The measured loss factors are compared with the theoretical results, which were calculated for oil at 40° C and 100° C respectively (the data for shell oil at 20° C were not available during the study). It can be seen that the measured loss factors are quite close to the predicted values. Because the double pipe system with oil gap sealed by thin "*rubber film*" had less mechanical linkage between the inner and outer pipes, the loss factors are slightly larger than these for the system sealed by "*silicone rubber*". Measured loss factors of the squeeze oil damped pipes were of the order of 10^{-2}. These are higher than the loss factors measured for the squeeze air damped pipe. Although measured values of loss factors with oil damping at high temperature were not obtained in this study, it can stated from the theory and principle of damping discussed above that the viscosity of oil is strongly affected by temperature, and so is the loss factor. The damping caused by the silicon rubber seals was very small compared with the oil damping. The damping created by the seal can be neglected. This can be proved by reference to figure 4.7, where the diameter of inner pipe and the seal material were the same as in the oil damped pipe system. The damping from the silicon rubber seal must be less than that from the air damped pipe system where silicon rubber was used.
Comparing the loss factors measured for an industrial pipe (see figure 5.14), where loss factors were below $2x10^{-3}$ except at frequencies below 400 Hz, with those measured for air or oil damped pipes, it is clear that damping created by air and oil in the double pipe system is significant. Loss factors are the order of $6x10^{-3}$ to $1.5x10^{-2}$ for air damping and the order of $7x10^{-3}$ to $3x10^{-2}$ for oil damping at most measured frequency points.

4.6 CONCLUSIONS.

From the results of the experiments, the following points can be made:

1). The squeeze film damping mechanism was verified by the measurement of the loss factor of a double pipe system in reduced air pressures.

2). Measured loss factors associated with air damping in the double pipe system agreed quite well with predicted values. It was also found, as predicted that damping is low at the conditions where the two pipes vibrate in-phase.

3). Although data were only measured for the oil damping system at 20^0 C, the plot of measured loss factors versus frequency was very similar in shape to theoretically predicted curves for higher temperatures.

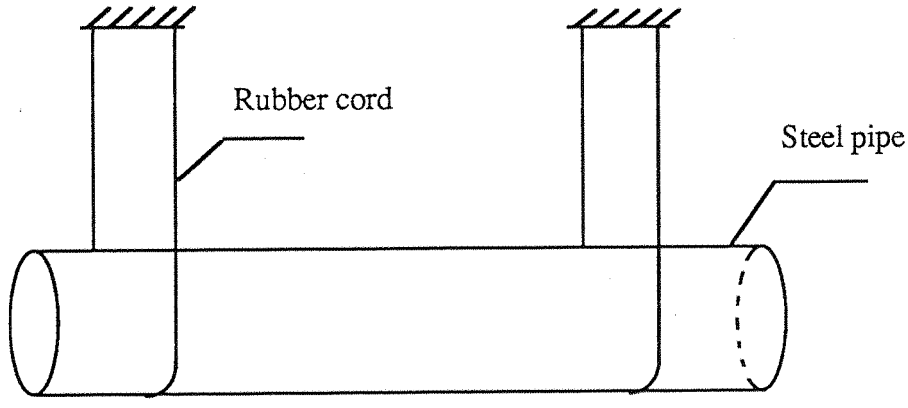

Figure 4.1 A steel pipe suspended by rubber cords.

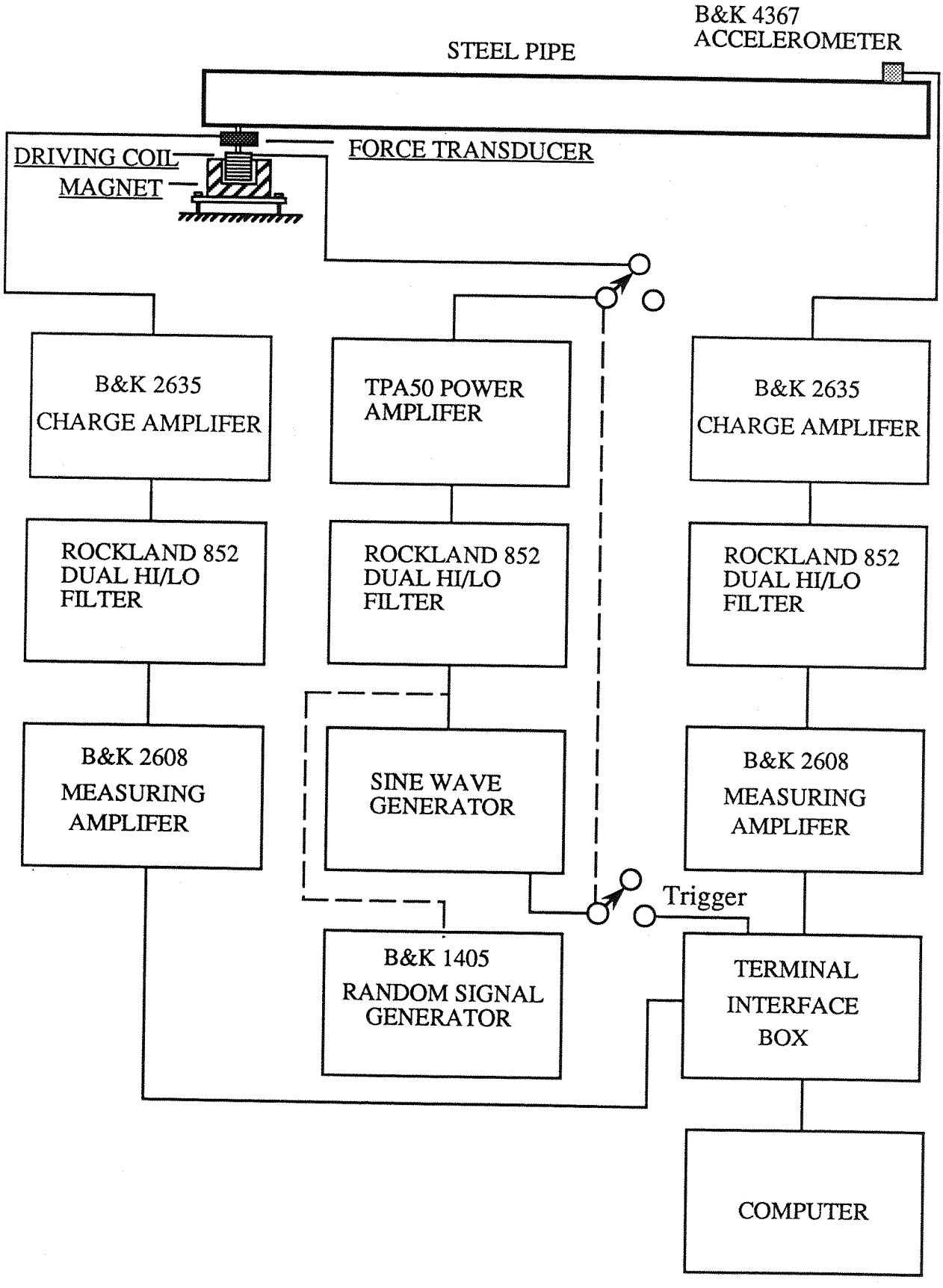

Figure 4.2 Instrumentation for loss factor measurements.

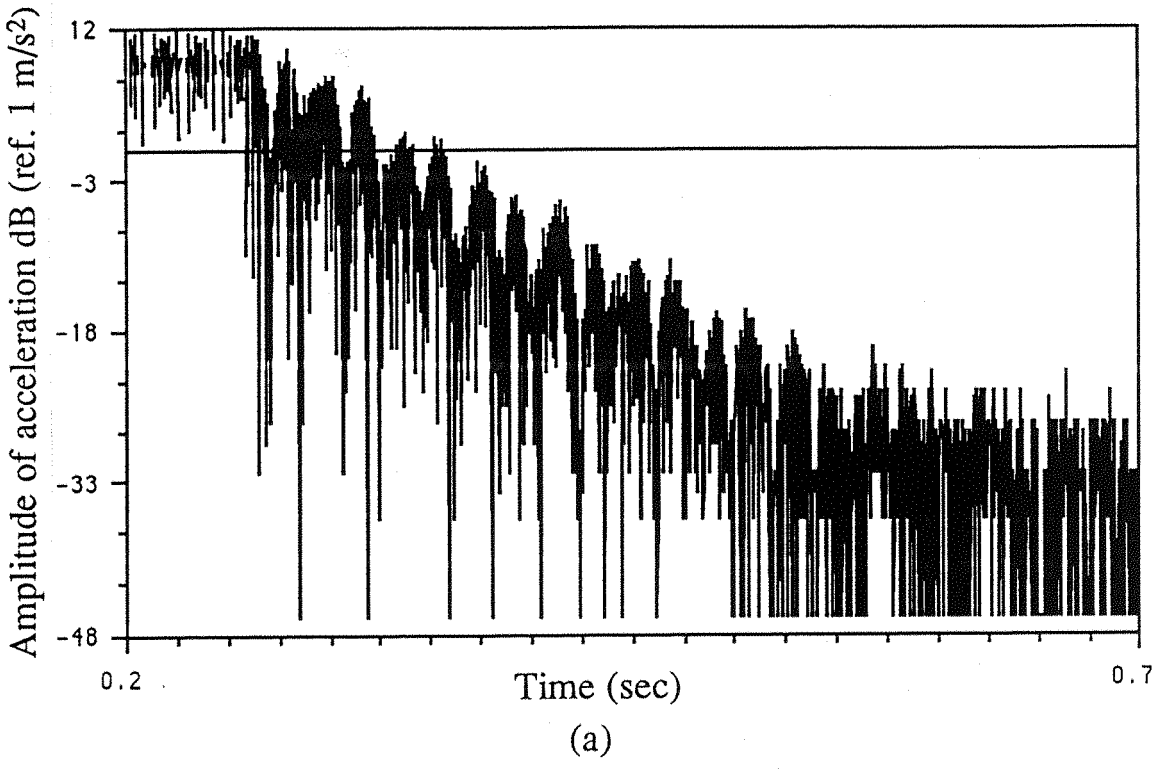

(a)

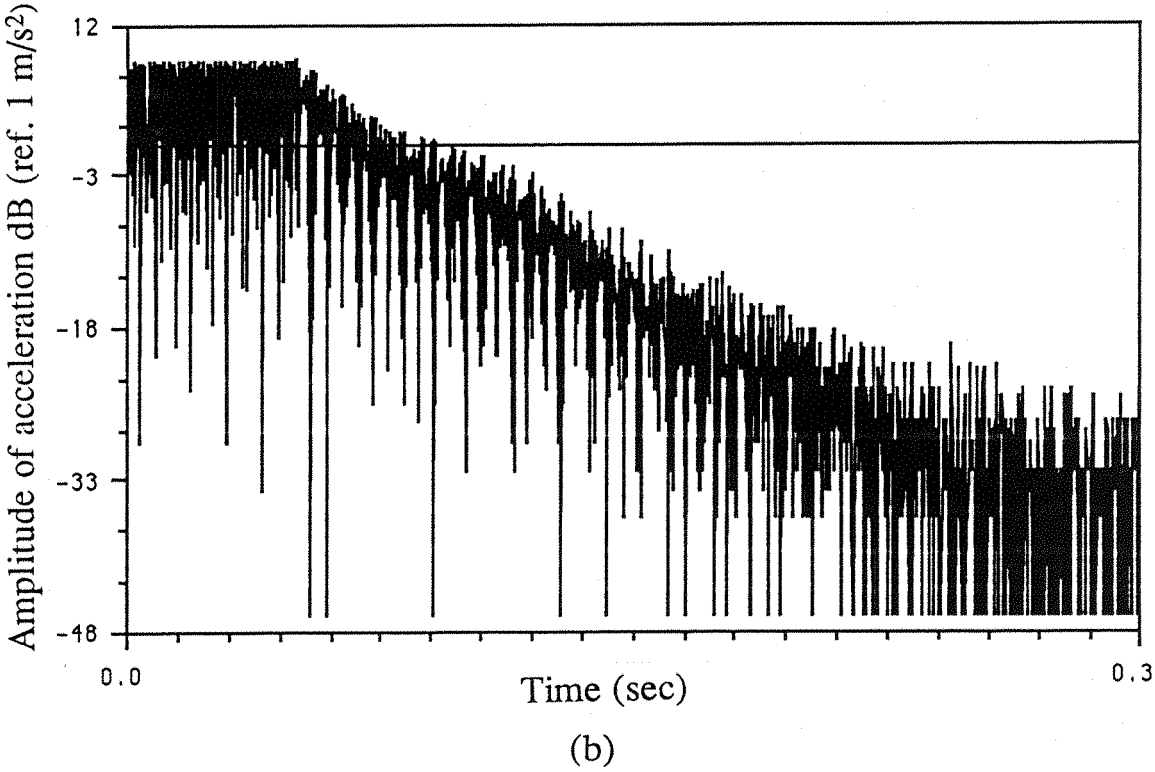

(b)

Figure 4.3 Decay curves of acceleration.

(a) f = 464 Hz, (b) f = 1191 Hz.

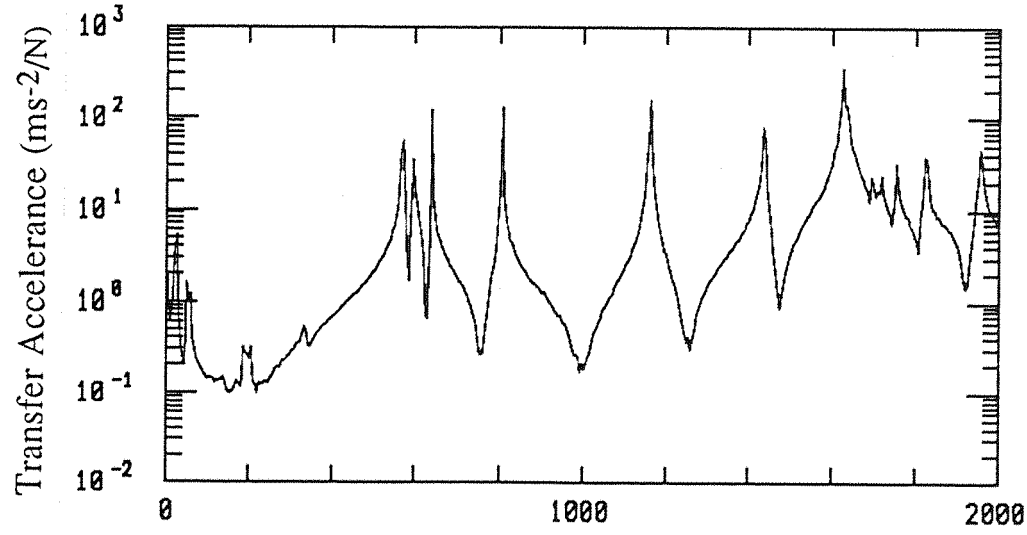

(a)

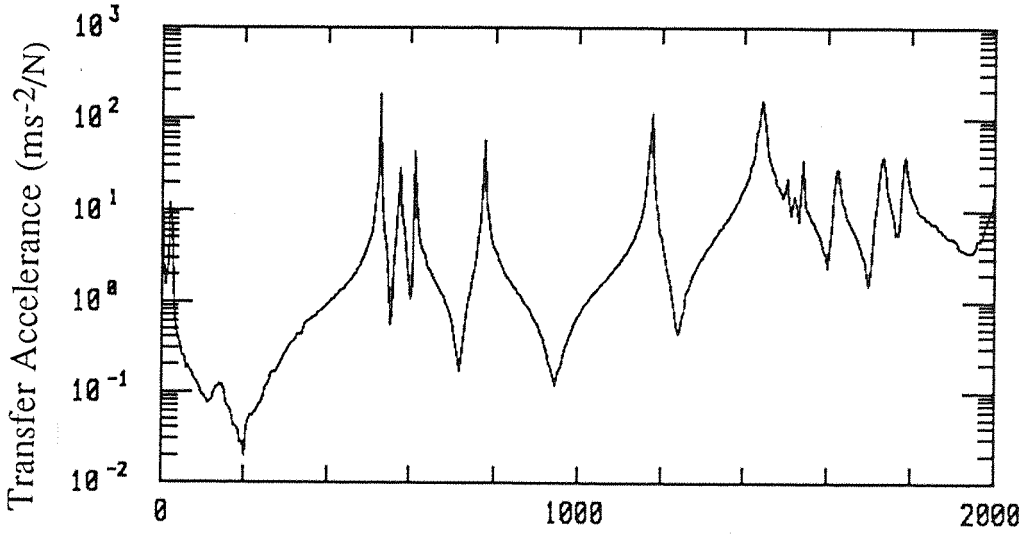

(b)

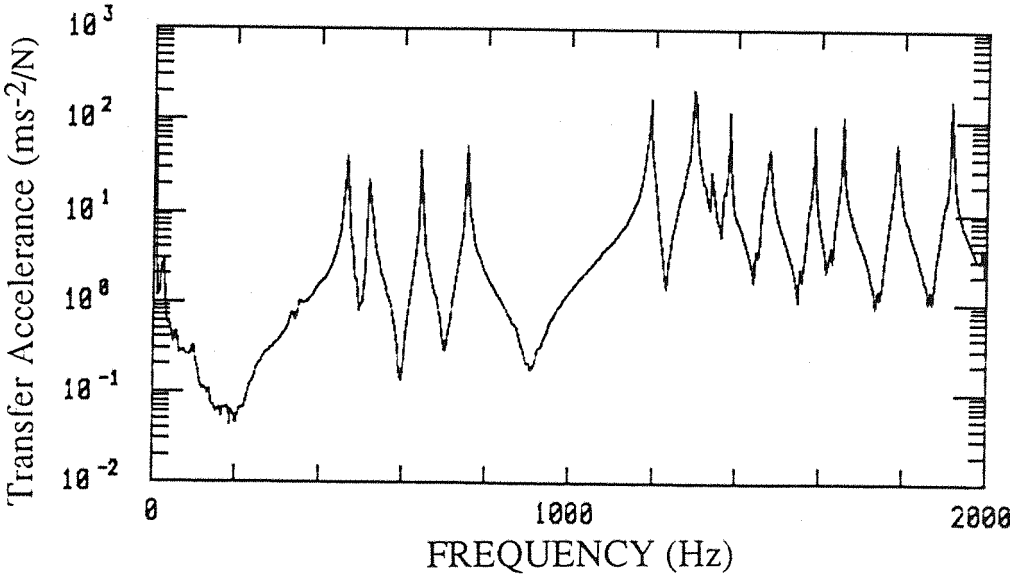

(c)

Figure 4.4 Transfer accelerance of a steel pipe.

(a) pipe 1, (b) pipe 2, (c) pipe 3.

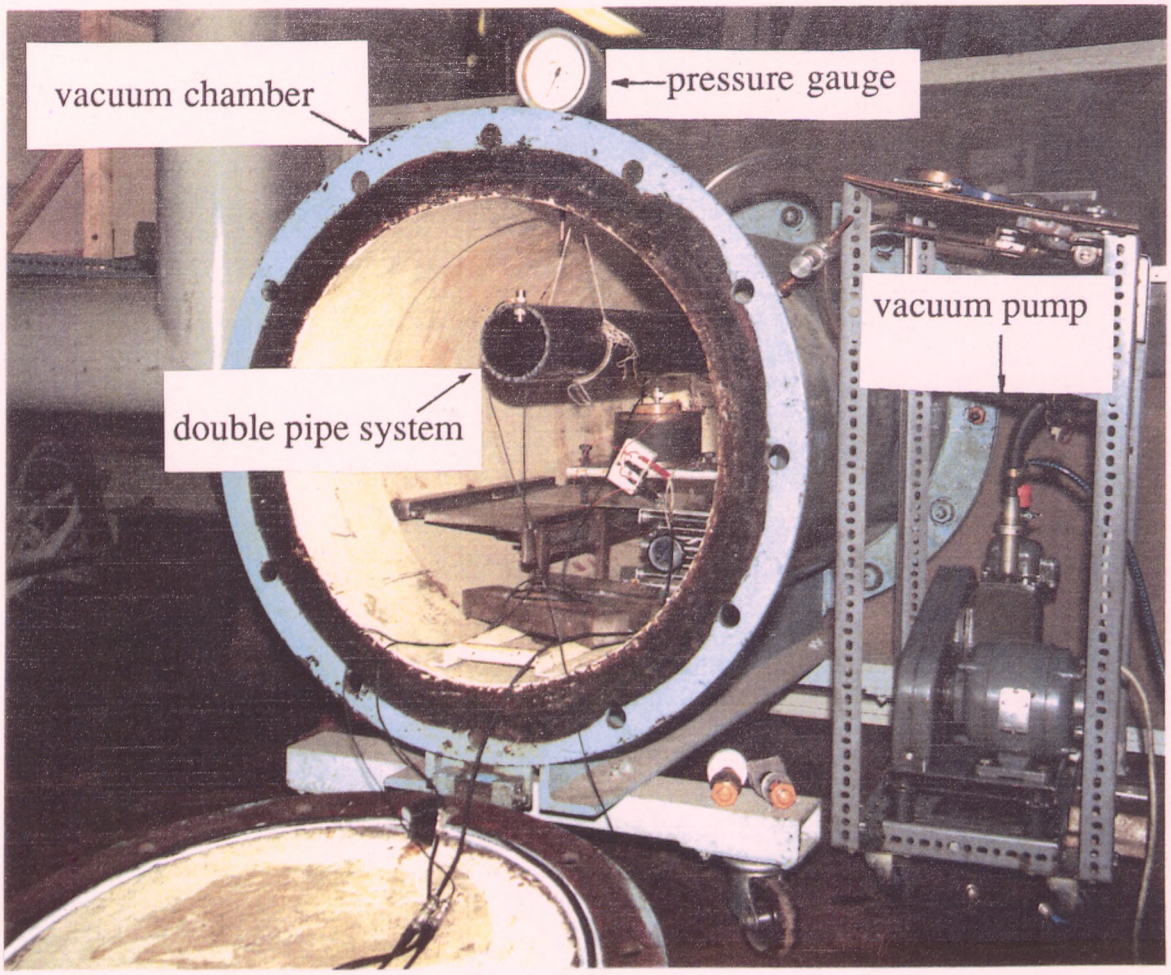

Figure 4.5 A double pipe system suspended in a vacuum chamber.

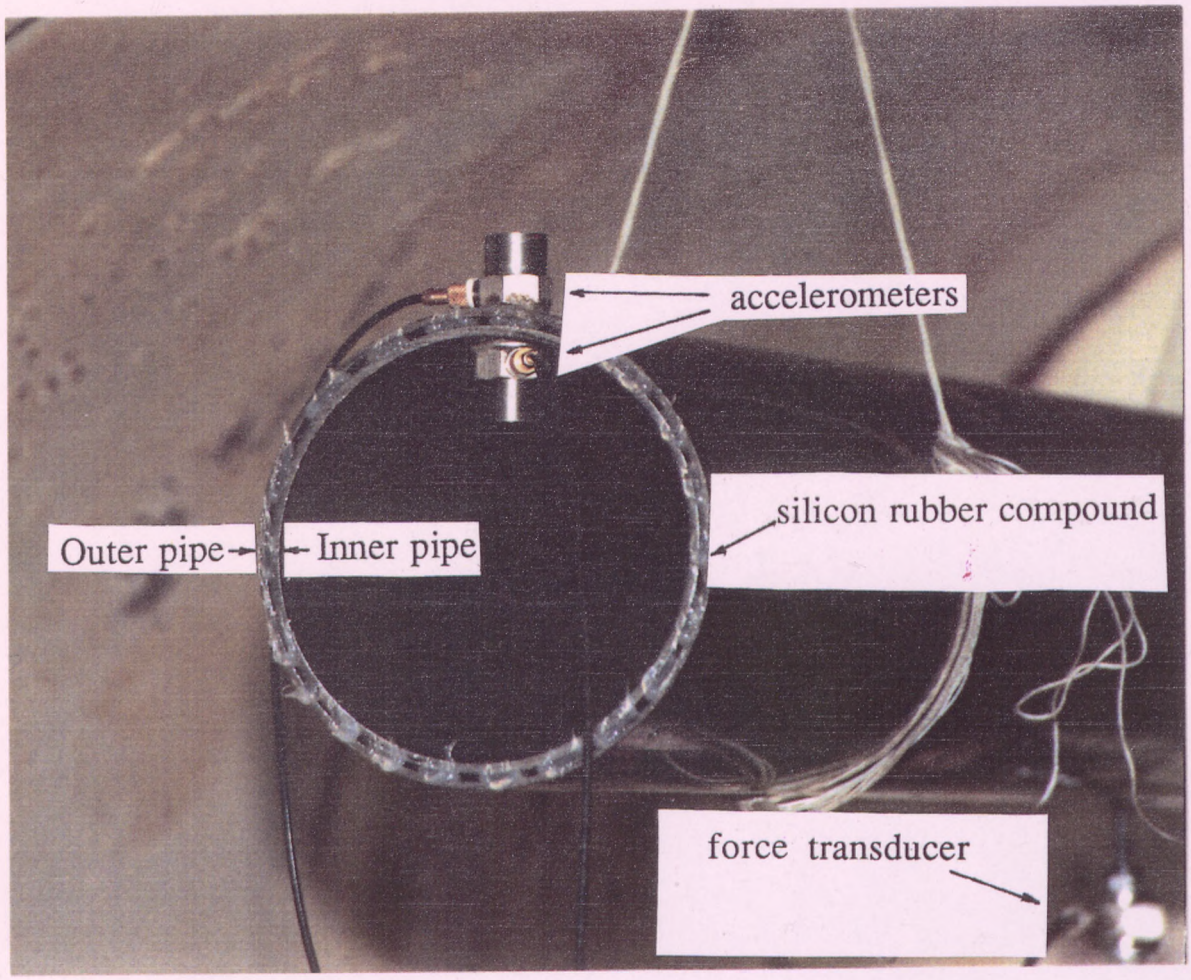

Figure 4.6 Two concentric pipes with air clearance gap for loss factor and mode shape tests.

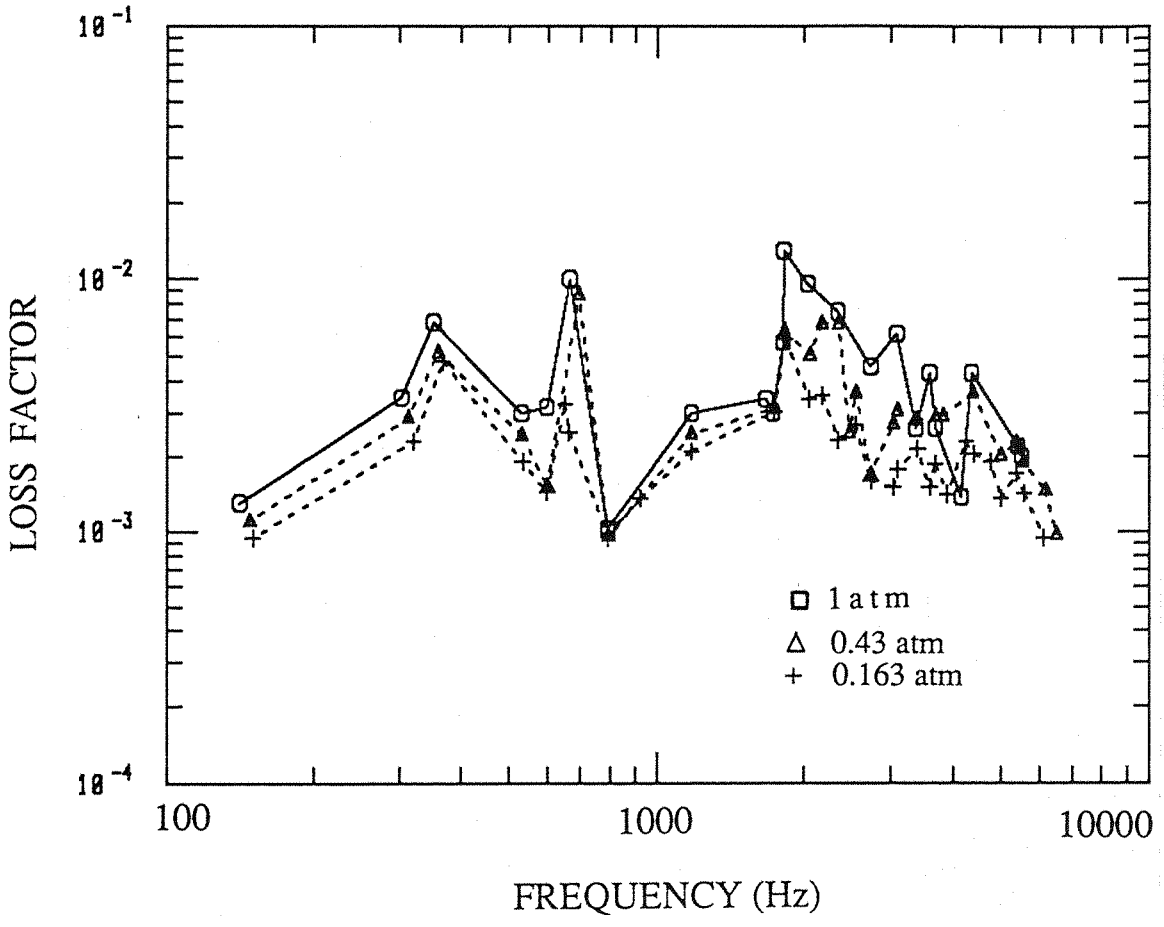

Figure 4.7 Measured loss factors of a double pipe system in reduced air pressure conditions.

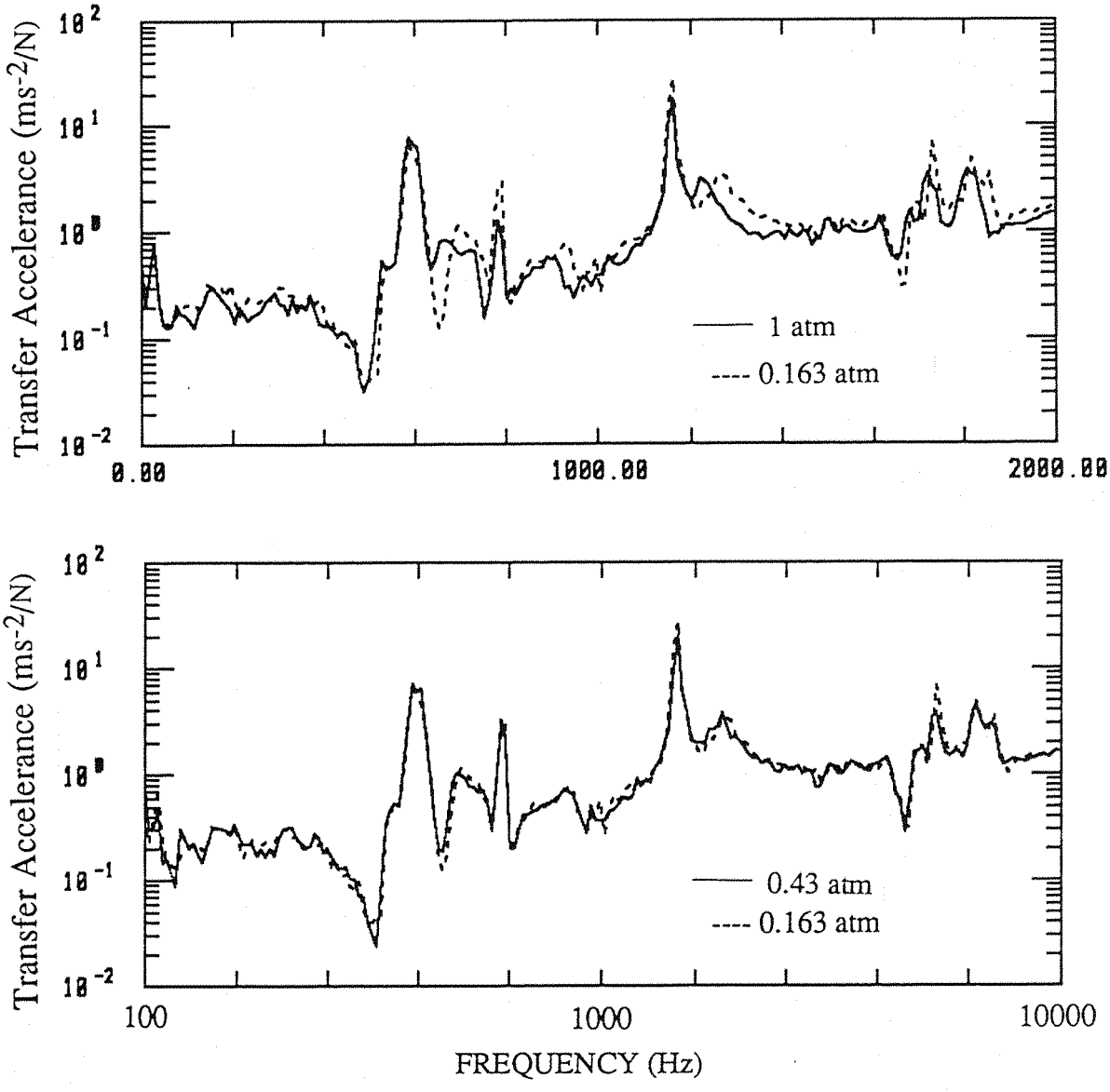

Figure 4.8 Measured transfer accelerance of double pipe system in reduced air pressure conditions.

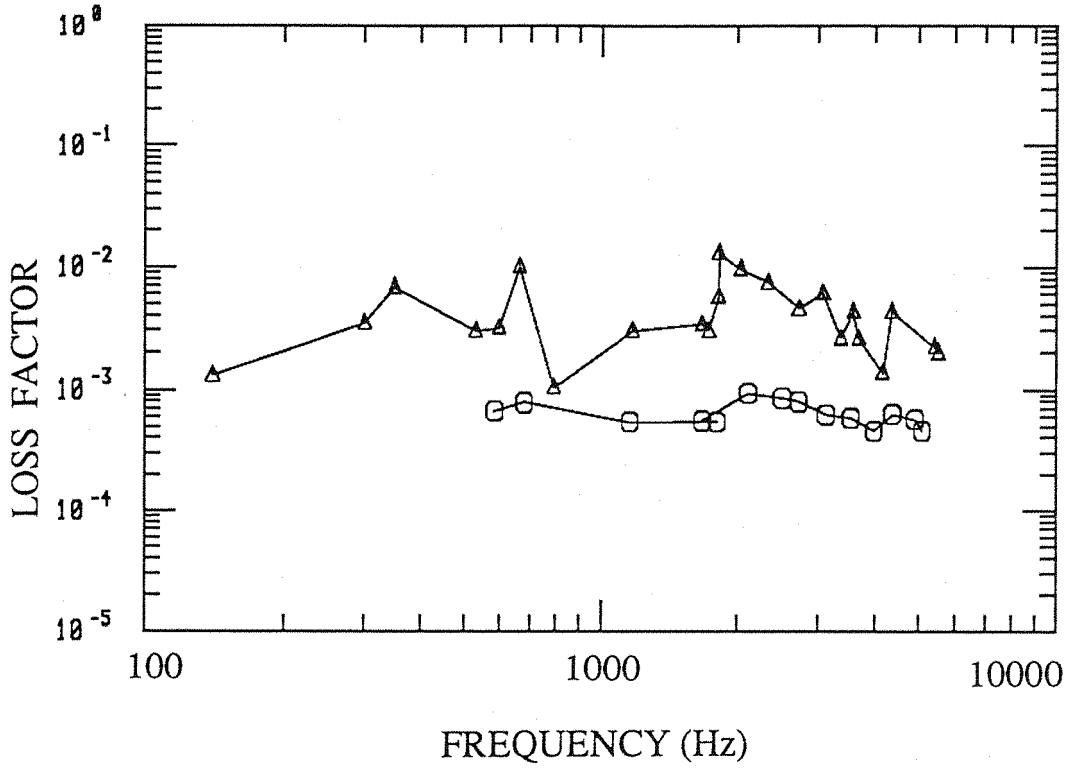

Figure 4.9 Comparison of loss factors between a steel pipe and double pipe system with 1.5 mm air gap.

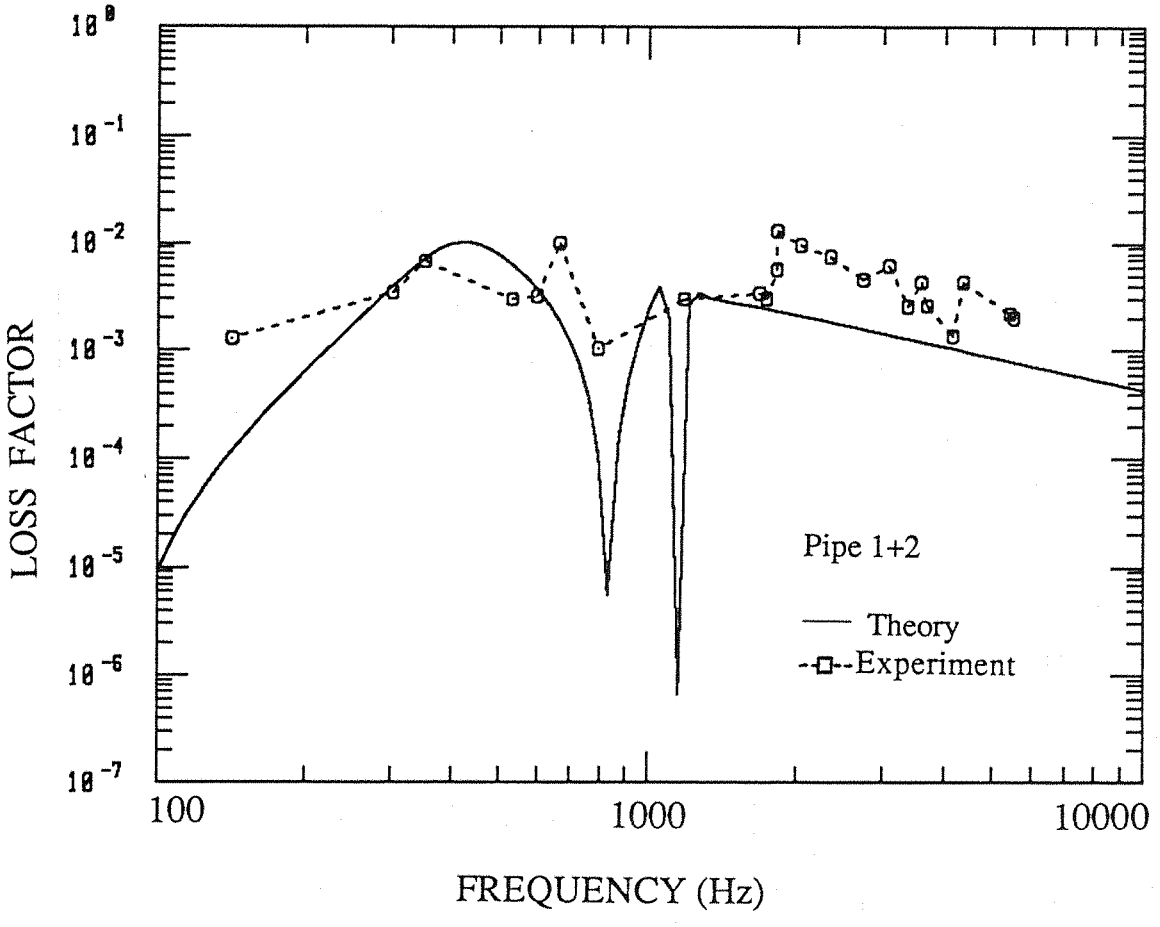

Figure 4.10 Comparison of theoretical and experimental loss factors for pipe 1+2.

r_1= 47.5 mm, h_1= 2.0 mm, h_2 = 2.15 mm, h = 1.5 mm, T = 20^0 C.

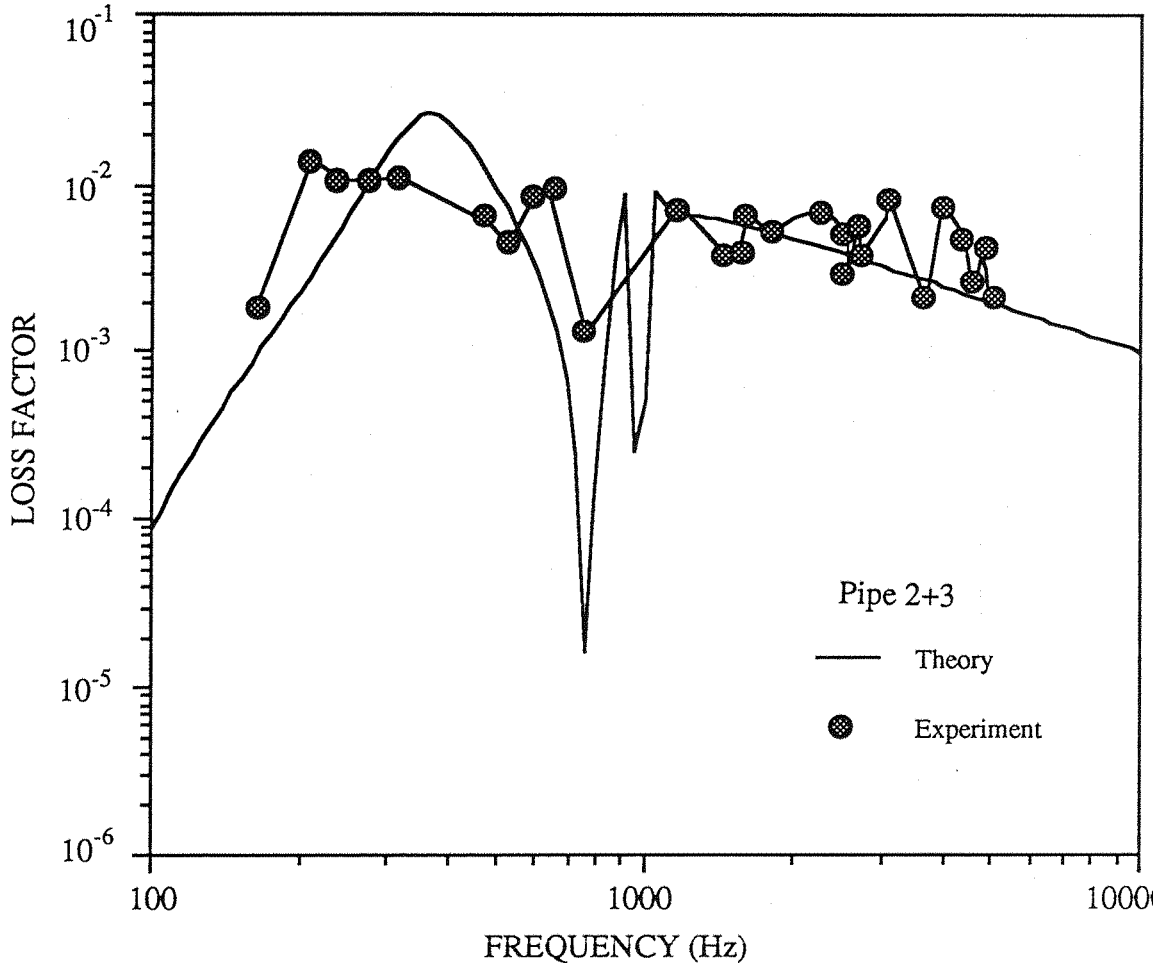

Figure 4.11 Comparison of theoretical and experimental loss factors for pipe 2+3.

r_1= 51.15 mm, h_1= 2.15 mm, h_2 = 2.0 mm, h = 0.85 mm, T = 20^0 C.

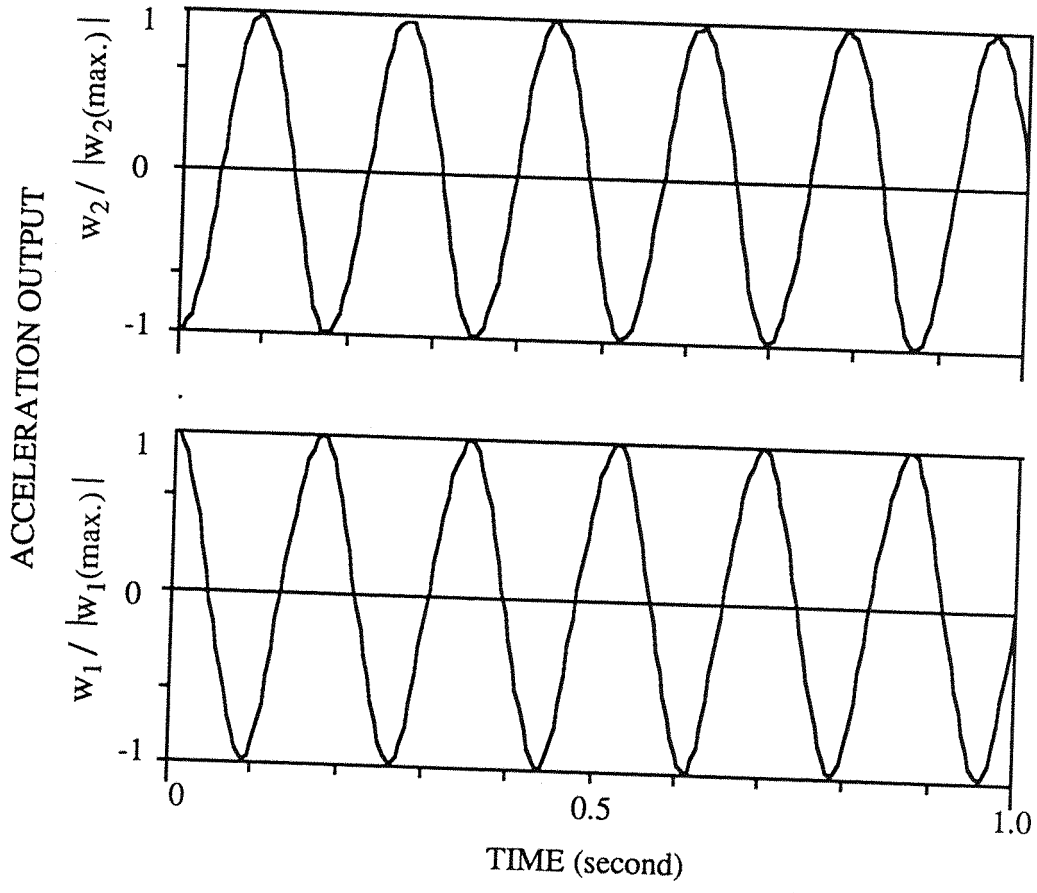

- w_1 = measured acceleration of inner pipe,
  $|w_1(max.)|$ = maximum amplitude of w_1,
+ w_2 = measured acceleration of outer pipe,
  $|w_2(max.)|$ = maximum amplitude of w_2.

(note signs of w_1 and w_2 above).

Figure 4.12 (a) Measured responses with two modes in phase.

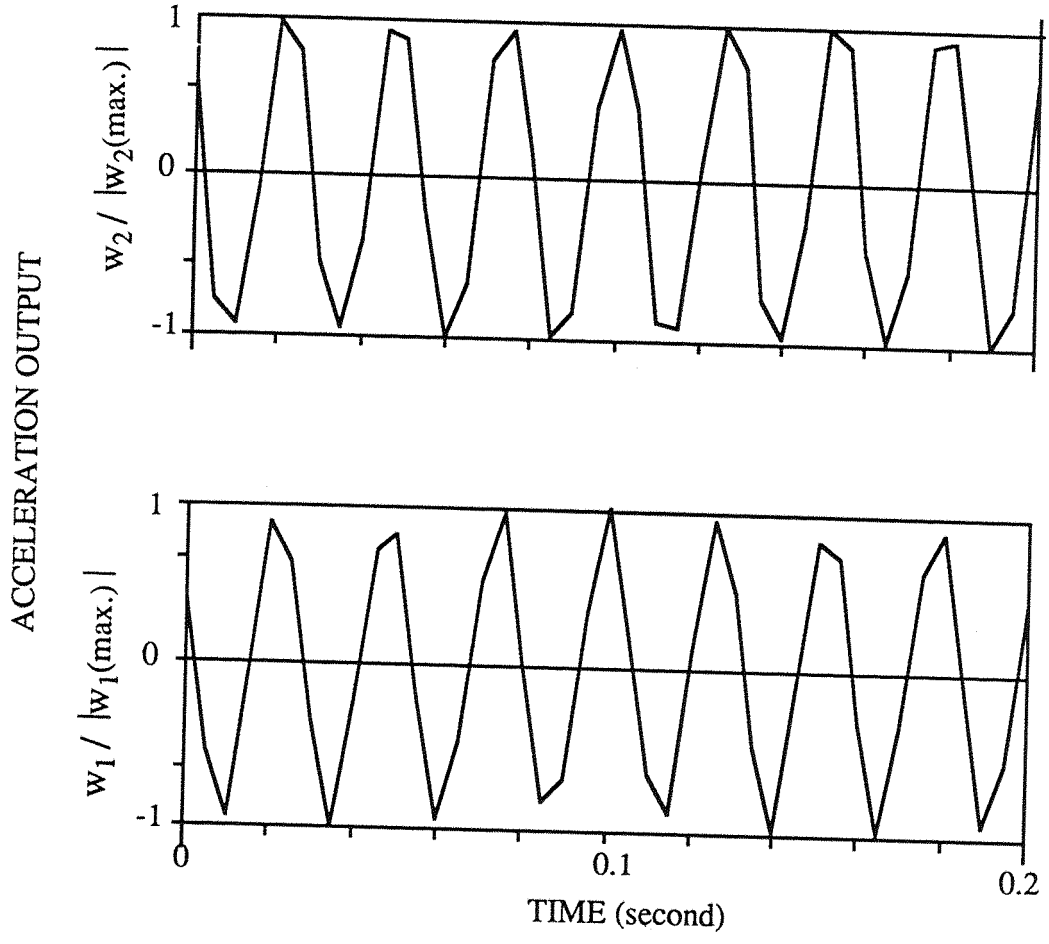

- w_1 = measured acceleration of inner pipe,
  $|w_1(max.)|$ = maximum amplitude of w_1,
+ w_2 = measured acceleration of outer pipe,
  $|w_2(max.)|$ = maximum amplitude of w_2.

(note signs of w_1 and w_2 above).

Figure 4.12 (b) Measured responses with two modes out of phase.

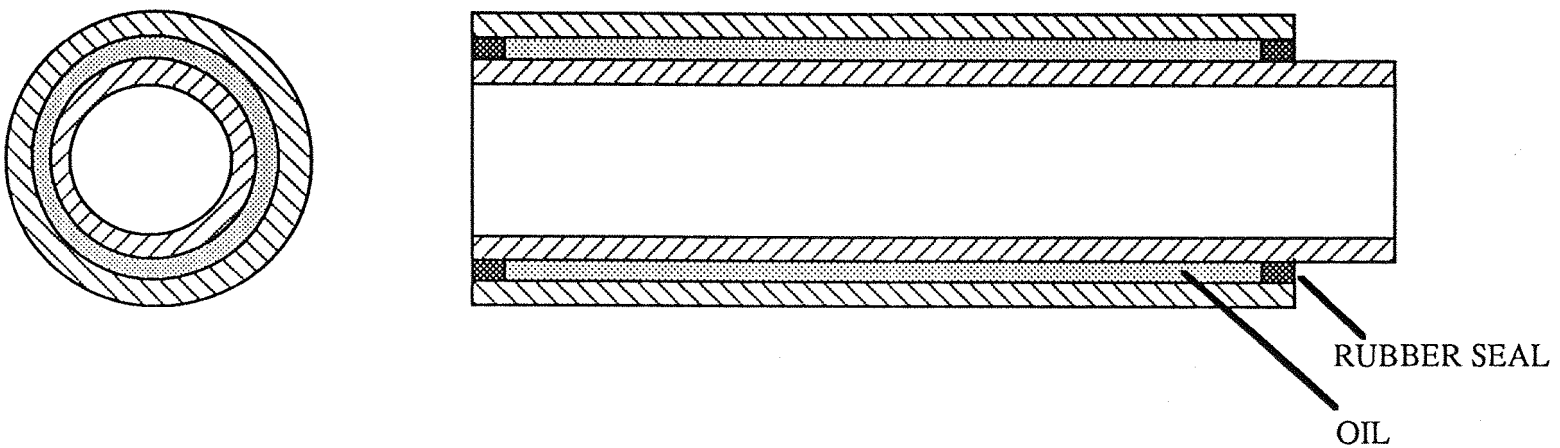

Figure 4.13 Seal arrangement for containing oil in the gap between the two pipes.

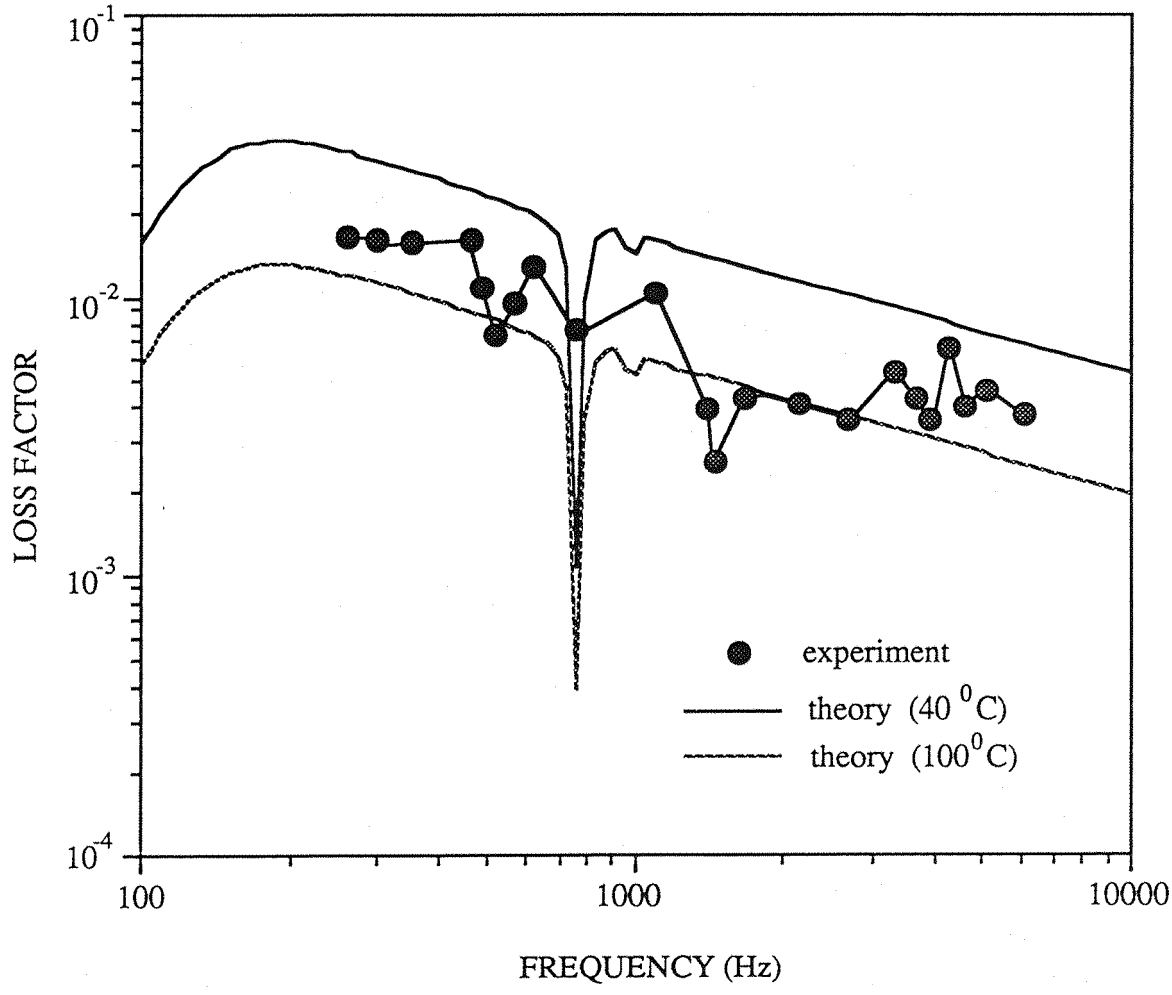

Figure 4.14 Comparison of theoretical and experimental loss factor.

Double pipes with Shell Oil (SAE 10W/40) filled and oil sealed by silicone rubber compound.

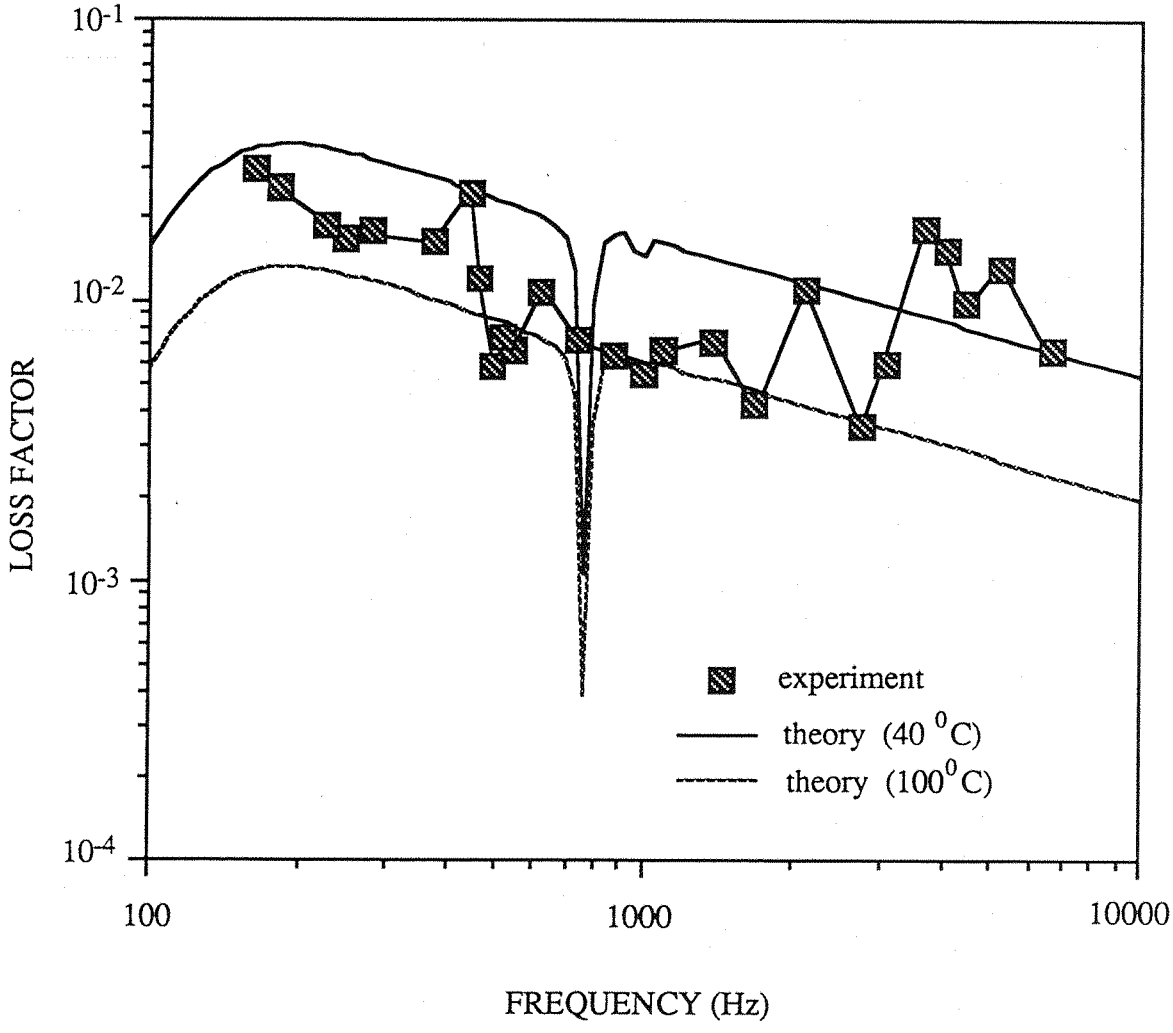

Figure 4.15 Comparison of theoretical and experimental loss factors.

Double pipe with Shell Oil (SAE 10W/40) filled and oil sealed by thin rubber film.

CHAPTER 5. PIPE DAMPING DUE TO FRICTION DEVICES AND LAGGING.

5.1 INTRODUCTION.

To meet the requirement of increasing damping by a robust method which may be used at high temperatures, another approach, dry friction damping, was employed to decrease vibration and noise radiation from a pipe system.

The design of the friction devices follows from reference [51], where a metal spring was used to decrease the noise radiation from a mining drill. To damp the pipe vibration in this study, various size of wire rope and a coiled steel spring were used to act as friction damping devices on a pipe. The aim of experimental investigation here was to study the friction damping characteristics of the two types of device when applied to a pipe.

Most previous researches in the field of friction damping have been following three quantitative relations of friction force which express the magnitude of the friction force as a function of the principal macroscipically observable variables, namely the applied load, the size of the region of contact and sliding velocity. The three quantitative relations are:
1). The friction force is proportional to the normal force N, that is $F=\mu N$, where μ is the coefficient of friction.
2). The friction force is independent of the apparent area of contact A_a. Thus large and small objects have the same coefficient of friction.
3). The friction force is independent of the sliding velocity v. This implies that the force required to initiate sliding will be the same as the force required to maintain sliding at any specified velocity.
However, in Rabinowicz and Kragelskii's researches [71, 72], it was stated that the third principle might not be obeyed in some circumstance as friction coefficient is a function of velocity or a frequency dependent factor. This will be discussed in this chapter.

In this study, a series of experiments were carried out to investigate the loss factors from carefully arranged friction devices on a pipe and the variation of loss factor with frequency and normal load. Although theoretical work is not available within the scope of this chapter because of limited time for this project, a general discussion of friction damping is given for these kinds of damping devices.

5.2 FRICTION DAMPING OF A PIPE IN FLEXURAL VIBRATION WITH WRAPPED COILED STEEL SPRINGS AND WIRE ROPES.

The need for a robust damping mechanism which can operate at high temperatures has already been stated and the successful applications of coiled spring around rods in noise reduction lead to this investigation of the two types of device shown in figure 5.1.

The coiled steel spring is supposed to vibrate independently when a pipe is in vibration. Friction forces occur between the contacting surfaces of pipe and spring, then energy is dissipated by friction. The wire rope consists of a group of thin wires. Energy is dissipated either by friction between the wire rope and the pipe or by friction among those wires within the wire rope, i.e., there is "internal dissipation" within the rope and not in the "spring".

5.2.1 Description of the coiled spring damping system.

1). Dimensions of coiled spring.
The coiled steel spring was made of thin steel wire as shown in figure 5.1(a). Three sizes of spring were used in the experiment. The dimensions of coiled springs used in experiments are

	D_s (mm)	d_s (mm)	l_s (mm)
spring 1	12	1.6	7.1
spring 2	8.0	1.6	6.0
spring 3	7.5	1.1	3.8

where

D_s = diameter of spring coil,
d_s = diameter of spring wire,
l_s = spacing between two spring coils.

2). A pipe with coiled steel spring wound around it.
A coiled steel spring was wrapped around a pipe as shown in figure 5.1(b). Both ends of spring were attached to the ends of the pipe via two collars. The ends of the spring were attached to the collars which could be rotated in opposite directions and then clamped to the pipe to pretension the spring.

5.2.2 Description of wire rope damping system.

Wire rope is simply several strands of wire twisted or wound, together. Some of the types are commonly called "cable" and are used to carry electricity, support bridges and in many other practical ways. In the present experiment, two wire ropes were used, description and dimensions of which are shown in figure 5.2(a). A wire rope consists of number of strands and every strand contains a number of steel wires. The dimensions of two wire ropes are

	D_w (mm)	d_w (mm)	N_s	N_w
wire rope 1	4	1.4	19	4
wire rope 2	5	1.6	19	6.

where

D_w = diameter of wire rope,
d_w = diameter of a wire,
N_s = number of strands of wire rope,
N_w = number of wires per strand.

A wire rope was wrapped around a pipe shown in figure 5.2(b). Both ends of wire rope were fixed onto the pipe by two collars. By this arrangement the structure of the wire rope provided many contacting points on the pipe. It is expected that a portion of the energy associated with relative motion of the strands of wire would be converted by friction into thermal energy and vibrational energy would be dissipated.

5.2.3 Measurements of loss factor and accelerance.

Loss factors were measured by use of the decay time method (see equation 4.1 and figure 4.2). The approach to measurement was the same as that in chapter 4. A steel pipe was used in the experiments. Dimensions of pipe are: length = 1080 mm, mean radius = 50 mm, thickness of pipe wall = 2 mm. The damped pipe was suspended by nylon or rubber string as shown in figure 5.3. Flexural vibration was excited by coil and magnet system. Transfer accelerance was measured from the signals of exiting force and acceleration response. The transfer accelerance is defined as

$$\text{Transfer Accelerance} = \frac{a_{\text{output}}(\omega)}{F_{\text{input}}(\omega)} \qquad (5.1)$$

where

$a_{output}(\omega)$ = acceleration,

$F_{input}(\omega)$ = force.

5.2.4 Measurement of loss factors of a wire rope damped pipe.

The characteristics of friction damping by a wire rope were investigated and the loss factors of a wire rope damped pipe were measured. The measured loss factors are plotted versus frequency for the pipe-rope system in figure 5.4, in which lower solid line is for a plain pipe and the other two lines are the loss factors for 4 mm and 5 mm diameter wire ropes respectively.

There are some interesting points which arise from the results, as follows;

1). wire rope is considerably effective in damping the vibration of a pipe. The loss factor is improved from order of 10^{-3} for plain pipe to the order of 10^{-2} for a damped pipe.
2). Because there is no pretension added to the wire rope, the only friction force comes from weight or gravitation of the wire rope itself, which is

$$\mu N \approx \mu g \frac{(\rho_w \pi D_w^{2})}{4} \int_0^{\pi} R \sin\theta \, d\theta$$

$$= \mu g \frac{(\rho_w \pi^2 D_w^2 R)}{2} \quad \text{when } R \gg d \tag{5.2}$$

where

N = normal force to surface of pipe wall,

μ = coefficient of dry friction,

g = constant of gravitation,

ρ_w = density of wire rope,

D_w = diameter of wire rope,

R = radius of pipe.

Comparing various diameter of wire ropes with the same material, it comes out clearly that a large diameter of wire rope gives high friction force according to above description. The friction force occurs, of course, only in the top half circle of the wire rope.

3). High friction force should normally give high damping. But the measured loss factors of the 5 mm wire rope were low compared with those of the 4 mm wire rope within the frequency range of about 500 ~ 2000 Hz. There may be two reasons for this contradiction. First, vibration velocities of the pipe are low at lower frequency, so that wire rope as a friction damper is nearly stuck, or excitation frequency is too low to overcome the static friction or to cause slip. In this case, damping is controlled by relative slip between the interface of the surfaces of the pipe wall and the wire rope rather than by normal force. Thus, light wire rope is assumed to be more active or moving more quickly than a heavy one. The second reason is that friction damping occurs among the wires of the wire rope itself. For the same reason, at a given excitation force, light wire rope moves more rapidly, therefore high damping is achieved.

4). In the mid frequency range (>2000 Hz), the vibration velocity for high frequency response is high enough to cause slip, so friction force is controlling damping. In the high frequency range the wire rope is moving freely. In this case the loss factor for light weight wire rope will decrease at a certain frequency, which can be seen at frequencies above 3500 Hz in figure 5.4.

5.2.5 Measurement of loss factors of a coiled spring damped pipe.

A coiled spring is supposed to undergo a strong local vibration when it is wrapped around a pipe. Friction damping is affected mostly by the nature of the spring. When the spring receives energy from the main vibrating structure and produces local vibration, friction occurs at some contacting point, so energy is dissipated. In this case, friction damping does not only depend on the weight of spring but also on the spring rate or stiffness. Normal forces exerted on the surface of a pipe wall are from gravity and the stress in the spring while the spring is in vibration. The spring can be either compressed or extended; the deflection of spring can be expressed as [73]

$$\delta = \frac{8 F D_s^3 n}{G d_s^4} \qquad (5.3)$$

where

δ = deflection of spring,

F = force exerted on spring,

D_s = mean coil diameter of spring,

d_s = diameter of spring wire,

G = modulus of rigidity of spring material,

n = number of active coils.

The spring rate or stiffness K_s is

$$K_s = \frac{F}{\delta} = \frac{G\, d_s^4}{8\, D_s^3\, n} \tag{5.4}$$

For a given exerted force and diameter of spring wire, the spring with large mean coil diameter of spring has low stiffness and high deflection, so high friction damping will be produced. Figures 5.5 to 5.6 give loss factors of a pipe with coiled springs of diameter 12 mm and 8 mm which were compared with these of an undamped pipe. Loss factors of the 12 mm diameter spring system are great than those associated with the 8 mm spring, each having the same diameter of spring wire.

To study friction damping with various pretensions of the spring, one collar to which the end of the spring was fixed, was twisted through 120^0 and 240^0. The extended lengths of the spring are

$$l_1 = 0.67\ \pi\ R \text{ and } l_2 = 1.33\ \pi\ R.$$

Pretensions are equal to $l_1 K_s$ and $l_2 K_s$ for 120^0 and 240^0 respectively. As discussed in section 5.2.4, spring with high pretension will "stick" at low frequency and move in contact with the pipe but will yield effective friction for high frequency vibration.
Although the spring with low pretension had high friction damping in the low frequency range, it became less effective at high frequencies because the spring lost its friction when the vibration velocities were high. The appropriate curves in figures 5.5 and 5.6 clearly show this effect. When the spring pretension is changed, the resonance frequency of the pipe will change because the distribution of added mass changed. High pretension results in more added mass and lower resonance frequency as shown in figure 5.7, which gives measured accelerances of the pipe with various pretensions of the spring. Figure 5.8 shows the same type of results as discussed above, where a very small diameter spring wire was used, although the loss factor levels were low as it was less effective as a friction device.

Observing figure 5.5, 5.6 and 5.8, it was found that the loss factors were generally very low in the frequency range 500 ~ 600 Hz and there was no friction damping at all from all springs with high pretension. How is this effect related to a certain mode shape of the vibrating pipe? In the next section the effect of mode shapes of the pipe will be discussed.

5.3 Measured Natural Frequencies and Mode Shapes of a Pipe.

To identify the first two circumferential modes of a pipe, two accelerometers were fixed at one end of the pipe as shown in figure 5.9. Transfer functions a_1/f and a_2/f were measured. The definition of transfer function is

$$H_i(\omega) = \frac{G_{a_i a_i}}{G_{a_i f}} \tag{5.5}$$

where

$i = 1,2,$

G_{aa} = acceleration spectral density,

G_{af} = cross spectral density of acceleration and force,

a_1 = acceleration of lower point of inner pipe wall,

a_2 = acceleration of upper point of outer pipe wall.

Comparing the phase of transfer functions of inner and outer pipes (H_1 and H_2), the first circumferential number n=1 can be recognized as in-phase motion occurs, the mode with n=2 can be seen as out-of-phase. Typical results of transfer accelerance are shown in figure 5.10, where resonance frequencies and phases are given.

The measured resonance frequencies and mode shapes are compared with results from shell theory of chapter 2 in table 5.1.

Table 5.1 Comparison of measured natural frequencies and mode shapes with theoretical results.

Length of pipe = 1080 mm, mean radius = 50, thickness = 2 mm

n	m	theory (Hz)	experiment (Hz)	phase of H_2/H_1
1	2	504	517	+
2	1	561	561	-
2	2	737	717	-
2	3	1056	1053	-
1	3	1260	1323	+

n = circumferential mode, m = axial mode.

Measured results showed quite good agreement with theoretical values. It can be seen that the low loss factors in figures 5.5, 5.6 and 5.7 are at 561 Hz, the frequency of the mode with n=2 and m=1, where spring friction is supposed to be less effective.

5.4 POSSIBLE EXPLANATION OF FRICTION DAMPING ON A PIPE BY USING SINGLE DEGREE FREEDOM SYSTEM MODELLING.

5.4.1 Natural frequency of a helical spring.

As discussed in the previous section, independent vibration may occur in the coiled spring of a spring damped pipe system. The lowest natural frequency of a helical spring may be calculated according to reference [73] as

$$f_s = \frac{2\, d_s}{\pi D_s n} \sqrt{\frac{Gg}{32\gamma}} \qquad (5.6)$$

where

f_s = lowest natural frequency of spring,
d_s = diameter of spring wire,
D_s = diameter of spring coil,
G = modulus of rigidity of spring material,
g = acceleration due to gravity,
γ = weight density of spring material,
n = number of active coils.

The fundamental natural frequencies of the steel springs in figure 5.1(a) were calculated as below,

	n	Natural frequency f_s (Hz)
Spring 1	44	90
Spring 2	52	172
Spring 3	82	85

where the following coefficients were used
$G=79.6x10^9$ N/m^2, $r=\gamma/g=7850$ Kg/m^3, n=the spring wound around the pipe for one circle.

Further study on the effect of the natural frequency of a helical spring on the friction damping of the spring damped pipe should be carried out in future research.

5.4.2 Relationship between the force normal to the surface of a pipe and the slipping velocity of a coiled spring or wire rope.

A multi degree of freedom system representation of a spring in contact with a pipe is given in figure 5.11 (a). A series of masses and springs with friction force is used to model a spring or wire rope wound around a pipe. One mass and one spring represent one turn of the spring. One turn of the spring is modelled in figure 5.11 (b), where N is the normal force exerted on a mass. For a coiled spring N occurs due to pretension and gravity and for a wire rope N is due to gravity only. If the driving force $F \geq \mu N$, relative motion of the spring mass will take place. The sign of the frictional force varies with the sign of the velocity y. An equation of motion of such a mass spring system is

$$m\ddot{y} + K y = F(t) - \mu N \operatorname{sgn}(\dot{y}) \tag{5.7}$$

where

y= displacement of spring mass.
μ = coefficient of dry friction,
m = mass of spring
K = stiffness of spring

If v(t) is assumed to be of the form

$$y(t) = A \cos \omega t,$$

and

$$\dot{y}(t) = - A \omega \sin \omega t,$$

then $$\ddot{y}(t) = - A \omega^2 \cos \omega t,$$

$$\operatorname{sgn}(\dot{y}) = \operatorname{sgn}(-A\omega \sin\omega t)$$
$$= -\frac{4}{\pi}\frac{A}{|A|}\sin \omega t + \ldots \tag{5.8}$$

Neglecting the higher order term, equation (5.7) becomes

$$m\ddot{y} + K y - \frac{4}{\pi}\frac{A}{|A|}\sin \omega t = F \cos(\omega t + \gamma) \qquad (5.9)$$

Substituting $y(t) = A \cos \omega t$ into equation (5.9), $|A|$ can be immediately written as

$$|A| = \frac{\sqrt{A_0^2 - (4\ a/p)^2}}{|1 - \omega^2/\omega_0^2|}$$

where

$A_0 = F/K$,

$a = \mu N/K$.

If $\omega_0^2 = K/m$, and the force F is applied at certain frequency ω, then

$$|A| = C_1 \sqrt{1 - C_2 (\frac{N}{F})^2} \qquad (5.10)$$

where

$$C_1 = \frac{F}{K\ |1 - \omega^2/\omega_0^2|}$$

$$C_2 = (4\ \mu / \pi)^2 .$$

$|A|/C_1$ can be expressed as a function of $\frac{N}{F}$ as shown in figure 5.12, where the velocity decreases rapidly when normal force increases.

The normal force for a coiled spring $N = \frac{K\ l_s}{n}$, $l_s = l + \delta$, where l is the length of spring.

The normal force for a wire rope $N = g\frac{\rho\ \pi^2\ d^2\ R}{2}$, g = gravity constant.

5.4.3 Relationship between coefficient of friction and slipping velocity.

It is well known that the force required to start sliding is usually greater than the force required to maintain sliding, and this gives rise to the notion that there are two coefficients of friction - static (for surface at rest) and kinetic (for surface in motion).

The kinetic friction coefficient is a function of velocity. A plot of kinetic friction coefficient versus velocity will generally have a positive slope at low sliding velocity and a negative slop at high sliding velocity.

The relationship between velocity and coefficient of friction can be expressed by an empirical equation [71] as

$$\mu = (a + b\,\dot{y})\, e^{-c\,\dot{y}} + d \qquad (5.11)$$

where a, b, c and d are constant for various materials, an example here is given in iron-iron surface,

$$a = 0.022,\ b = 0.274,\ c = 0.59,\ d = 0.11$$

Figure 5.12 shows the relationship of velocity and friction coefficient of iron-iron surfaces. The friction between a steel spring and a steel pipe should follow the same rule.

5.4.4 Parameters which affect friction damping.

Discussion in sections 5.4.2 and 5.4.3 shows the relationships between normal force and slipping velocity, coefficient of friction and slipping velocity respectively. The coefficient of friction has a key role in friction damping.

Under a given excitation, the coefficient of friction is function of slipping velocity, and the velocity depends on the normal force, which acts on the slipping mass and causes friction damping. Hence, coefficient of friction finally depends on the normal force. A possible optimum point exists at which the magnitude of the normal force produces the highest friction damping.

The slipping velocity also depends on frequency of excitation as high velocities usually occur at high frequency. There are therefore two important parameters which control

friction. These are excitation frequency and normal force. These two factors are considered separately here when friction damping is discussed.

1). At a given frequency.
The expression for velocity is

$$\dot{y} = |A|\omega \cos(\omega t + \theta),$$

The velocity is function of normal force, from equation (5.10), as

$$\dot{y} = \text{constant } f(N).$$

In the case of a wire rope damped pipe, the normal force is a function of the weight of the wire rope, so is the friction. For a coiled spring, the normal force is either a function of the weight of the spring or a function of pretension in the spring. For a light weight spring, friction is controlled by pretension, but it may also be controlled by weight when the spring is heavy.

2). At a given normal force.
Slipping velocity is controlled by excitation frequency range and so is the friction damping.

5.5 DISCUSSION.

Concerning the optimum design of a friction damping system, both the normal force produced by spring and frequency range must be considered.

Friction damping definitely depends on the range of frequencies involved. Heavy wire rope or a coiled spring with high pretension may not have high friction damping at low frequencies because their slipping velocities are low from equation 5.8. Higher friction damping may occur at high frequencies.

For a light weight wire rope or a coiled spring with low pretension, the friction damping is low because the normal forces are low .

To design the optimum friction damping system for a pipe, a size of wire rope or coiled spring as well as the pretension of a coiled spring can be chosen depending on the frequency range of interest.

5.6 FRICTION DAMPING OF AN INDUSTRIAL PIPE BY MINERAL WOOL LAGGING.

(i) Design.

Mineral wool lagging is often used at power stations to lag pipes. There is a need to investigate damping of this type of pipe system. This is required in order to ascertain the levels of damping present in a lagged pipe and to compare them with the loss factors achievable by other methods investigated. Figure 5.13 is an industrial pipe with wrapped mineral wool lagging and a 1 mm thickness steel cleading* cover on the outside. By adjusting the clips, which clamped the steel clearly shown in figure 5.13, conditions approximately to constrained and unconstrained lagging can be achieved. The experimental method and measurement used for investigating the damping of this structure here as already described in chapter 4 and figures 4.1 and 4.2.

(ii) Results.

The pipe tested is practical one used in power stations and the measured loss factors are given in figure 5.14. Data are given for the plain pipe and the pipe covered with constrained or unconstrained lagging. Loss factors of the plain pipe varied from $1.5x10^{-3}$ ~ $5x10^{-3}$ and increased to $1x10^{-2}$ ~ $2.5x10^{-2}$ with lagging, through the frequency range examined. Constrained lagging produced the highest loss factors.

* Cleading is a term usually used in the power industry.

5.7 CONCLUSIONS.

1). Wire rope wrapped around a pipe can produce high damping. Damping was produced either from friction between the surface of the wire rope and the pipe wall or from friction between strands of rope.

2). Friction damping may depend on the weight of wire rope. The optimum loss factor will depend on weight and frequency. It is suggested that further investigation be carried to determine the optimum size of wire to give high loss factors in a given frequency range.

3). The level of loss factor produced by a coiled steel spring device is determined by the size of the spring and pretension and is also frequency dependent. There is an optimum slipping velocity of the spring, where higher coefficients of friction may be reached. This velocity depends only on spring force normal to the surface of the pipe induced by gravity and pretension. To determine the optimum size of a coiled spring and optimum pretension for a given frequency range, further experiments and research are needed.

4). When a pipe vibrates in its first bending mode and the second circumferential mode, loss factors caused by friction damping by both a wire rope or a coiled spring are very low because of relative low slipping velocity.

At high frequency, a high pretension coiled spring produces high damping. A low pretension coiled spring system has high a loss factor at low frequency but low loss factor at high frequency.

5). Mineral wool lagging will increase damping on industrial pipes. Constrained lagging will produce higher loss factors than unconstrained lagging.

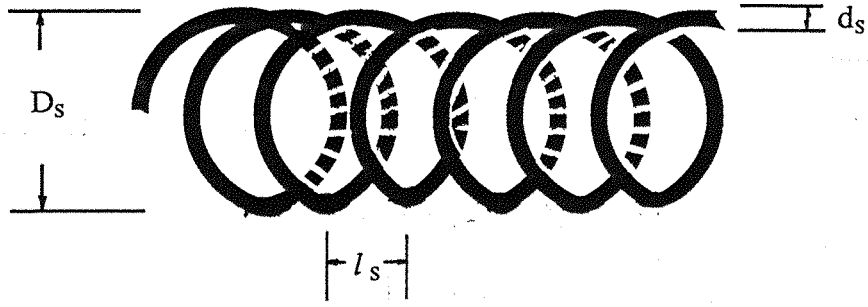

	D_S (mm)	d_S (mm)	l_S (mm)
spring 1	12	1.6	7.1
spring 2	8.0	1.6	6.0
spring 3	7.5	1.1	3.8

Figure 5.1 (a) Structure and dimensions of coiled steel spring.

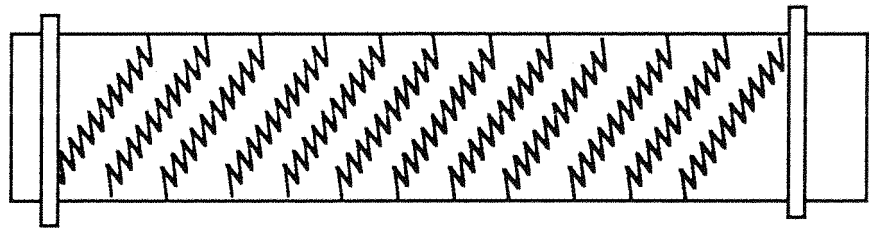

Figure 5.1 (b) A steel pipe with a wrapped steel spring.

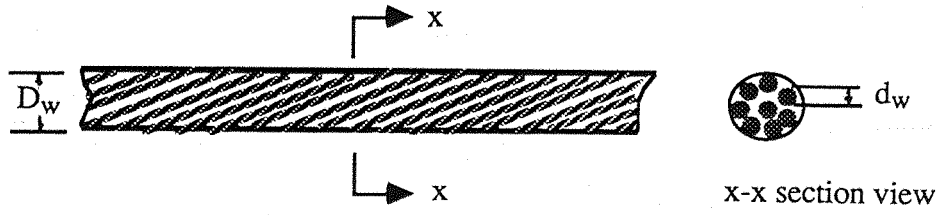

	D_w	d_w
wire rope 1	4	1.4
wire rope 2	5	1.6

Figure 5.2(a) Structure and dimensions of wire rope.

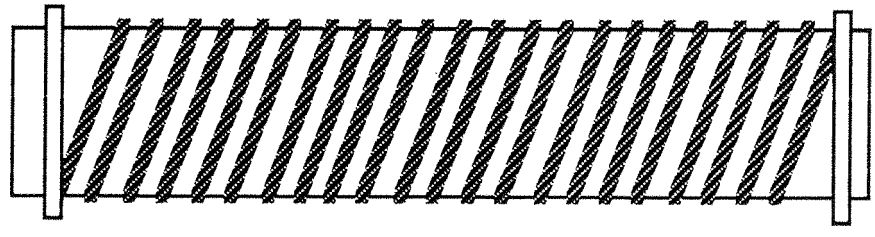

Figure 5.2 (b) A steel pipe with a wrapped wire rope.

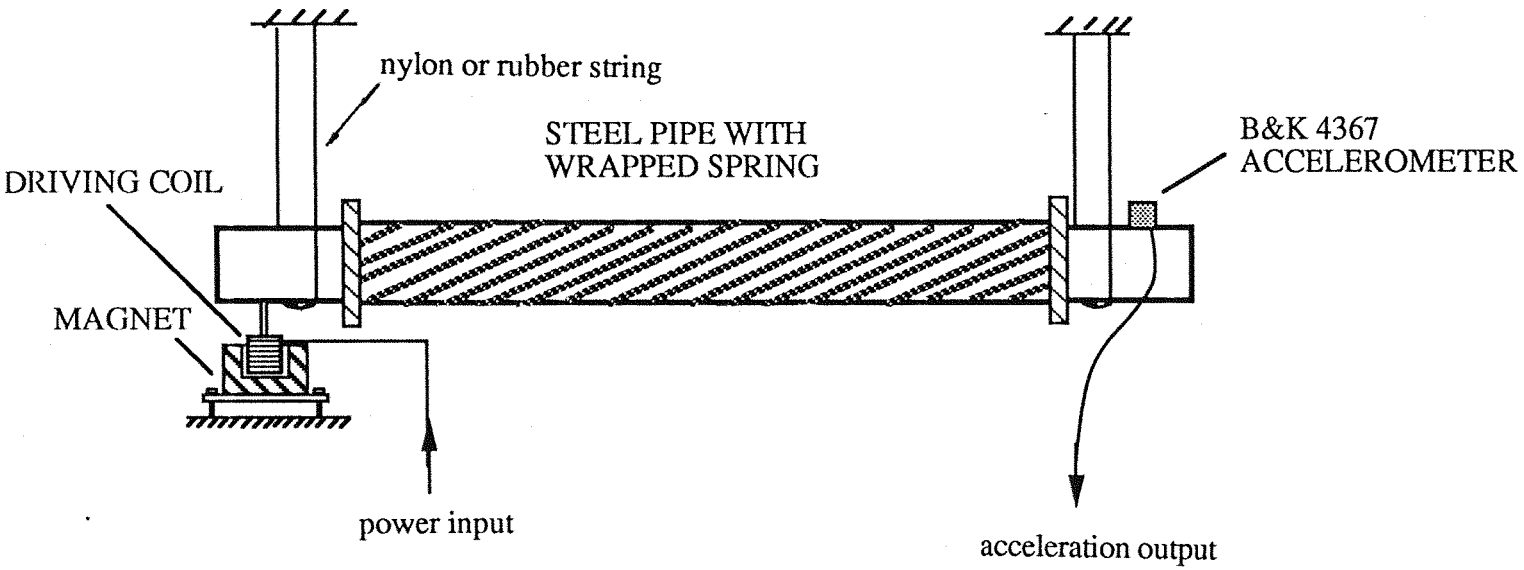

Figure 5.3 Excitation and acceleration measurement of a friction damped pipe with free-free boundary conditions.

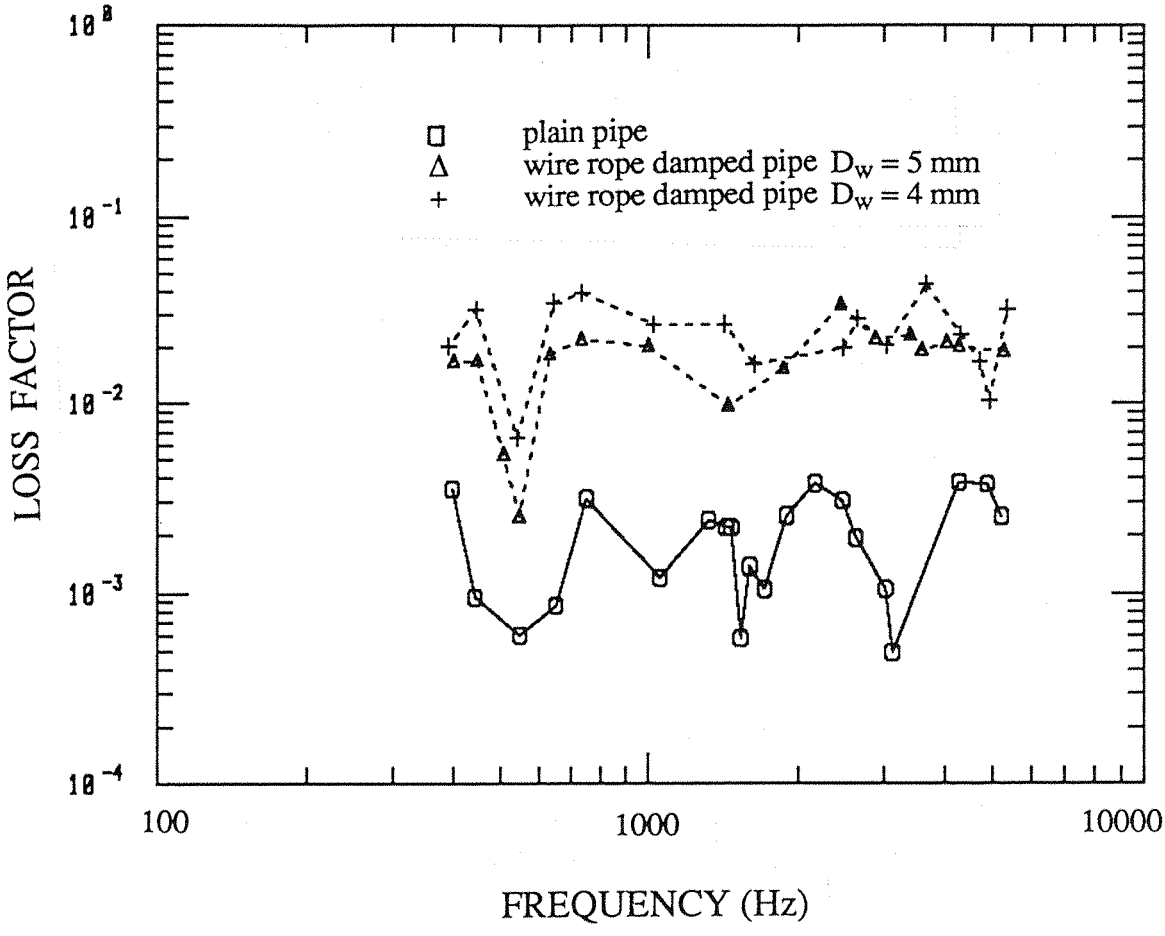

Figure 5.4 Measured loss factors of a plain pipe and wire rope damped pipe in flexural vibration.

D_w = diameter of wire rope.

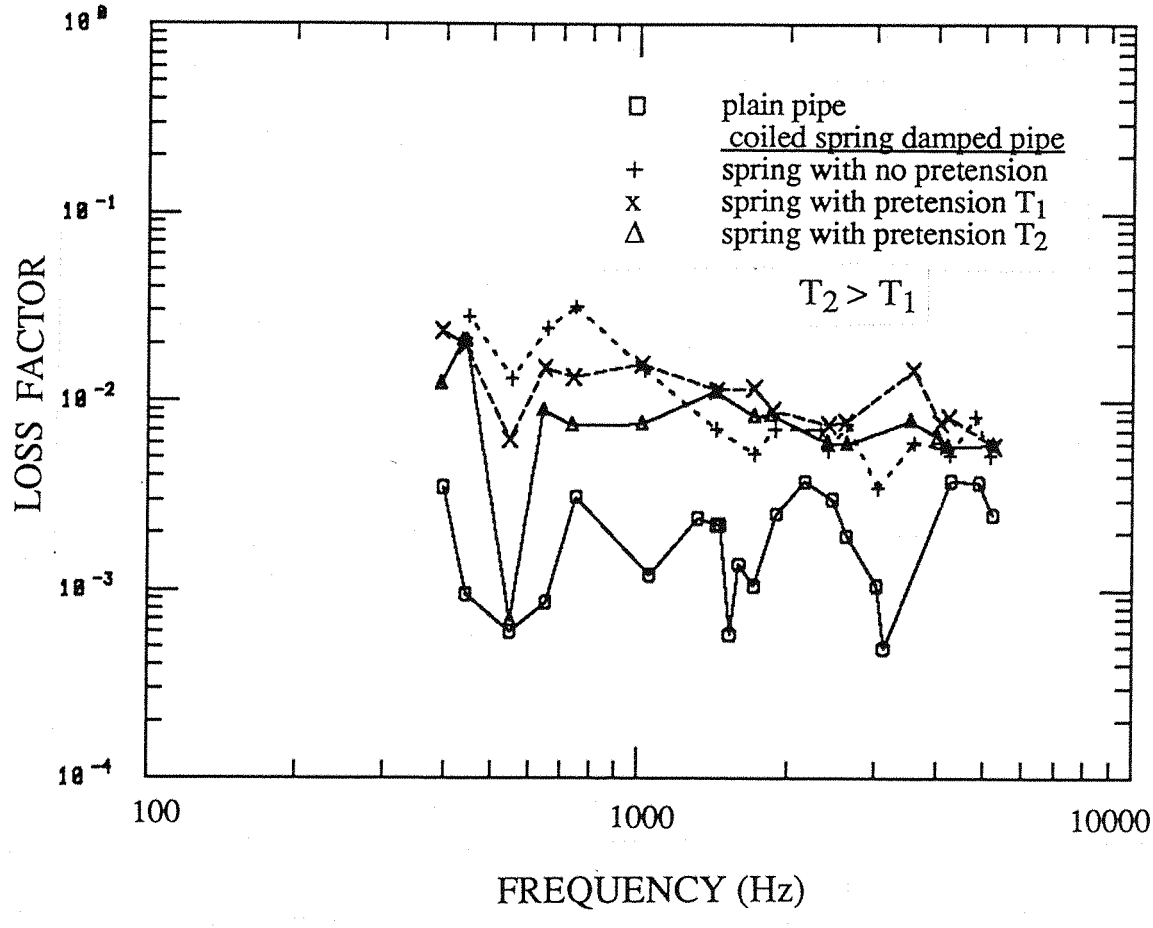

Figure 5.5 Measured loss factors of a plain pipe and coiled steel spring 1 damped pipe in flexural vibration.

T_1= the extended length of spring is 0.67 π R,
T_2= the extended length of spring is 1.33 π R,
R = mean radius of pipe, diameter of spring 1 = 12 mm.

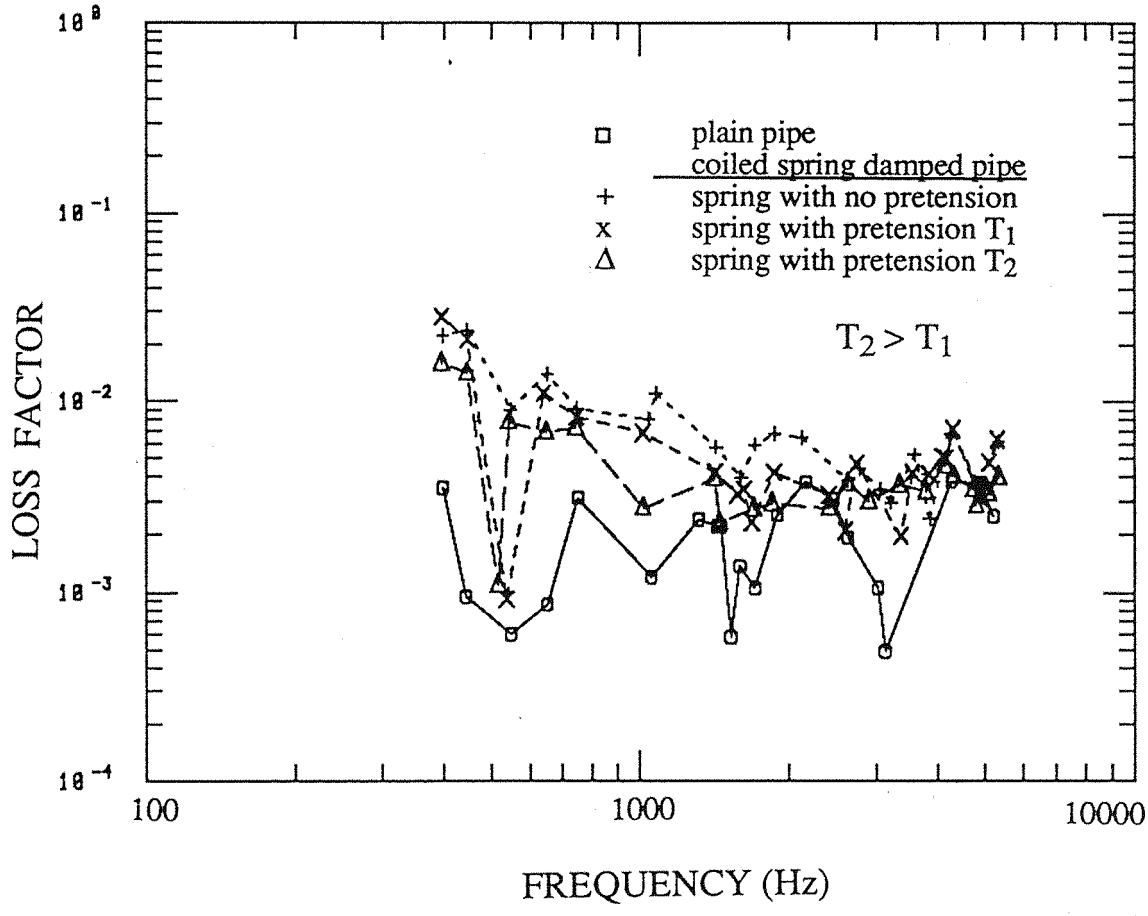

Figure 5.6 Measured loss factors of a plain pipe and coiled steel spring 2 damped pipe in flexural vibration.

T_1= the extended length of spring is 0.67 π R,
T_2= the extended length of spring is 1.33 π R,
R = mean radius of pipe, diameter of spring 2 = 8 mm.

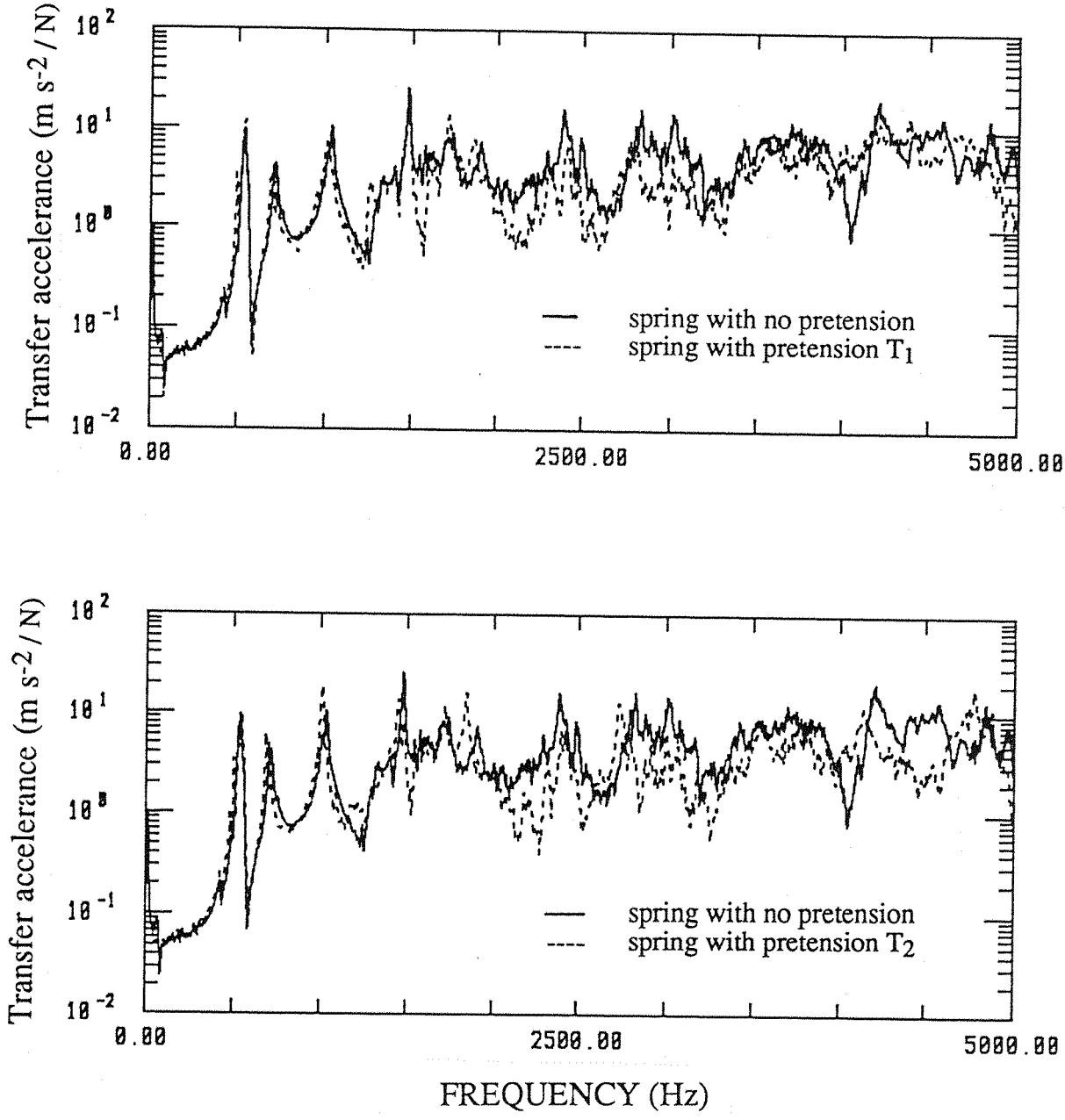

T_1= the extended length of spring is 0.67 π R,
T_2= the extended length of spring is 1.33 π R,
R = mean radius of pipe, diameter of spring = 12 mm.

Figure 5.7 Measured transfer accelerances of the coiled spring damped pipe with various pretensions of spring.

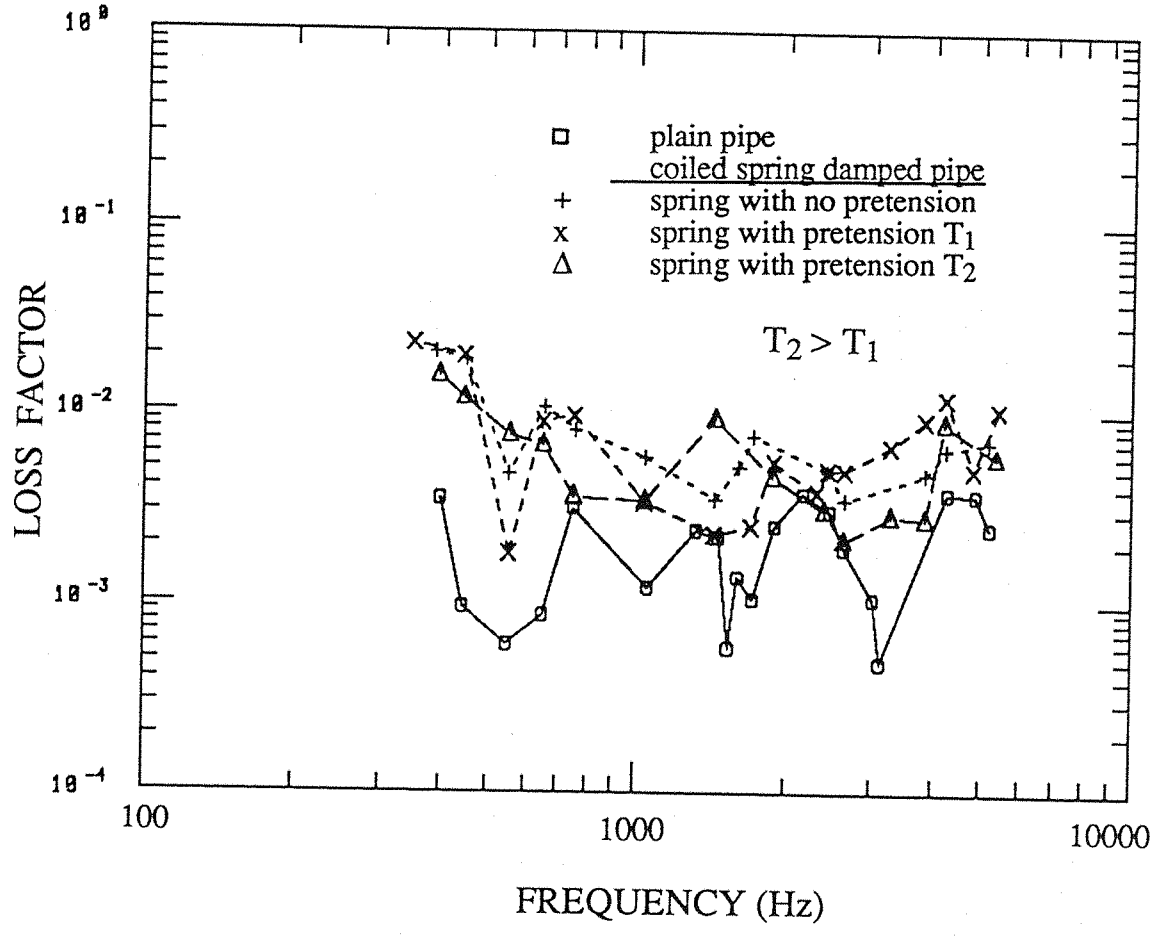

Figure 5.8 Measured loss factors of a plain pipe and coiled steel spring 3 damped pipe in flexural vibration.

T_1= the extended length of spring is 0.67 π R,
T_2= the extended length of spring is 1.33 π R,
R = mean radius of pipe, diameter of spring 3 = 7.5 mm.

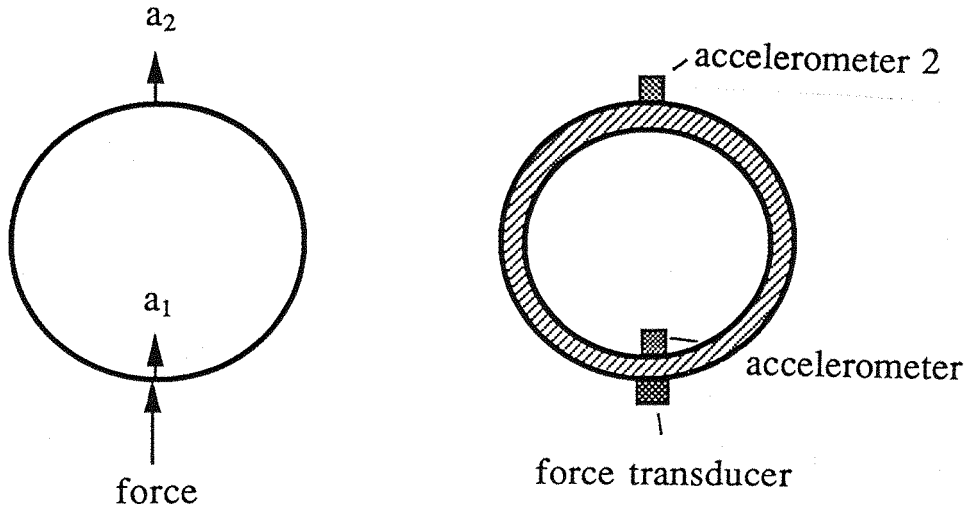

Figure 5.9 Arrangement for verifying the first two circumferential modes of a plain pipe.

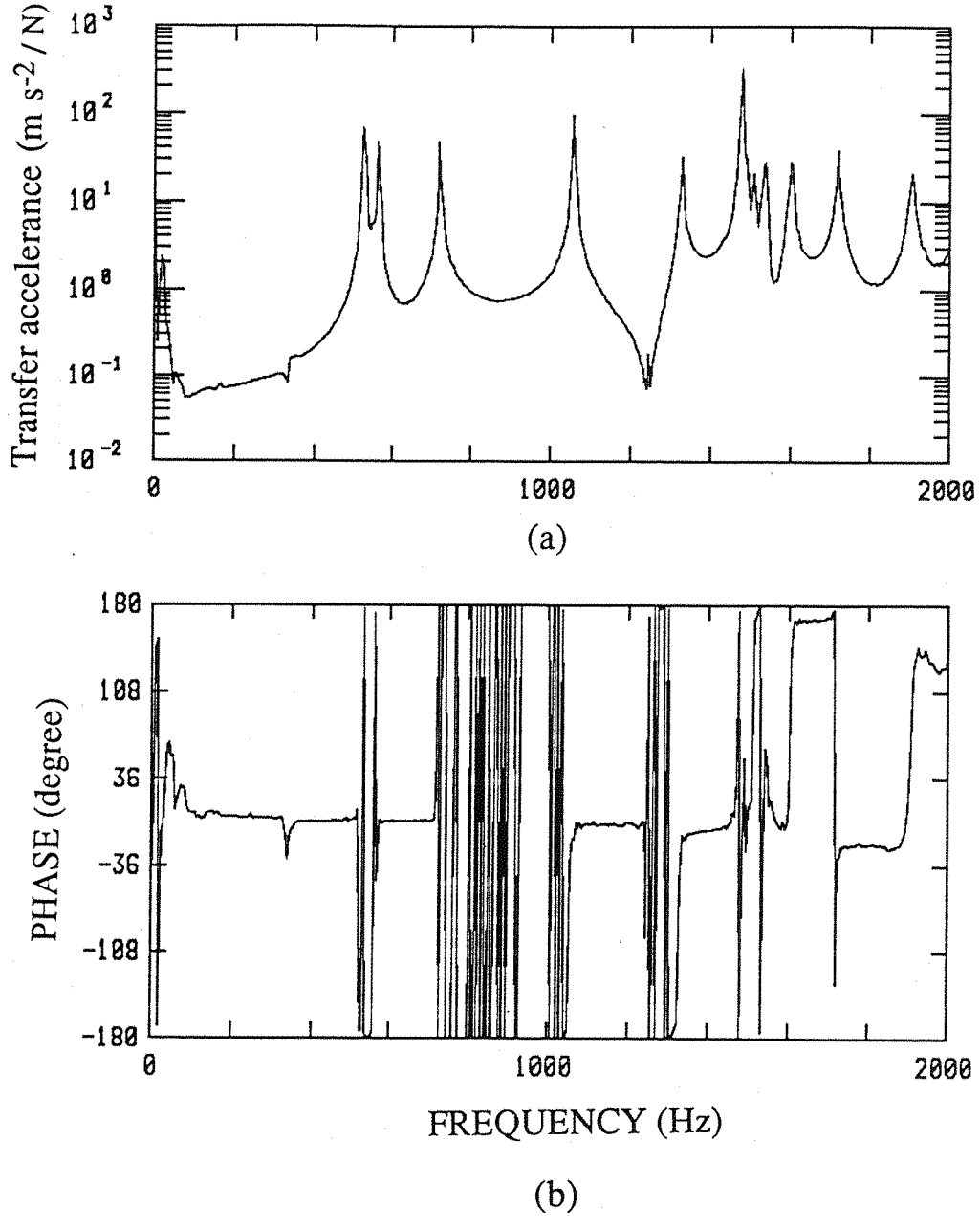

Figure 5.10 Measured transfer accelerance of a plain pipe (length = 1080 mm).

(a) Modulus, (b) Phase.

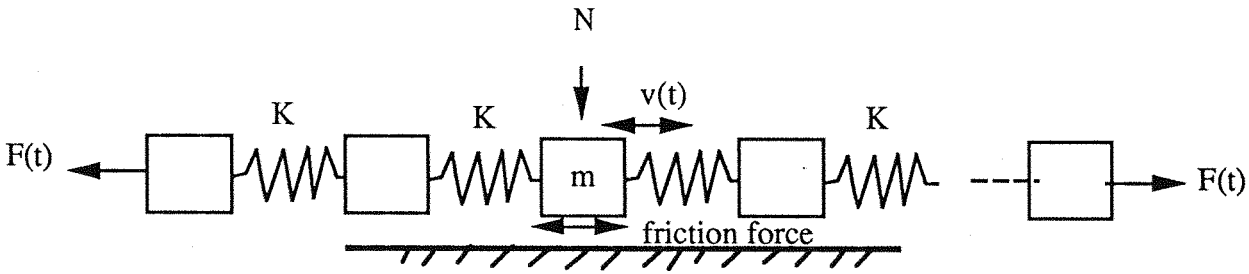

(a) A multi degree of freedom model of a spring around a pipe.

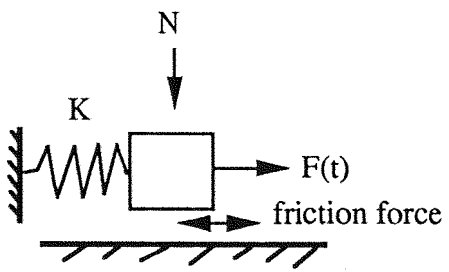

(b) One degree of freedom system with friction damping.

K=stiffness of spring, m=mass, v(t)=velocity of mass m,
F(t)=driving force, N=normal force.

Figure 5.11 Friction damping models.

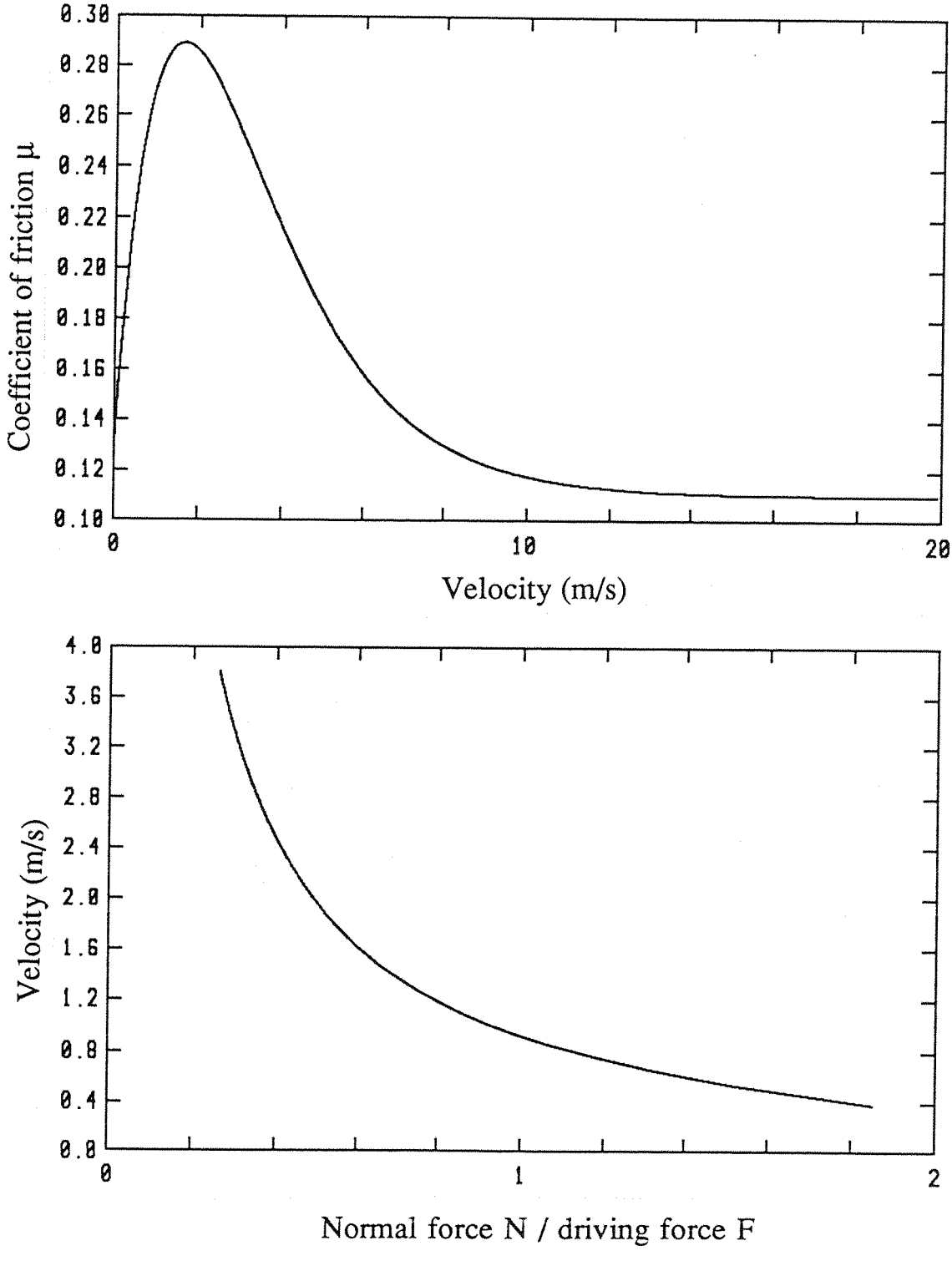

Figure 5.12 Calculated coefficient of friction versus velocity and velocity versus normal force.

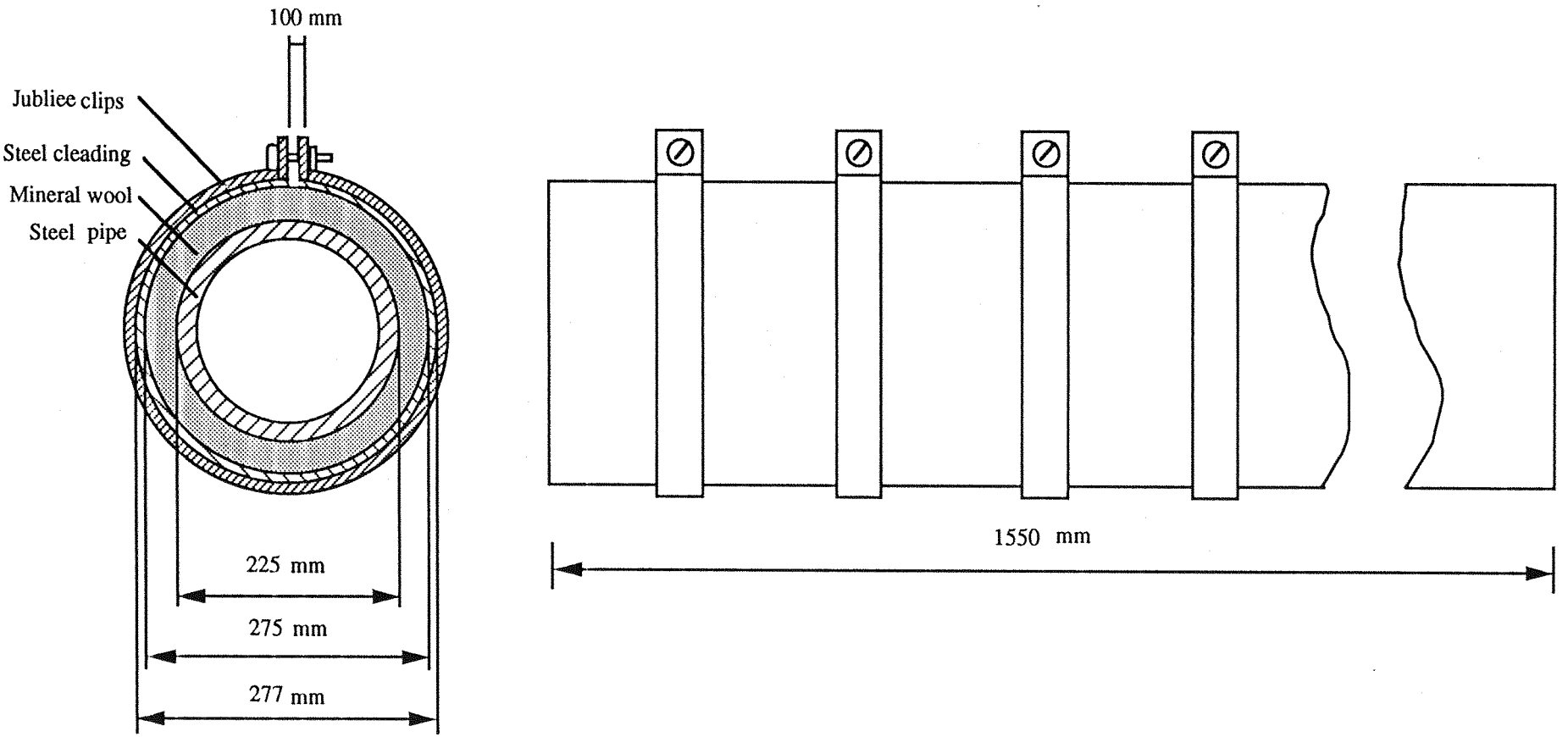

Figure 5.13 A pipe with wrapped mineral wool and steel "cleading".

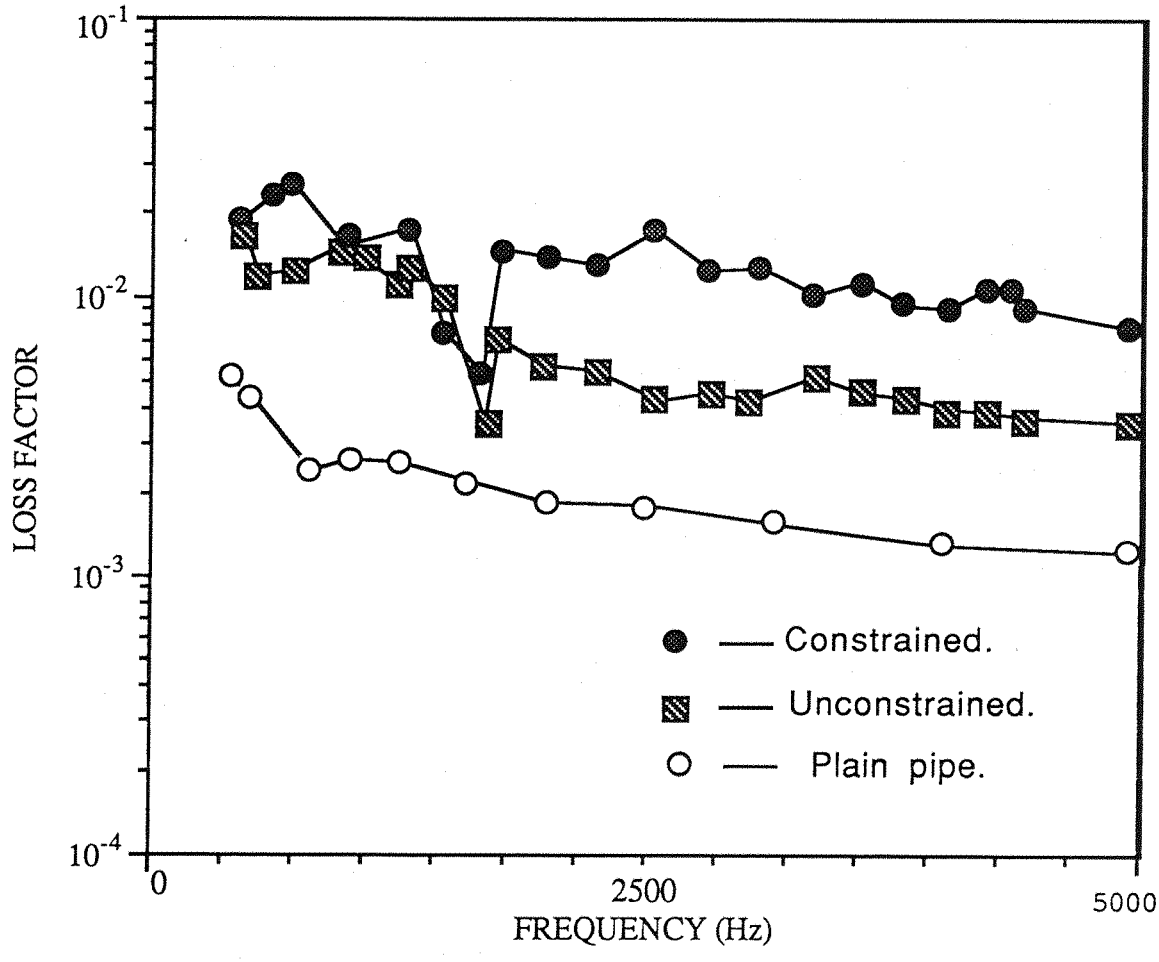

Figure 5.14 Comparison of measured loss factors of a plain industrial pipe and the pipe with constrained or unconstrained mineral wool lagging.

CHAPTER 6. SOUND TRANSMISSION LOSS THROUGH PIPE WALLS.

6.1 INTRODUCTION

In the previous chapters, the investigation involved studies of the vibration behaviour of pipes and the approaches to increasing the damping of a thin cylindrical shell to control vibration transmission and noise radiation from pipework. This type of problem has been also referred to as the control of "structure borne sound".

The approaches explored in the present study to produce damping for vibration control on a double pipe system included squeeze film damping by gas or liquid pumping in the annular gap between two pipes and friction damping by attached devices such as spring or wire rope or lagging. Further questions arise, such as, are these damping devices also effective in reducing sound radiation and how much sound energy will be transmitted through a pipe with those damping devices? In this chapter, acoustic properties of the damped pipes are studied experimentally.

6.1.1 Definition of Sound Transmission Loss.

The transmission of fluid-borne sound from inside a pipe to the surroundings through the pipe wall is of practical interest in many industrial applications. The sound is radiated from the pipe to produce the resulting sound field in the environment. Only a portion of the internal sound energy is transmitted through the pipe wall and the process will depend on the nature of the internal sound field, the acoustical properties of the internal and external fluids, the geometry (thickness/diameter ratio) of the pipe and the acoustical and damping properties of the pipe material.

The "transmission loss" is often used to assess the ratio of sound power transmitted through a pipe wall. Transmission loss (TL) is conventionally defined as

$$TL = 10 \log_{10} (1/\tau) \tag{6.1}$$

where τ is the transmission coefficient

$$\tau = \frac{I(\text{external})}{I(\text{internal})} = \frac{\text{Acoustic intensity of transmitted wave}}{\text{Acoustic intensity of incident wave}} \tag{6.2}$$

The transmission loss of a pipe differs considerably from that of the more usual flat plate case. For the cylindrical geometry of a pipe, it must be recognized that there are several deviations from the often studied ideal case. First, the radiated power is typically proportional to the surface area of the pipe while the incident power is proportional to the cross sectional area. The transmission loss for a given specimen is also a function of the ratio of length to diameter. Secondly, the sound field exciting the pipe interior is certainly not isotropic in the frequency range of interest due to the limitations of propagation within the cylindrical geometry. Third, the sound field is not homogeneous because of attenuation due to dissipation and radiation.

The approach of defining TL on the basis of power flow rather than internal mean square pressure has the significant virtue of obviating the need for dealing with the singularities in the mean square internal sound pressure at the cut-off frequency, which convey no net power down the pipe. It is appropriate at this point to denote two important frequencies for cylindrical shells. The first is the ring frequency, defined as

$$f_r = C_L / \pi D \tag{6.3}$$

where

C_L = the longitudinal wave speed in the pipe wall,

D = diameter of the pipe,

the ring frequency can be thought as the upper limit for curvature effects, since it represents the frequency at which the time for stress wave propagation becomes sufficiently long so that the phase change around the pipe circumference is large.

The second is pipe wall critical frequency, which is defined from the flat plate equation as

$$f_c = (c^2 / 2\pi)\,(m/B)^{1/2} \approx c^2 / 1.8\, C_L h \tag{6.4}$$

where

c = speed of sound in the fluid,

m = mass per unit surface area of pipe wall,

B = the bending stiffness per unit width of the pipe wall,

h = the thickness of the pipe wall.

When the adjacent fluids differ in sound speed on either side, a different critical frequency for each side must be defined. When the critical frequency f_c is computed to be less than the ring frequency f_r, the physical significance of f_c is questionable since curvature of the walls will have a greater significance in determining the flexual wave speed in the wall.

In practice, the sound transmission loss is given as

$$TL = 10 \log [<P^2> S/4\rho_0 c W_t] \qquad (6.5)$$

where

$<P^2>$ = the space-average mean square pressure in inside a pipe,
S = the sound radiation surface area,
W_t = the sound power transmitted through a measured surface,
ρ_0 = the density of air,
c = sound speed of air.

The item W_t/S is the sound intensity. By using simple calculation referred to a reference sound intensity level $I_0 = 1 \times 10^{-12}$ w/m^2 and reference sound pressure level $p_{ref} = 20 \times 10^{-6}$ N/m^2, sound transmission loss can be rewritten as

$$TL = <L_p> - L_I - 6.1 \ \text{(dB)} \qquad (6.6)$$

where

$<L_p>$ = the space-averaged sound pressure level in the pipe,
L_I = the sound intensity level through a measured surface.

To measure the TL in practice, the measurements of sound pressure level L_p inside pipe and sound intensity level around the surface of the pipe are needed.

6.1.2 Sound Intensity and its Measurement.

Sound intensity is defined as the vector quantity pu,

$$I = p(t)\, u(t) \qquad (6.7)$$

where

p(t) is the instantaneous acoustic pressure at a point, u(t) is the instantaneous particle velocity vector.

The sound intensity level is defined as

$$L_I = 10 \log_{10}[I/I_0] \quad dB \tag{6.8}$$

where

I_0 = the reference sound intensity, 10^{-12} Wm^{-2}.

In practice, sound intensity can be estimated by measuring a pressure difference Δp, which exists between points along an axis separated by a distance Δr. For time stationary fields, the time average intensity component is given by

$$I_n \approx \frac{1}{2\rho_0 \Delta r} p_1 p_2 (\phi_1 - \phi_2) \tag{6.9}$$

where

$\phi_1 - \phi_2$ = phase different of p_1 and p_2.

The frequency domain equivalent of equation (6.9) is

$$I_n(\omega) \approx - \frac{I_m\{G_{12}(i\omega)\}}{r_0 \omega \Delta r} \tag{6.10}$$

where G_{12}= the cross spectral density of the two pressure signals. The logarithmic measure of I is the sound intensity level.

This measurement can be achieved by use of a sound intensity probe, which consists of two nominally identical microphones placed Δr apart, as shown in figure 6.1.

Since sound intensity is a power flux density, practical procedures are required for sampling the continuous normal intensity distribution over a chosen measuring surface. There are basically two distinct sampling methods:

1). 'point sampling': a intensity probe is held stationary at discrete points on the surface for the period of time to adequately and precisely estimate the sound intensity.

2). 'scanned sampling': a intensity probe is traversed or swept along a continuous path over a portion of a measurement surface and time average estimate is obtained by this way.

In this research, the 'scanned sampling' method was used.

6.1.3. Sound Pressure Level and its Measurement in a Pipe.

The definition of sound pressure level is

$$L_p = 20 \log_{10} (p / p_{ref}) \qquad (6.11)$$

where the sound reference pressure in air is

$$p_{ref} = 20 \text{ m Pa } (20 \times 10^{-6} \text{ Nm}^{-2}).$$

In the measurements, the space-averaged and time averaged sound pressure level was measured at the end of a closed pipe, as will be described in section 6.2.

6.2 INSTRUMENTATION AND TEST PROCEDURES.

A series of experiments were set up for investigating acoustic properties of a damped pipe. The sound transmission loss through the wall of a damped pipe with air or oil squeeze film damping, or friction damping was measured. An industrial pipe (a pipe practically used in power stations) covered by an unconstrained or constrained mineral glass fibre layer was also tested.

6.2.1 Acoustic Excitation in a Pipe.

Two sizes of pipe were used in the experiments. The pipes were acoustically excited by a loudspeaker at one end of each pipe.

The loudspeaker consisted of a power drive unit and an acoustic horn. The power drive unit used was model DCR 100 (100 watts power and 8 Ω resistance) and the designed cut-off frequency is 500 Hz. To drive a damped pipe with a diameter of less than 120 mm , a plastic tube was used to connect the pipe to the loudspeaker drive unit as shown in figure 6.2 a. The other end of the pipe was covered by a circular plastic plate.

To drive an industrial pipe, which has large diameter (over 200 mm diameter), a horn was designed to connect the drive unit to the pipe as shown in figure 6.2 b. The other end of pipe was enclosed by a rigid plate, where sound pressure was measured. The sound power is transmitted through the pipe wall as shown in figure 6.3.

The radii of the horn inlet and exit governed by the diameter of the drive unit and the radius of the pipe. The length of the horn was designed according to the cut-off frequency of the drive unit. The design of the acoustic horn was based upon the need to be coupled to the end of the pipe and the consideration of the frequency range. The design work is shown in appendix 6.1. The horn was made of polyester resin mixed with C.S.M. (chopped strand glass fibre mat). The dimension of the horn and the loudspeaker assembly are given in figures 6.4 and 6.5.

6.2.2 Acoustical Shield against Background Noise.

Although the in-situ intensity measurement method is practically available and has proved to be of great advantage, extraneous noise sources may still disturb the sound field and create serious bias errors in the sound power estimate, especially when the extraneous noise sources are stronger than the sound source of interest. For example, when scanning to measure sound power along a pipe wall, there are strong sound power radiations from both the ends of the pipe, the coupler and the body of the loudspeaker. The extraneous sound itself has a different phase compared with the sound inside the pipe and may result in cancellation or enhancement. To solve this problem during the TL test, an acoustical shield was placed between the loudspeaker and the "driven" end of the pipe. The other end of the pipe was covered by thick plastic foam to prevent sound radiation from the source to the test area via this path. The arrangement of acoustical shield is illustrated in figure 6.6.

6.2.3 Test Configurations.

Sound transmission loss tests were performed on the two kinds of damped pipes, which were damped by squeeze damping and friction damping.

A double pipe system with air or oil gap

A double pipe system, which consisted of two concentric pipes, is indicated in figure 6.6, where the inner pipe was acoustically excited. The dimensions (in mm) of the double pipe system were

	Inner diameter	Outer diameter	Length	air or oil gap
Inner pipe	98	102.3	1080	
				0.85
Outer pipe	104	108	1000.	

The two pipes were connected by two means. First, three screws were mounted in tapped holes close to each end of the outer pipe; the screws were at 120^0 to each other and held the inner pipe relative to the outer pipe. The second connection was at the ends of the pipes where the gaps were filled with silicone rubber compound; there were air holes in the seal for the air gap but the ends were completely sealed for the oil filled case. The seal and pipe spacing method are shown in figure 6.6.

The pipe damped by a coiled spring or a wire rope.

A pipe was damped either by a coiled spring or a wire rope, which were the same as shown in figures 5.1 and 5.2, and was also excited by loudspeaker for the acoustical measurements. The dimensions of the pipe were the same as the inner pipe above (d=

98 mm, D = 102.3 mm, L =1080 mm). The details of the test springs and wire ropes were:

1. a pipe with coil spring

	spring 1	spring 2	spring 3
diameter of spring coil (mm)	12	8	7.5
diameter of spring wire (mm)	1.6	1.6	1.1
pitch between two coils (mm)	7	6	3.8

2. a pipe with wire rope wound around it

	wire rope 1	wire rope 2
diameters of rope (mm)	5	4

An industrial pipe wrapped with mineral wool and single or double cladding.

A mineral wool lagging was wrapped on a pipe. The mineral wool layer was covered by a steel cladding or double cladding with 1 mm air gap, which was rolled into a cylindrical shape and gripped by clips. The design is shown in figure 5.13, and the sketch of double claddings is in figure 6.7. The dimensions of the industrial pipe were inner diameter d = 204 mm,

outer diameter D = 219 mm,

length = 1583 mm.

The thickness of mineral wool = 25 mm.

The dimensions of the double cladding were

thickness of inner steel cladding: 1 mm,

thickness of outer steel cladding: 1 mm,

air gap between two claddings: 0.5 - 1.2 mm.

The air gap between the two claddings was controlled by 1 mm thickness rubber supports, but the gap dimensions varied according to the radii of the steel cladding,

which was made of rolled plate. Clips around the outside of the pipe were used to constrain the lagging system.

6.2.4 Measurements of Sound Intensity and Sound Pressure.

(1). Sound intensity measurement;

The instrumentation for TL measurement is shown in figure 6.8. The test pipe with loudspeaker attached was suspended by rubber cords on a frame as shown in figure 6.9. The baffle and rubber foam at the two ends of the pipe were removed for clarity, when the photograph was taken. A random noise generator and power amplifier system were used to drive the loudspeaker, and the radiated sound was detected by condenser microphone from which the signals were fed to an analyser (B&K 2032 Dual Channel Signal Analyser).

The scanning method was used to measure the sound intensity normal to the pipe wall and the surface of the lagging materials. The route and area which was scanned by the sound intensity probe are shown in figure 6.10a.; 400 samples were acquired in the scanning measurement on damped pipes and on an industrial pipe.

A typical measured sound intensity around a plain pipe obtained by use of the scanning method is shown in figure 6.11.

(2). Internal sound pressure measurement.

Sound pressure was measured at the end of the pipe. The instrumentation used for the measurements is shown in figure 6.12. A circular plate with three holes was used as a cover at the end of the pipe; 1500 samples were acquired from 15 points at the end of the pipe, where the cover plate was rotated. The measurement positions are shown in figure 6.10 b.

A typical measured sound pressure within a plain pipe is shown in figure 6.13.

6.3. PREDICTION OF SOUND TRANSMISSION LOSS.

By computing an impedance for the pipe wall in terms of a harmonic forcing function and relating the transmission coefficient in the form of equation (6.2) to a model of the interior sound field [74][75], the transmission loss for a thin shell, for the frequency range below 0.8 f_r is given by

$$TL_1 = 10\,Log_{10}(C_L m/\rho_0 c\, D) + 5\,Log_{10}[(f/f_r) - (f/f_r)^2] + 1.5\ dB \qquad (6.12)$$

where

ρ_0 = density of fluid,

m = mass per unit surface area of pipe wall,

$\rho_0 c$ = the impedance of the acoustic medium,

C_L = the longitudinal wave speed in the pipe wall,

D = diameter of the pipe.

The theory for calculating transmission loss across air gaps is based on reference [61]. for a given layer the incremental TL is

$$\Delta TL = 20\,Log_{10}\,|P_I / P_T|\ dB \qquad (6.13)$$

where P_I / P_T is the ratio of incident to transmitted sound pressure for the air layer. The transmitted pressure ratio P_I / P_T is

$$P_I / P_T = \frac{\cosh\,[bh + \coth^{-1}\,(Z_2/Z_B)]}{\cosh\,[\coth^{-1}\,(Z_2/Z_B)]} \qquad (6.14)$$

where

$b = \omega/c_0(j + \eta_{air})$,

= the propagation constant of the air layer,

c_0 = speed of sound within the air gap,

η_{air} = acoustic air gap loss factor,which describe the decay of a plane wave propagating into a semi-infinite lossy medium, 0.4 is used in this study,

h = thickness of air gap,

$Z_2 = j\,\omega\,m + \rho_0 c_0$,

= impedance of the air gap,

$j\,\omega\,m$ = the inner wall mechanical impedance,

$\rho_0 c_0$ = the impedance of the air inside the cylinder,

$Z_B = \rho_0 c_0$.

The total sound transmission loss of a double pipe system with air gap is

$$TL = TL_1 + \Delta TL \qquad (6.15)$$

A rigourous analysis is not possible within the scope of this study, however, some possible mechanisms of TL through an air gap will be discussed in the following paragraphs.

6.4 ACOUSTICAL CHARACTERISTICS OF THE PIPES WITH DAMPING AND ACOUSTICAL TREATMENTS.

6.4.1. Transmission Loss of a Double Pipe System with Air or Oil in the Annulus.

Measurements of TL were made for a double pipe system with an air or oil filled gap, and the results are compared with the TL of plain pipe as shown in figure 6.14. TL of a double pipe system with 0.85 mm air gap was improved 5 ~ 10 dB when the pipes were connected by screws. The TL of the same double pipe system but sealed with silicone rubber was improved, particularly at some frequencies in the low frequency range (600 ~ 2000 Hz).

The TL of oil filled double pipe system improved only a little in the high frequency range and was worse at low frequencies compared with the plain pipes. As oil may not be as good as an acoustical isolator, the effect of oil in the gap is to add mass to the pipe system, and a little TL improvement can be achieved by the added mass of oil according to 'mass law'. The sound transmission loss, "mass law" is

$$TL = 20\,Log_{10}(m\,f) - 20\,Log_{10}(\rho_0\,c\,/\pi) \qquad (6.16)$$

Sound transmission loss TL will decrease at two kinds of resonance frequencies; the mass-air-mass resonance frequency of the double pipe system and the acoustical

resonance frequency in the air filled pipe. The mass-air-mass resonance frequency [76] of a double pipe system is

$$\omega_0 = \left[\left(\frac{\rho_0 c^2}{h}\right)\left(\frac{m_1 + m_2}{m_1 m_2}\right)\right]^{1/2} \qquad (6.17)$$

where

m_1, m_2 = mass per unit area of inner and outer pipes with air gap,

ρ_0, c and h are same as in equations(6.12 - 6.14).

The mass-air-mass resonance frequency f_0 is 732 Hz for the air gapped double pipe system used here.

The acoustical resonance frequency Ω is

$$\Omega_{np} = (k^{np} r)\,(c_i / c_l') \qquad (6.18)$$

where

Ω_{np} = nondimensional resonance frequency of acoustical modes of n and p (see figure 6.15),

$= \omega_{np} / \omega_r$,

ω_{np} = resonance frequency of acoustical modes of n and p,

ω_r = ring frequency,

k^{np} = radial wave number of acoustical mode of n, p,

r = radius of pipe

c_i = speed of sound in the containing fluid (air),

c_l' = longitudinal wave speed in the pipe material,

Values of $(k^{np} r)$ can be found in reference [76]. The first three acoustical resonance frequencies f_{np} for the inner pipe used here are

f_{10} = 2006 Hz, f_{20} = 3325 Hz, f_{01} = 4175 Hz.

Measured sound transmission losses for a plain pipe and air gapped double pipe system are compared with predicted values in figure 6.16 a and b. It can clearly seen that TL is

low in the regions of the frequencies of the acoustical modes f_{10}, f_{20} and f_{01}, the lowest TL occurring at the second acoustical mode f_{20}. The effects of these modes on TL by these mode are clear, both for the plain pipe and the double pipe system. At the mass-air-mass resonance frequency (f_0 = 730 Hz), the effect on the TL of the double pipe system can be clearly seen in figure 6.16 b.

The predicted transmission losses are reasonably consistent with the experimental data in relation to the simple nature of the models used and the assumptions made, the two sets of experimental data being very similar in nature and only slightly different in level. The following interpretations may be useful for study of noise control by use of a double pipe system.

(1). For the frequencies below the mass-air-mass resonance frequency, the structural damping has negligible influence, this could explain the low values of TL at low frequencies.
(2). At the mass-air-mass resonance frequency f_0 TL is minimised. At frequencies close to f_0, TL is damping controlled [76], so that TL is high at frequencies close to f_0 in the experimental results and the same tendency is apparent in the predicted curve.
(3). At frequencies above f_0, TL is mass controlled. The increase of TL in the double pipe system at high frequencies assumed because of the added mass of the outer pipe.

6.4.2 Sound Transmission Loss of a Pipe with Friction Damping Treatments.

From the previous chapter it is clear that adding the spring and cable to a pipe increased structural damping. Experiments are carried out to ascertain any effects on the transmission loss. Measured TL values for a pipe wrapped by 12 mm, 8 mm and 7.5 mm diameter coiled springs with various pretensions (the same as chapter 5) are shown

in figures 6.17, 6.18 and 6.19. It is clear from these three figures that TL has been improved in a frequency range of 500 ~ 1500 Hz and frequencies above 2000 Hz.

To control noise radiation from an acoustically excited pipe, a damping treatment is obvious normally only effective at resonance frequencies [59]. For the convenience of study, the first a few vibration resonance frequencies of the pipe in figure 5.1 are re-listed here; 504 (1,2), 561(2,1), 737 (2,3), 1056 (2,4) Hz ...., where the numbers in parentheses (n,m) indicate the modal behaviours in the circumferential direction (n) and the axial direction (m) of the pipe. At frequencies below the lowest resonance frequency, mass and damping are not important as this is the stiffness controlled region. At the first few resonance frequencies, damping became important in controlling the sound radiation. This is indicated in the results shown in figures 6.17 to 6.19. Above the first few resonance frequencies, the mass generally became most influential. It must be emphasised here that

(a). it can not be concluded that for all frequencies above the first few resonance frequencies, the TL of pipe is always mass controlled.

(b). high damping does not necessarily produce high TL, it may enhance the sound radiation.

There is no improvement in sound transmission loss ΔTL at 2000 Hz. It could be assumed that there may be a coincidence frequency of a structural mode and an acoustical mode in this region. Above 2000 Hz, TL is mass controlled and ΔTL is about 20 dB. The mass controlled region extends up to the 'critical frequency', this is not discussed here.

The effect of spring pretension is variable below the first acoustical mode. Above this frequency, the various pretensions were found to have little effect on TL in these experiments.

Similar conclusions can be drawn from the results of the tests on the wire rope damped pipes, which are shown in figure 6.20. At the first acoustical mode, ΔTL is very small for 5 mm and 4 mm wire rope damped pipes. ΔTL varies below this frequency. Above the first acoustical mode, TL is assumed to be as mass controlled, and TL gradually increases with increasing frequency as for the coiled spring damped pipe. The increase of TL with increasing frequency is in accordance with the theory of the mass law of acoustical transmission loss.

6.4.3 Sound Transmission Loss through an Industrial Pipe with Mineral Wool Covered by Single or Double Partitions.

The TL of a plain industrial pipe was measured. The results were compared with the prediction shown in figure 6.21 and table 6.1. The measured and predicted values of TL, are fairly close in the frequency range above 1000 Hz.

To study the effects of the resonance frequencies of structural and acoustical modes on TL and their possible coincidence point, the structural and acoustical resonance frequencies of the plain pipe are listed as follows,

Resonance frequencies:

structure

n	m	theory (Hz)	experiment (Hz)
1	2	456	439
2	1	460	503
2	2	482	—
2	3	646	679
2	4	943	918
1	3	1069	1055

acoustic (theory)

f_{10} = 1000 Hz, f_{01} = 2082 Hz, f_{11}= 2897 Hz, f_{30} = 2282 Hz.

At the first structural resonance frequency, TL is low. At the first two acoustical resonance frequencies, TL appeared lower than that in the low frequency range. At frequencies above f_{10} and f_{01} TL obeys the mass law.

When the plain pipe was wrapped with mineral wool and single wall cladding, TL increased by 5 ~ 25 dB as shown in figure 6.22. Above 1000 Hz, the increment ΔTL was greater according to the mass law effect.

However, for a pipe wrapped with mineral wool and covered by double wall cladding (which had a 1 mm air clearance), the TL generally increased by less than 5 dB for most of the frequency range compared that with single wall cladding.

There was no obvious increment of TL when constraint was applied to both the single wall and double wall covered mineral wool layers; the results are shown in figures 6.22 and 6.23. A general comparison of results for the plain pipe, and the pipe with mineral wool constrained by double and single wall cleading can be seen in figure 6.24.

6.5 DISCUSSIONS

6.5.1 Sound Intensity Measurement.

Because sound intensity is a vector quantity, measurement can be carried out in normal noise environment. The reason is that when a certain area is chosen for scanning measurement, the average incident sound intensity will be cancelled by reflected sound intensity from the surface. This means that in a measurement close to a non-sound-source body, sound intensity should be zero. In the experiments reported upon here, it was found that if the external sound intensity of the noise source was not stronger than

that radiated from the measuring surface, the measured results would only be slightly affected by noise. Furthermore, even a strong noise source could only affect the sound intensity measurement in the low frequency range (e.g. < 1000 Hz). In the experiments, reliable results could be achieved by simply covering the loudspeaker with plastic foam or using a wooden plate having twice the area of the end of the pipe as a baffle to isolate the noise radiated externally from the source.

6.5.2 Coupling between structural modes and acoustical modes.

The acoustical coupling between the fluid contained in a pipe and the structure is very much dependent upon the relative axial phase speeds (or axial wave numbers) of the wave guide modes in the two media. In the cases of coupling between a metal pipe and low pressure gases, the coupling modes may be assumed to retain their uncoupled characteristics. It was stated in a previous study [76] that the only waves of equal circumferential order n may couple. In most practical cases, coincidence between the lower order shell modes and the acoustical modes of low radial order p occurs at frequencies close to the acoustical mode cut off frequency.

A high density of coincidences appears around the ring frequency and at the frequencies of coincidence a reduction in transmission loss can be observed.

6.5.3 The relationship between transmission loss and damping for a double pipe system.

From this study, it was shown that TL is increased with added damping only at the first few structural resonance frequencies. The double pipe system with oil or air in the gap exhibited increased damping. The double partitions effect is also important in producing the mass-air-mass resonance effect but this, of course, did not occur with oil filling. The air gap double partitions effect did produce some effect on the lagged pipe where 5~10 dB extra transmission loss occurred at high frequencies.

6.5.4 Transmission loss of a mineral wool covered pipe.

Mineral wool, normally with metal cover, is used in industry to reduce noise radiation from pipes. The mechanism of increasing TL within mineral wool is that it absorbs the sound energy during the multiple reflection of sound between two metal surfaces, within which the mineral wool layer is sandwiched. Using a double partition cover, instead of single partition, does not enhance the sound absorbing effect. Mineral wool is effective only at high frequencies.

6.6 CONCLUSIONS.

(1). A double pipe system with an air gap may improve sound transmission loss by 5 ~ 10 dB but an oil filled gap is less effective for minimising acoustical energy transmission through the wall of a pipe.

(2). Friction damping is effective for increasing TL but only at the first few structural resonance frequencies. At high frequencies, the TL obeys the mass law effect.

(3). Mineral wool with a steel sheet cover (cladding) increases sound transmission loss by 5 ~ 10 dB at lower frequencies and about 25 dB at high frequencies. Double partitions will not greatly enhance the sound absorbing effect.

Table 6.1 Sound pressure and transmission loss of a plain pipe.

f (Hz)	500	630	800	1000	1250	1600	2000	2500	3150	4000	5000
<Lp>	126.5	126.8	128.0	126.5	124.9	121.0	129.9	124.5	121.0	122.8	119.4
Lw1	70.5	60.5	64.5	64.3	66.1	69.6	68.9	69.7	65.4	65.1	60.0
Lw2	69.2	59.5	63.4	66.4	65.5	70.7	68.9	68.4	65.1	64.7	60.1
Lw3	71.6	63.8	62.8	65.9	68.8	68.5	69.9	69.7	66.1	64.8	60.0
Lw4	66.4	60.7	61.0	60.1	64.8	67.2	68.9	69.8	64.4	64.4	60.1
TL1	50.4	60.7	57.9	56.6	53.2	45.8	55.4	49.2	50.0	52.1	53.8
TL2	51.7	61.7	59.0	54.5	53.8	44.7	55.4	50.5	50.3	52.5	53.7
TL3	49.3	57.4	59.6	55.0	50.5	46.9	54.4	49.2	49.3	52.4	53.8
TL4	54.5	60.5	61.4	60.8	54.5	48.2	55.5	49.1	51.0	52.8	53.7

<Lp> = the space average sound pressure level in the pipe (dB).
L_{wi} = the ith test of sound intensity level (dB).
TL_i = the ith test of sound transmission loss (dB).

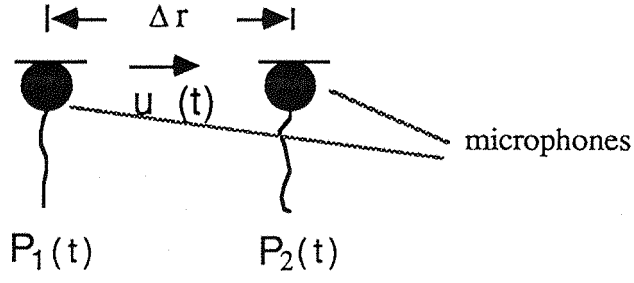

$P_1(t)$, $P_2(t)$ = the measured sound pressure level,
$U(t)$ = the particle velocity,
Δr = the distance between two microphones.

Figure 6.1 Principle of two-microphone sound intensity measurement.

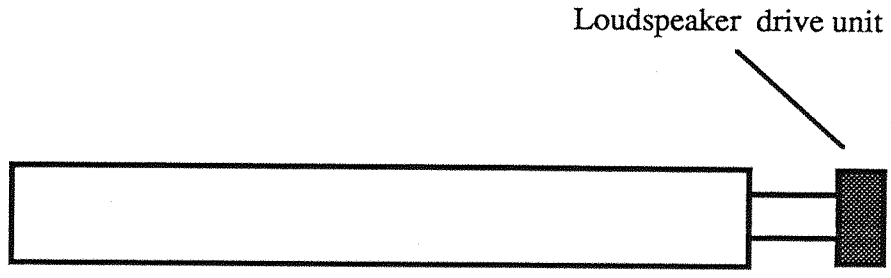

(a)

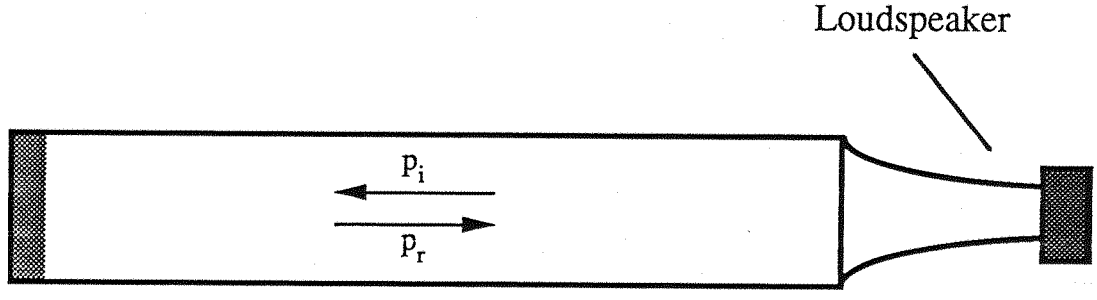

(b)

Figure 6.2 Acoustic excitation in a pipe.

(a) Loudspeaker connected to a small pipe.
(b) Loudspeaker connected to a large pipe.

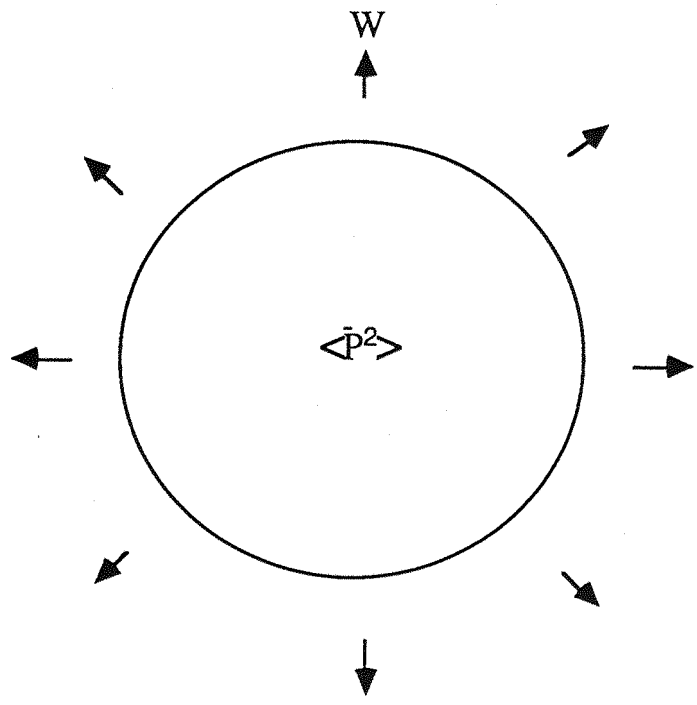

W —— Radiated sound energy

<p̄²> —— Mean square pressure

Figure 6.3 Power of sound transmitted through the pipe.

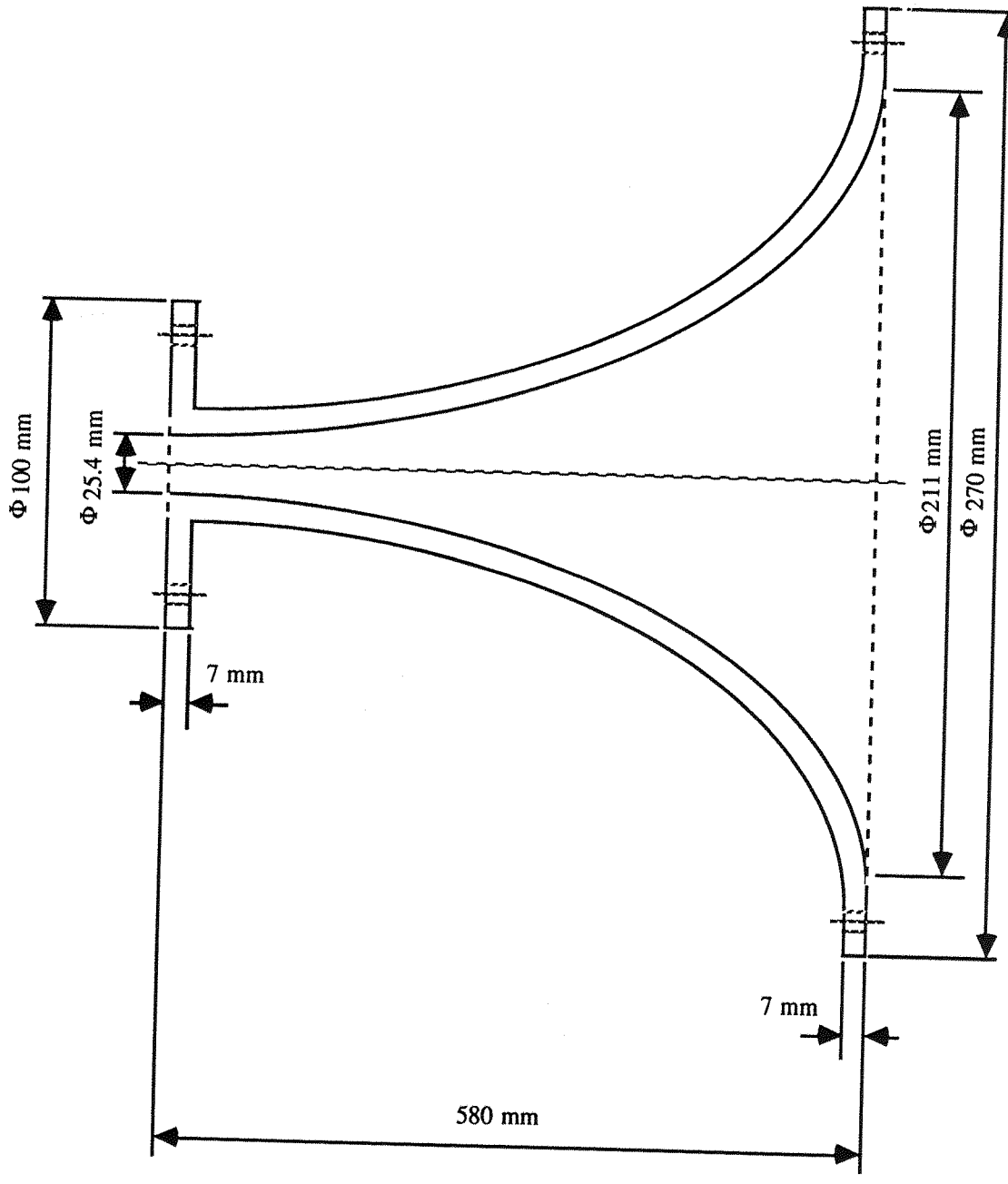

Figure 6.4 Cross section view of a horn.

Material: Polyester resin mixed with C.S.M. (chopped strand mat).

Figure 6.5 Loudspeaker.

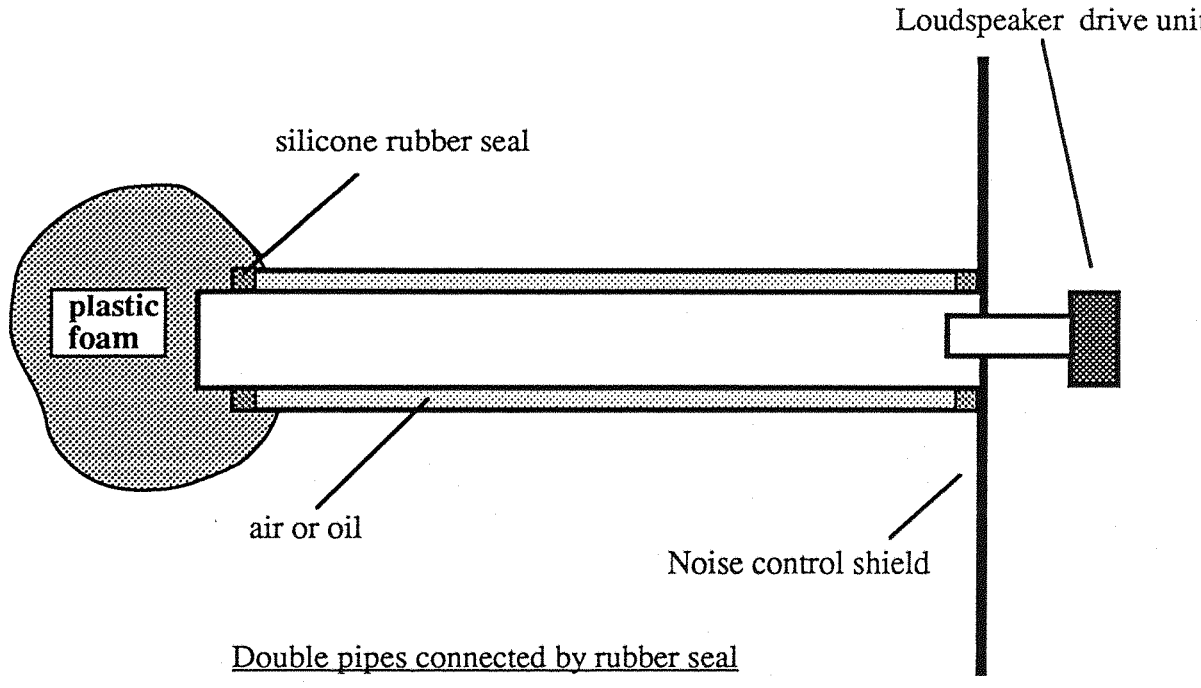

Double pipes connected by rubber seal

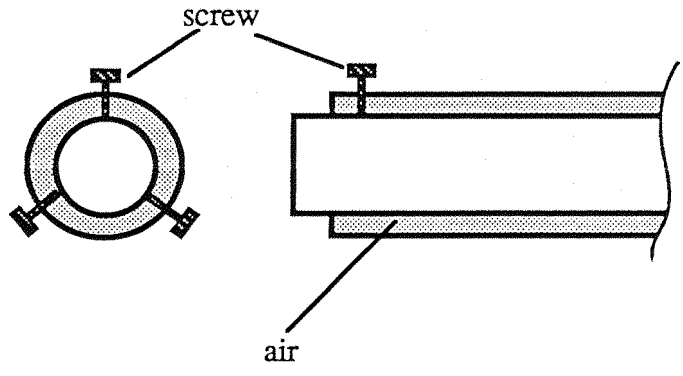

Double pipes connected by three screws

Figure 6.6 Acoustically excited double pipe system with air or oil annular gap.

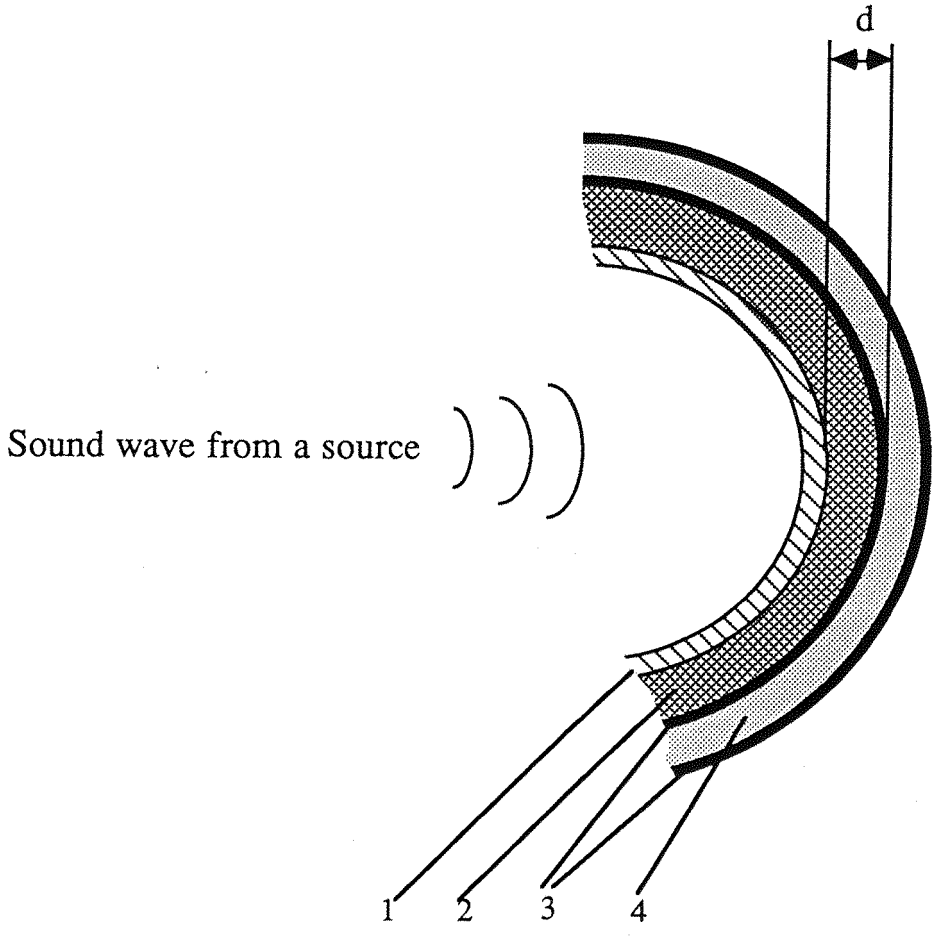

Figure 6.7 Structure of a pipe with wrapped porous acoustical material and double cladding.

1. Vibrating pipe
2. Acoustic porous material
3. Layers of rolled steel plates
4. Air gap

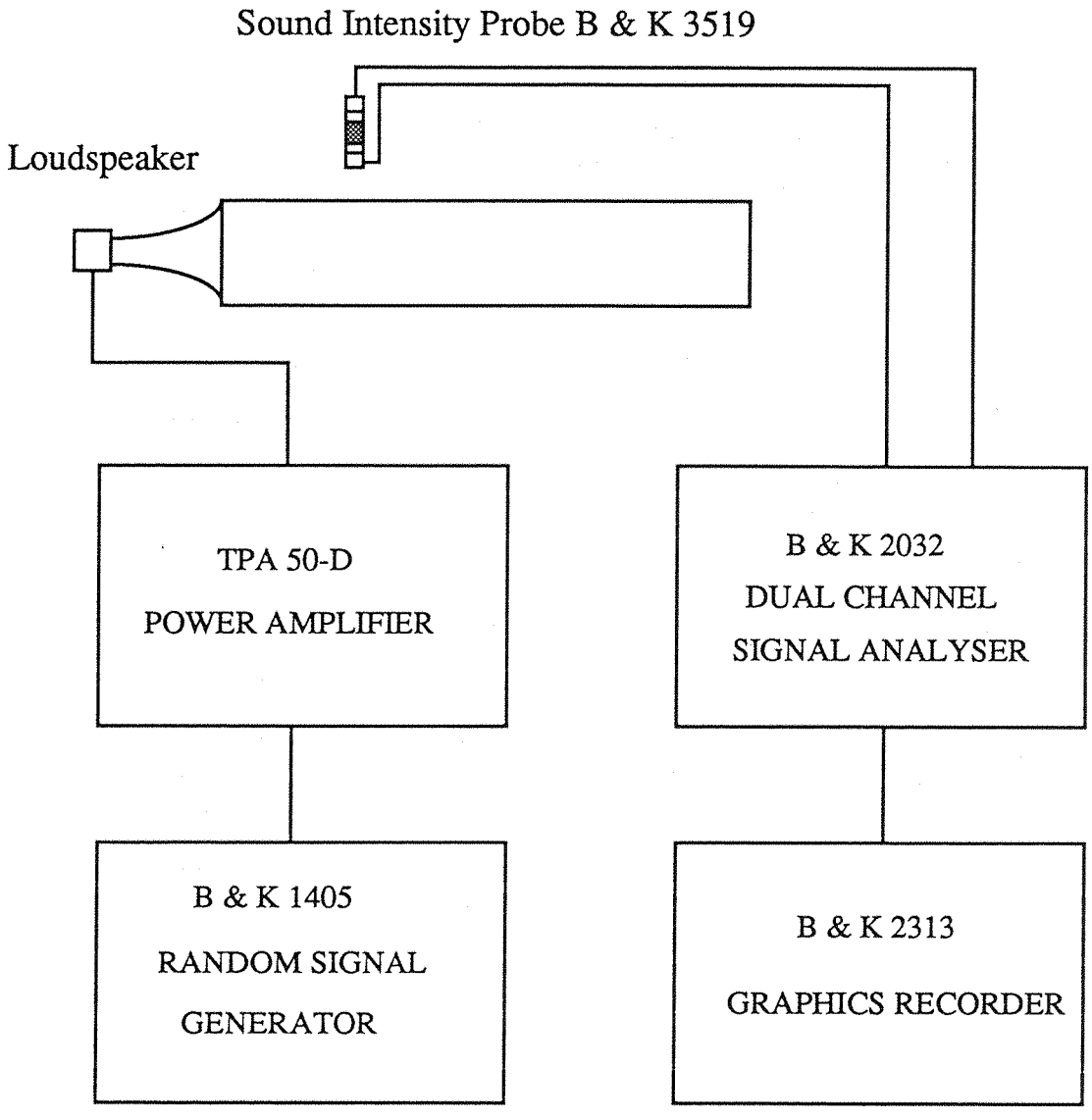

Figure 6.8 Sound Intensity Measurement

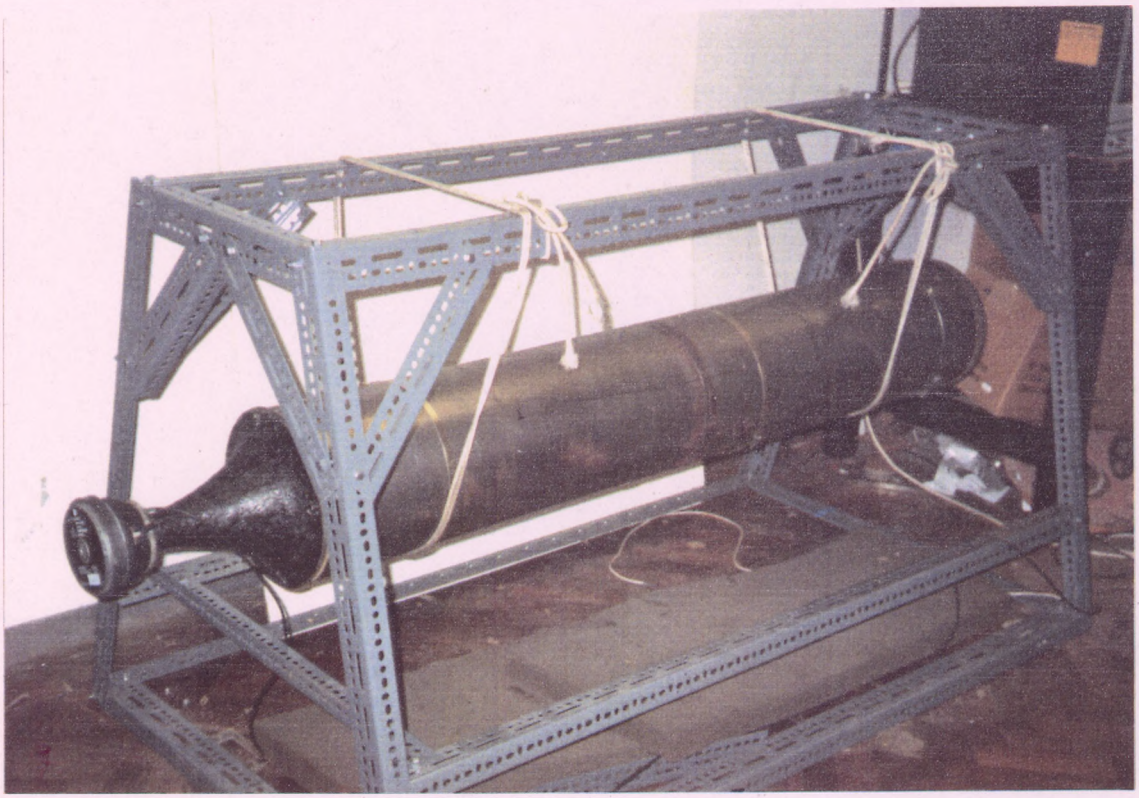

Figure 6.9 A pipe with loudspeaker attached and suspended on a frame.

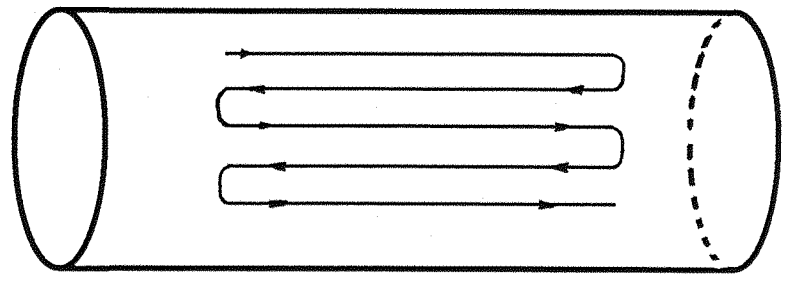

Figure 6.10a External scanning route for sound intensity measurement.

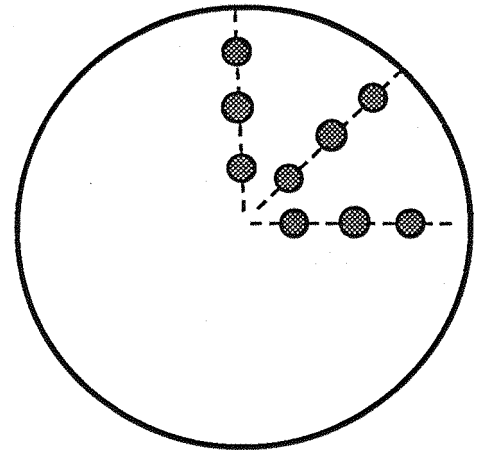

Figure 6.10b Positions for internal sound pressure measurement.

● — measuring point

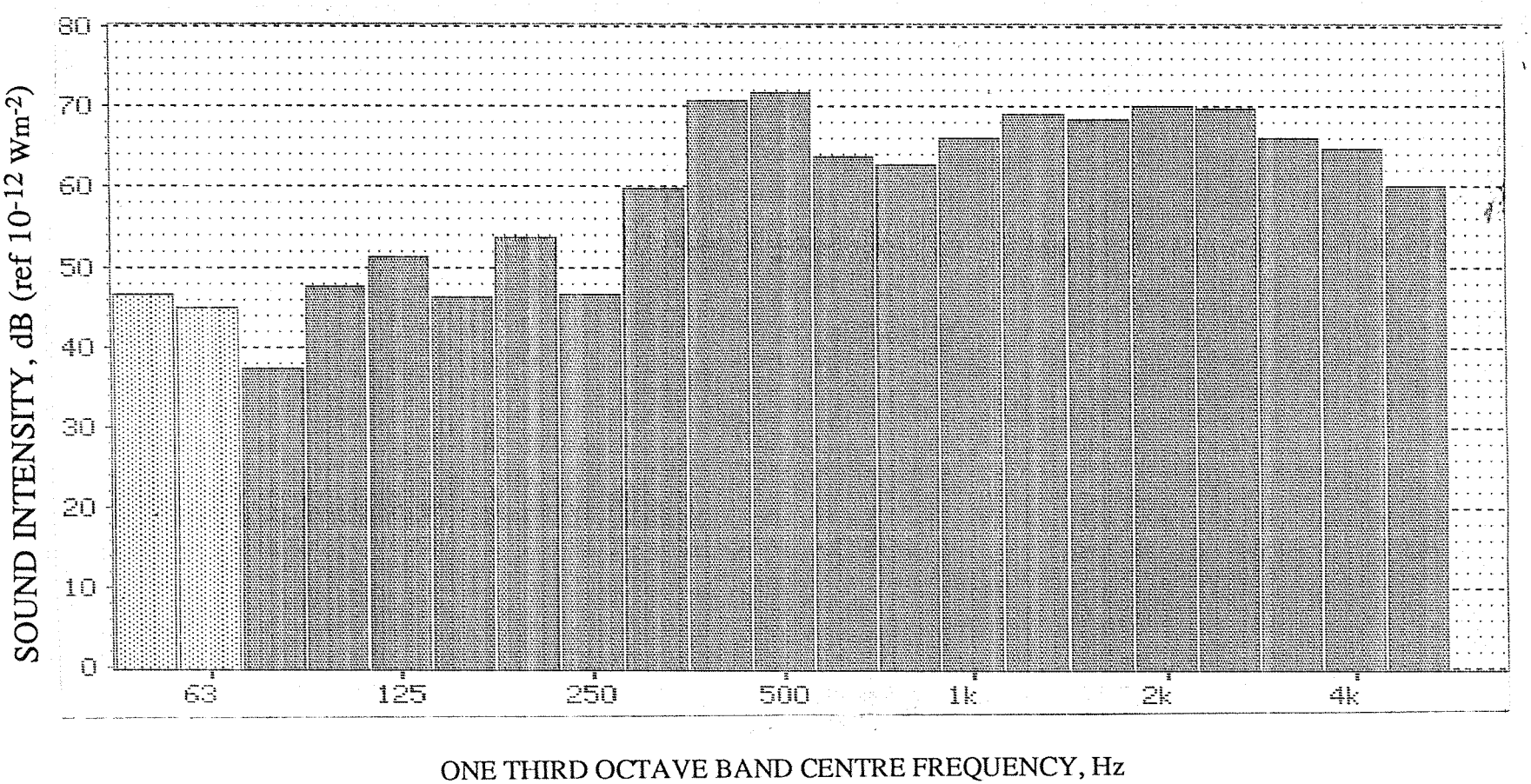

Figure 6.11 Sound intensity normal to the surface of a plain pipe.

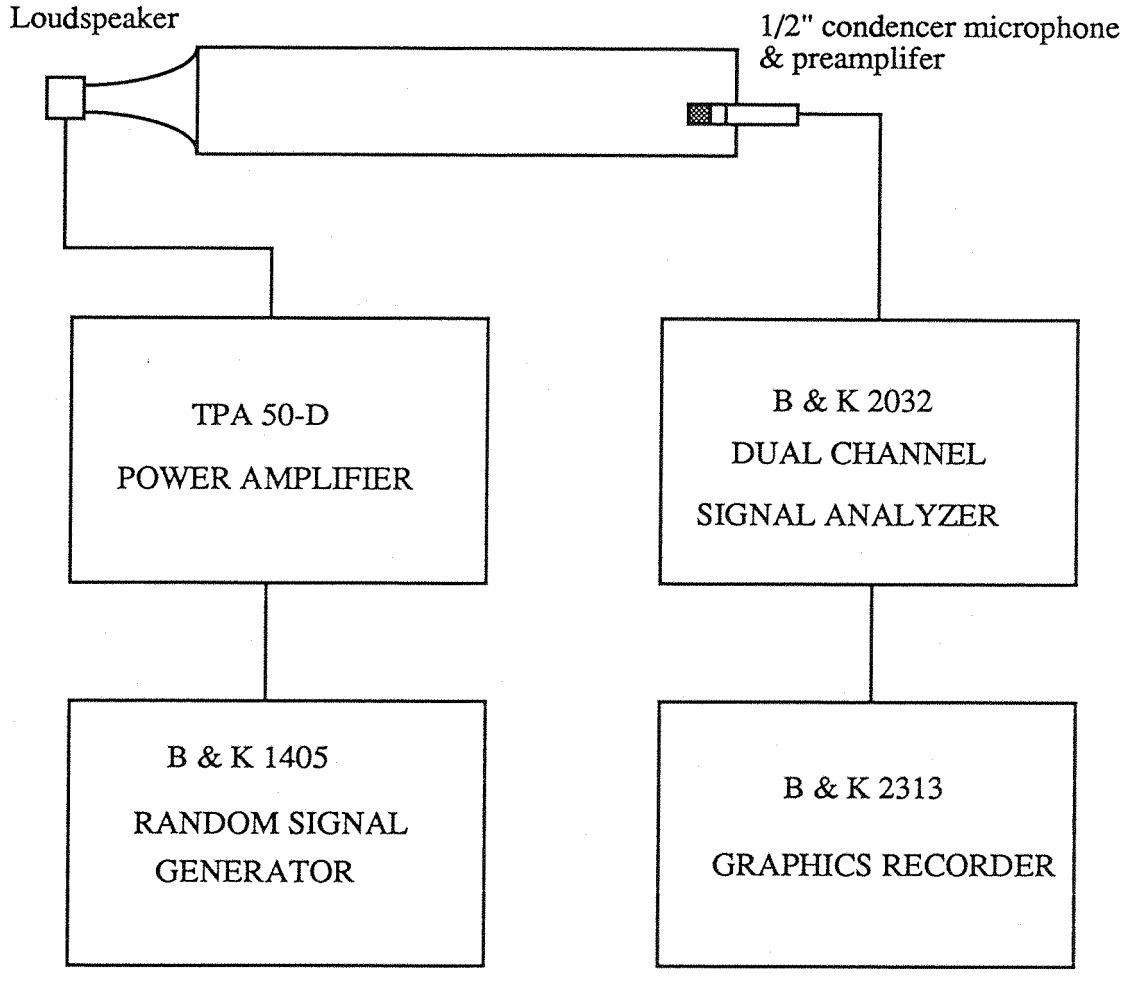

Figure 6.12 Sound Pressure measurement.

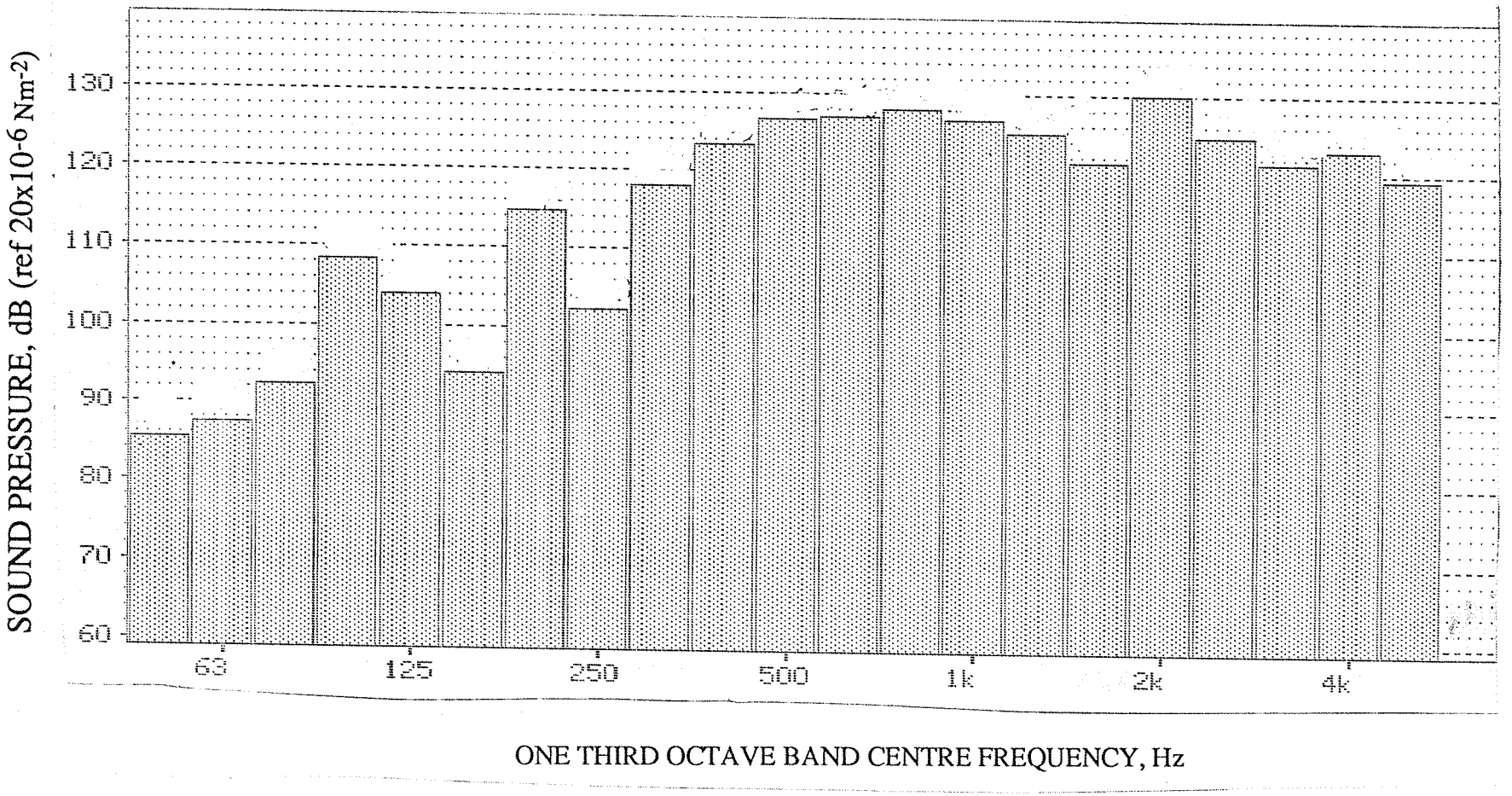

Figure 6.13 Sound pressure at the closed end of a plain pipe.

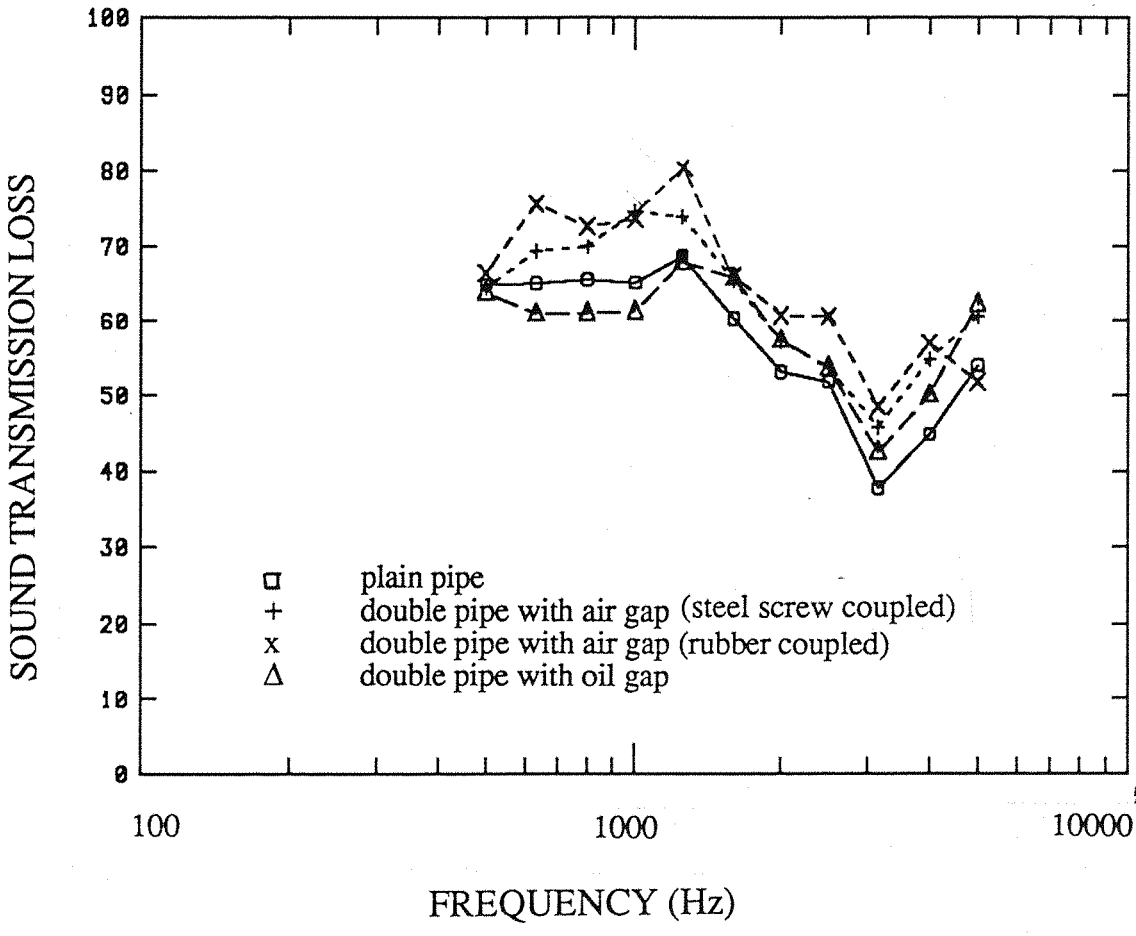

Figure 6.14 Measured sound transmission loss a plain pipe and double pipe system with air or oil in the annular gap.

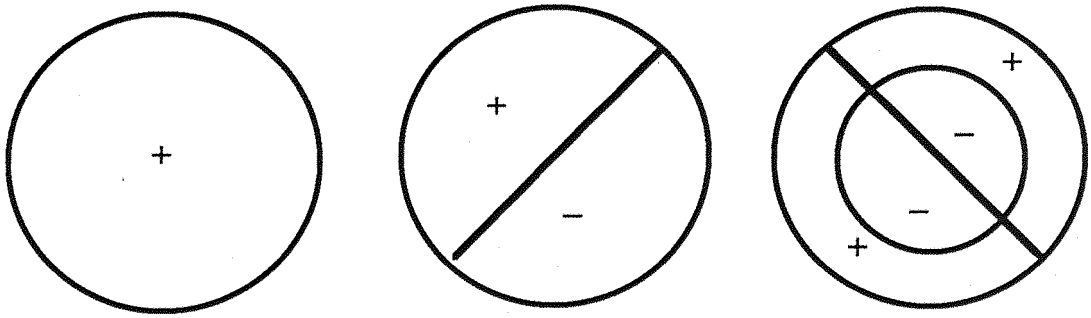

mode order	n = 0 p = 0	n =1 p = 0	n = 1 p = 1

Figure 6.15 Cross-sectional distribution of pressure phase and nodal surfaces of acoustical modes of a pipe.

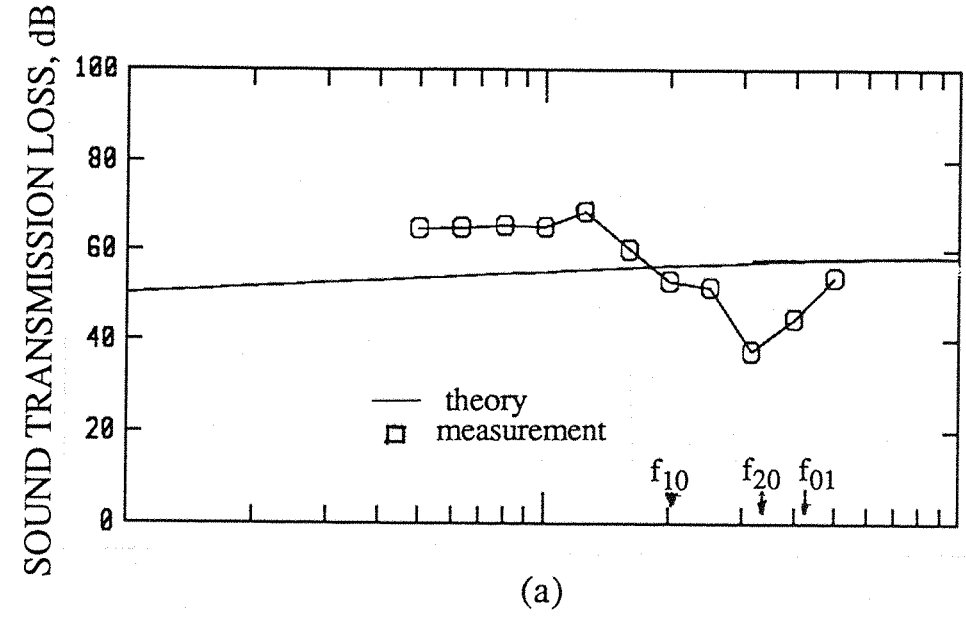

(a)

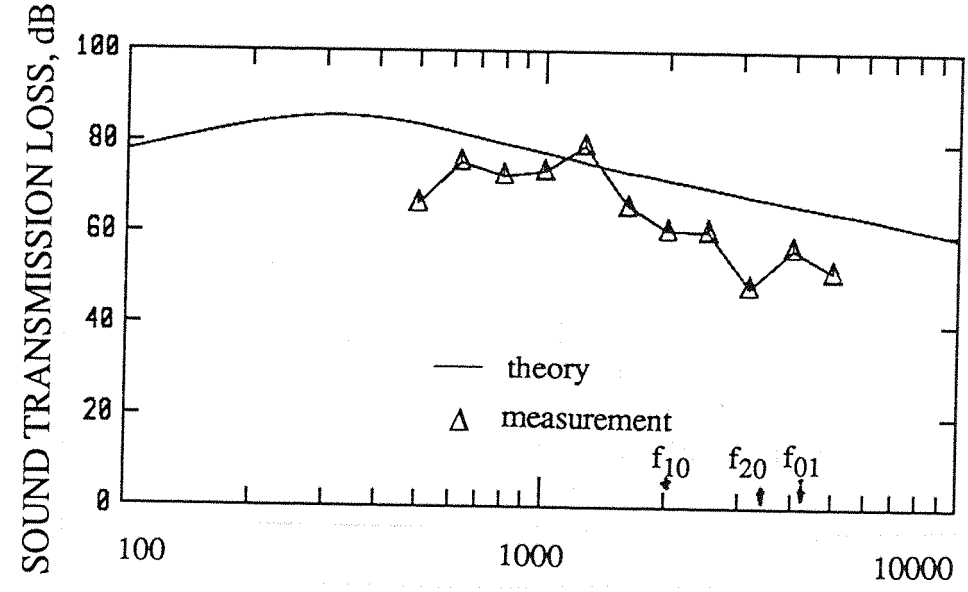

(b)

Figure 6.16 Comparison of predicted and measured sound transmission losses of a plain pipe and double pipe with air gap.

(a) plain pipe. (b) double pipe with air gap.

f_{10} = 2006 Hz, f_{20} = 3325 Hz, f_{01} = 4175 Hz.

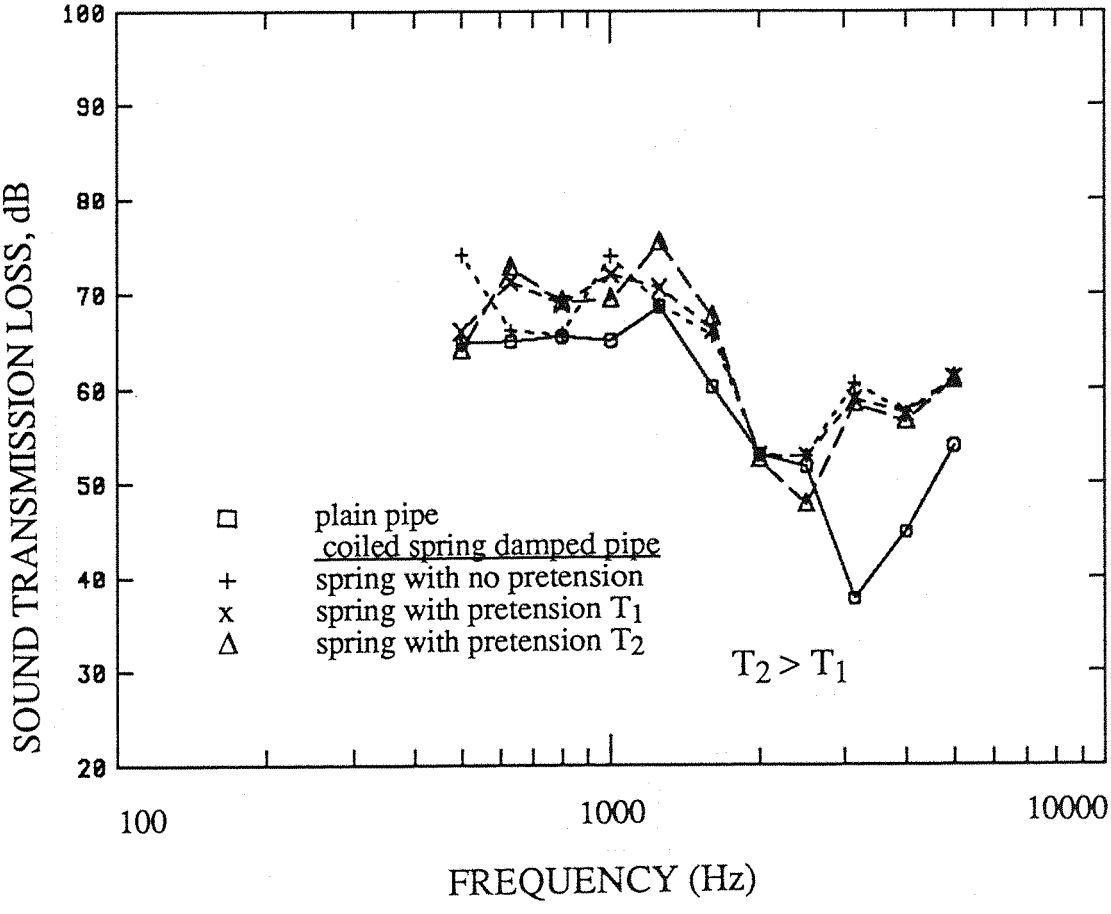

Figure 6.17 Measured sound transmission loss of a plain pipe and a pipe wrapped with a coiled spring.

T_1= the extended length of spring is 0.67 π R,

T_2= the extended length of spring is 1.33 π R,

R = mean radius of pipe, diameter of spring 1 = 12 mm.

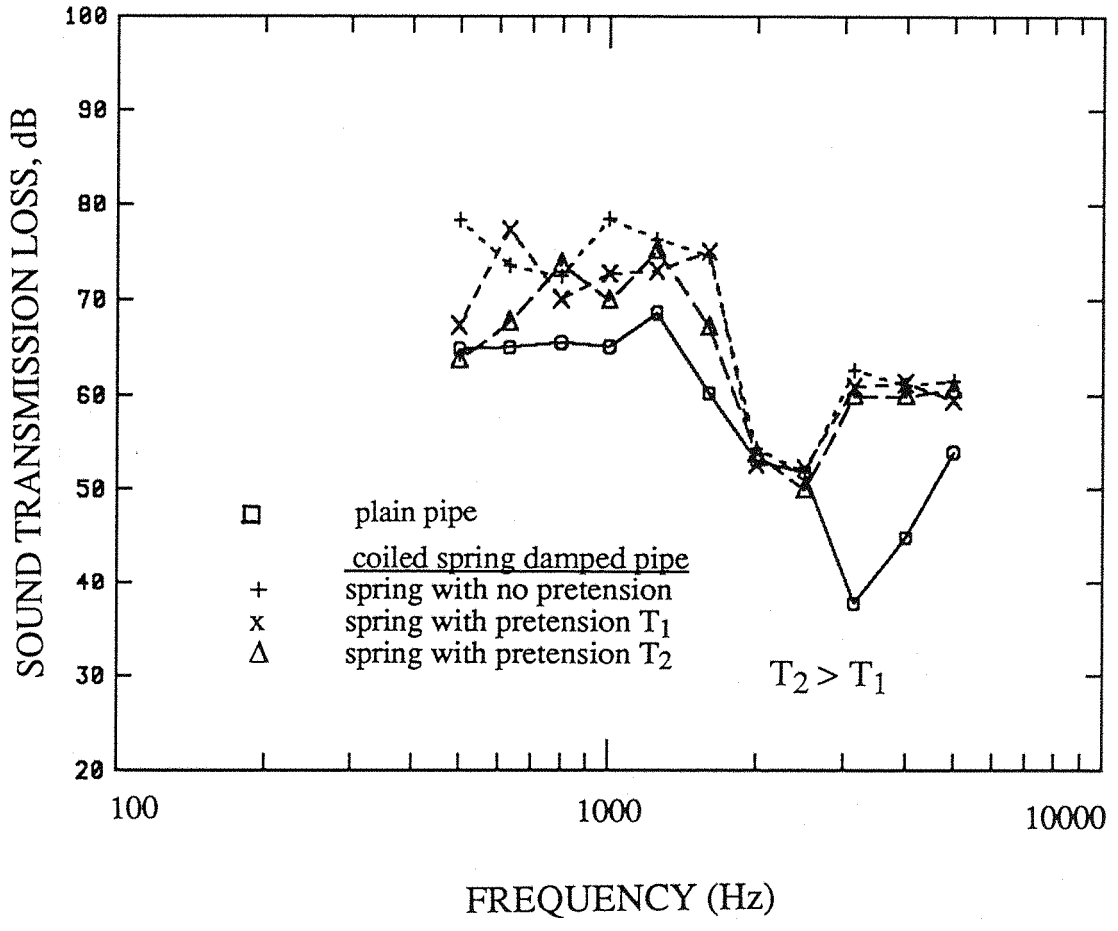

Figure 6.18 Measured sound transmission loss of a plain pipe and a pipe wrapped with a coiled spring.

T_1= the extended length of spring is 0.67 π R,
T_2= the extended length of spring is 1.33 π R,
R = mean radius of pipe, diameter of spring·2 = 8 mm.

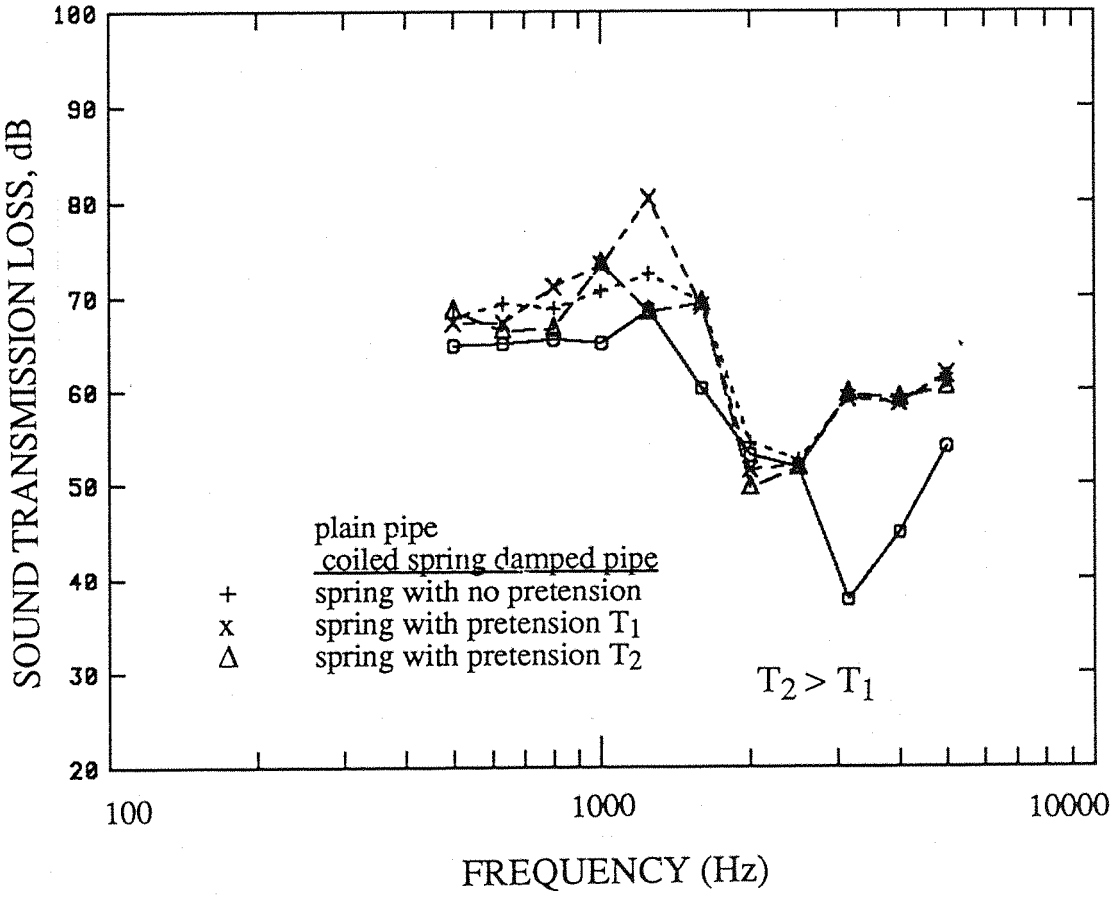

Figure 6.19 Measured sound transmission loss of a plain pipe and a pipe wrapped with a coiled spring.

T_1= the extended length of spring is 0.67 π R,
T_2= the extended length of spring is 1.33 π R,
R = mean radius of pipe, diameter of spring 3 = 7.5 mm.

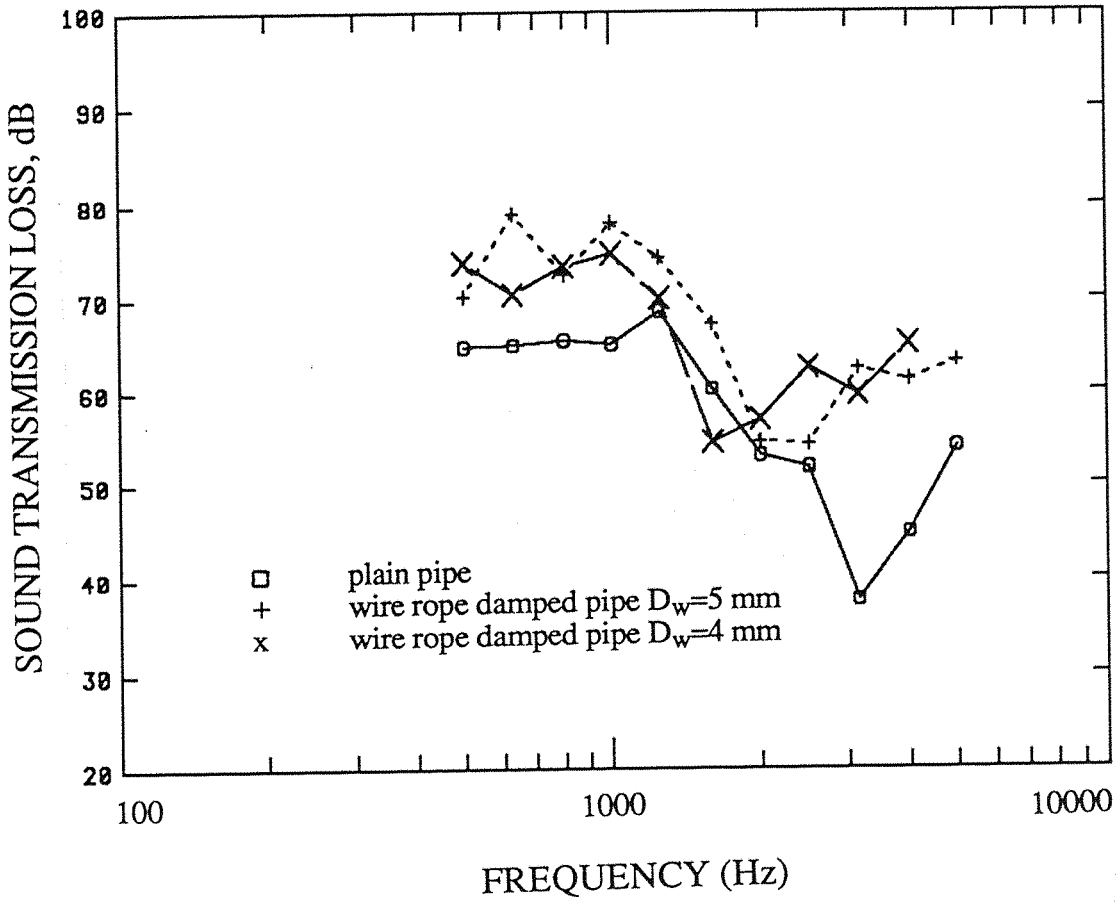

Figure 6.20 Measured sound transmission loss of a plain pipe and a pipe wrapped with a wire spring.

D_w = diameter of wire rope.

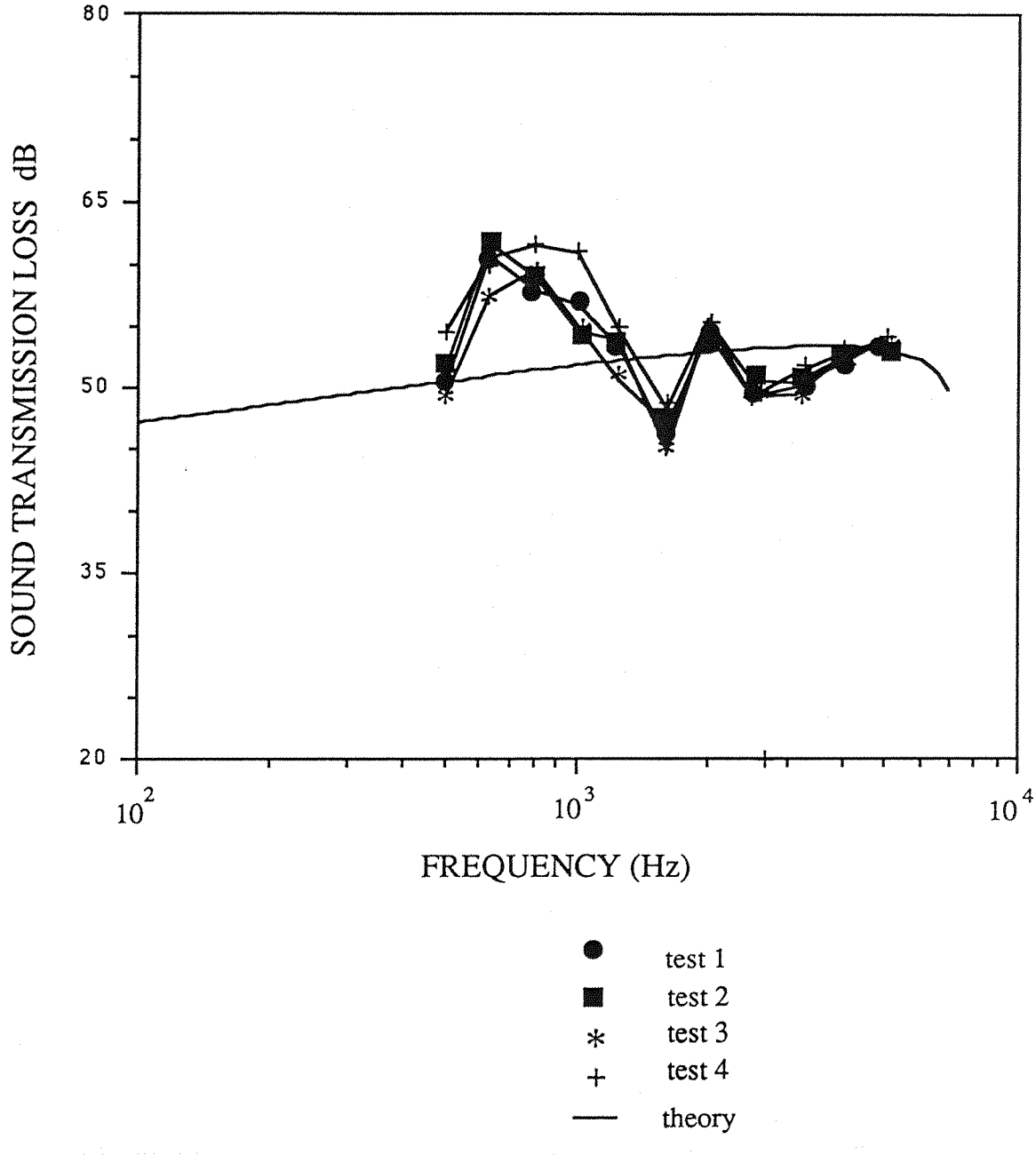

Figure 6.21 Comparison of theoretical and experimental results for sound transmission loss for a plain pipe (the "industrial pipe").

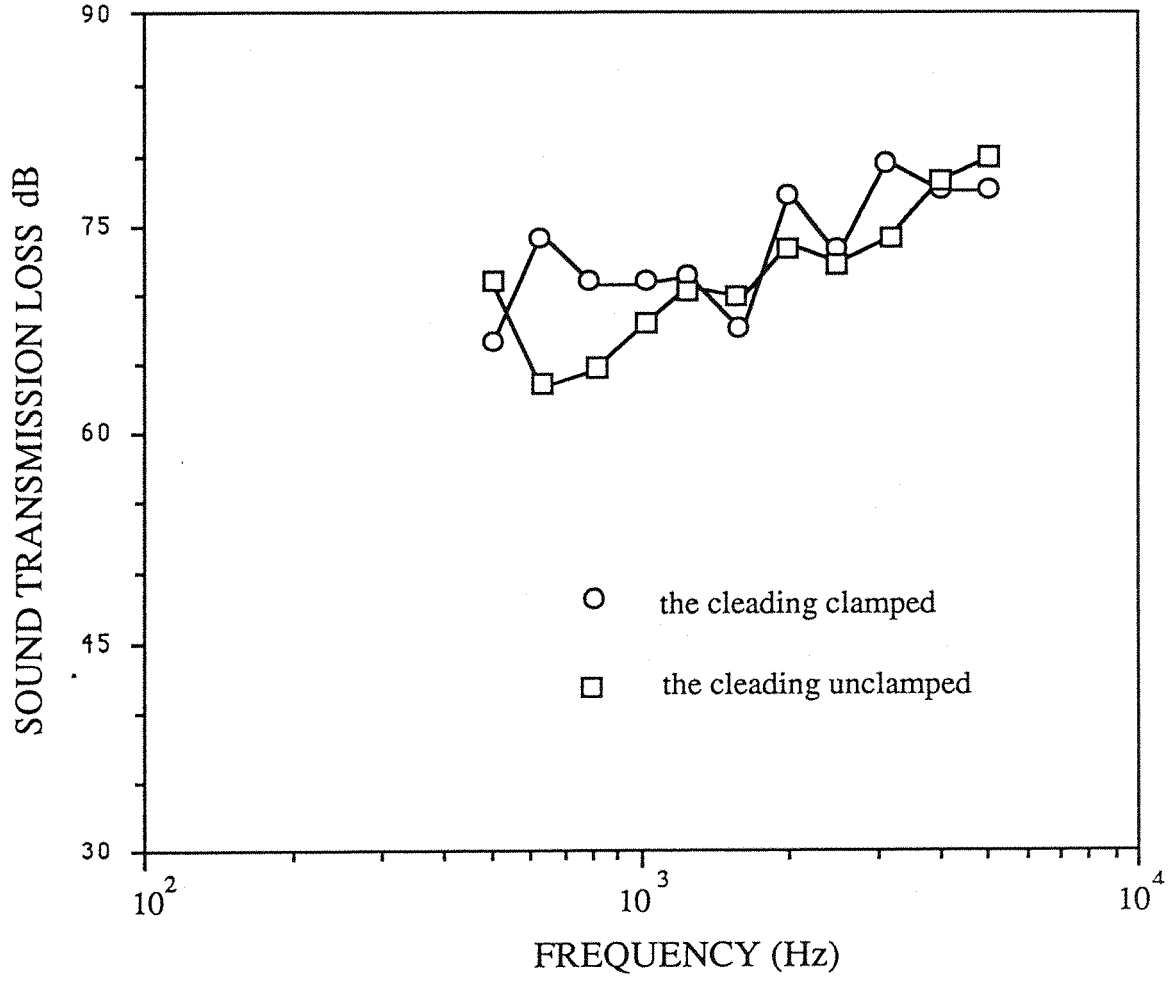

Figure 6.22 Measured sound transmission loss for a pipe wrapped with mineral wool and single wall cleading.

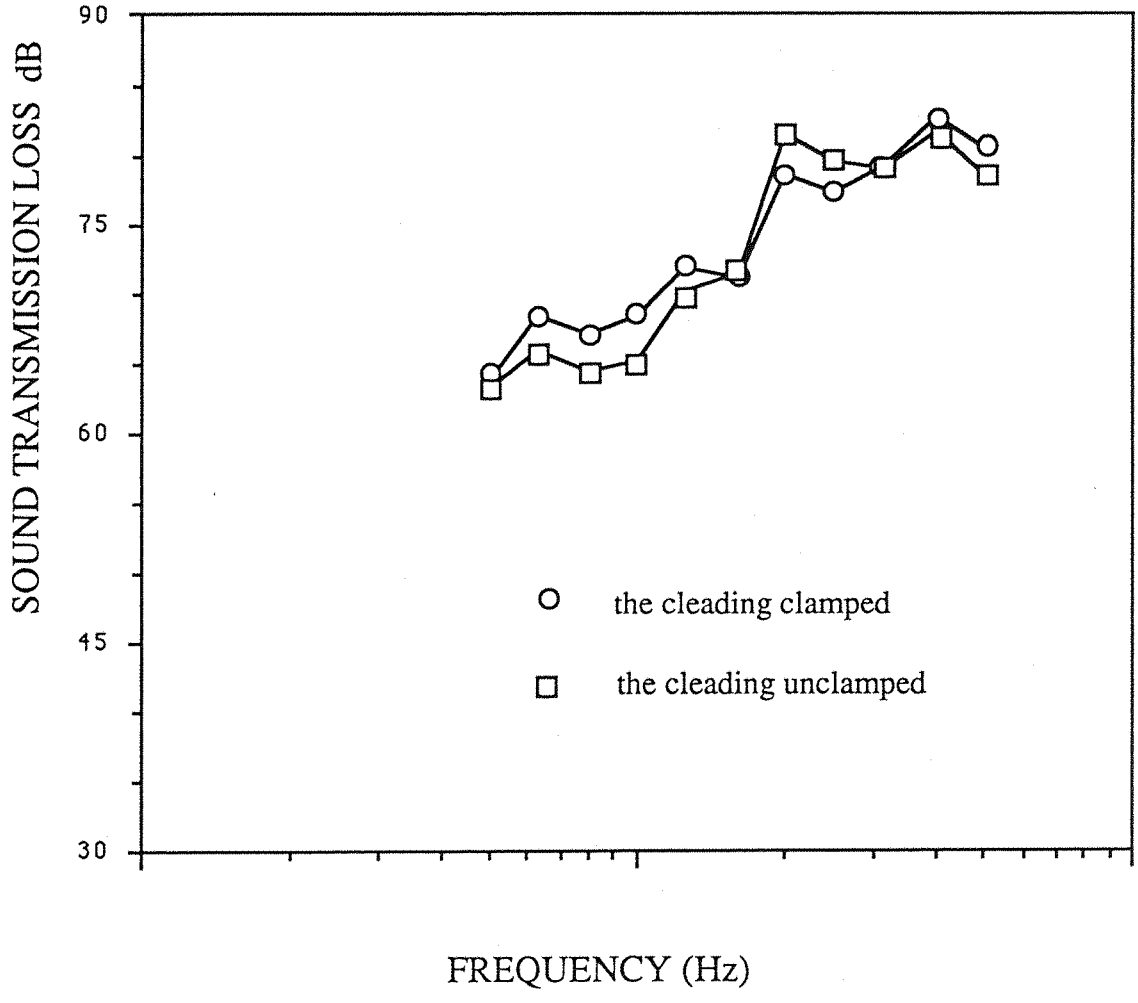

Figure 6.23 Measured sound transmission loss for a pipe wrapped with mineral wool and double wall cleading.

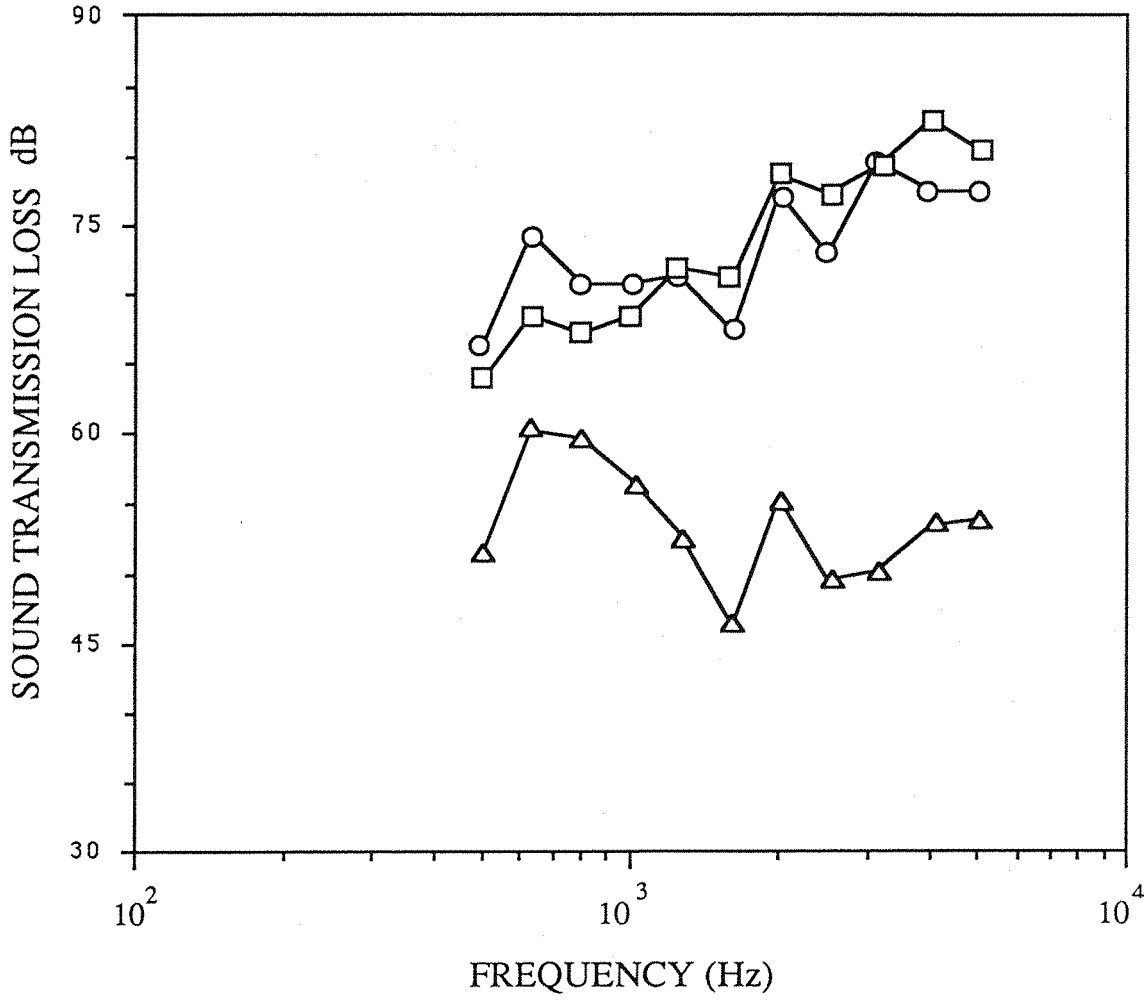

△ single pipe

○ pipe wrapped with mineral wool and single wall cleading.

□ pipe wrapped with mineral wool and double wall cleading.

Figure 6.24 Comparison of sound transmission loss between the single pipe and the pipe wrapped with mineral wool.

CHAPTER 7. CONCLUSIONS.

Mechanical vibration, vibration transmission, noise radiation and their control in industrial pipework have been studied for many years, both experimentally and theoretically. Following this basis of established research, the study presented here has sought to develop simple, robust and effective methods for increasing the damping of industrial pipework by techniques which could be used at elevated temperatures. Two principal techniques for increasing the structural damping of pipes have been investigated, squeeze film damping in a concentric pipe system and the addition of friction devices in the form of a spring or wire rope wound around the outside of a pipe. It is clear that any such techniques should be investigated both theoretically and experimentally at laboratory scale and the implications of the damping levels achieved be assessed in relation to the damping levels likely to be encountered in industrial pipework, this has been done.

A theoretical model has been developed for predicting the loss factors of a concentric, thin-walled pipe system with gas or liquid in the annulus; this necessitated reappraisal of methods for predicting the free vibration characteristics of thin shells. Thin shell analysis has been extended in this thesis and the results applied to the concentric pipe problem. Theoretical studies on friction damping were necessarily somewhat limited in this work and the simple model was employed to study the significance of parameters involved in the process. Experiments were carried out to validate the shell theory, to obtain measured loss factors for comparison with theoretical predictions in the concentric pipe damping system and the friction damping systems were investigated experimentally. The damping values obtained have been carefully appraised in relation to the loss factors of a plain pipe, i.e. an indication of "improvement" by the proposed damping techniques has been obtained; the data were also compared with experimentally determined loss factors of a section of "industrial" pipe with various lagging systems which is used in the electrical power generation industry. Finally, no such study would have been complete without consideration of acoustic transmission loss of the systems discussed above, i.e. the transmission of sound from inside a pipe to the external surrounding medium; this was done in the last chapter of the thesis and comparisons were made.

The principal conclusions from the work carried out in this thesis are that using improved thin shell theory it is possible to predict the lower, shell-type natural frequencies of pipes. Subsequently, a theoretical model has been successfully developed which enables the loss factors of a double pipe system to be predicted with

a reasonable degree of accuracy over a wide frequency range with air or oil in the gap; the reasonable degree of accuracy has been proven by comparison of theoretical results with experimental data. The limited parameter studies carried out with coiled spring and wire rope friction damping systems wound around a pipe have shown that in limited frequency ranges these devices can improve significantly the damping of a plain pipe; industrial lagging also increases structural damping. The relationship between structural damping and sound radiation from pipes with internal acoustic sources has been examined. The experimental results suggest that sound energy radiated from the surface of a pipe can be reduced at some structural resonance frequencies by the vibration control methods investigated in this work. Experimentally determined sound transmission loss data for a broad frequency range are given for all of the systems considered.

More detailed conclusions on the various aspects of the study are given below.

7.1 PREDICTION OF NATURAL FREQUENCIES AND MODE SHAPES OF THIN-WALLED PIPES.

Using the equations of motion for a thin circular cylindrical shell, the exact solution for natural frequencies for the symmetric and antisymmetric modes was derived in the form of a matrix. Thus, this theoretical solution applied to prediction of the natural frequencies and mode shapes of thin-walled pipe precisely. Numerical results for natural frequencies and mode shapes of a thin-walled pipe with free-free, free-clamped and clamped-clamped boundary conditions have been obtained. The theoretical results agreed quite well with published data.

Furthermore, as was shown by the numerical results for the natural frequencies and mode shapes, it may be suggested that Rayleigh and Love modes might not be independent modes and could be considered as a special case of the first axial wave mode of shell vibration with free-free boundary conditions when the shell is either very long or very short.

7.2. SQUEEZE FILM DAMPING OF A DOUBLE PIPE SYSTEM.

The squeeze film damping mechanism has been studied theoretically and a better understanding of the processes involved has been achieved. Damping is created in the double pipe system mainly from the viscous property of gas or liquid which converts

mechanical energy into thermal energy when the gas or liquid is "squeezed" and flows between the two vibrating walls of the pipes. From the study of the fluid dynamic properties of squeezed flow, it has been found that the kinematical viscosity and velocity gradient within the air or liquid filled gap have key roles in the level of loss factor achieved in a double pipe system. Kinematical viscosity depends only on the properties of the chosen fluid at certain temperature and pressure conditions. At normal ambient pressure conditions, temperature is the only factor to affect the kinematical viscosity of gas or liquid. The loss factor of an air gapped double pipe system can be increased at high temperatures because of the high kinematical viscosity of air at high temperature. An oil gapped double pipe system, only produces high damping at normal ambient temperature, or even lower temperatures, as the kinematical viscosity of oil decreases at elevated temperatures.

The velocity gradient in the fluid will be strongly dependent on the size of the gap between the two pipes, and it also strongly depends on the mode shapes of two vibrating pipes. A narrow annular gap will create high damping. An optimum thickness of this gap exists for the highest loss factor in the double pipe system according to the present theoretical study.

In the experiments, the loss factors achieved were approximately $3x10^{-3} \sim 1x10^{-2}$ by air damping and $4x10^{-3} \sim 2x10^{-2}$ by oil damping in the double pipe system. Comparing these values with the loss factors of approximately $5\sim9x10^{-4}$ for a plain pipe and $2x10^{-3}$ for an industrial pipe, indicates that the double pipe system can reasonably increase damping. However, the measured loss factors with oil damping were slightly low compared with the predicted values although the loss factors should be quite high according to the theory. A high loss factor can be achieved by an optimally designed narrow air or oil filled annular gap in the double pipe system.

Loss factors are largest with out-of-phase modal vibration. In-phase modal vibration is less effective in modal damping. Only the first three circumferential modes apparently contribute to squeeze film damping. The highest loss factors occur in the first circumferential modes or bending modes. In practice it is beneficial to create a high damping in the double pipe system as the bending mode of a pipe is always strongly excited in service.

7.3 FRICTION DAMPING SYSTEMS USING A SPRING, WIRE ROPE OR MINERAL WOOL LAGGING ATTACHED TO A PIPE.

Experimental studies have been carried out on friction damping of a pipe with three different devices wrapped around it. It can be suggested that magnitudes of loss factors achieved for a friction damped pipe depend on the coefficient of friction and the friction force between the damping device and the pipe surface. The coefficient of friction is normally a constant for a given pair of materials, but it is also a function of the relative velocity between two contacting surfaces. The arrangement of friction devices will control the friction forces. The addition to the effect of the dimensions of a coiled spring, loss factors are affected by pretension of the spring and the mode shapes of the vibrating pipe. High loss factors can be achieved for the pipe with a high pretension coiled spring in a *high* frequency range, and with a low pretension coiled spring in a *low* frequency range.

One or two of the lower circumferential and axial modes of a vibrating pipe were found less affected by both coiled spring and wire rope friction damping. It was also found in the experiments that the friction force of wire rope is a function of its weight. Further investigation is needed to optimise the size of wire rope to give high loss factors in a chosen frequency range.

Constrained mineral wool lagging produces high loss factors in industrial pipes due to high inter-lagging material friction.

The loss factors achieved with friction damping were approximately $7x10^{-3} \sim 3x10^{-2}$ by the coiled spring, $2 \sim 3x10^{-2}$ by the wire rope and about $1 \sim 2x10^{-2}$ by constrained mineral wool lagging. Therefore, the loss factors are considerably increased by the friction damping devices comparing with those values for the plain pipe and the industrial pipe. It also has been found that the loss factors created by the friction damping devices are higher than those created by the double pipe system, particularly in the higher frequency range.

7.4 SOUND TRANSMISSION LOSS OF THE PIPE WITH VARIOUS DAMPING SYSTEMS.

The frequencies of interest in this study of noise reduction in pipe systems fall within the audio frequency range, which is generally well below the ring frequency and critical frequency of industrial pipes and the pipe system examined here. Sound

transmission loss has been measured for a double pipe system, the friction damped pipe and lagged pipes with acoustic excitation inside the pipe.

Noise radiation from the surface of pipe wall can only be decreased in a low frequency range by means of structural damping, squeeze film damping and friction damping or lagging, because only within the frequency range covering the first few resonant structural modes, damping is controlling the response of the pipe system. Although sound transmission loss may be achieved at high frequencies, it is not because of structural damping treatment, but the results of acoustical treatment. For example, sound radiation is mass controlled at high frequency for a double pipe system and the mineral wool lagging wrapped pipe, where sound radiation is shielded by mass "blocking" and sound energy is absorbed by the acoustical material.

The sound transmission loss produced by the means of structural damping is limited, for example by friction damping or squeeze film damping. By the use of the mineral wool lagging with steel sheet, the sound transmission loss through a pipe wall can be increased by 5 ~ 10 dB at lower frequencies and over 20 dB at high frequencies. The transmission loss levels of the lagged pipe were about 65 dB to 85 dB in the frequency 500 to 6000 Hz compared with about 45 dB to 60 dB TL levels for a plain pipe.

7.5 RECOMMENDATION FOR FURTHER WORK.

On the basis of the present studies, further investigations should be carried out on the following topics.

Theoretical and experimental studies of coupled mode shapes and natural frequencies of a double pipe system with a gas or liquid filled gap would be useful in further investigation of squeeze film damping.

In order to achieve the highest loss factor in a double pipe system, it is necessary to determine an optimum ratio of the thickness of the air or liquid gap to the diameter of the inner pipe and the ratio of the thicknesses between inner and outer pipes.

On friction damping, further theoretical study is required. Practically, an optimum size of the wire rope device for the highest loss factors at given frequency range needs to be determined. The relationship between pretension of the spring and loss factor from friction damping should be investigated. Furthermore, it would be very useful to

try various materials to improve the friction damping due to constrained lagging on an industrial pipe.

Theoretical study should also be carried out on sound transmission loss of a plain pipe and a double pipe system or a lagged pipe based on fluid-structure interaction, where both the structural modes and acoustic modes are concerned.

REFERENCES

[1] Leissa, W., Vibration of Shells, Ohio State Univ. Columbus, Ohio. NASA, Washington, D.C. 1973.

[2] Warburton, G.B., "Vibration of Thin Cylindrical Shells," *J. Mech. Enging. Soc.* Vol. 7 Dec. 1965, pp 399-407.

[3] Forsberg, K.,"Influence of Boundary Conditions on the Modal Characteristics of Thin Cylindrical Shells," *AIAA* Vol. 2, No. 12, 1964, pp 2150-2157.

[4] Arnold,R. N.& Warburton, G. B., "Flexural Vibrations of the Walls of Thin Cylindrical Shells having Freely Supported Ends," Proc. Roy. Soc. (London), ser. A. 197, June 1949, pp 238-256.

[5] Leissa, A. W. and Iyer, K. M., "Modal Response of Circular Cylindrical Shells with Structural Damping," *J. Sound and Vibration*, 77(1), 1981, pp 1-10.

[6] Gottenberg, W.G., "Experimental Study of the Vibrations of a Circular Cylindrical Shell," *J. Acousti. Soc. Am.*, Vol. 32, No. 8, Aug. 1960, pp 1002-1006.

[7] Crandall S. H., "The Role of Damping in Vibration Theory," *J. Sound and Vibration*, 11(1) 1970, pp 3-18.

[8] Baker, W. E. and Allen, F. J., The Damping of Thin Beams in Air, Aberdeen Proving Ground B.R.L. Report No.1033, 1957.

[9] Baker, W. E., Woolam, W. E. and Young, D., "Air and Internal Damping of Thin Cantilever Beams," *Int. J. Mech. Sci.*, Vol 9, 1967, p 743.

[10] Clarkson B. L. & Pope R. J., "Experimental Determination of Modal Densities and Loss Factors of Flat Plates and Cylinders," *J. Sound and Vibration*, 77(4) 1981, pp 535-549.

[11] Ranky M. F. & Clarkson B. L., "Frequency Average Loss Factors of Plates and Shells," *J. Sound and Vibration*, 89(2) 1983, pp 309-323.

[12] Nashif, A.D., Jones, D. I. G. and Henderson, J. P., Vibration Damping, John Wiley & Sons, 1985.

[13] Oberst, H. and Frankenfeld, K., "Uber die Dampfung der Biegeschwingungen dunner Bleche durch festhaftende Belage," *Acustica*, 2, 1952, pp181-194.

[14] Rogers, L. C. and Nashif, A. D., "Computerized Processing and Empirical Representation of Viscoelastic Material Property Data and Preliminary Constrained Later Damping Treatment Design," *Shock Vib. Bull.*, 48(2), 1978, pp23-37.

[15] Jones, D. I. G., Nashif, A. D. and Parin, M. L., "Parametric Study of Multiple-layered Damping Treatments on Beams," J. Sound & Vibration, 29(4), 1973, pp 423-434.

[16] Ungar E.E., "Energy Dissipation at Structural Joints; Mechanisms and Magnitudes.", Air Force Flight Dynamics, Laboratory Report FDL-TDR-64-98, August 1964.

[17] Ungar E. E. & Carbonell J. R., "On Panel Vibration Damping due to Structural Joints.", *AIAA Journal*, 4(8), 1966.

[18] Maidanik G., "Energy Dissipation Associated with Gas-pumping in Structural Joints", *J. Acoust. Soc. Am.*, Vol. 40, No. 5, 1966, pp 1064-1072.

[19] Möser von M., "Damping of Structure-borne Sound by the Viscosity of a Layer between Two Plates", *Acustica*, Vol. 46, 1980, pp 210-217.

[20] Trochidis von A., "Vibration Damping due to Air or Liquid Layers", *Acustica*, Vol. 51, 1982, pp 201-212.

[21] Chow, L. C., Damping of Plates with Attached Fluid or Elastic Layers, Ph.D Thesis, ISVR, University of Southampton, England, 1987.

[22] Chen S. S., "Free Vibration of a Coupled Fluid/Structural System", *J. Sound and Vibration*, 21(4) 1972, pp 387-398.

[23] Chen S. S., "Dynamics of a Rod-shell System Conveying Fluid", *Nuclear Engineering and Design*, 30, 1974, pp 223-233.

[24] Chen S. S., et al, "Added Mass and Damping of a Vibrating Rod in Confined Viscous Fluids", *T. ASME, J. Applied Mechanics*, 1976, pp 325-329.

[25] Fritz R. J., "The Effect of Liquids on the Dynamic Motions of Immersed Solids", *J. Eng. for Industry, T. ASME*, 1972, pp 167-173.

[26] Levin L. & Milan D., "Coupled Breathing Vibrations of Two Thin Cylindrical Coaxial Shells in Fluid", Vibration Problems in Industry Proc. Int. Symp., Paper No. 616, 1973.

[27] Au-Yang M. K., "Free Vibration of Fluid-coupled Coaxial Cylindrical Shells of Different Lengths", *T. ASME, J. Applied Mechanics*, 1976, pp 480-484.

[28] An-Yang M. K., "Generalized Hydrodynamic Mass for Beam Mode Vibration of Cylinders Coupled by a Fluid Gap", *T. ASME, J. Applied Mechanics*, 1977, pp 172-173.

[29] Yeh T. T. & Chen S. S., "Dynamics of a Cylindrical Shell System Coupled by Viscous Fluid", *J. Acoust. Soc. Am.*, Vol. 62, No. 2, 1977, pp 262-270.

[30] Yeh T. T. & Chen S. S., "The Effect of Fluid Viscosity on Coupled Tube/Fluid Vibrations", *J. Sound and Vibration*, 59(3) 1978, pp 453-467.

[31] Mulcahy T. M., "Fluid Forces on Rods Vibrating in Finite Length Annular Regions", *T. ASME, J. Applied Mechanics*, Vol. 47, 1980, pp 234-240.

[32] Fox M. J. H. & Whitton P. N., "The Damping of Structural Vibration by Thin Gas Films", *J. Sound and Vibration*, 73(2) 1980, pp 279-295.

[33] Brown S. J., "A comparison of Experimental and Theoretical Vibration Results for Narrow Gap, Fluid-coupled, Coaxial Flexible Cylinders", ASME 80-C2/PVP-104, pp 1-12.

[34] Dowell E. H., "Bounds on Modal Damping by a Component Modes Method using Lagrange Multipliers", *T. ASME, J. Applied Mechanics*, Vol. 47, 1980, pp 211-213.

[35] Chung H. et al, "Analysis of a Cylindrical Shell Vibrating in a Cylindrical Fluid Region", *Nuclear Engineering and Design* 63, 1981, pp 109-120.

[36] Garner G. & Chandra S., "Fluid-structure Coupling between a Finite Cylinder and a Confined Fluid", *T. ASME, J. Applied Mechanics*, Vol. 51, 1984, pp 857-862.

[37] Private information from M. Heckl and U. Schober, Institut für Technische Akustic, Technishe Universität Berlin, Berlin, Germany.

[38] Bowden, F. P. and Tabor, D., Friction and Lubrication of Solids, Oxford University Press (London), 1964.

[39] Zhuravlev, V. A., "On the Physical Basis of the Amontons-Coulomb Law of Friction", *J. Tech. Phys.* (USSR), Vol. 10, 1940, p. 1447.

[40] Greenwood, J. A. and Williamson, J. B. P., "The Contact of Nominally Flat Surfaces", Proc. 2nd Int. Conf. on Electric Contacts, Graz, Austria, 1964.

[41] Den Hartog, J. P., "Forced Vibrations with Combined Coulomb and Viscous Friction", Trans. ASME, APM-53-9, 1931, pp 107-115.

[42] Dowell, E. H., "The Behaviour of a Linear, Damped Modal System with a Non-Linear Spring-Mass-Dry Friction System Attached", *J.Sound and Vibration*, 89(1), 1983 pp 65 - 84.

[43] Ferr, A. A.& Dowell, E. H., "The Behaviour of a Linear Damped Modal System with a Non-Linear Spring-Mass-Dry Friction /damper System Attached", *J.Sound and Vibration*, 101(1), 1985 pp 55 - 74.

[44] Parnes, R., "Response of an Oscillator to a Ground Motion with Coulomb Friction Slippage", J.Sound and Vibration, 94(4), 1984 pp 469 - 482.

[45] Shaw, S. W., "On the Dynamic Response of a System with Dry Friction", *J.Sound and Vibration*, 108(2), 1983 pp 305 - 325.

[46] Gordon, C. K. Yeh, "Forced Vibrations of a Two-Degree-of Freedom System with Coulomb and Viscous Damping", J.(1), *J. Acoust. Soc. Am.*, Vol. 39, pp 14 - 24.

[47] Srinivasan, A. V., Gutts, D. G. and Sridhar, S., Turbojet Engine Blade Damping, NASA CR 165406, USA, July 1981.

[48] Jezequel, L., "Structural Damping by Slip in Joints", Tran. ASME, J. Mechanical Design, 81-DET-139, 1981, pp 1-8.

[49] Beards, C. F., "The Damping of Structural Vibration by Rotational Slip in Joints", *J.Sound and Vibration*, 53(3), 1977 pp 333 - 340.

[50] Earles, S. W. E. and Williams, E. J., "A Linearized Analysis for Frictionally Damped Systems", *J.Sound and Vibration*, 24(4), 1972 pp 444 - 458.

[51] Stimpson, G. and Richards, E. J., "Noise Reduction During Rock Drilling", Proceedings of the Institute of Acoustics, Spring Conference 1981, University of New Castle upon Tyne, 1981.

[52] Mlakar, P. F. and Walker, R. E., "Response of a Helical Spring Considering Hysteretic and Viscous Damping", The Shock and Vibration Bulletin, Bulletin 48 Part 2, Sept. 1978, pp 63-74.

[53] Cutchins, M. A. and Cochran, J. E., "An Investigation of the Damping Phenomena in Wire Rope Isolators", The Role of Damping in Vibration and Noise Control, DE-Vol. 5. The 1987 ASME Design Technology Conferences - 11th Biennial Conference on Mechanical Vibraion and Noise, Boston, M.A. Sept. 1987, pp 197-204.

[54] Holmer, C. I., "Transmission of Sound through Pipe Walls in the Presence of Flow", *J. Sound and Vibration*, 70(2), 1980, pp 275-301.

[55] Manning, J. E., "Noise reduction by a Cylindrical Shell", *J. Acoust. Soc. Am.*, Vol. 39, 1966, p 1245.

[56] Szechenyi, E., "Sound Transmission through Cylinder Walls Using Statistical Considerations", *J. Sound and Vibration*, 19, 1971, pp 83-94.

[57] Koval, L. R., "Sound Transmission into a Laminated Cylindrical Shell ", *J. Sound and Vibration*, 71 (4), 1980, pp 523-530.

[58] Beranek, Leo L.(editor), Noise and Vibration Control, McGRAW-Hill, 1971.

[59] Beranek, Leo L., Noise Reduction, Robert E. Krieger Publishing Company, Huntington, New York, 1980.

[60] Koval, L. R., "On the Transmission into a Thin Cylindrical Shell under 'Flight Conditions' ", *J. Sound and Vibration*, 48 (2), 1976, pp 265-275.

[61] Balena, F. J. and el, "Single- and Double-Wall Cylinder Noise Reduction", *J. Aircraft*, Vol. 20, No. 5, 1983, pp 434-439.

[62] Fahy, F. J., Sound Intensity, Elsevier Science Publishers Ltd, London and New York, 1989.

[63] Donnell, L.H., A Discussion of Thin Shell Theory. Proc. Fifth Intern. Congr. Appl. Mech., 1938

[64] Flügge, W., Stresses in Shells. Springer-Verlag (Berlin) 1962.

[65] Rayleigh, Lord: "Note on the Free Vibration of an Infinitely Long Shell", *Proc. Roy. Soc.*, Vol. 45, 1889, p.445.

[66] Love, A.E.H., A Theatise on Mathematical Theory of Elasticity. Fourth ed., Dover Pub., Inc. (New York) 1944.

[67] Sewall, J.L. & Naumann, E.C., "An Experimental and Analytical Vibration Study of Thin Cylindrical Shells with and without Longitudinal Stiffeners", NASA TN D-4750, Sep. 1968.

[68] L. D. Landau and E. M. Lifshits, Fluid Mechanics, 1982, Pergamon Press.

[69] Tse, F. S., Morse, I. E. and Hinkle, R. T., Mechanical Vibrations Theory and Applications, second edition, 1978 Allyn and Bacon Inc.

[70] Shell Oil Data Sheet, Shell Lubricants U.K., London.

[71] Rabinowicz, E., Friction and Wear of Materials, 1965, John Wiley and Sons, Inc.

[72] Kragelskii, I. V., Friction and Wear, 1965, London Butterworths.

[73] Harris, C. M. & Crede, C. E., Shock and Vibration Handbook, Second Edition, 1976, McGraw-Hill book company.

[74] Harris, C. M., Handbook of Noise Control, McGrw - Hill, Inc. 1957.

[75] Bies, D. A. & Jansen, C. H., Engineering Noise Control, Unwin Hyman Ltd, 1988.

[76] Fahy, F. J., Sound and Structrual Vibration, Academic Press Inc. Ltd, London, 1985.

APPENDIX 2

a. Deduction of components of displacement for circular cylindrical shell.

The equation of motion for thin circular cylindrical shells in matrix form is

$$\begin{bmatrix} a_{11} & a_{12} & a_{13} \\ a_{21} & a_{22} & a_{23} \\ a_{31} & a_{32} & a_{33} \end{bmatrix} \begin{bmatrix} U_0 \\ V_0 \\ W_0 \end{bmatrix} = 0 \qquad (2.14)$$

where

$$a_{11}=\alpha^2-[0.5(1-\nu)(1+\beta)n^2-\Omega]$$
$$a_{12}=0.5(1+\nu)n\alpha$$
$$a_{13}=-\beta\alpha^3+[\nu-0.5(1-\nu)n^2\beta]\alpha$$
$$a_{21}=-0.5(1+\nu)n\alpha$$
$$a_{22}=0.5(1-\nu)(1+3\beta)\alpha^2+(\Omega^2-n^2)$$
$$a_{23}=0.5(3-\nu)\beta n\alpha^2-n$$
$$a_{31}=-\beta\alpha^3+[\nu-0.5(1-\nu)\beta n^2]\alpha$$
$$a_{32}=-0.5(3-\nu)\beta n\alpha^2+n$$
$$a_{33}=\beta\alpha^4-2\beta n^2\alpha^2+[1+\beta(n^2-1)^2-\Omega]$$

Using (2.19) and (2.16), equation (2.17) can be written as

$$W(x) = C_1'\cosh \alpha_1 x/R + C_2'\sinh \alpha_1 x/R + C_3'\cos \alpha_2 x/R + C_4'\sin \alpha_2 x/R + \exp(\alpha_3 x/R)(C_5'\cos \alpha_4 x/R + C_6'\sin \alpha_4 x/R) + \exp(-\alpha_3 x/R)(C_7'\cos \alpha_4 x/R + C_8'\sin \alpha_4 x/R) \qquad (A2.1a)$$

$$U(x) = C_2'K_1\cosh \alpha_1 x/R + C_1'K_1\sinh \alpha_1 x/R + C_4'K_3\cos \alpha_2 x/R - C_3'K_3\sin \alpha_2 x/R + \exp(\alpha_3 x/R)[(C_5'K_5+C_6'K_6)\cos \alpha_4 x/R + (C_6'K_5-C_5'K_6)\sin \alpha_4 x/R)] + \exp(-\alpha_3 x/R)[(C_8'K_6-C_7'K_5)\cos \alpha_4 x/R - (C_8'K_5+C_7'K_6)\sin \alpha_4 x/R)] \qquad (A2.1b)$$

$$V(x) = C_1'K_2\cosh \alpha_1 x/R + C_2'K_2\sinh \alpha_1 x/R + C_3'K_4\cos \alpha_2 x/R + C_4'K_4\sin \alpha_2 x/R + \exp(\alpha_3 x/R)[(C_5'K_7+C_6'K_8)\cos \alpha_4 x/R + (C_6'K_7-C_5'K_8)\sin \alpha_4 x/R)] + \exp(-\alpha_3 x/R)[(C_7'K_7-C_8'K_8)\cos \alpha_4 x/R + (C_8'K_7+C_7'K_8)\sin \alpha_4 x/R)] \quad (A2.1c)$$

where

$$C_1' = B_1 + B_2, \quad C_3' = B_3 + B_4, \quad C_5' = B_5 + B_6, \quad C_7' = B_7 + B_8,$$
$$C_2' = B_1 - B_2, \quad C_4' = i(B_3 - B_4), \quad C_6' = i(B_5 - B_6), \quad C_8' = i(B_8 - B_7)$$

equation (A2.1) can be rewritten in another form

$$U(x) = C_2K_1\cosh \alpha_1 x/R + C_1K_1\sinh \alpha_1 x/R + C_4K_3\cos \alpha_2 x/R - C_3K_3\sin \alpha_2 x/R + \cos \alpha_4 x/R[(C_6K_5+C_7K_6)\cosh \alpha_3 x/R + (C_5K_5+C_8K_6)\sinh \alpha_3 x/R)] + \sin \alpha_4 x/R[(C_8K_5-C_5K_6)\cosh \alpha_3 x/R + (C_7K_5-C_6K_6)\sinh \alpha_3 x/R)] \quad (2.21a)$$

$$V(x) = C_1K_2\cosh \alpha_1 x/R + C_2K_2\sinh \alpha_1 x/R + C_3K_4\cos \alpha_2 x/R - C_4K_4\sin \alpha_2 x/R + \cos \alpha_4 x/R[(C_5K_7+C_8K_8)\cosh \alpha_3 x/R + (C_6K_7+C_7K_8)\sinh \alpha_3 x/R)] + \sin \alpha_4 x/R[(C_7K_7-C_6K_8)\cosh \alpha_3 x/R + (C_8K_7-C_5K_8)\sinh \alpha_3 x/R)] \quad (2.21b)$$

$$W(x) = C_1\cosh \alpha_1 x/R + C_2\sinh \alpha_1 x/R + C_3\cos \alpha_2 x/R + C_4K_3\sin \alpha_2 x/R + \cos \alpha_4 x/R(C_5\cosh \alpha_3 x/R + C_6\sinh \alpha_3 x/R) + \sin \alpha_4 x/R(C_7\cosh \alpha_3 x/R + C_8\sinh \alpha_3 x/R) \quad (2.21c)$$

where

$$C_1=C_1', \quad C_2=C_2', \quad C_3=C_3', \quad C_4=C_4',$$
$$C_5=C_5'+C_7', \quad C_6=C_5'-C_7', \quad C_7=C_6'+C_8', \quad C_8=C_6'-C_8',$$

or written in matrix form

$$\begin{bmatrix} U(x) \\ V(x) \\ W(x) \end{bmatrix} = \begin{bmatrix} A_{11} & A_{12} & \dots & A_{18} \\ A_{21} & A_{22} & \dots & A_{28} \\ A_{31} & A_{32} & \dots & A_{38} \end{bmatrix} \begin{bmatrix} C_1 \\ C_2 \\ \vdots \\ C_8 \end{bmatrix} \qquad (2.22)$$

where

$A_{11}= K_1 \sinh \alpha_1 x/R$
$A_{12}= K_1 \cosh \alpha_1 x/R$
$A_{13}=-K_3 \sin \alpha_2 x/R$
$A_{14}= K_3 \cos \alpha_2 x/R$
$A_{15}= K_5 \cos \alpha_4 x/R.\sinh \alpha_3 x/R - K_6 \sin \alpha_4 x/R.\cosh \alpha_3 x/R$
$A_{16}= K_5 \cos \alpha_4 x/R.\cosh \alpha_3 x/R - K_6 \sin \alpha_4 x/R.\sinh \alpha_3 x/R$
$A_{17}= K_6 \cos \alpha_4 x/R.\cosh \alpha_3 x/R + K_6 \sin \alpha_4 x/R.\sinh \alpha_3 x/R$
$A_{18}= K_6 \cos \alpha_4 x/R.\sinh \alpha_3 x/R + K_6 \sin \alpha_4 x/R.\cosh \alpha_3 x/R$

$A_{21}= K_2 \cosh \alpha_1 x/R$
$A_{22}= K_2 \sinh \alpha_1 x/R$
$A_{23}= K_4 \cos \alpha_2 x/R$
$A_{24}= K_4 \sin \alpha_2 x/R$
$A_{25}= K_7 \cos \alpha_4 x/R.\cosh \alpha_3 x/R - K_8 \sin \alpha_4 x/R.\sinh \alpha_3 x/R$
$A_{26}= K_7 \cos \alpha_4 x/R.\sinh \alpha_3 x/R - K_8 \sin \alpha_4 x/R.\cosh \alpha_3 x/R$
$A_{27}= K_8 \cos \alpha_4 x/R.\sinh \alpha_3 x/R + K_7 \sin \alpha_4 x/R.\cosh \alpha_3 x/R$
$A_{28}= K_8 \cos \alpha_4 x/R.\cosh \alpha_3 x/R + K_7 \sin \alpha_4 x/R.\sinh \alpha_3 x/R$

$A_{31}= \cosh \alpha_1 x/R$
$A_{32}= \sinh \alpha_1 x/R$
$A_{33}= \cos \alpha_2 x/R$
$A_{34}= \sin \alpha_2 x/R$
$A_{35}= \cos \alpha_4 x/R.\cosh \alpha_3 x/R$
$A_{36}= \cos \alpha_4 x/R.\sinh \alpha_3 x/R$
$A_{37}= \sin \alpha_4 x/R.\cosh \alpha_3 x/R$
$A_{38}= \sin \alpha_4 x/R.\sinh \alpha_3 x/R$

b. Operators of determinant $B_{i,j}$.

$$|B_{ij}| = 0 \tag{2.27}$$

$B_{11} = b_1 \cosh\gamma_1$
$B_{12} = b_1 \sinh\gamma_1$
$B_{13} = b_2 \cos\gamma_2$
$B_{14} = b_2 \sin\gamma_2$
$B_{15} = b_3 \cos\gamma_4 \cosh\gamma_3 - b_4 \sin\gamma_4 \sinh\gamma_3$
$B_{16} = b_3 \cos\gamma_4 \sin\gamma_3 - b_4 \sin\gamma_4 \cosh\gamma_3$
$B_{17} = b_3 \sin\gamma_4 \cosh\gamma_3 + b_4 \cos\gamma_4 \sinh\gamma_3$
$B_{18} = b_3 \sin\gamma_4 \sinh\gamma_3 + b_4 \cos\gamma_5 \cosh\gamma_3$

$B_{21} = b_1$
$B_{22} = 0$
$B_{23} = b_2$
$B_{24} = 0$
$B_{25} = b_3$
$B_{26} = 0$
$B_{27} = 0$
$B_{28} = b_4$

$b_1 = [K_1\alpha_1+\nu(nK_2-1)+\beta\alpha_1^2]/R$
$b_2 = [-K_3\alpha_2+\nu(nK_4-1)+\beta\alpha_2^2]/R$
$b_3 = [(K_5\alpha_3-K_6\alpha_4)+\nu(K_7-1)+\beta(\alpha_1^2-\alpha_1^2)]/R$
$b_4 = [(K_6\alpha_3+K_5\alpha_4)+\nu K_8+\beta\alpha_3\alpha_4)]/R$

$B_{31} = b_5 \cosh\gamma_1$
$B_{32} = b_5 \sinh\gamma_1$
$B_{33} = b_6 \cos\gamma_2$
$B_{34} = b_6 \sin\gamma_2$
$B_{35} = b_7 \cos\gamma_4 \cosh\gamma_3 - b_8 \sin\gamma_4 \sinh\gamma_3$
$B_{36} = b_7 \cos\gamma_4 \sinh\gamma_3 - b_8 \sin\gamma_4 \cosh\gamma_3$
$B_{37} = b_7 \sin\gamma_4 \cosh\gamma_3 + b_8 \cos\gamma_4 \sinh\gamma_3$
$B_{38} = b_7 \sin\gamma_4 \sinh\gamma_3 + b_8 \cos\gamma_5 \cosh\gamma_3$

$B_{41} = b_5$
$B_{42} = 0$

$B_{43} = b_6$

$B_{44} = 0$

$B_{45} = b_7$

$B_{46} = 0$

$B_{47} = 0$

$B_{48} = b_8$

$b_5 = [\alpha_1^2+\nu n(K_2-n)+K_1\alpha_1]/R^2$

$b_6 = [-\alpha_2^2+\nu n(nK_4-n)-K\alpha_2]/R^2$

$b_7 = [(\alpha_3^2-\alpha_4^2)+\nu n(K_7-n)+(K_5\alpha_3-K_6\alpha_4)]/R^2$

$b_8 = [2\alpha_3\alpha_4+\nu nK_8+(K_6\alpha_3+K_5\alpha_4)]/R^2$

$B_{51} = b_9 \sinh\gamma_1$

$B_{52} = b_9 \cosh\gamma_1$

$B_{53} = b_{10} \sin\gamma_2$

$B_{54} = b_{10} \cos\gamma_2$

$B_{55} = b_{11} \cos\gamma_4 \sinh\gamma_3 + b_{12} \sin\gamma_4 \cosh\gamma_3$

$B_{56} = b_{11} \sin\gamma_4 \cosh\gamma_3 + b_{12} \sin\gamma_4 \sinh\gamma_3$

$B_{57} = b_{11} \sin\gamma_4 \sinh\gamma_3 - b_{12} \cos\gamma_4 \cosh\gamma_3$

$B_{58} = b_{11} \sin\gamma_4 \cosh\gamma_3 - b_{12} \cos\gamma_4 \sinh\gamma_3$

$B_{61} = 0$

$B_{62} = b_9$

$B_{63} = 0$

$B_{64} = -b_{10}$

$B_{65} = 0$

$B_{66} = b_{11}$

$B_{67} = -b_{12}$

$B_{68} = 0$

$b_9 = [\alpha_1K_2(1+\beta)-n(K_1+\beta\alpha_1)]/R$

$b_{10} = [-\alpha_2K_4(1+\beta)+n(K_3+\beta\alpha_2)]/R$

$b_{11} = [(\alpha_3K_7-\alpha_4K_8)(1+\beta)-n(K_5+\beta\alpha_3)]/R$

$b_{12} = [-(\alpha_4K_7+\alpha_3K_8)(1+\beta)+n(K_6+\beta\alpha_4)]/R$

$B_{71} = b_{13} \sinh\gamma_1$

$B_{72} = b_{13} \cosh\gamma_1$

$B_{73} = b_{14} \sin\gamma_2$

$B_{74} = b_{14} \cos\gamma_2$

$B_{75} = b_{15} \cos\gamma_4 \sinh\gamma_3 + b_{16} \sin\gamma_4 \cosh\gamma_3$

$B_{76} = b_{15} \sin\gamma_4 \cosh\gamma_3 + b_{16} \sin\gamma_4 \sinh\gamma_3$

$B_{77} = b_{15} \sin\gamma_4 \sinh\gamma_3 - b_{16} \cos\gamma_4 \cosh\gamma_3$

$B_{78} = b_{15} \sin\gamma_4 \cosh\gamma_3 - b_{16} \cos\gamma_4 \sinh\gamma_3$

$B_{81} = 0$

$B_{82} = b_{13}$

$B_{83} = 0$

$B_{84} = -b_{14}$

$B_{85} = 0$

$B_{86} = b_{15}$

$B_{87} = -b_{16}$

$B_{88} = 0$

$b_{13} = [\alpha_1^3+K_1\alpha_1^2+0.5(3-\nu)n\alpha_1K_2-(2-\nu)n^2\alpha_1+0.5(1-\nu)n^2K_1]/R^3$

$b_{14} = [\alpha_2^3+K_3\alpha_2^2-0.5(3-\nu)n\alpha_2K_4+(2-\nu)n^2\alpha_2-0.5(1-\nu)n^2K_3]/R^3$

$b_{15} = [\alpha_3(\alpha_3^2-3\alpha_4^2)+K_5(\alpha_3^2+\alpha_4^2)-2K_6\alpha_3\alpha_4+0.5(3-\nu)n(\alpha_3K_7-\alpha_4K_8)-(2-\nu)n^2\alpha_3$
$+0.5(1-\nu)n^2K_5]/R^3$

$b_{16} = [\alpha_4(\alpha_4^2-3\alpha_3^2)-K_6(\alpha_3^2-\alpha_4^2)-2K_5\alpha_3\alpha_4-0.5(3-\nu)n(\alpha_4K_7+\alpha_3K_8)+(2-\nu)n^2\alpha_4$
$-0.5(1-\nu)n^2K_6]/R^3$

$$\gamma_1 = \frac{\alpha_1 L}{R} \quad , \quad \gamma_2 = \frac{\alpha_2 L}{R} \quad , \quad \gamma_3 = \frac{\alpha_3 L}{R} \quad , \quad \gamma_4 = \frac{\alpha_4 L}{R}$$

c. Equations for natural frequency with clamped-clamped boundary conditions.

Substituting clamped-clamped boundary conditions for equation (2.22), equation (2.26) becomes

$$\left|\begin{array}{cc} \begin{matrix} B_{11} & B_{13} & B_{15} & B_{18} \\ B_{21} & B_{23} & B_{25} & B_{28} \\ B_{31} & B_{33} & B_{35} & B_{38} \\ B_{41} & B_{43} & B_{45} & B_{48} \end{matrix} & 0 \\ 0 & \begin{matrix} B_{12} & B_{14} & B_{16} & B_{17} \\ B_{22} & B_{24} & B_{26} & B_{27} \\ B_{32} & B_{34} & B_{36} & B_{37} \\ B_{42} & B_{44} & B_{46} & B_{47} \end{matrix} \end{array}\right| = 0 \qquad (2.29)$$

where

$B_{11} = k_1 \sinh\gamma_1$

$B_{12} = k_1 \cosh\gamma_1$

$B_{13} = - k_3 \sin\gamma_2$

$B_{14} = k_3 \cos\gamma_2$

$B_{15} = k_5 \cos\gamma_4 \sinh\gamma_3 - k_6 \sin\gamma_4 \cosh\gamma_3$

$B_{16} = k_5 \cos\gamma_4 \cos\gamma_3 - k_6 \sin\gamma_4 \sinh\gamma_3$

$B_{17} = k_6 \cos\gamma_4 \cosh\gamma_3 + k_5 \sin\gamma_4 \sinh\gamma_3$

$B_{18} = k_6 \cos\gamma_4 \sinh\gamma_3 + k_5 \sin\gamma_5 \cosh\gamma_3$

$B_{21} = k_2 \cosh\gamma_1$

$B_{22} = k_2 \sinh\gamma_1$

$B_{23} = k_4 \cos\gamma_2$

$B_{24} = k_4 \sin\gamma_2$

$B_{25} = k_7 \cos\gamma_4 \cosh\gamma_3 - k_8 \sin\gamma_4 \sinh\gamma_3$

$B_{26} = k_7 \cos\gamma_4 \sinh\gamma_3 - k_8 \sin\gamma_4 \cosh\gamma_3$

$B_{27} = k_8 \cos\gamma_4 \sinh\gamma_3 + k_7 \sin\gamma_4 \cosh\gamma_3$

$B_{28} = k_8 \cos\gamma_4 \cosh\gamma_3 + k_7 \sin\gamma_4 \sinh\gamma_3$

$B_{31} = \cosh\gamma_1$

$B_{32} = \sinh\gamma_1$

$B_{33} = \cos\gamma_2$

$B_{34} = \sin\gamma_2$

$B_{35} = \cos\gamma_4 \cosh\gamma_3$

$B_{36} = \cos\gamma_4 \sinh\gamma_3$

$B_{37} = \sin\gamma_4 \cosh\gamma_3$

$B_{38} = \sin\gamma_4 \sinh\gamma_3$

$B_{41} = \frac{d_1}{R} \sinh\gamma_1$

$B_{42} = \frac{d_1}{R} \cosh\gamma_1$

$$B_{43} = \frac{-d_2}{R} \sin\gamma_2$$

$$B_{44} = \frac{d_2}{R} \cos\gamma_2$$

$$B_{45} = \frac{d_3}{R} \cos\gamma_4 \sinh\gamma_3 - \frac{d_4}{R} \sin\gamma_4 \cosh\gamma_3$$

$$B_{46} = \frac{d_3}{R} \cos\gamma_4 \cosh\gamma_3 - \frac{d_4}{R} \sin\gamma_4 \sinh\gamma_3$$

$$B_{47} = \frac{d_3}{R} \sin\gamma_4 \sinh\gamma_3 + \frac{d_4}{R} \cos\gamma_4 \cosh\gamma_3$$

$$B_{48} = \frac{d_3}{R} \sin\gamma_4 \cosh\gamma_3 + \frac{d_4}{R} \cos\gamma_4 \sinh\gamma_3$$

$$\gamma_1 = \frac{\alpha_1 L}{2R} \quad , \quad \gamma_2 = \frac{\alpha_2 L}{2R} \quad , \quad \gamma_3 = \frac{\alpha_3 L}{2R} \quad , \quad \gamma_4 = \frac{\alpha_4 L}{2R}$$

d. Equation of Natural Frequency with Clamped-Free Boundary Conditions.

Substituting clamped-free boundary condition into equation (2.23) with x = - L/2 and x = L/2, the natural frequency equation is written as

$$| D_{ij} | = 0 \qquad (2.30)$$

where

$$D_{ij} = B_{ij} \text{ of (2.29)} \quad \text{when } i = 1, 2, 3, 4 \quad , \quad j = 1, 2, 3, \ldots 8$$

when i > 4

$$D_{51} = d_1 \cosh\gamma_1$$
$$D_{52} = - d_1 \sinh\gamma_1$$
$$D_{53} = d_2 \cos\gamma_2$$
$$D_{54} = - d_2 \sin\gamma_2$$
$$D_{55} = d_3 \cos\gamma_4 \cosh\gamma_3 - d_4 \sin\gamma_4 \sinh\gamma_3$$
$$D_{56} = - d_3 \cos\gamma_4 \sinh\gamma_3 + d_4 \sin\gamma_4 \cosh\gamma_3$$
$$D_{57} = - d_3 \sin\gamma_4 \cosh\gamma_3 - d_4 \cos\gamma_4 \sin\gamma_3$$
$$D_{58} = d_3 \sin\gamma_4 \sinh\gamma_3 + d_4 \cos\gamma_4 \cosh\gamma_3$$
$$D_{61} = d_5 \cosh\gamma_1$$
$$D_{62} = - d_5 \sinh\gamma_1$$
$$D_{63} = d_6 \cos\gamma_2$$
$$D_{64} = - d_6 \sin\gamma_2$$

$D_{65} = d_7 \cos\gamma_4 \cosh\gamma_3 - d_8 \sin\gamma_4 \sinh\gamma_3$

$D_{66} = - d_7 \cos\gamma_4 \sinh\gamma_3 + d_8 \sin\gamma_4 \cosh\gamma_3$

$D_{67} = - d_7 \sin\gamma_4 \cosh\gamma_3 - d_8 \cos\gamma_4 \sinh\gamma_3$

$D_{68} = d_7 \sin\gamma_4 \sinh\gamma_3 + d_8 \cos\gamma_4 \cosh\gamma_3$

$D_{71} = - d_9 \sinh\gamma_1$

$D_{72} = d_9 \cosh\gamma_1$

$D_{73} = - d_{10} \sin\gamma_1$

$D_{74} = - d_{10} \cos\gamma_1$

$D_{75} = - d_{11} \cos\gamma_4 \sinh\gamma_3 - d_{12} \sin\gamma_4 \cosh\gamma_3$

$D_{76} = d_{11} \cos\gamma_4 \cos\gamma_3 + d_{12} \sin\gamma_4 \sinh\gamma_3$

$D_{77} = d_{11} \sin\gamma_4 \sinh\gamma_3 - d_{12} \cos\gamma_4 \cosh\gamma_3$

$D_{78} = - d_{11} \sin\gamma_4 \cosh\gamma_3 + d_{12} \cos\gamma_4 \sinh\gamma_3$

$D_{81} = - d_{13} \sinh\gamma_1$

$D_{82} = d_{13} \cosh\gamma_1$

$D_{83} = - d_{14} \sin\gamma_2$

$D_{84} = - d_{14} \cos\gamma_2$

$D_{85} = - d_{15} \cos\gamma_4 \sinh\gamma_3 - d_{16} \sin\gamma_4 \cosh\gamma_3$

$D_{86} = d_{15} \cos\gamma_4 \cosh\gamma_3 + d_{16} \sin\gamma_4 \sinh\gamma_3$

$D_{87} = d_{15} \sin\gamma_4 \sinh\gamma_3 - d_{16} \cos\gamma_4 \cosh\gamma_3$

$D_{88} = - d_{15} \sin\gamma_4 \cosh\gamma_3 + d_{16} \cos\gamma_4 \sinh\gamma_3$

APPENDIX 3.1 Differential Operators Used in the Equation of Motion for the Cylindrical Shell.

A. Mathematical Operators in Cylindrical Co-ordinates.

$\phi = \phi(r, \theta, z)$,

$\mathbf{a} = \mathbf{a}(r, \theta, z)$,

$$\nabla \cdot \mathbf{a} = \frac{\partial a_r}{\partial r} + \frac{1}{r}\frac{\partial a_\theta}{\partial \theta} + \frac{\partial a_z}{\partial z} + \frac{a_r}{r} \qquad \text{(A3 1.1)}$$

$$\nabla \times \mathbf{a} = \left(\frac{1}{r}\frac{\partial a_z}{\partial \theta} - \frac{\partial a_\theta}{\partial z}\right)\mathbf{r} + \left(\frac{\partial a_r}{\partial z} - \frac{\partial a_z}{\partial r}\right)\theta + \frac{1}{r}\left(\frac{\partial r a_\theta}{\partial r} - \frac{\partial a_r}{\partial \theta}\right)\mathbf{z} \qquad \text{(A3 1.2)}$$

$$\nabla \phi = \frac{\partial \phi}{\partial r}\mathbf{r} + \frac{1}{r}\frac{\partial \phi}{\partial \theta}\theta + \frac{\partial \phi}{\partial z}\mathbf{z} \qquad \text{(A3 1.3)}$$

Laplacian operator is:

$$\nabla^2 = \frac{1}{r}\frac{\partial}{\partial r}\left(r\frac{\partial}{\partial r}\right) + \frac{1}{r}\frac{\partial^2}{\partial \theta^2} + \frac{\partial^2}{\partial z^2} \qquad \text{(A3 1.4)}$$

B. The Components of the Stress Tensor in Cylindrical Co-ordiantes r, θ, z.

$$\sigma_{rr} = -p + 2\mu\frac{\partial v_r}{\partial r}, \qquad \text{(A3 1.5)}$$

$$\sigma_{r\theta} = \mu\left(\frac{1}{r}\frac{\partial v_r}{\partial \theta} + \frac{\partial v_\theta}{\partial r} - \frac{v_\theta}{r}\right), \qquad \text{(A3 1.6)}$$

$$\sigma_{\theta\theta} = -p + 2\mu\left(\frac{1}{r}\frac{\partial v_\theta}{\partial \theta} + \frac{v_r}{r}\right), \qquad \text{(A3 1.7)}$$

$$\sigma_{\theta z} = \mu\left(\frac{\partial v_\theta}{\partial z} + \frac{1}{r}\frac{\partial v_z}{\partial \theta}\right), \qquad \text{(A3 1.8)}$$

$$\sigma_{zz} = -p + 2\mu\frac{\partial v_z}{\partial z}, \qquad \text{(A3 1.9)}$$

$$\sigma_{zr} = \mu\left(\frac{\partial v_z}{\partial r} + \frac{\partial v_r}{\partial z}\right) \qquad \text{(A3 1.10)}$$

C. Differential Operators Used in the Equation of Motion of a Pipe.

$$[\mathbf{D}_{d\text{-}m}] = \begin{bmatrix} [R^2\frac{\partial^2}{\partial x^2}+\frac{(1-\nu)}{2}\frac{\partial^2}{\partial\theta^2}-\Omega^2\frac{\partial^2}{\partial t^2}] & R\frac{(1+n)}{2}\frac{\partial^2}{\partial x\partial\theta} & R\nu\frac{\partial}{\partial x} \\ R\frac{(1+\nu)}{2}\frac{\partial^2}{\partial x\partial\theta} & [\frac{(1-\nu)}{2}R^2\frac{\partial^2}{\partial x^2}+\frac{\partial^2}{\partial\theta^2}-\Omega^2\frac{\partial^2}{\partial\theta^2}] & \frac{\partial}{\partial\theta} \\ R\nu\frac{\partial}{\partial x} & \frac{\partial}{\partial\theta} & [1+\beta\nabla^4+\Omega^2\frac{\partial^2}{\partial t^2}] \end{bmatrix}$$

(A3 1.11)

where $\nabla^4 = \nabla^2\nabla^2$, $\nabla^2 = R^2\frac{\partial^2}{\partial x^2} + \frac{\partial^2}{\partial\theta^2}$, $\Omega^2 = rR^2(1-\nu^2)\omega^2/E$, E is Young's modulus, ν the Poisson's ratio, r the density of material.

$$[\mathbf{D}_{mod}] = \begin{bmatrix} [\frac{(1-\nu)}{2}\frac{\partial^2}{\partial\theta^2}] & 0 & -R^3\frac{\partial^3}{\partial x^3}+\frac{(1-\nu)}{2}R\frac{\partial^3}{\partial x\partial\theta^2} \\ 0 & \frac{3}{2}R^2(1-\nu)\frac{\partial^2}{\partial x^2} & -\frac{(3-\nu)}{2}R^2\frac{\partial^3}{\partial x^2\partial\theta}+\frac{\partial^2}{\partial\theta^2} \\ -R^3\frac{\partial^3}{\partial x^3}+\frac{(1-\nu)}{2}R\frac{\partial^2}{\partial\theta^2} & -\frac{(3-\nu)}{2}R^2\frac{\partial^3}{\partial x^2\partial\theta} & 1+2\frac{\partial^2}{\partial\theta^2} \end{bmatrix}$$

(A3 1.12)

APPENDIX 3.2. Derivation of the Stream Function.

When the coefficient of viscosity of the fluid is considered constant, the Navier-Stokes equation can be expressed in the following form,

$$\frac{DV}{Dt} = -\frac{1}{\rho}\nabla p + \frac{\nu_0}{3}\nabla(\nabla\cdot\mathbf{V}) + \nu_0\nabla^2\mathbf{V} \qquad \text{(A3 2.1)}$$

for an incompressible fluid with constant viscosity, equation (A3 2.1) becomes,

$$\frac{DV}{Dt} = -\frac{1}{\rho}\nabla p + \nu_0\,\nabla^2\mathbf{V} \qquad \text{(A3 2.2)}$$

where

$$\frac{DV}{Dt} = \frac{\partial V}{\partial t} + (\mathbf{V}\cdot\nabla)\mathbf{V} \qquad \text{(A3 2.3)}$$

in cylindrical coordinates, the velocity of the fluid is

$$\mathbf{V} = V_r\,\mathbf{r} + V_\theta\,\theta + V_z\,\mathbf{z} \qquad \text{(A3 2.4)}$$

The correction term $(\mathbf{V}\cdot\nabla)\mathbf{V}$ is second order in the fluid velocity [3.48], and therefore, if $\mathbf{V}$ is small (as it often is for sound waves), equation (A3 2.3) can be expressed as its first order of approximation,

$$\frac{DV}{Dt} \approx \frac{\partial V}{\partial t}$$

The term $\frac{\partial V}{\partial t}$ is denoted as the local contribution of acceleration in non-steady flow. And the term $(\mathbf{V}\cdot\nabla)\mathbf{V}$ is the convective contribution due to translation. In fact, when oscillatory motion in a viscous fluid is considered, the term $(\mathbf{V}\cdot\nabla)\mathbf{V}$ should again be negligible. Let l be the order of magnitude of the dimension of the oscillating body. In the case of pipe vibrating with fluid, l is the diameter of the pipe, and $l = d$, where $l >> \delta$, and

$$\delta = \sqrt{2\,\nu_0\,\omega} \qquad \text{(A3 2.5)}$$

where δ is called the depth of penetration of the wave. The amplitude of the oscillations should be small in comparison with the dimensions of the body:

$$l^2 \omega >> \nu_0 \quad \text{and} \quad u << l \tag{A3 2.6}$$

where ω = circular frequency,

u = amplitude of the displacement of the vibrating body.

In this case, it should be noticed, the Reynolds number need not be small. The above inequality is obtained by estimating the magnitude of $(\mathbf{V}\cdot\nabla)\mathbf{V}$. The operator $(\mathbf{V}\cdot\nabla)$ denotes differention in the direction of the velocity. Near the surface of the body, however, the velocity is nearly in the tangential direction and the velocity changes appreciably only over distances of the order of the dimension of the body. Hence

$$(\mathbf{V}\cdot\nabla)\mathbf{V} \sim V^2/l \sim u^2 \omega^2/l .$$

Since the velocity itself is of the order of $u\omega$. The derivative $\partial\mathbf{V}/\partial t$, however, is of the order of $v\omega \sim u\omega^2$. Comparing these, it is seen that

$$(\mathbf{V}\cdot\nabla)\mathbf{V} << \partial\mathbf{V}/\partial t \tag{A3 2.7}$$

If $u << l$, the terms $\partial\mathbf{V}/\partial t$ and $\nu_0 \nabla^2\mathbf{V}$ are then easily seen to be of the same order.

By introducing the vector of vorticity, curl Ω,

$$\Omega = -\nabla^2\psi \tag{A3 2.8}$$

and from (A3 2.2) the pressure can be eliminated for two dimensional flow, we obtain

$$\frac{D\Omega}{Dt} = \nu_o \nabla^2\Omega \tag{A3 2.9}$$

Considering equation (A3 2.7), we have

$$\frac{\partial\Omega}{\partial t} = \nu_o \nabla^2\Omega \tag{A3 2.10}$$

or

$$\nabla^4\psi - \frac{1}{\nu_o}\frac{\partial}{\partial t}\nabla^2\psi = 0 \qquad \text{(A3 2.11)}$$

$$\nabla^2(\nabla^2\psi - \frac{1}{\nu_o}\frac{\partial}{\partial t}\psi) = 0 \qquad \text{(A3 2.12)}$$

Equation (A3 2.12) can be expressed as

$$\nabla^2\psi = 0 \qquad \text{(A3 2.13a)}$$

$$\nabla^2\psi - \frac{w}{n_0}\psi = 0 \qquad \text{(A3 2.13b)}$$

To solve equation (A3 2.13a), let ψ have the form

$$\psi = \psi(r)\sin(n\theta)\exp[j(\omega t - k_z z)] \qquad \text{(A3 2.14)}$$

For two dimensional flow

$$\nabla^2\psi = \frac{\partial^2\psi}{\partial r^2} + \frac{1}{r^2}\frac{\partial^2\psi}{\partial\theta^2} + \frac{1}{r}\frac{\partial\psi}{\partial r} + \frac{\partial^2\psi}{\partial z^2}$$

$$= 0 \qquad \text{(A3 2.15)}$$

This is the Euler equation. When $n > 0$, its solution is

$$\psi(r) = Ar^n + Br^{-n} \qquad \text{(A3 2.16)}$$

Equation (A3 2.13b) is the standard Bessel equation, so that the solutions of (A3 2.13a,b) are

$$\psi(r) = Ar^n + Br^{-n} + CI_n(kr) + DK_n(kr) \qquad \text{(A3 2.17)}$$

where A, B, C, D are constants and n = circumferential wave number,
$I_n(kr)$, $K_n(kr)$ = modified first and second order Bessel functions,
$k^2 = k_z^2 + j\,\omega/\nu_o$,

k_z = axial wavenumber,
ω = circular frequency.

APPENDIX 3.3 Deduction of the Velocity Profile between Two Pipes and the Loss Factor of the System.

Radial and tangential velocities of pumping flow can be expressed as

$$V_r = \frac{n}{r}[\, Ar^n + Br^{-n} + C\, I_n(kr) + D\, K_n(kr)] \qquad \text{(A3 3.1)}$$

$$V_\theta = -A(nr^{n-1}) + B[nr^{-(n+1)}] - Ck\, I_n'(kr) - Dk\, K_n'(kr) \qquad \text{(A3 3.2)}$$

where

A,B,C,D = constants,

I_n, K_n = modified first and second order Bessel functions.

$$I_n(z) \sim \frac{e^z}{\sqrt{2\pi z}}\left\{1 - \frac{\xi-1}{8z} + \frac{(\xi-1)(\xi-9)}{2!\,(8z)^2} - \frac{(\xi-1)(\xi-9)(\xi-25)}{3!\,(8z)^3} + \ldots\right\} \qquad \text{(A3 3.3)}$$

$$K_n(z) \sim \frac{e^{-z}}{\sqrt{2\pi z}}\left\{1 + \frac{\xi-1}{8z} + \frac{(\xi-1)(\xi-9)}{2!\,(8z)^2} - \frac{(\xi-1)(\xi-9)(\xi-25)}{3!\,(8z)^3} + \ldots\right\} \qquad \text{(A3 3.4)}$$

where $\xi = 4n^2$

$z = kr$.

Using Taylor's theorem as

$$f(z) = \sum_{m=0}^{\infty} b_m (Z-a)^m,$$

$$b_m = \frac{1}{m!} f^{(m)}(a),$$

$$m = 0,1,\cdots$$

here , let m=2, and the function f(z) is expanded as a second order series.

if the function f(z) is a Bessel function $I_n(z)$ or $K_n(z)$ and is expanded at the point $r=r_1$, let

$$z = k(r_1 + y)$$

then

$$f(z) = f(kr_1) + f'(kr_1)(z-r_1) + \frac{f''}{2}(kr_1)(z-r_1)^2$$
$$= f(kr_1) + f'(kr_1)y + \frac{f''(kr_1)}{2}y^2, \qquad \text{(A3. 3.5)}$$

when r_1 is fixed f(z) is the only function of y and where

$$y = 0 \sim h.$$

By using

$$I_n'(kz) = \frac{nk}{z} I_n(kz) + k\, I_{n+1}(kz) \qquad \text{(A3. 3.6)}$$
$$K_n'(kz) = \frac{nk}{z} K_n(kz) - k\, K_{n+1}(kz) \qquad \text{(A3. 3.7)}$$

Equations (A3. 3.3) and (A3. 3.4) can be rewritten as

$$I_n(kr) = I_n(kr_1)\, H_1(y) + I_{n+1}(kr_1)\, H_2(y) + I_{n+2}(kr_1)\, H_3(y) \qquad \text{(A3. 3.8)}$$
$$K_n(kr) = K_n(kr_1)\, H_1(y) - K_{n+1}(kr_1)\, H_2(y) + K_{n+2}(kr_1)\, H_3(y) \qquad \text{(A3. 3.9)}$$

where

$$H_1(y) = 1 + n\frac{y}{r_1} + \frac{1}{2}n(n-1)\left(\frac{y}{r_1}\right)^2$$
$$H_2(y) = ky\left[1 + \frac{1}{2}(2n+1)\left(\frac{y}{r_1}\right)\right]$$
$$H_3(y) = \frac{1}{2}(ky)^2.$$

By this expression,

$$I_n(kr)\big|_{y=0} = I_n(kr_1),$$

$$K_n(kr)\big|_{y=0} = K_n(kr_1),$$

$$I_n(kr)\big|_{y=h} = I_n(kr_2),$$
$$= I_n(kr_1)\, H_1(h) + I_{n+1}(kr_1)\, H_2(h) + I_{n+2}(kr_1)\, H_3(h),$$

$$K_n(kr)\big|_{y=h} = K_n(kr_2),$$
$$= K_n(kr_1)\, H_1(h) - K_{n+1}(kr_1)\, H_2(h) + K_{n+2}(kr_1)\, H_3(h),$$

where

$I_n(kr_1)$ and $K_n(kr_1)$ can be written as the form of

$$I_n(kr_1) = \frac{e^{kr_1}}{\sqrt{2\pi kr_1}} F_n(kr_1),$$

$$I_{n+i}(kr_1) = \frac{e^{kr_1}}{\sqrt{2\pi kr_1}} F_{n+i}(kr_1),$$

$$K_n(kr_1) = \sqrt{\frac{\pi}{2kr_1}}\, e^{-kr_1}\, G_n(kr_1),$$

$$K_{n+i}(kr_1) = \sqrt{\frac{\pi}{2kr_1}}\, e^{-kr_1}\, G_{n+i}(kr_1),$$

or $I_{n+i} = q_1\, F_{n+i}(kr_1),$

$$K_{n+i} = q_2\, G_{n+i}(kr_1),$$

where

$$q_1 = \frac{e^{kr_1}}{\sqrt{2\pi kr_1}},$$

$$q_2 = \sqrt{\frac{\pi}{2kr_1}}\, e^{-kr_1},$$

$$F_n(kr_1) = \left\{ 1 - \frac{\xi-1}{8kr_1} + \frac{(\xi-1)(\xi-9)}{2!\,(8kr_1)^2} - \frac{(\xi-1)(\xi-9)(\xi-25)}{3!\,(8kr_1)^3} + \ldots \right\},$$

$$G_n(kr_1) = \left\{ 1 + \frac{\xi-1}{8kr_1} + \frac{(\xi-1)(\xi-9)}{2!\,(8kr_1)^2} - \frac{(\xi-1)(\xi-9)(\xi-25)}{3!\,(8kr_1)^3} + \ldots \right\}.$$

In the computing procedure, there is an ill conditioned point when using a very large value of q_1 or small value of q_2. To overcome this difficulty, the following deduction is used.

The equation of motion (equation 3.26) of a double pipe system is

$$\{[A_{ij}] - [B_{ij}][C_{ij}]\,[a_{ij}]^{-1}\}\;[\;\bar{v}_1\;\;\bar{w}_1\;\;\bar{v}_2\;\;\bar{w}_2]^T = 0 \qquad \text{(A3. 3.10)}$$

As Bessel functions are only in the matrices of C_{ij} and a_{ij}, $[C_{ij}]$ and $[a_{ij}]$ are written as

$$[a_{ij}] = \begin{bmatrix} a_{11} & a_{12} & q_1 a'_{13} & q_2 a'_{14} \\ a_{21} & a_{22} & q_1 a'_{23} & q_2 a'_{24} \\ a_{31} & a_{32} & q_1 a'_{33} & q_2 a'_{34} \\ a_{41} & a_{42} & q_1 a'_{43} & q_2 a'_{44} \end{bmatrix} \qquad \text{(A3. 3.11)}$$

$$[c_{ij}] = \begin{bmatrix} c_{11} & c_{12} & q_1 c'_{13} & q_2 c'_{14} \\ c_{21} & c_{22} & q_1 c'_{23} & q_2 c'_{24} \\ c_{31} & c_{32} & q_1 c'_{33} & q_2 c'_{34} \\ c_{41} & c_{42} & q_1 c'_{43} & q_2 c'_{44} \end{bmatrix} \qquad \text{(A3. 3.12)}$$

where

$q_l\, c'_{ij} = c_{ij}$,

$q_l\, a'_{ij} = a_{ij}$,

$j=3,4, \qquad l = 1,2.$

in which the $q_1F_n(kr)$ and $q_2G_n(kr)$ are substituted for $I_n(kr)$ and $K_n(kr)$.

$$[a_{ij}]^{-1} = [A_{ij}] / |a_{ij}|$$

$$= \begin{bmatrix} A_{11} & A_{21} & \cdot & A_{41} \\ A_{12} & A_{22} & \cdot & \cdot \\ A_{13} & \cdot & \cdot & \cdot \\ A_{14} & \cdot & \cdot & A_{44} \end{bmatrix} \qquad \text{(A3. 3.13)}$$

$$|a_{ij}| = \begin{vmatrix} a_{11} & a_{12} & q_1 a'_{13} & q_2 a'_{14} \\ a_{21} & a_{22} & q_1 a'_{23} & q_2 a'_{24} \\ a_{31} & a_{32} & q_1 a'_{33} & q_2 a'_{34} \\ a_{41} & a_{42} & q_1 a'_{43} & q_2 a'_{44} \end{vmatrix}$$

$$= q_1 q_2 \begin{vmatrix} a_{11} & a_{12} & a'_{13} & a'_{14} \\ a_{21} & \cdot & \cdot & \cdot \\ \cdot & \cdot & \cdot & \cdot \\ \cdot & \cdot & \cdot & a'_{44} \end{vmatrix} \qquad \text{(A3. 3.14)}$$

$$A_{11} = q_1 q_2 \begin{vmatrix} a_{22} & a'_{23} & a'_{24} \\ a_{32} & \cdot & \cdot \\ \cdot & \cdot & a'_{44} \end{vmatrix}$$

$$A_{12} = q_1 q_2 \begin{vmatrix} a_{21} & a'_{23} & a'_{24} \\ a_{31} & \cdot & \cdot \\ \cdot & \cdot & a'_{44} \end{vmatrix}$$

$$A_{13} = q_2 \begin{vmatrix} a_{21} & a_{22} & a'_{24} \\ a_{31} & \cdot & \cdot \\ \cdot & \cdot & a'_{44} \end{vmatrix} \qquad A_{14} = -q_1 \begin{vmatrix} a_{21} & a_{22} & a'_{23} \\ a_{31} & \cdot & \cdot \\ \cdot & \cdot & a'_{43} \end{vmatrix}$$

so that

$$[a_{ij}]^{-1} = \frac{\begin{bmatrix} A_{11} & A_{21} & \cdot & A_{41} \\ A_{12} & A_{22} & \cdot & \cdot \\ \frac{1}{q_1} A'_{13} & \cdot & \cdot & \cdot \\ \frac{1}{q_2} A'_{14} & \cdot & \cdot & \frac{1}{q_2} A'_{44} \end{bmatrix}}{\begin{vmatrix} a_{11} & a_{12} & a'_{13} & a'_{14} \\ a_{21} & \cdot & . & . \\ . & . & \cdot & . \\ . & . & . & a'_{44} \end{vmatrix}} \qquad \text{(A3. 3.15)}$$

$$[c_{ij}][a_{ij}]^{-1} = \begin{bmatrix} c_{11} & c_{12} & q_1 c'_{13} & q_2 c'_{14} \\ c_{21} & c_{22} & q_1 c'_{23} & q_2 c'_{24} \\ c_{31} & c_{32} & q_1 c'_{33} & q_2 c'_{34} \\ c_{41} & c_{42} & q_1 c'_{43} & q_2 c'_{44} \end{bmatrix} \begin{bmatrix} A_{11} & A_{21} & \cdot & A_{41} \\ A_{12} & A_{22} & \cdot & \cdot \\ A'_{13}/q_1 & \cdot & \cdot & \cdot \\ A'_{14}/q_2 & \cdot & \cdot & A'_{44}/q_2 \end{bmatrix} \Big/ \begin{vmatrix} a_{11} & a_{12} & a'_{13} & a'_{14} \\ a_{21} & \cdot & . & . \\ . & . & \cdot & . \\ . & . & . & a'_{44} \end{vmatrix}$$

(A3. 3.16)

The terms q_1 and q_2 are cancelled in the equation for $[c_{ij}][a_{ij}]^{-1}$.

Rewrite equation (3.24) of chapter 3 as

$$[A\ B\ C\ D]^T = j\omega\,[a_{ij}]^{-1}[\ \bar{v}_1\ \ \bar{w}_1\ \ \bar{v}_2\ \ \bar{w}_2]^T \qquad \text{(A3. 3.17)}$$

substitute (A3. 3.17) for (A3. 3.1) and (A3. 3.2), and let $\bar{w}_1 = 1$, then

$$V_r = \frac{n}{r_1 + y}[t_{ri}]\,[a_{ij}]^{-1}\left[\frac{\partial\,\bar{w}_i}{\partial t}\right]^T \qquad \text{(A3. 3.18)}$$

$$V_\theta = [t_{\theta i}]\,[a_{ij}]^{-1}\left[\frac{\partial\,\bar{w}_i}{\partial t}\right]^T \qquad \text{(A3. 3.19)}$$

where

$$[t_{ri}] = [t_{r1}\ t_{r2}\ q_1 t_{r3}\ q_2 t_{r4}]$$

$$[t_{\theta i}] = [t_{\theta 1}\ t_{\theta 2}\ q_1 t_{\theta 3}\ q_2 t_{\theta 4}]$$

$$\left[\frac{\partial\,\bar{w}_i}{\partial t}\right]^T = \left[\frac{\partial\,\bar{w}_1}{\partial t}\ 1\ \frac{\partial\,\bar{v}_2}{\partial t}\ \frac{\partial\,\bar{w}_2}{\partial t}\right]^T,$$

$\frac{\partial\,\bar{w}_1}{\partial t}, \frac{\partial\,\bar{v}_2}{\partial t}, \frac{\partial\,\bar{w}_2}{\partial t}$ = velocities of pipes.

Obviously, the terms of q_1 and q_2 can be cancelled in the velocity profiles V_r and V_θ.

The stresses can also be obtained as

$$\tau_{rr} = \frac{n}{r_1 + y}[t_{ri}]\,[a_{ij}]^{-1}\left[\frac{\partial\,\bar{w}_i}{\partial t}\right]^T \qquad \text{(A3. 3.20)}$$

$$\tau_{r\theta} = [t_{\theta i}]\,[a_{ij}]^{-1}\left[\frac{\partial\,\bar{w}_i}{\partial t}\right]^T \qquad \text{(A3. 3.21)}$$

and then loss factor can be easily calculated from equation (3.33).

Loss factor

$$\eta = \frac{E_{dissipated}}{2\pi\, E_{total}}.$$

where energy dissipated is

$$E_{dissipated} = \int_{r_1}^{r_2} \int_{0}^{\frac{2\pi}{\omega}} \int_{0}^{L} \int_{0}^{2\pi} \mu[2(\varepsilon_{rr}^2+\varepsilon_{\theta\theta}^2) + \varepsilon_{r\theta}^2]\, dtdz\, rd\theta dr$$

Total energy in the system is

$$E_{total} = \frac{1}{2}\rho \int_0^L \int_0^{2\pi} \sum_{i=1}^{2} h_i R_i \left[\left(\frac{\partial v_i}{\partial t}\right)^2 + \left(\frac{\partial w_i}{\partial t}\right)^2\right] dzd\theta$$

$$+\frac{1}{2}\rho_o \int_{r_1}^{r_2} \int_0^L \int_0^{2\pi} (V_\theta^2 + V_r^2)\, rd\theta\, drdz$$

$$\varepsilon_{rr} = \frac{\partial V_r}{\partial r},$$

$$\varepsilon_{\theta\theta} = \frac{1}{r}\frac{\partial V_\theta}{\partial \theta} + \frac{V_r}{r},$$

$$\varepsilon_{r\theta} = \frac{1}{r}\frac{\partial V_r}{\partial \theta} + \frac{\partial V_\theta}{\partial r} - \frac{V_\theta}{r}.$$

$$\varepsilon_{rr} = An(n-1)\, r^{n-2} - Bn(n+1) r^{-(n+2)} + C\left[\frac{n}{r} I_n'(kr) - \frac{n}{r^2} I_n(kr)\right] + D\left[\frac{n}{r} K_n'(kr) - \frac{n}{r^2} K_n(kr)\right]$$

$$\varepsilon_{\theta\theta} = An(n-1) r^{n-2} + Bn(n+1) r^{-(n+2)} + C\left[\frac{n}{r^2} I_n(kr) - \frac{k}{r} I'_n(kr)\right] + D\left[\frac{n}{r^2} K_n(kr) - \frac{k}{r} K'_n(kr)\right]$$

$$\varepsilon_{r\theta} = -An(n-1)r^{n-2} - Bn(n+1)r^{-(n+2)} + C\left[-\frac{n}{r^2} I_n(kr) + \frac{1}{r} I'_n(kr) - I''_n(kr)\right]$$
$$+ D\left[-\frac{n}{r^2} K_n(kr) + \frac{1}{r} K'_n(kr) - K''_n(kr)\right]$$

where

$$I'_n(z) = \frac{\partial I_n(z)}{\partial z},$$

$$K'_n(z) = \frac{\partial K_n(z)}{\partial z},$$

$$z = kr.$$

Appendix 3.4: Flow Chart of the Computer Program for predicting the Loss Factor of the Double Pipe Damping System.

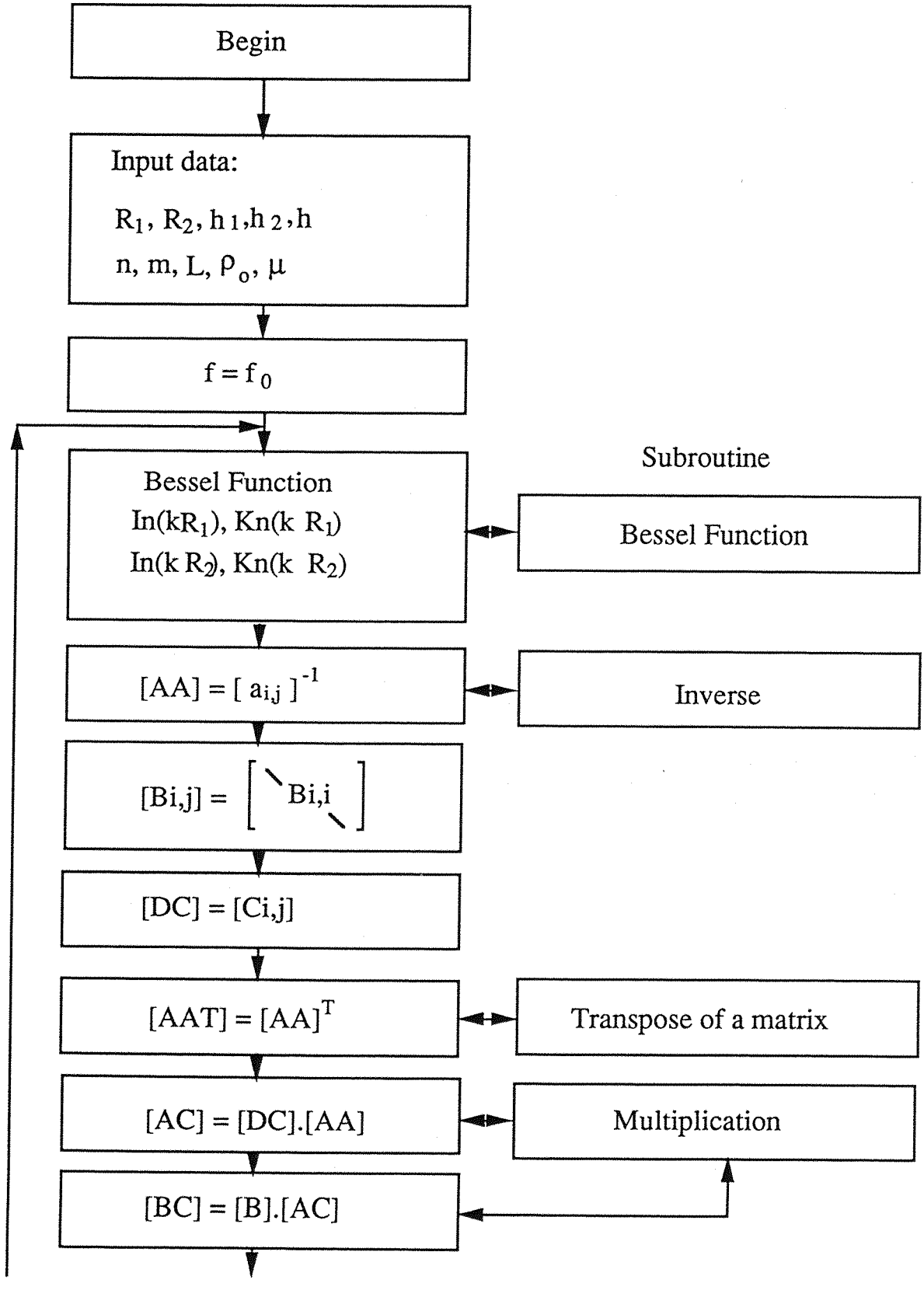

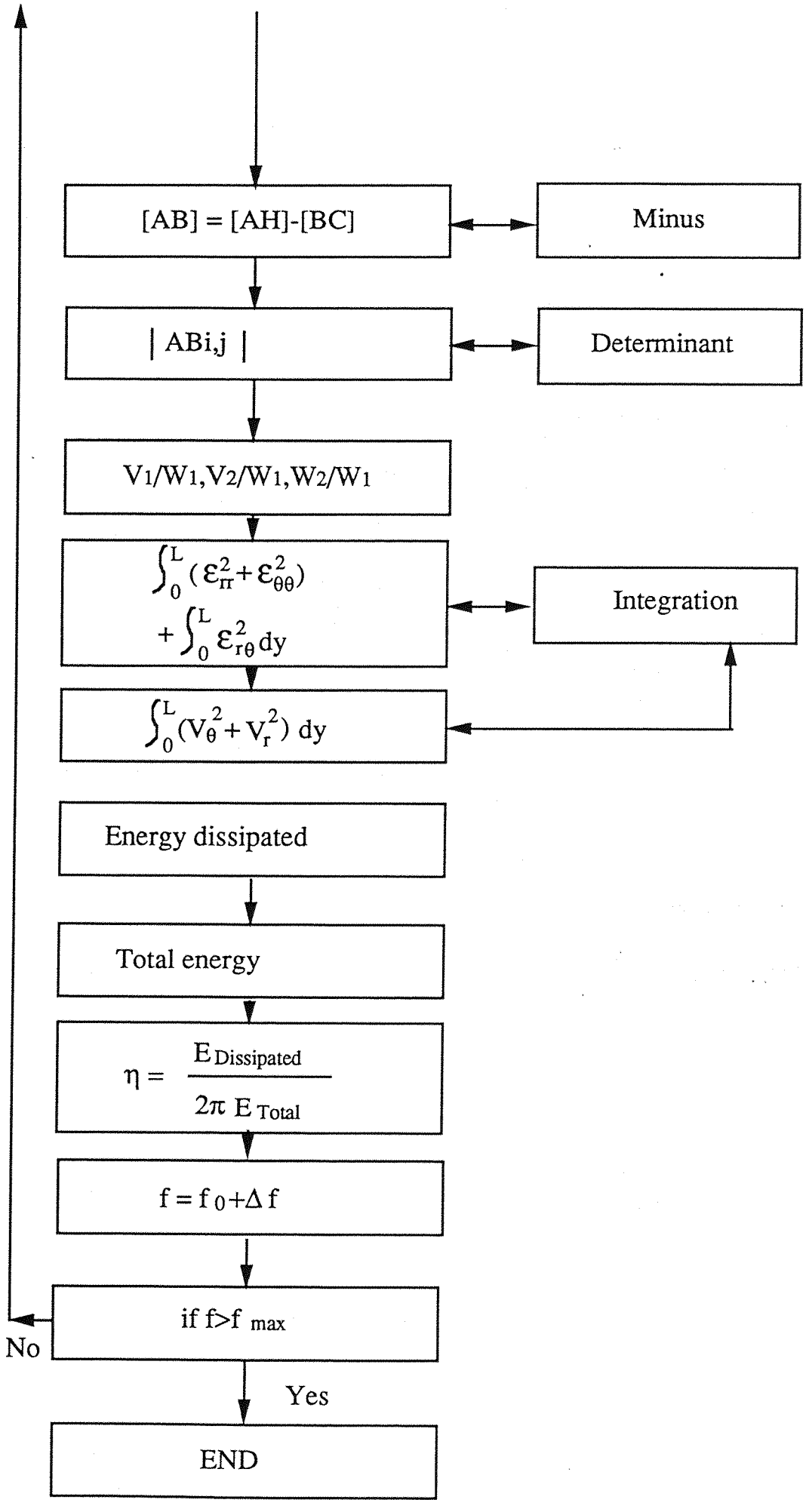
[AB] = [AH]-[BC]
Minus
| ABi,j |
Determinant
V1/W1,V2/W1,W2/W1
$\int_0^L (\varepsilon_{rr}^2 + \varepsilon_{\theta\theta}^2) + \int_0^L \varepsilon_{r\theta}^2 dy$
Integration
$\int_0^L (V_\theta^2 + V_r^2)\, dy$
Energy dissipated
Total energy
$\eta = \frac{E_{Dissipated}}{2\pi E_{Total}}$
$f = f_0 + \Delta f$
if f>f max
No
Yes
END

APPENDIX 6. Design of an acoustic horn.

The basic equation of an acoustic horn is [29]:

$$\frac{\partial^2 p}{\partial x^2} + \frac{\partial p}{\partial x}\frac{\partial}{\partial x}(\ln S(x)) = \frac{1}{c^2}\frac{\partial^2 p}{\partial^2 t} \qquad \text{(A 6.1)}$$

where

p = the pressure of sound in the acoustic horn,
x = distance of axis from the throat of horn,
c = speed of sound,

The plane wave solution is

$$p = \left(\frac{B}{y}\right) e^{-j(\omega/c)\,(\tau x - ct)} \qquad \text{(A 6.2)}$$

where

B = constant,
y = radius of horn at distance of x,
τ = transmissibility,

$$= \sqrt{1 - \left(\frac{\omega_c}{\omega}\right)^2},$$

ω_c = cut off frequency,
C_h = the flare constant,

for an exponential horn, the radius of the horn is

$$y = y_0 \exp(C_h x/2) \qquad \text{(A 6.3)}$$

where y_0 = radius of throat at x = 0.
Section area is

$$S = S_0 \exp(C_h x) \qquad \text{(A 6.4)}$$

where $S_0 = \pi (2y)^2$.

Sound pressure is

$$p = p_0 \exp\left[-\frac{C_h x}{2} - j\frac{\omega}{c}(\tau x - ct)\right]. \qquad \text{(A 6.5)}$$

Particle velocity is

$$v = \frac{1}{\rho_0 c}\left[\tau - j\frac{\omega_c}{\omega}\right]p \qquad \text{(A 6.6)}$$

and resistance rate is

$$R_A = \rho_0 c\sqrt{1 - \left(\frac{\omega_c}{\omega}\right)^2} \qquad \text{(A 6.7)}$$

radiated power is,

$$P_A = \frac{1}{2} v_0^2 S_0 \rho_0 c\sqrt{1 - \left(\frac{\omega_c}{\omega}\right)^2} \qquad \text{(A 6.8)}$$

If the radii of the throat and the mouth of horn are y_0 and y_1 respectively, the length of the horn can be written as

$$L = \frac{2}{C_h}\ln\frac{y_1}{y_0} \qquad \text{(A 6.9)}$$

and from equation (A 6.3), the profile of the horn can be determined.

For cut off frequency of 500 Hz, $2y_0$ = 25.4 mm and $2y_1$ = 211 mm, the designed length of horn is 580 mm.